



**HAL**  
open science

# Photocontrolled biomimetic communication between molecules and nanosystems in confined compartments

Robin Bofinger

► **To cite this version:**

Robin Bofinger. Photocontrolled biomimetic communication between molecules and nanosystems in confined compartments. Other. Université Sciences et Technologies - Bordeaux I, 2013. English. NNT : 2013BOR14933 . tel-01124146

**HAL Id: tel-01124146**

**<https://theses.hal.science/tel-01124146>**

Submitted on 6 Mar 2015

**HAL** is a multi-disciplinary open access archive for the deposit and dissemination of scientific research documents, whether they are published or not. The documents may come from teaching and research institutions in France or abroad, or from public or private research centers.

L'archive ouverte pluridisciplinaire **HAL**, est destinée au dépôt et à la diffusion de documents scientifiques de niveau recherche, publiés ou non, émanant des établissements d'enseignement et de recherche français ou étrangers, des laboratoires publics ou privés.

# THÈSE

PRÉSENTÉE A

**L'UNIVERSITÉ BORDEAUX 1**

ÉCOLE DOCTORALE DES SCIENCES CHIMIQUES

Par

**Robin BOFINGER**

POUR OBTENIR LE GRADE DE

**DOCTEUR**

SPÉCIALITÉ : CHIMIE ORGANIQUE

**Photocontrolled biomimetic communication between molecules  
and nanosystems in confined compartments**

Directeur de thèse : Dr. Nathan D. MCCLENAGHAN

Soutenue le : à renseigner

Devant la commission d'examen formée de :

M. HUNTER, Christopher  
M. SENEQUE, Olivier  
M. JULLIEN, Ludovic  
M. LECOMMANDOUX, Sébastien  
Mme. ODA, Reiko  
M. MCCLENAGHAN, Nathan

Professeur des Universités, Sheffield  
Chargé de Recherche (HDR) CNRS  
Professeur des Universités, ENS Paris  
Professeur des Universités  
Directeur de Recherche CNRS  
Directeur de Recherche CNRS

Rapporteur  
Rapporteur  
Examineur  
Examineur  
Examineur  
Directeur de thèse

---

---

---

## Acknowledgements

First of all I would like to express my sincere gratitude to my supervisor Dr. Nathan D. McClenaghan for giving me the opportunity to carry out this doctoral research in his group and the advice and inspiration concerning the research project. Beside the scientific part I want to respectfully thank him for nourishment and feasts in his place and for the Belgium beer night, but we don't talk about Belgium beer night.

During this multidisciplinary thesis I had the pleasure to collaborate with the group of Prof. Sébastien Lecommandoux at the LCPO and Dr. Reiko Oda at the IECB. I want to thank both collaboration partners for their contribution and the fruitful discussion concerning the work, but above all for the patience when I asked for the third time: "Sorry, but can you explain that again".

I want to thank in particular my invited jury members namely Olivier Sénèque, Christopher Hunter and Ludovic Jullien for taking the time to evaluate my work and for the suggestions to improve the quality of my work.

My deep gratitude goes in particular to the founding bodies of the project. This Ph.D. thesis was financed by the ERC (FP7/2007-2013) "Ideas" program, grant agreement N°208702. All the work presented in this thesis corresponds to and directly contributed to the objectives of the project ("COMMOTION"). Equally, support from the initiative d'excellence at Bordeaux via a project "Projet exploratoire premier soutien" is greatly appreciated.

I also want to thank the people who directly contributed to this work namely Dr. Julie Thevenot for excellent confocal microscopy experiments along with Guillaume Raffy who are in my eyes magicians on the instrument. Guillaume Vives, Pinar Batat and Gedminas Jonusauskas are gratefully acknowledged for the participation with precursors and transient absorption measurements and Jean-Marc Vincent for his guidance on some ultrafast catalysts.

The CESAMO group, who helped me with fluorine NMR samples and mass spectroscopy, is highly acknowledged. I want to thank Jean-Michel, Noël, Claire, Patricia and the rest of the

---

---

team especially for the last few weeks before I had to hand in this manuscript and I came only with very urgent samples to measure.... and they did.

A big thanks goes to the people who made my everydaylife in the lab a pleasant experience. During the three years I conducted my thesis I had the pleasure to meet many people from all over the world. So thanks to HP, Arnaud, Aurélien, Peter Verwilst, Luca, Cedric, Quentin and Sergey for making life in the lab despite crazy hours quite lively. I want to thank as well my combatants in other labs with whom I spend my leisure time when there was some. Suresh, Kitkat, Salem and the rest of the NSysA doctorants and postdocs for the good times we had.

Natürlich darf ich die Leute in Deutschland nicht vergessen die ich während dieser drei Jahre ziemlich vernachlässigt habe, allen voran meine Familie die mich maximal zweimal im Jahr zu sehen bekam. Ganz besonders möchte ich auch meinen Freunden danken die in dieser Zeit so gut wie gar nichts von mir hörten. Einen ganz speziellen Dank natürlich an Alex der mir das Gefühl gab, auch wenn ich mich mal wieder ewig nicht gemeldet hatte, dass wir uns erst letzte Woche das letzte mal gesehen haben.

So finally I kept the last acknowledgements for my hearts person, my adorable girlfriend Léa Messenger. I want to thank her especially for her love and support in the last few months and for an awesome time together during these three years.

The final line is reserved for all the people I forgot to mention because I was very late for preparing my manuscript and there might be the chance that some people who deserved to be mentioned here, didn't find the way on these pages. So a big thank you to them for whatever they did.

---

## Résumé de thèse :

# Communication moléculaire biomimétique entre molécules et nanosystèmes photocontrôlés en compartiments confinés.

**Robin Bofinger**

L'objectif de cette thèse est l'étude du transfert des ions entre nanocompartiments confinés afin de mimer la communication cellulaire des systèmes biologiques. Pour cette raison, nous avons envisagé une approche multidisciplinaire combinant une gamme de techniques dans différents domaines de chimie tels que la chimie supramoléculaire, la chimie des matériaux et la photochimie (utilisation de molécules photoactives). Après une introduction du sujet de thèse et une étude bibliographique des domaines de chimie utilisés, les résultats accomplis se présentent en quatre chapitres.

Le premier chapitre de résultats se focalise sur la synthèse et l'étude d'un nouveau fluorophore à base de BODIPY (bore-dipyrométhène) portant un cycle aromatique perfluoré. La photostabilité de ce fluorophore s'est révélée trois fois supérieure à celle de la fluorescéine, utilisée comme standard pour la microscopie de fluorescence.

Dans un premier temps, le cycle perfluoré a montré une bonne réactivité avec les amines et les thiols, groupements fonctionnels d'intérêt biologique. De plus, une réaction simultanée de ce fluorophore avec des amines et des thiols en solution montrait une conversion sélective de 99 % en produit thiolé.

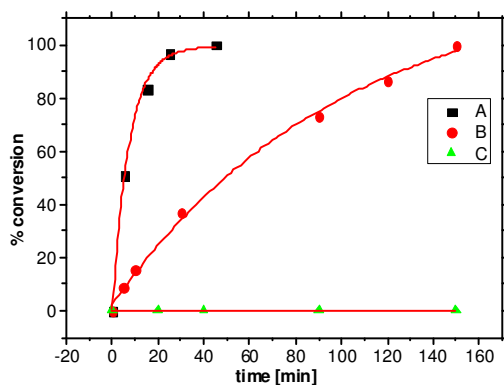


**Image 01 :** Réactivité du perfluorophenyl BODIPY avec différents groupes fonctionnels : thiol (noir, A), amine primaire (rouge, B) et amine secondaire (vert, C).

Cette meilleure réactivité peut donner lieu à des applications pour le labelling des aminoacides tels que la cystéine ou la lysine. Ainsi, en considérant à la fois cette réactivité et le rendement quantique du produit thiolé qui est 90-fois supérieur à celui du produit aminé en milieu aqueux, un contraste de  $10^4$  entre les deux produits a pu être obtenu.

Dans un deuxième temps, afin d'obtenir un dérivé qui peut être utilisé pour la fonctionnalisation de surface portant des alcynes, un azoture a été introduit en position 4 du cycle aromatique, en utilisant la chimie unique de ce type de cycle perfluoré. En employant un cuivre (II) pré-catalyseur photo-réductible en présence de BODIPY-azoture, il a été possible de greffer le fluorophore sur la surface portant des alcynes via formation d'une liaison triazolique. Ces surfaces ont ensuite été observées par microscopie confocale avec la technique FLIM (fluorescence lifetime imaging microscopy), permettant ainsi d'observer à la fois l'intensité de fluorescence et la durée de vie. De plus, nous avons montré que la quantité des molécules greffées sur la surface dépend de la puissance du laser et du temps d'irradiation. Toutefois, la résolution du motif micrométrique greffé s'est révélée surtout dépendre de la viscosité du solvant utilisé comme montré par des expériences dans du toluène puis du cyclohexanol. Ainsi, cette étude préliminaire peut donner lieu à une nouvelle méthode pour greffer fluorophores aux surfaces sans photomasque en utilisant la microscopie confocale.

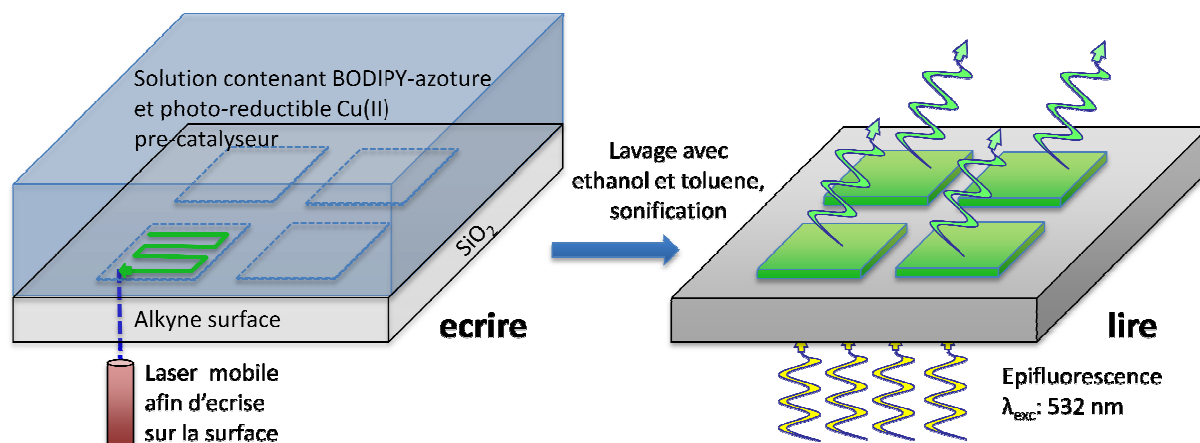


**Image 02** : Principe de fonctionnalisation d'une surface portant des groupes alcynes avec des composés BODIPY-azoture en présence de pré-catalyseur  $\text{Cu(II)}$  photo-réductible.

L'objectif principal de cette thèse était surtout dédié au transfert d'ions entre molécules et nanocompartiments. Pour ce faire, les études suivantes ont été menées.

Dans le deuxième chapitre de résultat, des senseurs moléculaires fluorescents de type fluoroionophore ont tout d'abord été synthétisés. Ces fluoroionophores sont basés sur une partie de reconnaissance BAPTA (1,2-bis(o-aminophenoxy)ethane-N,N,N',N'-tetraacetic acide) et une partie fluorophore à base de BODIPY, furane ou naphthalimide. L'étude de ce senseur moléculaire hydrosoluble, notamment le BAPTA-BODIPY, a montré une augmentation de l'intensité de fluorescence entre 23 et 122 fois par rapport l'intensité initiale, par complexation avec des ions de type  $\text{Ca}^{2+}$  en conditions pseudo-intracellulaires.

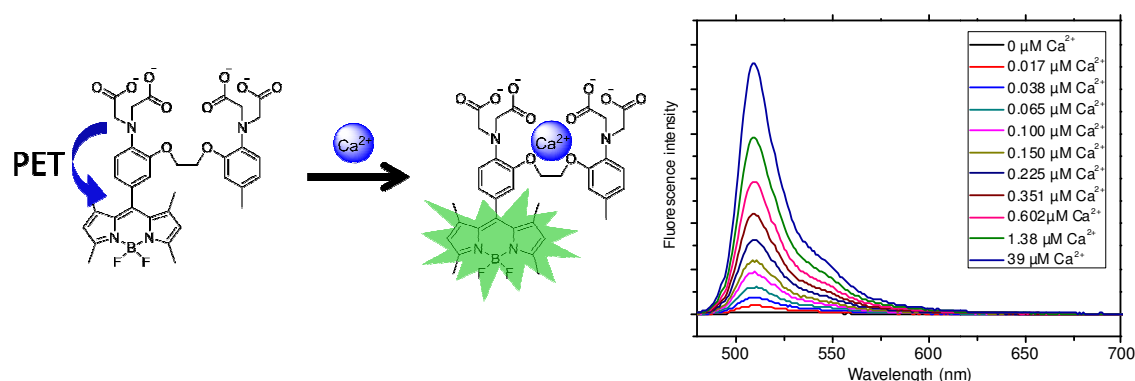


**Image 03 :** Augmentation de la fluorescence par complexation du fluoroionophore hydrosoluble de type BAPTA-BODIPY avec le  $\text{Ca}^{2+}$ .

Par mesure d'absorption transitoire, la vitesse de transfert des électrons a également pu être déterminée, et ce pour la première fois entre des ionophores de type BAPTA et fluorophores de type BODIPY. Les constantes de vitesse obtenues sont de  $3.3 \times 10^{12}$  pour une connexion directe entre fluorophore et ionophore et de  $8.3 \times 10^{11}$  lorsque les deux parties sont séparées par un groupement phényle.

Afin de pouvoir incorporer ces fluoroionophores dans la membrane des vésicules formées par des amphiphiles fluorés, nous avons ensuite synthétisé des amphiphiles senseurs de  $\text{Ca}^{2+}$  basés sur le BAPTA comme motif de reconnaissance et sur le naphthalimide, le BODIPY ou le furan comme fluorophore. Les constantes de dissociation ont été déterminées par titrage avec du  $\text{Ca}^{2+}$ . Les valeurs obtenues (entre  $0.076 - 0.724 \mu\text{M}$ ) se sont révélées similaires à celles obtenues pour des molécules portant un groupement de BAPTA.

Ces études, dédiées à la préparation d'un fluoroionophore récepteur pour le transfert d'ions, ont été suivies dans la deuxième partie de ce chapitre par la synthèse d'un agent photolabile hydrosoluble et amphiphile. Des molécules pouvant libérer des ions par irradiation ont donc été synthétisées, en utilisant le motif de reconnaissance EGTA (ethylene glycol tetraacetic acid) portant un groupement photo-actif DMNPE (1-(4,5-dimethoxy-2-nitrophenyl)ethyl).

Afin d'exécuter ces études de transfert des ions entre molécules et nanocompartiments, une version hydrosoluble et une version amphiphile ont ensuite été synthétisées et caractérisées. Le transfert des ions photoinduit a été réalisé en conditions pseudo-intracellulaires pour mettre en place les conditions pour le transfert des ions entre vésicules.

Ensuite, dans le troisième chapitre de résultats, les fluoroinophores ont d'abord été incorporés dans la membrane de vésicules de type fluoré. Les propriétés de fluorescence et les constantes de dissociation ont alors été déterminées en milieu confiné. Les résultats ont montré une baisse de l'affinité pour le  $\text{Ca}^{2+}$ , causée par la charge de surface des vésicules. Aussi, l'augmentation de la fluorescence s'est avérée plus faible dans la membrane du à l'effet hydrophobe, ce qui induit une inhibition du transfert des électrons. Pour cette raison, une fluorescence non négligeable a aussi été observée en absence de  $\text{Ca}^{2+}$ . Notons que le transfert d'ions photo-induit entre les vésicules de type éjecteur et les vésicules de type récepteur a été réalisé en milieu pseudo-intracellulaire.

L'étape suivante consistait à encapsuler ces deux types de vésicules dans un compartiment vésiculaire géant à base de copolymère à bloc (polymersome). Pour ce faire, des vésicules de type hydrocarboné et fluorocarboné ont été utilisées. Le processus d'encapsulation de vésicules hydrocarbonées dans les polymersomes a conduit de façon surprenante à la formation de nanostructures mélangées, telles que des vésicules polymère-amphiphile hybride. Le processus d'encapsulation de vésicules fluorocarbonées a quant à lui donné lieu à des structures de type vésicules emprisonnées dans les polymersomes géants. Ces deux types de nanostructures sont illustrées en image 04.

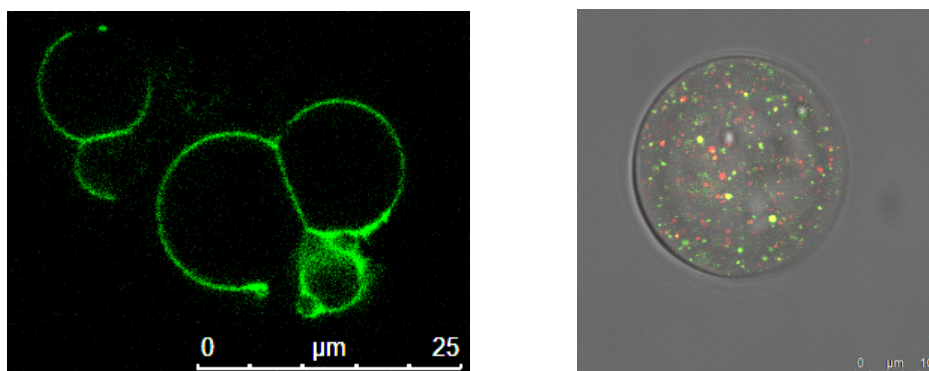


**Image 04 :** *Gauche : Vésicules de type hybride polymère-amphiphile. Droite : Vésicule fluorocarbonée dans un micro-compartiment de polymersome géant.*

Enfin, des vésicules fluorocarbonées incorporant dans la membrane des senseurs de  $\text{Ca}^{2+}$  photolabiles d'une part et des senseurs moléculaires fluorescents d'autre part, ont été

encapsulées dans des polymersomes géants. Ce type de nanostructure multi-compartimentalisée a ensuite été irradié, induisant 1) la libération des ions  $\text{Ca}^{2+}$  complexés aux vésicules de type éjecteur, puis 2) leur transfert vers les vésicules de type récepteur fluorescent. Aussi, une augmentation de fluorescence a été enregistrée. La cinétique de libération des ions  $\text{Ca}^{2+}$  a également été déterminée, par suivi de la vitesse d'augmentation de fluorescence. La cinétique observée s'est avérée du même ordre que la cinétique de décomplexation observée pour les molécules de type DMNPE en solution.

Le dernier chapitre s'est focalisé sur l'approche de multi-compartimentalisation en utilisant des vésicules fluorées incorporant des fluorophores émettant dans le bleu, le vert ou le rouge. En suivant la même procédure d'encapsulation développée dans les chapitres précédents, des microstructures émettant la lumière blanche ont été obtenues. Toutefois, si ces objets sont observés par microscopie confocale, tout compartiment portant de vésicules de couleur différente a pu être observé, comme imagé en image 05.

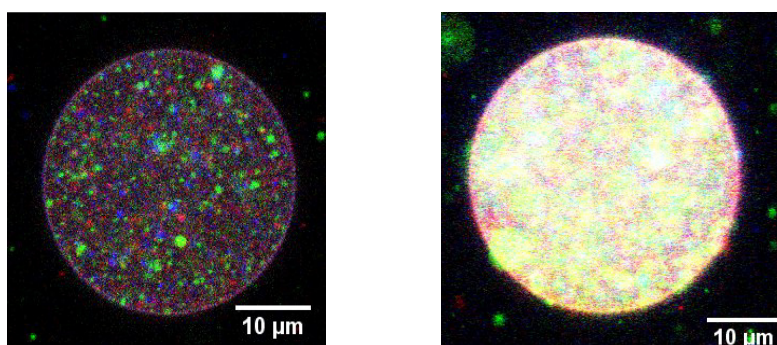


**Image 05 :** à gauche : *polymersome multi-compartimentalisé émettant la lumière blanche observé par microscopie confocale* ; à droite: *le même polymersome observé par microscopie pseudo-épifluorescente*.

En résumé, le but de ce projet de thèse visait au développement du transfert d'ions photoinduit entre compartiments confinés. Nous avons montré avec succès la préparation de tels systèmes, en développant des vésicules fluorées encapsulées dans polymersomes géants. Ces systèmes multicompartimentalisés ont ensuite été exploités pour des études de transfert d'ions, mais aussi pour l'obtention de la lumière blanche en milieu confiné. De plus, nous avons également développé un nouveau fluorophore de type BODIPY et montré son utilisation potentielle pour des applications dans la fonctionnalisation de surface ou le marquage de protéines.

---

<b>1</b>	<b>Introduction .....</b>	<b>5</b>
1.1	Ions in biology.....	5
1.2	Goal of the project.....	7
1.3	Supramolecular chemistry.....	8
1.3.1	Cation binding motifs.....	9
1.4	Stimulus induced ion movement and release .....	12
1.5	A short introduction to photochemistry .....	14
1.5.1	Absorption of light .....	14
1.5.2	Electronic transitions and excited state .....	14
1.5.3	Deexcitation processes .....	16
1.5.4	Characteristics of fluorescence emission.....	17
1.6	Photochromism and light triggered ion release.....	18
1.6.1	Photochromism .....	18
1.6.2	Light induced ion release .....	19
1.7	Cation sensors and molecular sensing processes .....	21
1.7.1	Photoinduced electron transfer (PET).....	21
1.7.2	Photoinduced charge transfer (PCT).....	29
1.8	Biomimetic nanodomains and self-assembled cell mimicry.....	34
1.9	Conclusion.....	34
<b>2</b>	<b>F<sub>5</sub>-BODIPY for selective labeling, fluorescence studies and surface patterning .....</b>	<b>42</b>
2.1	Introduction .....	41
2.1.1	Post-functionalization of the BODIPY core.....	42
2.2	Synthesis and selective labeling of F <sub>5</sub> -BODIPY ( <b>59</b> ).....	46
2.2.1	Synthesis and crystal structure of F <sub>5</sub> -BODIPY ( <b>59</b> ).....	46
2.2.2	S <sub>N</sub> Ar on the perfluorophenyl ring of F <sub>5</sub> -BODIPY ( <b>59</b> ) with thiol and amine conjugates .....	47
2.3	Spectroscopical studies of F <sub>5</sub> -BODIPY ( <b>59</b> ) and its substitution products ( <b>60,61</b> and <b>62</b> ).....	50
2.3.1	Single molecule studies of F <sub>5</sub> -BODIPY ( <b>59</b> ) in PMMA .....	56
2.4	Conclusion.....	58
2.5	Perspectives and preliminary results of photoinduced surface patterning using an azide-BODIPY ( <b>63</b> ) and click chemistry .....	59
2.5.1	Chemistry of azide-BODIPY ( <b>63</b> ) and photoinduced click reaction in solution.....	60
2.5.2	Surface patterning using azide-BODIPY ( <b>63</b> ) and [Cutren(CH <sub>2</sub> PhtBu) <sub>3</sub> ](kt) <sub>2</sub> ( <b>64</b> ) .....	63
2.6	Summary .....	69
<b>3</b>	<b>Synthesis and characterisation of fluorescent Ca<sup>2+</sup>-sensors and photolabile Ca<sup>2+</sup>-decaging agents.....</b>	<b>74</b>
3.1	Synthesis and spectral studies of water soluble Ca <sup>2+</sup> -sensors based on BAPTA and BODIPY .....	73
3.1.1	Synthesis of BAPTA-BODIPYs ( <b>72</b> and <b>76</b> ).....	73
3.1.2	Single crystal X-ray diffraction studies of ester protected BAPTA-BODIPYs ( <b>71</b> and <b>75</b> ) .....	77
3.1.3	Quantum chemical calculations of model compounds for BAPTA-BODIPYs ( <b>72</b> and <b>76</b> ) .....	78
3.1.4	Spectral characterization of BAPTA-BODIPY ( <b>72</b> and <b>76</b> ) and their corresponding esters ( <b>71</b> and <b>75</b> ).....	80
3.1.5	Ca <sup>2+</sup> complexation studies of BAPTA-BODIPYs ( <b>72</b> and <b>76</b> ).....	81
3.1.6	Time-resolved transient absorption studies of BAPTA-BODIPYs ( <b>72</b> and <b>76</b> ).....	84

---

3.1.7	Intermediate conclusion .....	88
3.2	Synthesis and spectral characterization of amphiphilic Ca <sup>2+</sup> -sensors .....	88
3.2.1	Synthesis of BAPTA based amphiphilic fluorionophores bearing naphthalimide (79), BODIPY (82) and furan (97) fluorophores .....	88
3.2.2	Ca <sup>2+</sup> -complexation studies and spectral characterization of BANIF (79), C <sub>8</sub> F <sub>17</sub> -BAPTA-BODIPY (82) and C <sub>8</sub> F <sub>17</sub> -fura red (97) .....	93
3.3	Water soluble and amphiphilic nitrobenzyl-based Ca <sup>2+</sup> -decaging agents .....	98
3.3.1	Synthesis of Ca <sup>2+</sup> -decaging agents DMNPE-4 (99) and amphiphilic DMNPE-4 (122 and 124) .....	103
3.3.2	Spectral characterization and Ca <sup>2+</sup> binding studies of DMNPE-4 (99) and C <sub>14</sub> H <sub>29</sub> -DMNPE-4 (124) .....	105
3.4	Ca <sup>2+</sup> -transfer between DMNPE-4 (99) and BAPTA-BODIPY (72) under pseudo intracellular conditions .....	109
3.5	Conclusion .....	112
<b>4</b>	<b>Ca<sup>2+</sup>-transfer between self-assembled synthetic vesicles and in microcompartments .....</b>	<b>116</b>
4.1	Introduction .....	116
4.1.1	Amphiphiles and liposome formation .....	116
4.1.2	Fluorinated amphiphiles and vesicles .....	118
4.1.3	Polymersomes .....	119
4.1.4	Multicompartmentalized systems .....	120
4.2	Ion transfer between synthetic vesicles .....	122
4.2.1	Ca <sup>2+</sup> -decaging hydrocarbon vesicles preparation and ion release .....	122
4.2.2	Ca <sup>2+</sup> -sensing fluorinated vesicles preparation and spectral properties .....	126
4.2.3	Photoinduced Ca <sup>2+</sup> transfer between hydrocarbon and fluorocarbon vesicles .....	130
4.3	Multicompartmentalization of fluorocarbon and hydrocarbon vesicles in PB- <i>b</i> -PEO polymersomes .....	134
4.4	Molecular ion transfer in the aqueous compartment of PB- <i>b</i> -PEO vesicles .....	139
4.4.1	Ca <sup>2+</sup> sensing vesicles in the confocal microscope .....	142
4.4.2	Ion transfer between fluorocarbon vesicles in PB- <i>b</i> -PEO polymersomes .....	145
4.5	Conclusion .....	151
<b>5</b>	<b>White light emitting multicompartmentalized supramolecular assemblies .....</b>	<b>155</b>
5.1	Introduction .....	155
5.1.1	White light emission in supramolecular chemistry .....	157
5.2	Synthesis of RGB fluorophores based on coumarin, fluorescein and BODIPY ....	162
5.3	Formation of fluorinated R G B vesicles via thinfilm hydration .....	165
5.4	Spectral characterisation of fluorophores BODred (150), C <sub>8</sub> F <sub>17</sub> -fluorescein (152), Pacific-C <sub>8</sub> F <sub>17</sub> (156) and vesicle formulation B1, G1 and R1 .....	166
5.5	White light emission of mixed fluorocarbon vesicles bearing red, green and blue fluorophores .....	168
5.6	White light emission in multicompartmentalized polymersomes .....	173
5.7	Conclusion .....	176
<b>6</b>	<b>General conclusion and perspectives .....</b>	<b>180</b>
<b>7</b>	<b>Experimental section .....</b>	<b>185</b>

---

## Abbreviations:

### Chemicals and bio molecules:

Alq<sub>3</sub> = tris(8-hydroxyquinolino)aluminium

BAPTA = 1,2-bis(o-aminophenoxy)ethane-tetraacetic acid

DDP = di-*n*-dodecyl phosphate

DHP = di-*n*-hexadecyl phosphate

DLPC = 1,2-dilauroyl-*sn*-glycero-

DMPC = 1,2-dimyristoyl-*sn*-glycero-3-phosphocholine

DOPC = 1,2-di-(9*Z*-octadecenoyl)-*sn*-glycero-3-phosphocholine

DPPE = 1,2-dipalmitoyl-*sn*-glycero-phosphoethanolamine

DTDAB = di-tetradecylammonium bromide

EGTA = (ethylene glycol tetraacetic acid

HEEDTA = N-(2-hydroxyethyl) - ethylenediamine N,N',N'-triacetic acid

MOPS = 3-[N-morpholino]propanesulfonic acid

PGE = polyglycerol

Poly(AAc-*co*-DSA) = Poly(acrylic acid-*co*-distearin acrylate)

TMEDA = N,N,N',N'-Tetramethyl-1,2- *b*-polyethanediamine

ATP = adenosine triphosphate

cAMP = cyclic adenosine N,N,N',N'-monophosphate

DDAB = di-*n*-dodecylammonium

DIPEA = N,N-Diisopropylethylamine

DMNPE = dimethoxynitrophenyl 3-phosphocholine

DOAB = di-*n*-octadecylammonium bromide

DOPS = dioleoylphosphatidylserine

Dppf = [1,1-bis(diphenylphosphino)- 3-ferrocene]

EDTA = Ethylenediaminetetraacetic acid

HBTU = N,N,N',N'-Tetramethyl-O-(1*H*-benzotriazol-1-yl)uroniumhexafluorophosphate

HMTA = Hexamethylenetetramine

PB-*b*-PEO = polybutadiene-*b*-poly(ethylene oxide)

PMMA = Poly(methyl methacrylate)

PTMC-*b*-PGA = poly(trimethylene carbonate)- (<sub>L</sub>-glutamic acid)

TPEN = (N,N,N',N'-tetrakis(2-pyridylmethyl)- ethylenediamine

### Solvents:

AcOH = acetic acid

AcCN = acetonitrile

---

---

CHCl<sub>3</sub> = chloroform

DMF = dimethylformamid

DMSO = demethylsulfoxide

EtOH = ethanol

MeOH = methanol

PTE = petroleum ether

CDCl<sub>3</sub> = deuterated chloroform

DCM = dichloromethane

EtAc = ethylacetate

Et<sub>2</sub>O = diethyl ether

CD<sub>3</sub>OD = deuterated methanol

THF = tetrahydrofuran

### Materials:

MS = Mass spectrometrie

TLC = thin layer chromatography

NMR = Nuclear magnetic resonance

UV-Vis = ultraviolet-visible

### Units:

Hz = Hertz

nm = nanometer

cm = centimeter

ppm = part per million

°C = degree Celsius

mol = mole

A.U. = arbitrary units

s = seconds

MHz = Mega Hertz

µm = micrometer

M = mole per liter

kJ = kilo Joule

L = liter

mmol = millimole

min = minutes

h = hours

### Unclassified and symbols:

FRAP = Fluorescence Recovery after  
Photobleaching

LUMO = lowest unoccupied molecular orbital

MLV = multilamellar vesicles

$\lambda_{\text{exc}}$  = excitation wavelength

$\epsilon$  = extinction coefficient

$K_{\text{d}}$  = dissociation constant

HOMO = highest occupied molecular  
orbital

TTTR = time-tagged time resolved

SUV = small unilamellar vesicles

$\lambda_{\text{em}}$  = emission wavelength

$\tau$  = lifetime

rt = room temperature

---

---

## General introduction

The cell is the ultimate supramolecular system harnessing a wide range of supramolecular interactions such as ion-dipole, dipole-dipole, hydrophobic interactions or hydrogen bonding. A major area of supramolecular chemistry is dedicated to reproducing or mimicking certain aspects of these highly sophisticated architectures. Progress in the molecular biology domain allows a deeper understanding and gives access to a number of natural processes which gave rise to some machines exploiting the concepts nature is using for billions of years. Light is an environmental stimulus which is involved in natural processes such as photosynthesis or the mechanism of vision in the human eye. A part of supramolecular photochemistry is therefore dedicated to the exploitation of light as a trigger for molecular processes and interactions. In order to control and fine tune biological processes in a cell-like activation of enzymes when needed or triggering of adhesion to other cells, the nanocompartments inside of the cell need to communicate with one another. For this type of cellular communication a messenger is needed and among others the divalent cation  $\text{Ca}^{2+}$  emerged as one of the most ubiquitous ones. The goal of this thesis is the mimicry of this  $\text{Ca}^{2+}$  communication in rudimentary artificial systems by using the environmental stimulus light as a trigger to control the process. Advances in material science and self-assembly made it possible to create capsules which can resemble the membrane of cells. The progress in supramolecular chemistry gave us the understanding and the means to mimic a set of intracellular interactions, in particular between ions and receptors to create molecules which bind and release ions on command. Advances in supramolecular photochemistry yielded the tools to detect the presence and absence of ions via fluorescence reporters. The multidisciplinary approach of this project will make use of the aforementioned domains of chemistry to show an approach to the light controlled mimicry of cellular communication in artificial systems.

Chapter 1 of this thesis gives an introduction to supramolecular chemistry and highlights the importance of ions in biology. The underlying principles of photochemistry and fluorescent reporter molecules are also given.

Chapter 2 deals with the synthesis and characterisation of a novel boron-dipyrromethene (BODIPY) fluorophore and its application as a selective label, single molecule emitter and for surface patterning

---

Chapter 3 introduces fluorescent  $\text{Ca}^{2+}$  switches and decaging agents, their synthesis and spectroscopic characterisation. Photoinduced electron transfer rates for hydro soluble  $\text{Ca}^{2+}$ -sensors are determined, ion complexation studies for amphiphilic and water soluble sensors will be described and  $\text{Ca}^{2+}$ -transfer under pseudo-physiological conditions are shown.

Chapter 4 focuses on the preparation of self-assembled synthetic vesicles with the capability to sense  $\text{Ca}^{2+}$  through the incorporation of amphiphilic  $\text{Ca}^{2+}$ -sensors prepared in chapter 3 in their bilayer. Similarly, preparation of  $\text{Ca}^{2+}$ -decaging vesicles is described. Ion transfer between these self-assembled nanoobjects is studied via fluorescence spectroscopy. As a final approach towards the goal of the project the ion transfer between vesicles multicompartimentalized in the interior of giant polymersomes will be shown via confocal microscopy.

Chapter 5 takes the multicompartimentalization approach one step further on incorporating three different types of orthogonal emissive vesicles in the lumen of a giant polymersome to create white light-emitting microcompartments.

---

---

---

---

---

# **1 Introduction**

---

---

## 1.1 Ions in biology

Many ions play a vital role in biological systems. Among the most common ions one can find  $H^+$ ,  $Na^+$ ,  $K^+$ ,  $Ca^{2+}$ ,  $Mg^{2+}$ ,  $Cl^-$ ,  $PO_4^{3-}$ ,  $HCO_3^-$ , and  $OH^-$ . These ions play very different roles in cells or the human body. While  $Na^+$  is kept at rather low concentrations,  $K^+$  is the major counterion in the interior of a cell, therefore available in concentrations far higher than the other ions (table 01). The regulation of the ions is conducted by the  $Na^+/K^+$ -ATPase which exchanges 3 sodium ions from the interior of the cell for 2 potassium ions, creating a charge difference which is one of the mechanisms to keep the resting membrane potential of the cell.<sup>1</sup>

**Table 01:** Comparison of ion concentration inside and outside of mammalian cells.<sup>2</sup>

Cation	Intracellular concentration (mM)	Extracellular concentration (mM)
$Na^+$	5 – 15	145
$K^+$	140	5
$Mg^{2+}$	0.5	1 – 2
$Ca^{2+}$	$10^{-4}$	1 – 2
$H^+$	$7 \times 10^{-5}$ ( $10^{-7.2}$ M or pH 7.2)	$4 \times 10^{-5}$ ( $10^{-7.4}$ M or pH 7.4)
Anion		
$Cl^-$	5 – 15	110

$Mg^{2+}$  is second most abundant cation in the eukaryotic cell<sup>3</sup> and the major counterion of adenosine triphosphate (ATP), the so called fuel of the cells and other nucleic acids<sup>4</sup>. Indeed, when one talks about ATP generally this refers to the magnesium salt of ATP. Besides that,  $Mg^{2+}$  controls various enzymes and is part of cofactors. The most interesting ion for our studies is, however,  $Ca^{2+}$ , which is the richest element in the human body. This is mainly due to the presence in human bones. The reason we are interested in  $Ca^{2+}$  is however for its role in the signal transduction inside of eukaryotic cells. Several second messengers are known nowadays, with the complementary system cyclic adenosine monophosphate (cAMP) and  $Ca^{2+}$  among the most important ones.<sup>5</sup>

The crucial role of cAMP was discovered by Sutherland and Rall<sup>6</sup> who identified the molecule as a mediator for the hormones glucagon and ephedrine in the glycogen metabolism in the liver. Not very long after the discovery of cAMP as a second messenger,

---

$\text{Ca}^{2+}$  was established by Heilbrunn<sup>7</sup> even though the importance of  $\text{Ca}^{2+}$  in the event of muscle contraction had been shown much earlier by Ringer<sup>8</sup>. Nowadays, it is known that  $\text{Ca}^{2+}$  plays an essential role in almost all biological processes and is considered the universal messenger in biological systems. The free  $\text{Ca}^{2+}$  concentration in the cytosol is maintained rather low ( $10^{-4}$  mM) due to  $\text{Ca}^{2+}$ -ATPases located in the cell wall and endoplasmic reticulum<sup>9</sup>. Keeping a low concentration sets the stage for intracellular signal transduction. An increase in the intracellular  $\text{Ca}^{2+}$ -level is mostly achieved by voltage-guided  $\text{Ca}^{2+}$ -pumps which can increase the intracellular concentration >10-fold in milliseconds. In neurons the  $\text{Ca}^{2+}$  increase can be even faster.<sup>10</sup> One of the most prominent proteins which react to changes in  $\text{Ca}^{2+}$ -concentration is calmodulin (see figure 01), containing 4 high affinity binding sites. In the absence of  $\text{Ca}^{2+}$  the helices of calmodulin are packed so that their hydrophobic part is not exposed to the exterior. Upon binding  $\text{Ca}^{2+}$  the protein undergoes a conformational change so that the hydrophobic helices are exposed and other enzymes or proteins can bind.<sup>11</sup>

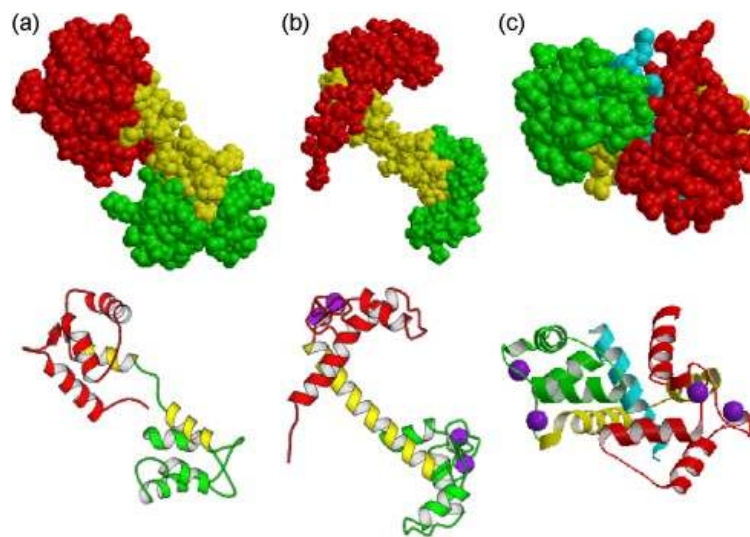


**Figure 01:** Schematic representation of the three structural forms of calmodulin. (a) apo-CaM structure. (b) Ca-CaM structure (c) CaM:smMLCK peptide complex structure. Each structure is shown as a cartoon and space-filling model.<sup>12</sup>

This is just one of many examples where  $\text{Ca}^{2+}$  triggers a cellular event. Others would include the release of neurotransmitters<sup>13,14</sup> or the involvement in programmed cell death.<sup>15</sup> Considering the universal application of  $\text{Ca}^{2+}$  as messenger in biological systems, the adaption of the  $\text{Ca}^{2+}$  based communication for artificial systems is a self-evident approach.

---

## 1.2 Goal of the project

In order to study ion transfer in artificial systems one can divide the process into three events. First event is the ion binding by a receptor molecule that, after receiving a stimulus, will eject the ion into the media. For this work light was chosen as the ion-ejecting stimulus. The second event is ion transfer or diffusion and finally the arrival of the ion and the detection by an appropriate reporter. Ion detection by reporter molecules can be achieved by a structural change or a change in physico-chemical properties.

In this thesis a photo-guided approach to biomimetic cellular communication in artificial systems is considered. Therefore  $\text{Ca}^{2+}$ -based communication will be established between vesicles representing  $\text{Ca}^{2+}$  storages in eukaryotic cells, in the interior of  $\mu\text{m}$ -scale giant polymersomes, which will represent the cell. Controlling this event by light will offer a real-time control over the ion transfer occurring inside the artificial cell mimicry. Detection of the ion is facilitated by fluorescent-switches as reporter molecules in the membrane of a second nanoobject, representing the receiving macromolecule inside the cell.

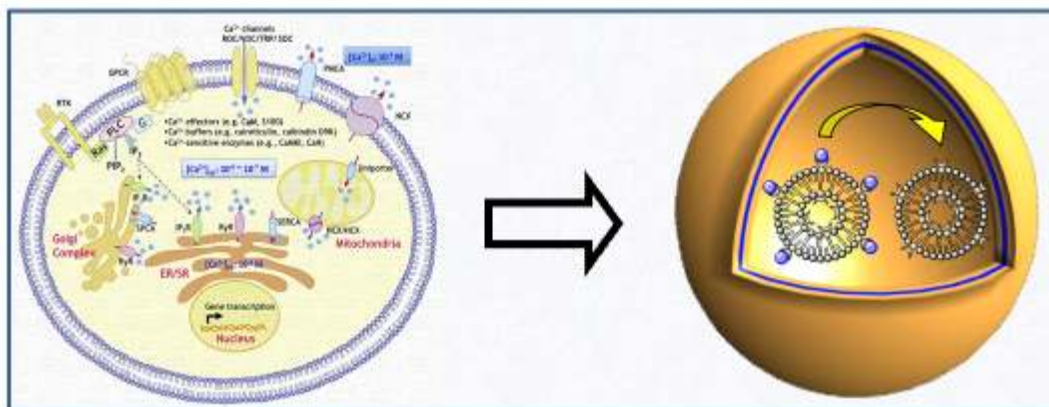


**Figure 02:** Schematic representation of ion transfer inside a cell and the adopted approach to photo-guided ion transfer in artificial microcapsules.

---

### 1.3 Supramolecular chemistry

Supramolecular chemistry was defined by one of its pioneers, Jean-Marie Lehn, who coined it as the “chemistry beyond the molecule”.<sup>16</sup> In its simplest form, supramolecular chemistry concerns the non-covalent bonds between host molecules and guest molecules. Even though supramolecular chemistry using artificial systems is a young discipline having been launched in the 1970’s, nature itself uses by definition supramolecular assemblies to operate since the beginning of life. In biological chemistry the supramolecular hosts are, for example, the receptor sites of enzymes and the guest molecules are ligands, ions, cofactors or drugs. Most of these interactions rely on supramolecular interactions such as ion-dipole, hydrogen bonding or hydrophobic interactions. In the cell for example, cations can not pass freely through the lipid bilayer, therefore as mentioned in chapter 1,  $\text{Na}^+/\text{K}^+$ -ATPase and other features need to transport ions actively or passively over the lipophilic barrier. Another mechanism for the transport of  $\text{K}^+$  ions over the mitochondria membrane is via the carrier mechanism. In this case, valinomycin wraps itself, due to ion-dipole interactions, around the potassium ion creating a hydrophobic supermolecule which can traverse the lipid bilayer.<sup>17,18</sup> The molecular structure and the molecular model are presented in figure 03.

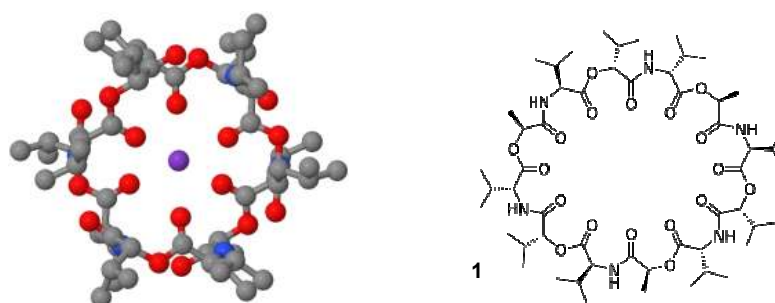


**Figure 03:** left: Valinomycin molecular model binding a potassium ion, right: chemical structure of valinomycin.

Beside the interactions mentioned, there are several other ways that molecules can interact with each other, without forming a real covalent bond. A way to quantify these interactions has been proposed in the group of Hunter<sup>19</sup> which can be applied to almost any type of supramolecular binding. A list of non-covalent interactions and their strengths is given in table 02. An important consideration for these interactions with regard to guest binding is the competitive nature of the medium. Indeed, highly polar protic solvents and elevated ionic strength found in Nature are typically not conducive with effective binding. These factors are considered below in guiding the choice of the calcium receptor.

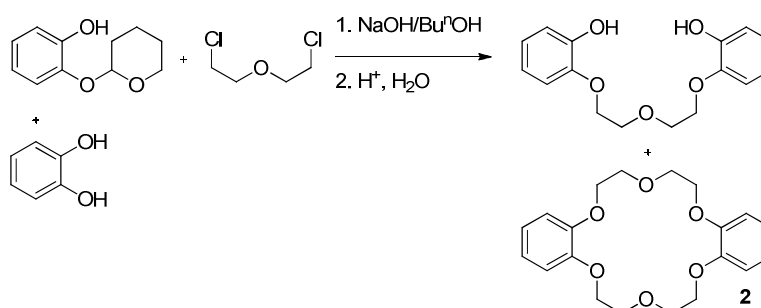
**Table 02:** Strength of molecular interactions.<sup>17</sup>

Interaction	strength
Covalent bond	145-1070 kJ/mol
Ion-ion	100-350 kJ/mol
Ion-dipole	50-200 kJ/mol
Dipole-dipole	5-50 kJ/mol
Hydrogen bond	4-60 kJ/mol
Ion- $\pi$	38-159 kJ/mol
$\pi$ - $\pi$	0-50 kJ/mol
Hydrophobic	< 8 kJ/mol

The part of supramolecular chemistry which directly impinges on this work will be discussed in more detail in the following sections. Working with  $\text{Ca}^{2+}$  as a messenger, molecules with a tendency to complex metal ions, called ionophores and possessing multiple ion dipole interactions to form a supramolecular interactions between ion and ligand will be regarded more closely.

### 1.3.1 Cation binding motifs.

One of the first supramolecular binding motifs for ions was accidentally discovered by Pedersen in 1967.<sup>20,21</sup> Due to a catechol impurity in his starting material, he obtained as a side product, during the synthesis of a linear diol which he hoped would act as a ligand for the vandylium ion, the so called dibenzo[18]crown-6 (**2**), which binds the potassium cation in its inner cavity. The synthesis of the first crown ether is shown in scheme 01. This gave rise to a new class of molecules which was named crown-ethers because of the crown-like shape.



**Scheme 01:** Serendipitous synthesis of the first crown-ether

---

The structural similarity to the biochemical valinomycin is evident and they have been used to bind a large variety of different cations throughout the years. Due to the spherical shape of inorganic cations, most cation-binding ionophores are of a macrocyclic nature. Selectivity for a specific ion depends on various factors. Some of these factors are the size complementarity between the cation and the host cavity which is depicted in figure 04. Furthermore, the electronic complementarity (HSAB theory), electrostatic charge, solvent polarity, degree of host preorganisation and the nature of the counter ion amongst others.<sup>22</sup> In nearly all cases cation binding is established through the interaction of the ion with Lewis-acids like ether oxygen or carboxylic acid oxygen. By altering the Lewis acid a different selectivity can be obtained. Ionophores bearing the soft sulphur atoms or nitrogen in their molecular backbone, tend to bind transition metals more strongly in many cases with respect to their oxygen counterparts.<sup>23</sup>

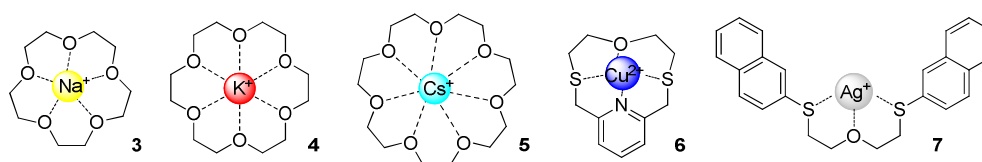


**Figure 04:** The influence of macrocycle size and the effect of the Lewis-acid nature on guest selectivity. From left to right, [15]crown-5 (3), [18]crown-6 (4) and [21]crown-7 (5) with their preferred guest ions. Copper (6) and silver (7) binding ligands with nitrogen and sulphur in their binding site.

The ion of interest for our study is however  $\text{Ca}^{2+}$ . One of the first binding units which was used in the preparation of  $\text{Ca}^{2+}$ -sensitive electrodes were phosphate esters. First attempts to prepare ionophores based on macrocycles were based on cryptands developed by Lehn and co-workers. The first cyclic ionophores were however not very selective.<sup>24</sup> A  $\text{Ca}^{2+}$ -selective probe which was developed for the use in ion selective electrodes was ETH-1001 which resembles in terms of structure  $\frac{1}{2}$  of a crown ether and forms readily 1:2 and 1:3 complexes.<sup>25</sup> One of the most widely used chelating agents is ethylenediaminetetraacetic acid (EDTA, 8). It displays high affinity constants for nearly all divalent ions and its strong chelating properties are widely used in medicine during the treatment of metal ion poisoning.<sup>26</sup> The discrimination between  $\text{Mg}^{2+}$  and  $\text{Ca}^{2+}$  is most important in biological systems because the intracellular  $\text{Mg}^{2+}$  concentration is about 4 - 5 orders of magnitude higher than that of  $\text{Ca}^{2+}$ . Therefore, ethylene glycol tetraacetic acid (EGTA, 9) was developed based on the design of EDTA (8) (see figure 05). EGTA (9) displays a large range of metal ion binding, like its predecessor but has a calcium binding constant which is about 5 orders of magnitude higher than the binding

---

constant for  $\text{Mg}^{2+}$  and is therefore very selective regarding these two ions. Some binding constants for EDTA (**8**) and EGTA (**9**) are depicted in table 03.

**Table 03:** Ion binding for EDTA (**8**) and EGTA (**9**), 25 °C, 0.1 M ionic strength (fully deprotonated)

Metal ion	$\text{pK}_{\text{ass}}$ EDTA	$\text{pK}_{\text{ass}}$ EGTA
$\text{Mg}^{2+}$	8.64	5.3
$\text{Ca}^{2+}$	11.0	10.9
$\text{Zn}^{2+}$	16.4	12.6
$\text{Cd}^{2+}$	16.4	16.5

Since biological systems are highly controlled environments and the presence of other divalent cations is rather low in the cytosol, EGTA (**9**) and its derivative 1,2-bis(o-aminophenoxy)ethane-N,N,N',N'-tetraacetic acid (BAPTA, **10**) (see scheme 02) are the most widely used calcium chelators / ionophores up to date. The low binding constant towards magnesium is based on the small ionic radius (0.09 nm) of  $\text{Mg}^{2+}$  which is the same size as  $\text{Li}^+$ . Therefore the hydration state is much higher compared to  $\text{Ca}^{2+}$  and ligand exchange occurs only slowly. EGTA (**9**) has been applied to prepare  $\text{Ca}^{2+}$ -buffer solutions<sup>27</sup> and was applied in several biological tests, in order to study for example the involvement of  $\text{Ca}^{2+}$  in brain ageing<sup>28</sup> or the control of various enzymes.<sup>29</sup> The BAPTA (**10**) molecule was first synthesized by Tsien and co-workers in 1980 and was developed as a pH insensitive alternative for EGTA (**9**) while maintaining the high selectivity for  $\text{Ca}^{2+}$  over  $\text{Mg}^{2+}$ .<sup>30</sup> The aliphatic amines of EGTA (**9**) which display a  $\text{pK}_{\text{ass}}$  between 8.5 and 9.5, were replaced by aromatic amines with a  $\text{pK}_{\text{ass}}$  of 5.97 and 6.36. This lower  $\text{pK}_{\text{ass}}$  results in a larger proportion of non-protonated BAPTA (**10**) receptor under physiological conditions. Therefore, the  $\text{Ca}^{2+}$  binding occurs faster since the EGTA (**9**) protons must dissociate first before  $\text{Ca}^{2+}$  can bind, while BAPTA skips this step. EGTA (**9**) and BAPTA (**10**) are high affinity  $\text{Ca}^{2+}$  binders with dissociation constants ( $K_d$ ) between 50 nM to 100 nM.<sup>31</sup>

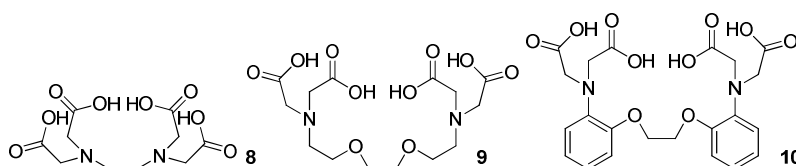


**Figure 05:** Molecular structure of EDTA (**8**), EGTA (**9**) and BAPTA (**10**)

---

After having defined the binding units of choice for  $\text{Ca}^{2+}$ , the state of the art of triggered ion movement will be discussed.

## 1.4 Stimulus induced ion movement and release

In order to study ion transfer, an ion must be ejected or moved from its binding cavity. Several different triggers to achieve ion movement are possible and the ones which were extensively studied are for example, a change in pH, binding of another ion or electro- and photochemical stimuli. The group of Shinkai showed that it is possible to mimic a syringe on a molecular level (**11**), see figure 05, where a silver ion is moved from one binding site, consisting of a crown ether, to another bearing a bis(ethoxyethoxy) unit linked by a 1,3-alternate-calix[4]arene, upon increasing the pH of the solution.<sup>32</sup> Upon increasing the pH the amine in the more complexing crown ether part gets protonated leading to a decrease in the binding affinity towards the silver ion. The ion is then transferred through the alternate calix[4]arene tube as judged by dynamic NMR measurements, towards the bis(ethoxyethoxy) subunit which has after protonation a higher  $K_a$  with respect to the protonated crown ether. This pH-induced ion movement could be reversed upon addition of a base. Another example of a pH-triggered  $\text{Cu}^{2+}$ -transfer (figure 06, **12**) is the polyaza-macrocyclic developed by Fabbrizzi and co-workers<sup>33</sup>. The  $\text{Cu}^{2+}$ -ion, which is located at the pyridine-amine binding site at a pH between 4 and 5, can be transferred to the amide-amine binding site of the molecule by increasing the pH above 10.5. The pH induced deprotonation of the amides increases the affinity towards the ion and along with the translocation of the ions the macrocycle undergoes rearrangement to fit its cavity to the ion. A prominent way to trigger ion transfer in biological systems is the binding to another ion which leads to a rearrangement in the binding site or a change in the electron density and therefore releases or translocates the ion of interest.

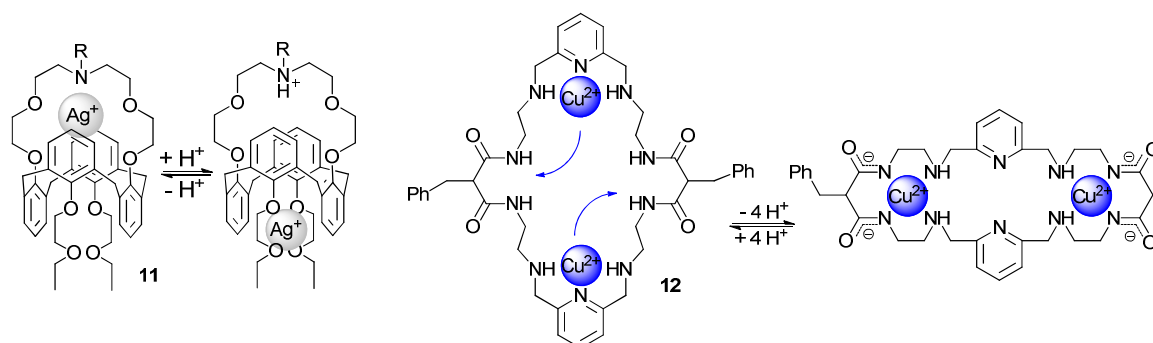


**Figure 06:** pH-triggered ion translocation left: molecular syringe translocating a silver ion from the crown ether cavity to the bis(ethoxyethoxy) binding site, right:  $\text{Cu}^{2+}$  translocation as proposed by Fabbrizzi and co-workers.

---

---

This chemically-induced ion translocation has the disadvantage that in order to move the ion acid or base needs to be added and side products can accumulate generally sitting in the amide-amine binding site of the molecule.

In order to achieve ion-triggered ion release one needs to look at the so called heterotropic negatively collaborative binding molecules. Rodriguez and co-workers synthesized a dicrown ether which is connected by a 2,2' bipyrazole linker (**13**, see figure 07).<sup>34</sup> In its initial state the molecule binds to a protonated diaminopentane. Upon the addition of a transition metal like  $Zn^{2+}$ , the bipyridine linker undergoes a conformational change, forcing the crown ether units apart and liberation of the diamine (figure 07, left).

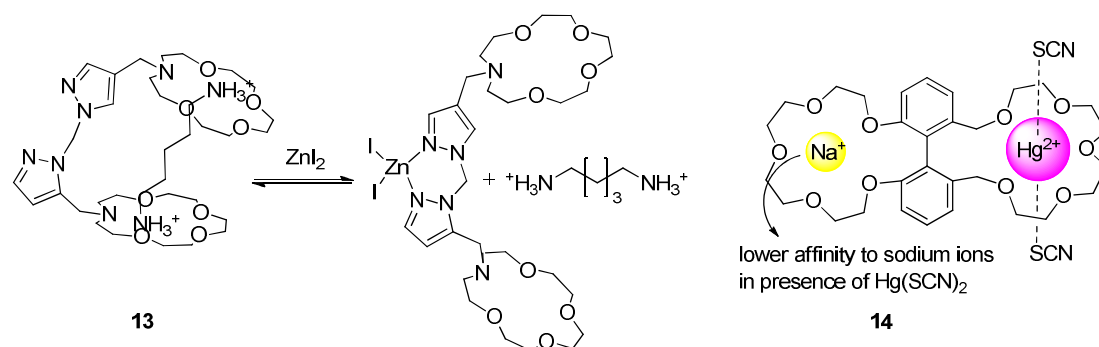


**Figure 07:** Example of an ion-induced ejection of 1,5-diaminopentane upon the addition of  $ZnI_2$  (**13**) (left) and sodium ejection from a dicrown ether (**14**) upon the addition of  $Hg^{2+}$  (right).

Another example where a conformational change leads to a decrease in binding affinity is the dicrown ether (**14**) prepared by Costero and co-workers (figure 07, right).<sup>35</sup> In this molecule a smaller crown ether with 2 phenolic oxygen and a larger ring are connected via a dibenzo-linker. The binding constant to sodium ions decreases in the presence of  $Hg(SCN)_2$  which binds to the larger cavity, leaving the smaller cavity free. Due to the steric hindrance after binding to mercury only three of the five crown ether oxygens are free to bind to sodium leading to a decreased binding affinity.

Light and electrons offer two attractive means to trigger ion release mainly because they avoid the “waste build-up” in reversible systems. In addition, light can be applied cleanly and remotely with high temporal and spatial resolution. While electrons are interesting in redox-active transition metal-based systems, they require wiring and electrode deposition during

---

---

usage. Reversible photo-guided ion release is based on the combination of ionophores with photoactive groups, which change either conformation or their electron density upon irradiation. But before the photocontrolled release of ion will be discussed, a short introduction into photochemistry will be given to highlight the underlying principles.

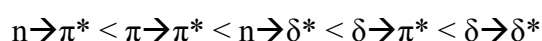
## 1.5 A short introduction to photochemistry

### 1.5.1 Absorption of light

Photochemistry studies the evolution of an excited molecule after the absorption of a photon and the subsequent transformation, be it a reaction induced by the absorption of a photon or the emission of another photon of a different wavelength like fluorescence or phosphorescence.<sup>36</sup> The minimum energy required for the electronic excitation of a molecule is around 150 to 170 kJ/mol and corresponds to a red light with a wavelength of around 700 to 800 nm. Irradiation with lower intensities is in general not sufficiently energetic to provoke electronic excitation. The maximum energy for the electronic excitation is in an order of 590 kJ/mol and corresponds to ultraviolet (UV) light with a wavelength of around 200 nm. Irradiation energies superior to that bear enough energy for bond dissociation.

### 1.5.2 Electronic transitions and excited state

A electronically excited state results from the excitation of an electron from the highest occupied molecular orbital (HOMO) to the lowest unoccupied orbital (LUMO) or a superior molecular orbital. A molecular orbital can be formed by linear combination of two s, s and p or two p atomic orbitals when they have a collinear axis of symmetry. Those bonds are called  $\delta$  orbitals. A  $\pi$  molecular orbital is formed from p atomic orbitals overlapping laterally, while non-binding electrons are in the n orbital.<sup>37</sup> Transitions upon excitation with photons can occur from all of these ground state orbitals to the antibinding orbitals denoted with  $\delta^*$  or  $\pi^*$ . The required energy for these transitions increase in the following order:



In figure 08 a schematic representation of the excitation of an electron from the ground state to a singlet excited state through a  $n \rightarrow \pi^*$  transition is given.

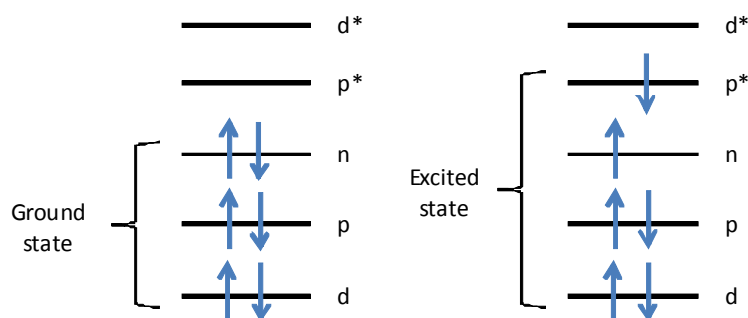


**Figure 08:** Excited state through a  $n \rightarrow \pi^*$  transition into a singlet excited state ( $S_1$ )

When one of the electrons with opposite spin is excited from the ground state ( $S_0$ ) in a higher orbital and the spin remains unchanged the excited state is called a singlet excited state ( $S_n$ ). In principle all excitation process are in first instance  $S_0 \rightarrow S_n$  transitions meaning the electron spin is preserved. The excited electron can also undergo a spin change which leads to a so called triplet state ( $T_n$ ) which is, according to Hund's rule, lower in energy (figure 09) .

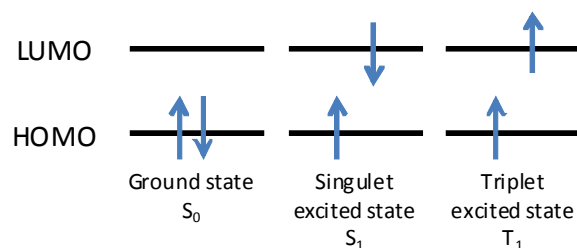


**Figure 09:** Electronic states

According to the Franck-Condon principle<sup>38,39</sup> the time required for an absorption of one quantum of light and for the transition of an electron into the excited state is as short as  $10^{-15}$  s. Compared to the vibrational period of an atomic nucleus ( $10^{-13}$  s) this time is rather short which means that an electronic transition occurs preferably to a vibrational state which has a wavefunction most similar to the state where it was excited from. This makes some transitions more likely than others and is responsible for the bands with different intensity in the absorption spectrum of a molecule.

### 1.5.3 Deexcitation processes

Once a molecule has absorbed a photon and passes to the excited-state several different deexcitation processes are possible. The Jablonski-Perrin diagram<sup>40</sup> visualizes all possible deexcitation processes in a graphical manner. A simplified version of this diagram is depicted in figure 10.

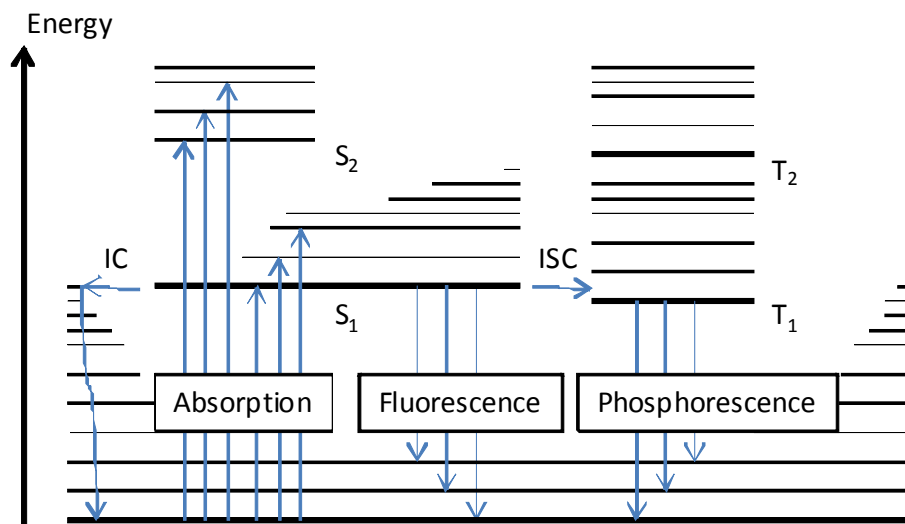


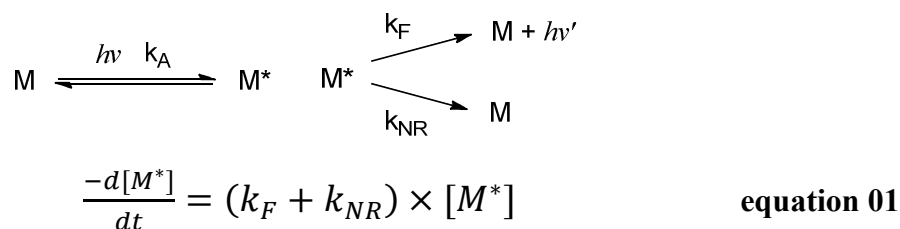
**Figure 10:** Simplified version of the Jablonski-Perrin Diagram

Fluorescence emission typically occurs from a singlet excited state (S<sub>1</sub>) with a short lifetime of 10<sup>-9</sup> to 10<sup>-7</sup> s and is independent of the excitation wavelength. The displacement to longer wavelength of the fluorescence emission with respect to the absorption spectrum due to the loss of energy in the excited-state via vibrational relaxation is called a Stokes shift.<sup>41</sup> Internal conversion (IC) describes a radiationless deexcitation process on a time scale of 10<sup>-11</sup> to 10<sup>-9</sup> s and occurs mostly between different excited states like S<sub>2</sub>→S<sub>1</sub> while internal conversion to the ground state can occur in molecules with low energy excited-states. Intersystem crossing (ISC) occurs on a time scale of 10<sup>-10</sup> to 10<sup>-8</sup> s and takes place between an singlet excited state and a close-lying triplet state. Intersystem crossing is therefore an internal change of the system including a electron spin change. Radiative deexcitation from the triplet excited state to the ground state is called phosphorescence and has a lifetime of 10<sup>-6</sup> to 1 s. The described processes are the principal deexcitation processes but several other deexcitation processes are possible like the transfer of an electron from another molecular fragment (PET) which will be described later on or a chemical conversion. The deexcitation process most pertinent for the presented work is fluorescence.

---

#### 1.5.4 Characteristics of fluorescence emission.

Excited molecules are very unstable and have a tendency to rapidly return to their respective ground state. Different processes of deexcitation have been described above. The radiative deexcitation from the  $S_1$  state is called fluorescence and the radiative rate constant is defined as  $k_F$ . Competitive non-radiative processes are internal conversion with a rate constant  $k_{IC}$  and intersystem crossing with a rate constant  $k_{ISC}$ . Non-radiative processes can be combined to give a rate constant  $k_{NR}$  to simplify the calculation. In the simplest case, a solution contains a fluorescent species  $M$  which is excited by a short light pulse ( $t = 0$ ) and a fraction of this molecules passes to the excited state  $S_1$ . The kinetics of deexcitation follow then the law in equation 1,



where  $[M^*]$  represents the population of molecules in the excited state  $S_1$ ,  $k_F$  the rate constant of the fluorescence deexcitation and  $k_{NR}$  the rate constant of non-radiative processes. The fluorescence intensity  $I_F$  is measured at a time ( $t$ ) and is proportional to the number of molecules in the excited state. The solution of this differential equation implies an exponential decay of the fluorescence intensity characterized by the fluorescence lifetime of the excited state corresponding to an average relaxation of the excited state  $S_1$ .  $I_F$  is defined in equation 02.

$$I_F(t) = k_F \times [M^*]_0 \times e^{\frac{-t}{\tau}} \quad \text{with } \tau = \frac{1}{k_F + k_{NR}} \quad \text{equation 02}$$

The measurement of the fluorescence lifetime of a solution containing a fluorophore is, in general, independent of the excitation wavelength. The fluorescence quantum yield ( $\phi_F$ ) is defined as the number of photons emitted by fluorescence divided by the number of photons absorbed. Generally the fluorescence quantum yield is measured and compared to a fluorescent sample of a known quantum yield (see experimental section). Knowing the fluorescence quantum yield ( $\phi_F$ ) and the fluorescence lifetime ( $\tau$ ) the rate constants for the photoprocess can be calculated according to equation 03.

$$\phi_F = \frac{k_F}{k_F + k_{NR}} = k_F \times \tau \quad \text{equation 03}$$

---

---

## 1.6 Photochromism and light triggered ion release

### 1.6.1 Photochromism

Photochromism is the reversible transformation of a chemical species between two molecular forms triggered by the absorption of photons. Generally the two structures possess different absorption spectra. During the photoisomerisation various physic-chemical parameters of the molecule change along with the absorption spectrum such as refractive index, dielectric constant, oxidation potential and geometrical structure.<sup>42</sup> Among the most prominent photochroms, the azobenzene (**15**) molecule is probably the best studied one. It exists mainly in two isomers which can be converted into one another by application of an external trigger such as light. The molecular structure of azobenzene (**15**) in its *trans*- and *cis*-form is shown in figure 11.

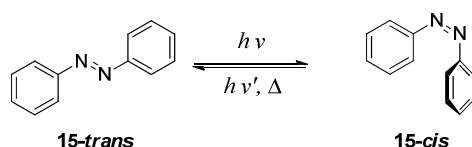


**Figure 11:** *trans*-*cis* isomerisation of an azobenzene molecule (**15**) applying an external trigger like light or temperature.

The *trans*-isomer is stable and the *cis*-isomer is metastable meaning it thermally converts back to its initial state over time. The energy difference between the two state is about 50 kJ/mol. The distance between carbon 4 and 4' is 9 Å in the *trans*-isomer and 5 Å in the *cis*-isomer.<sup>43</sup> This effect has been used for the synthesis of supramolecular structures such as dendrimers<sup>44</sup> or catenans.<sup>45</sup>

Another example are diarylethene compounds. A representative which is of this class of photochromes (**16**) is shown in figure 12.

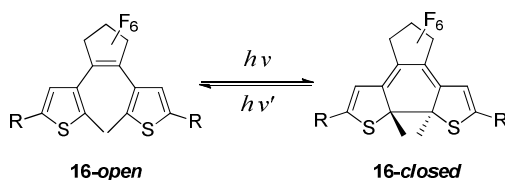


**Figure 12:** ring open-close isomerisation of an perfluoro dithienylethene (**16**) applying light as an external trigger.

Diarylethenes undergo a cyclisation reaction upon irradiation in the UV. The colorless open form converts into a closed form which appears in most cases blue to the human eye. The

---

---

process is reversible and upon irradiation with visible light the system undergoes cycloreversion.<sup>46</sup> The open ring isomer is not planar since free rotation of the aryl-group (here thienyl, **16**) is possible. The aromatic electrons are localised in the two thiophene units.<sup>47</sup> In the closed form the photochrome (**16-closed**) possesses a cyclohexadiene moiety and the  $\pi$ -electrons are conjugated over the whole structure.<sup>48</sup>

### 1.6.2 Light induced ion release

Some examples of ion-decaging ionophores harnessing photochromes will be presented after the introduction of a photo irreversible decaging molecule. An example for irreversible phototriggered ion release was presented by Chen.<sup>49</sup> A phenolic Schiff-base derivative shown in figure 13 binds to  $\text{Zn}^{2+}$ . Upon irradiation in the UV, the phenolic Schiff-base (**17**) can undergo a cyclisation reaction forming a 2-arylbenzoxazole. It was found that the binding affinity towards  $\text{Zn}^{2+}$  is greatly reduced after the formation of the 2-arylbenzoxazole.

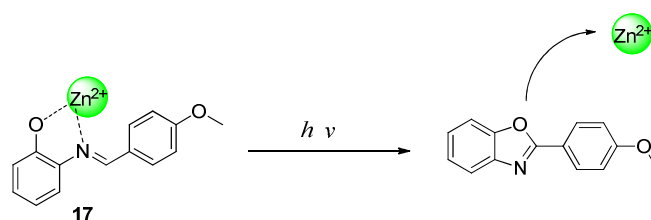


**Figure 13:** Phototriggered ejection of  $\text{Zn}^{2+}$  irradiation of an phenolic Schiff-base- $\text{Zn}^{2+}$  complex (**17**) via UV irradiation.

As mentioned earlier, upon irradiation in the UV range azobenzene (**15**) undergoes a conformational change from its thermodynamically more stable *trans*- form to the *cis*- form. The group of Shinkai implemented azobenzene into crown ether rings of different size (ranging from  $\text{O}_7$  to  $\text{O}_9$ ).<sup>50</sup> The *cis*-isomer of **18**, which is depicted in figure 14a shows a relatively high binding constant towards alkali metals. Once it is irradiated with visible light it isomerises back to its *trans*-form and releases the bound ion. While the *cis*-isomer forms the typical crown-ether like loop and shows the appropriate binding affinity of crown ethers, the *trans*-isomer displays a largely decreased binding affinity with respect to all alkali metal ions. The change in binding affinity is related to the linearly extended shape of the *trans*-isomer.

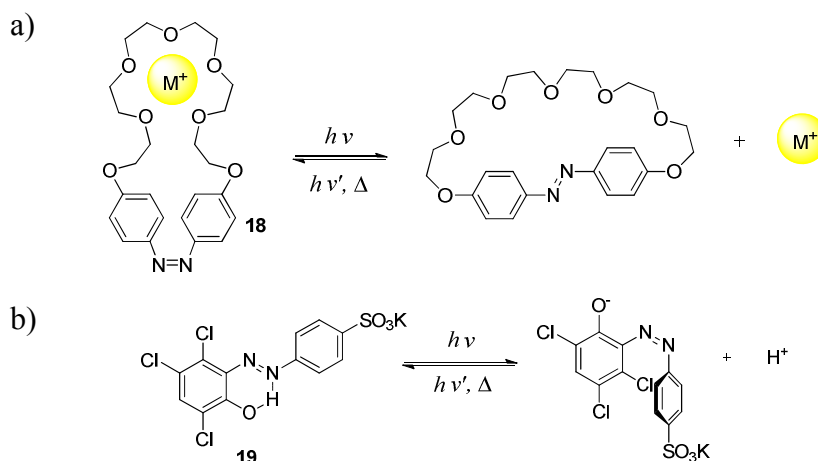


**Figure 14:** a) Azobenzenophane (**18**) crown ether synthesized by Shinkai and co-workers. Reversible ion release / uptake upon irradiation or thermal relaxation. b) Photocontrolled proton ejector based on an azobenzene chromophore (**19**).

A photoreversible proton ejector (figure 14b, **19**) has been designed in the group of Jullien.<sup>51</sup> The azobenzene moiety consists of one ring with an acidic hydroxyl group induced by the presence of three chlorine atoms on the same ring and a second ring bearing a sulfonic acid in order to improve the water solubility of the molecule. The acidic hydroxyl proton is complexed with one of the nitrogens in the *trans*-form of the azobenzene. Upon irradiation in the UV the azobenzene undergoes isomerisation and hydrogen bonding becomes sterically unfavourable, thus releasing a proton. The proton ejector (**19**) has been used to photocontrol the pH of an aqueous solution.

An example where a change in electron density, rather than a conformational change, is the trigger for ion release was given by Lapouyade and co-workers.<sup>52</sup> In this case an azacrown ether was used as the ion recognition unit which was connected to a non-symmetric dithienylethene as shown in figure 15.

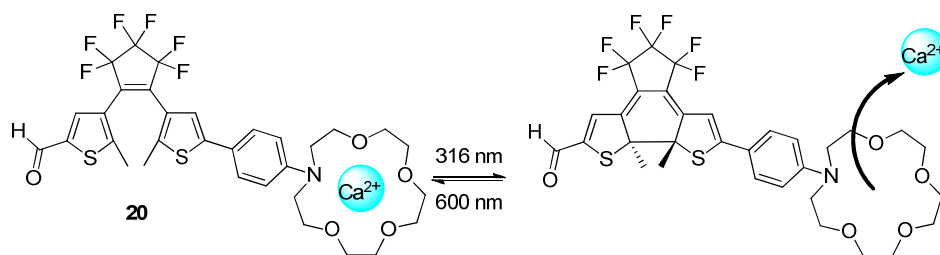


**Figure 15:** Reversible  $\text{Ca}^{2+}$  from aza-crown ether unit by modulation of the electron density of the amine using a dithienylethene chromophore in a non-competitive solvent.

---

In its open form **20** can bind tightly to one of several different ions in acetonitrile, among them  $\text{Ca}^{2+}$ . The binding constants obtained during titrations with calcium salts were comparable to those obtained for phenylazacrowns substituted with an electron-donating group. Upon irradiation with UV light dithenylethenes undergo photocyclisation reactions. As long as the molecule stays in the open form electronic communication between the two thiophene groups is minimized, once in the closed form, long range electron density transfer become possible. Therefore, the strong electron-withdrawing effect of the carbonyl group can lower the electron density of the amine in the aza-crown ring, which is a binding site for  $\text{Ca}^{2+}$  and therefore modulates the binding constant. This approach has different advantages compared to the azobenzenophane since both forms, open and closed, are stable at room temperature when not irradiated. However, both systems seem to work only in organic solvents and in order to mimic biological processes one would want to work under at pseudo-physiological conditions. Another means to liberate ions upon irradiation are decaging or uncaging molecules which have been used to liberate ions such as  $\text{Zn}^{2+}$ ,  $\text{Ag}^{+}$ <sup>53-55</sup>,  $\text{Cu}^{2+}$ <sup>56</sup> and biomolecules like glutamate<sup>57</sup> or cAMP<sup>58</sup> among others. A more detailed introduction to these types of molecules will be given in chapter 3.

Before ion sensors will be discussed, an introduction in the mechanisms of ion sensing by photoactive molecules utilising photoinduced electron transfer (PET) and photoinduced charge transfer (PCT) will be given in the next section.

## 1.7 Cation sensors and molecular sensing processes

### 1.7.1 Photoinduced electron transfer (PET)

Detecting cations is of great interest to many fields of research including biology, chemistry or clinical biochemistry<sup>59</sup> due to their involvement in numerous biological processes as highlighted earlier. This vast field of research has been reviewed in several articles.<sup>59,60</sup> Optical methods to detect ions has several advantages over other techniques due to being non-invasive relatively high increase of the output signal upon ion binding and the possibility to study the output with common microscopy and fluorescence techniques. Electrochemical methods for example have difficulties when it comes to small population of cells or single cell compartments. Therefore, the spatial resolution of fluorescence imaging methods make these

type of chemosensors especially attractive.<sup>61</sup> The ability to detect a change in ion concentration is based on the design of fluorionophores combining an ion binding and a fluorescent unit in one molecule. In figure 16 an example of a fluorionophore is given where the ionophore is an electron donor and the fluorophore is the electron acceptor.

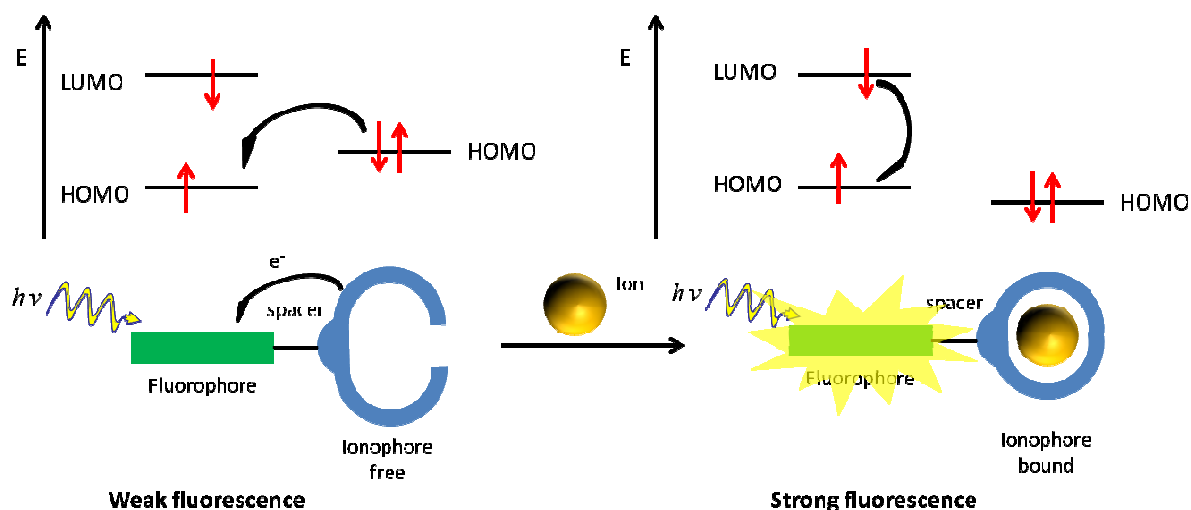


**Figure 16:** Principles of photoinduced electron transfer (PET) of an off-on fluoroionophore by reductive PET.

Upon irradiation, the fluorophore does undergo a transition to the excited-state which is depicted using Frontier Molecular Orbitals at the top of figure 16. The singlet state of the fluorophore with an electron in the highest occupied molecular orbital (HOMO) and an electron in the lowest unoccupied molecular orbital (LUMO) could in principle emit fluorescence. In the shown fluorionophore system, however, an electron from the HOMO of the ionophore can now be transferred to the HOMO of the fluorophore via PET causing fluorescence quenching of the latter which is favourable due to the energy level of the orbital. Upon cation binding the energy of the HOMO of the ionophore is decreased due to the presence of a cation and is now lower in energy than the HOMO of the fluorophore. Fluorescence quenching is therefore suppressed and the singlet excited state can follow deexcitation via fluorescence emission. This process is called reductive PET.

Conversely, the principle of oxidative PET is shown in figure 17. Here, in the absence of a cation the electron in the LUMO in the excited state of a fluorophore can be transferred to the LUMO of the ionophore due to its appropriate energy level, which causes quenching of the fluorescence. Once bound to the ion the LUMO of the ionophore increases its energy level and is no longer available for the deexcitation process. Thus, the fluorophore can undergo deexcitation via fluorescence emission.

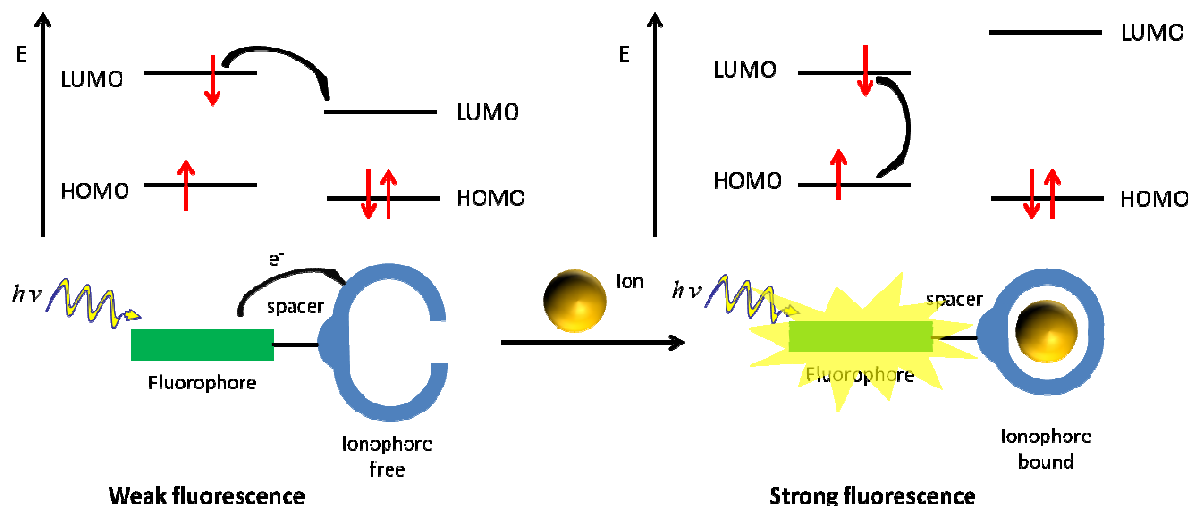


**Figure 17:** Principles of photoinduced electron transfer (PET) of an off-on fluoroionophore by oxidative PET.

In most PET-sensors, the electron pair of an aromatic or an aliphatic amine is involved in the quenching mechanism. Several examples which are sensitive to different cations such as  $\text{Zn}^{2+}$ ,  $\text{Fe}^{3+}$ ,  $\text{Hg}^{2+}$ ,  $\text{Cu}^{2+}$  and many others can be found in the literature.<sup>62-64</sup> A structural simple example of a fluoroionophore for potassium is based on an azacrown ether linked via a methylene spacer to an anthracene fluorophore developed in the group of de Silva<sup>65</sup> (**21**, figure 18). The molecule shows fluorescent enhancement up to 47 times its initial intensity upon binding potassium and sodium. Another macrocyclic off-on fluorescent ion switch was developed in the group of Czarnik<sup>66</sup> using a 18-crown ether where all the oxygens are replaced by nitrogens (**22**, figure 17), creating therefore a selectivity towards  $\text{Zn}^{2+}$ . The advantage of the system is that it could be used in aqueous solution but needs precise pH control due to the protonation of the amines which also leads to a quenching of the PET. If the pH was properly controlled fluorescence enhancement of up to 190-fold could be achieved upon metal binding.

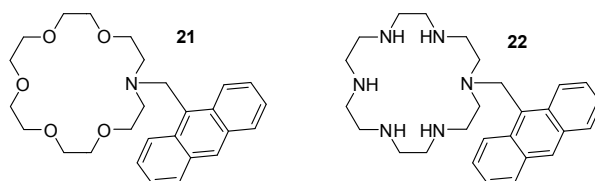


**Figure 18:** Anthracene-based macrocyclic off-on fluoroionophores sensitive to  $\text{K}^+$  and  $\text{Na}^+$  (**21**) developed by de Silva (left) and  $\text{Zn}^{2+}$  sensitive fluoroionophore developed by Czarnik (**22**) (right).

For the study that will be described in this thesis  $\text{Ca}^{2+}$ -selective ion sensors are of particular interest. When elaborated with ligating sites, receptors bearing an aromatic amine are

---

especially suited for fluorescent ion sensing under physiological conditions. Selective ion sensors for  $\text{Ca}^{2+}$  are in general based on the BAPTA binding unit described earlier. In principle to obtain a fluoroionophore literally thousands of combinations between ionophore and fluorophore are possible. Two  $\text{Ca}^{2+}$ -selective probes are highlighted in figure 19.

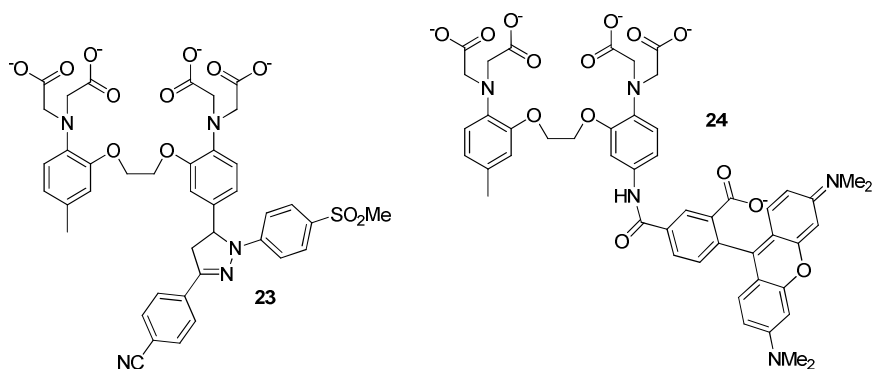


**Figure 19:**  $\text{Ca}^{2+}$  off-on fluoroionophores based on the BAPTA binding unit.

On the left side **23** developed in the group of de Silva<sup>67</sup> is shown. It combines the BAPTA-ionophore with a pyrazoline fluorophore. In this particular case the 5-methine part plays the role of the linker. Fluorescence enhancement upon ion binding of up to 90-fold has been recorded. The second  $\text{Ca}^{2+}$ -selective fluoroionophore (**24**) is based on the rhodamine fluorophore bearing an amide spacer.<sup>68</sup> Amides have been shown to serve as connectors which encourage PET via superexchange in several photoactive systems.<sup>69,70</sup> Since the boron-dipyrromethene (BODIPY) fluorophore will play an essential role in this thesis two ion sensors based on the BODIPY fluorophore will be presented. The first shown in figure 20 on the left (**25**) is a alkali and alkaline earth metal selective azacrown-BODIPY developed by Rurack *et al.*<sup>71</sup> Two bands of emission from the low energy (LE) state and the internal charge transfer (ICT) state have been observed to be solvent dependent with only LE-emission being visible in acetonitrile. Upon ion binding the fluorescence quantum yield increased due to the suppressed PET process.

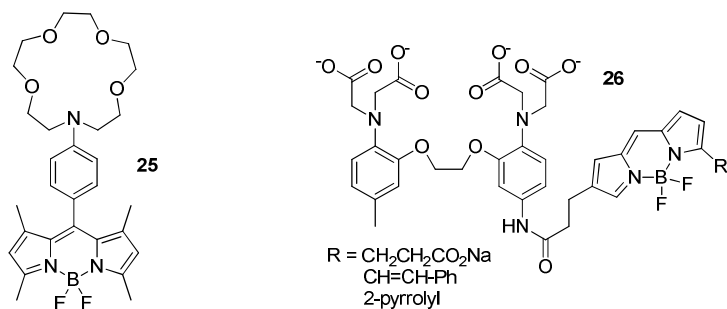


**Figure 20:** Fluorinophores based on the BODIPY fluorophore with an alkali and alkaline earth metals sensitive azacrown (**25**) (left) and  $\text{Ca}^{2+}$ -selective BAPTA-binding site (**26**) (right).

Figure 20 on the right side shows a series of BAPTA-BODIPY fluoroionophores with different substitution patterns which are linked together via a 3-propanamide linker (**26**).<sup>72</sup> The fluorescence is greatly quenched due to PET in aqueous medium. The binding affinities towards  $\text{Ca}^{2+}$  are in the range of 200 nM. Upon  $\text{Ca}^{2+}$  binding greatly enhanced fluorescence was obtained with no notable spectral shift due to the pH insensitivity of the fluorophore. The first example of fluorescent BAPTA sensors excitable in the visible light region were developed by Tsien.<sup>73</sup> In figure 21 some chemosensors from the **rhod** and the **fluo** series are depicted. The dyes were developed to overcome the problems which are imposed by UV-excitable dyes such as UV damage to cells upon irradiation, provoking autofluorescence from pyridine nucleotides and the lack of simultaneous application of  $\text{Ca}^{2+}$  decaging agents with UV excitable chemosensors. The latter reason is most important for the goal of the work in hand. These sensors, unlike their UV light-excitable counterparts, can be used in confocal fluorescence microscopy, two-photon excitation microscopy, and total internal reflection microscopy.<sup>74</sup> The first generation of **rhod** (**27-1**) and **fluo** (**28-1**) chemosensors bearing a hydroxyl group in the meta-position of the aniline showed strong pH dependency in the physiological range. This problem was overcome by omitting the hydroxyl group leading to the more potent **rhod-2** (**27-2**) and **fluo-2** (**28-2**) dyes.

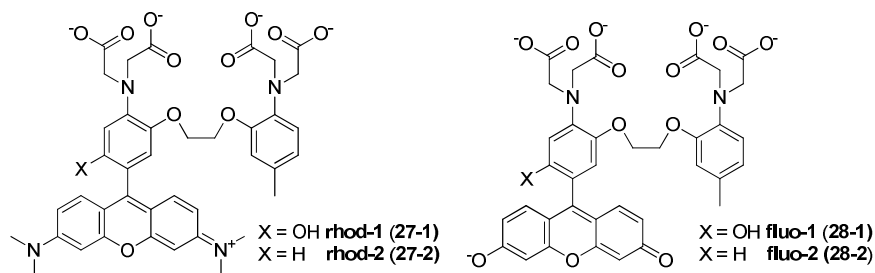


**Figure 21:** Visible light excitable  $\text{Ca}^{2+}$ -selective BAPTA based fluoroionophores developed by Tsien.

---

The fluorescence enhancement upon  $\text{Ca}^{2+}$  addition was determined to be 30-fold for **fluo-2** (28-2) and only 3.3 for **fluo-1** (28-1). The inverse case was seen for the rhodamine chemosensor which showed an increase in fluorescence intensity of 15-fold for **rhod-1** (27-1) and 3.4 for **rhod-2** (27-2). Ultimately those PET sensors gave rise to several similar fluoroionophores with substitutions on the fluorophore. Other fluorophores, such as BODIPY<sup>75</sup>, rhodamine<sup>76</sup> or naphthalimide<sup>77</sup> harnessing PET to detect micromolar  $\text{Ca}^{2+}$  levels have been developed over the years. Many BAPTA chemosensors are also commercially available and can be purchased in small quantities. Generally these PET sensors are used to understand biological processes involving  $\text{Ca}^{2+}$  for example in growth factors.<sup>78</sup>

Previous examples included only the case where fluorescence is increased upon metal ion binding but also the inverse case of PET systems are possible, the so called on-off switches which are much less popular than the previous case.

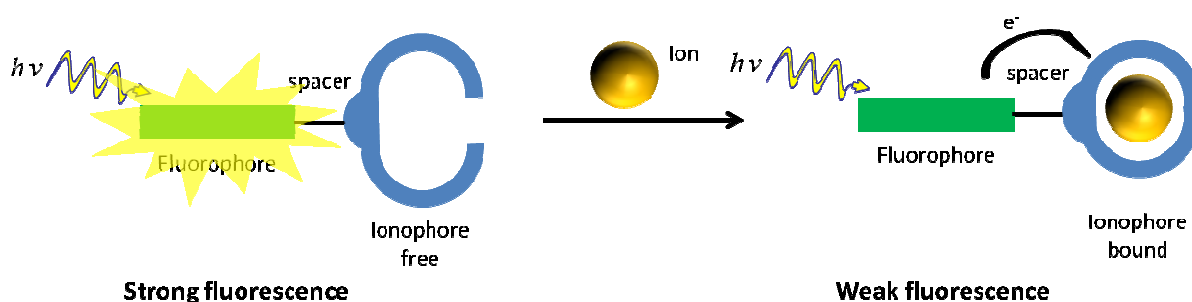


**Figure 22:** Photoinduced electron transfer principle of an "on-off" fluoroionophore

A schematic representation of this process is given in figure 22. The photoinduced electron transfer in this case is more complicated but in general it can be said that in the absence of an ion the fluorescence is unquenched in the fluoroionophore and upon ion binding the orbital of the ionophore reaches a favourable energy level for electron transfer from the fluorophore to the ionophore which leads to fluorescence quenching. Two examples are shown in figure 23. On the left side a "on-off" proton sensor (29) based on triphenyl substituted pyrazoline developed in the group of de Silva is shown.<sup>79</sup>

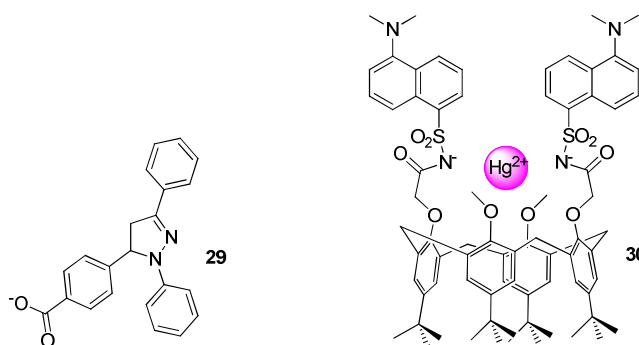


**Figure 23:** on-off fluorinophores for proton sensing based on a triphenyl pyrazoline (**29**) (left) and for mercury sensing based on a dansyl-substituted calyx-4-arene (**30**) (right).

Another example of Metivier *et al.*<sup>80</sup> is depicted on the right of figure 23 and shows a dansyl-substituted calix-4-arene (**30**), the binding of this compound being found to be highly specific towards  $\text{Hg}^{2+}$  showing PET from the dansyl fragments towards the ion centre when bound. No selectivity for other interfering cations like  $\text{Na}^+$ ,  $\text{K}^+$ ,  $\text{Ca}^{2+}$ ,  $\text{Cu}^{2+}$ ,  $\text{Zn}^{2+}$ ,  $\text{Cd}^{2+}$  and  $\text{Pb}^{2+}$  has been observed.

A generalized theory of electron transfer in chemical systems was introduced by Marcus<sup>81</sup> for which he received the Nobel prize in 1993. Concerning bimolecular electron transfer, after the excitation of a fluorophore it diffuses to the acceptor and forms an activated species. If electron transfer occurs between a fluorophore and an ionophore, a pair of radicals is formed, namely a radical cation and a radical anion. The electron transfer is then governed by kinetic and thermodynamic parameters. The Rehm-Weller equation (equation 04)<sup>82,83</sup> allows the estimation of the feasibility of electron transfer through readily quantifiable parameters. Electron transfer only occurs if the Gibbs energy ( $\Delta G^0$ ) for the reaction is negative or equal to zero.

$$\Delta G^0 = -E_{S,fluo.} - E_{red,fluo.} + E_{Ox.iono} - E_{ion\ pair} \quad \text{equation 04}$$

Here,  $E_{S,Fluo.}$  stands for the energy of the emissive excited state of the fluorophore,  $E_{red.fluo.}$  is the reduction potential of the fluorophore,  $E_{Ox.iono}$  is the the oxidation potential of the ionophore and  $E_{ion.pair}$  is the energy of the coulombic interaction of the radical ion pair that is formed. Electron transfer reactions are generally very fast with respect to the lifetime of the excited state. The presented PET systems are an exception to the described bimolecular calculations since electron donor and acceptor are present in the same molecule. According to

Marcus<sup>81</sup> the energy potentials of the donor-acceptor complex (**R**) and the charge separated state where the donor transferred an electron to the acceptor (**P**) can be represented in energy parabolas (figure 24). The energy transfer takes place when the system is at an intersecting point (a). Marcus theory allows the calculation of time constant of the electron transfer ( $k_{ET}$ ) from the activation energy ( $\Delta G^\ddagger$ ) or indirectly from the total Gibbs free energy ( $\Delta G^0$ ) given in equation 05 and 06.

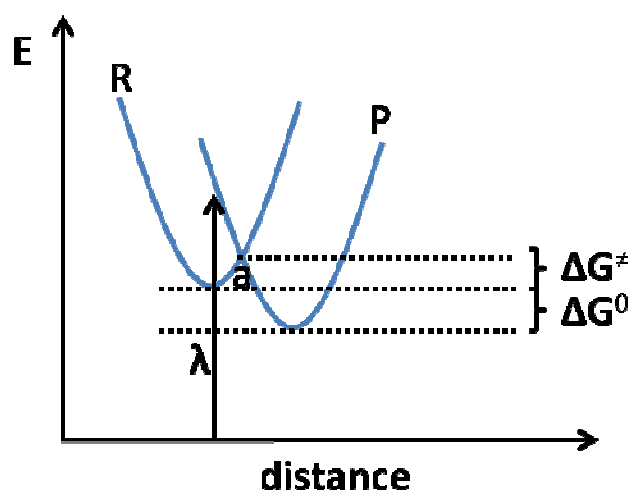


**Figure 24:** Energy profile of an electron transfer reaction

$$k_{ET} = \frac{2\pi}{h} \times (H_{el})^2 \times \frac{1}{\sqrt{4\pi\lambda k_b T}} \times \exp\left(-\left(\frac{\Delta G^\ddagger}{k_b T}\right)\right) \quad \text{equation 05}$$

$$\Delta G^\ddagger = \frac{(\lambda + \Delta G^0)}{4\lambda} \quad \text{equation 06}$$

In these equations  $H_{el}$  is the electronic coupling between the initial state and the final state,  $\lambda$  is the reorganization energy of the molecules which depends on the geometry of the complex state and state of the product,  $k_b$  is the Boltzmann constant,  $h$  is the Planck constant and  $T$  is the absolute temperature. With this equation the speed of the electron transfer can be predicted for many systems.

### 1.7.2 Photoinduced charge transfer (PCT)

Fluorophores containing an electron-donating group conjugated with an electron withdrawing group can undergo intramolecular charge transfer from the donor to the acceptor which is exalted upon excitation with light. A schematic example by Lord *et.al.*<sup>84</sup> of an anthracene fluorophore bearing a dimethyl amine as electron donating group and a 2-dicyanomethylene-3-cyano-2,5-dihydrofuran group as electron withdrawing part is shown in figure 25.

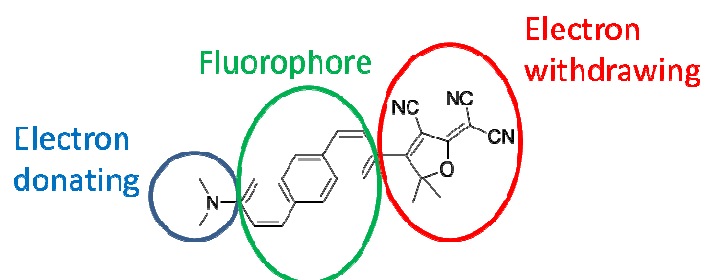


**Figure 25:** Schematic representation of a fluorophore capable of undergoing photoinduced charge transfer.

The resulting Stokes shift then depends on the environment and / or the microenvironment of the fluorophore. Therefore in fluoroionophores, binding a cation which interacts with the donor (or acceptor) can alter the internal charge transfer within the fluorophore and the resulting photophysical properties.<sup>85,86</sup> The different effects of cation binding on a donor or an acceptor site are described in figure 26.

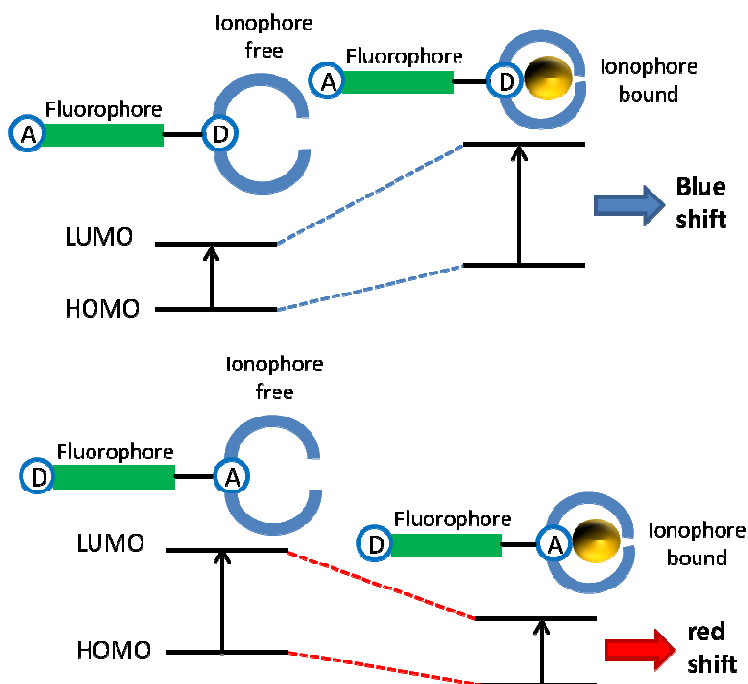


**Figure 26:** Spectral displacements of PCT sensors resulting from interaction of a bound cation with an electron-donating or an electron-withdrawing group.

---

When an electron-donating group such as an amine interacts with a cation the positive charge attracts the electrons from the amine group and thus reduces the charge transfer character. As a result, the absorption and emission spectra should experience a blue shift along with a decrease of the extinction coefficient due to the decrease in conjugation caused by the cation. The dipole moment is therefore concomitantly decreased. In the opposite case when a cation interacts with the electron-accepting group, the electron-withdrawing character of this group is enhanced and therefore the dipole moment experiences an increase. Absorption and emission spectra are in principle red-shifted and an increase in the extinction coefficient is often observed. The extent of this effect depends on the cation charge and the type of ionophore. For fluorophores that have a higher dipole moment in the excited state than in the ground state, cation-donor interactions destabilize the excited state more and lead to a blue shift. Conversely, if the cation interacts with an acceptor the excited state is more stabilized and leads therefore to a red-shift of the emission.

Most of the examples in the literature belong to the case where the cation interacts with a donor group.<sup>87,88</sup> Three examples based on an azacrown ionophore are given in figure 27.

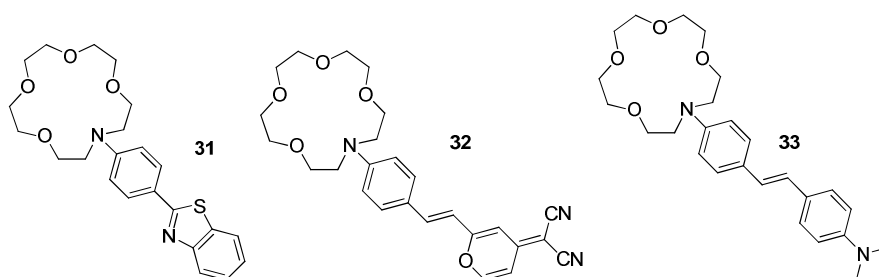


**Figure 27:** Crown ether based PCT ion sensors.

The two presented PCT-based ion sensors **31** developed by Mateeva *et al.*<sup>89</sup> connecting the azacrown to a benzothiazolylpenyl unit and **32** using a merocyanine fluorophore developed by and Bourson *et al.*<sup>90</sup> were tested for spectral changes upon  $\text{Ca}^{2+}$  binding. Upon ion addition, the absorption spectra of both fluorophores displayed a relatively large hypsochromic shift of the absorption maximum (**31** = 360 nm  $\rightarrow$  318 nm; **32** = 464 nm  $\rightarrow$  398 nm). The change in the emission maximum is, however, much smaller (**31** = 420 nm  $\rightarrow$  418 nm; **32** = 621 nm  $\rightarrow$  608 nm). The explanation for this lies in the nature of the excited state. Due to the positive polarization of the amine binding the cation, upon excitation a disruption of the bond between the nitrogen donor and the cation is induced. Thus, fluorescence is emitted from a species

---

---

which is no longer (or only weakly) bound to the cation and therefore the fluorescence emission maximum is only weakly influenced. This interpretation is supported by several studies about the photophysics of this kind of PCT ion sensor.<sup>91,92</sup> The third ion sensor **33** bears the ion-sensing group in the acceptor position of the molecule due to the electron rich character of the dimethylamine unit. Thus, upon  $\text{Ca}^{2+}$ -binding **33** gives a bathochromic shift in the absorption spectrum. Considerations made for the excited state equally apply here.

The aforementioned examples carrying an azacrown ionophore function well for  $\text{Ca}^{2+}$ -binding but are not highly specific. Many other ions such as  $\text{Li}^+$ ,  $\text{Ba}^{2+}$  or  $\text{K}^+$  bind with the same or increased selectivity to the ionophore.  $\text{Ca}^{2+}$ -selective PCT ion sensors are based on the BAPTA chelating agent developed by Tsien.<sup>30</sup> PCT-sensors have a distinct advantage over PET sensors since they can be internally calibrated against common microenvironmental variables by dual excitation wavelength monitoring and observing the ratio between the two emissions. A lot of BAPTA-based PET and PCT sensors are commercially available nowadays due to their application in determination of cytosolic  $\text{Ca}^{2+}$  concentrations.<sup>93</sup> Most prominent examples of BAPTA PCT sensors are shown in figure 28.

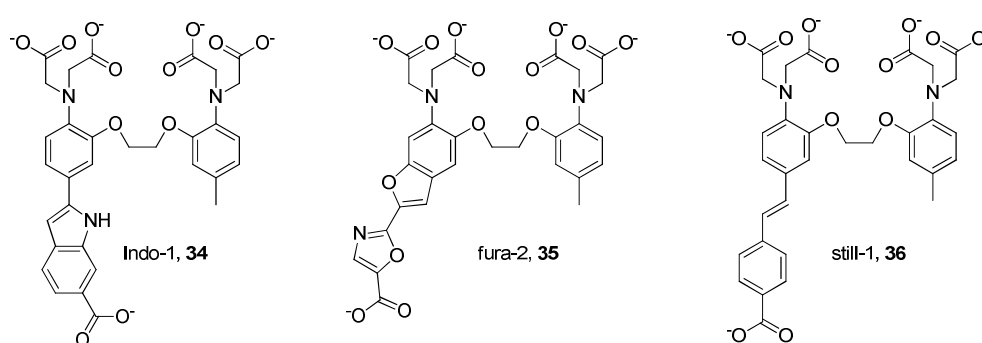


**Figure 28:** BAPTA based  $\text{Ca}^{2+}$ -selective PCT sensors.

In these fluoroionophores the fluorophore is a donor-acceptor molecule with an amine as the electron donor which is at the same time part of the ionophore and participates in the binding of  $\text{Ca}^{2+}$ . Upon  $\text{Ca}^{2+}$ -complexation in aqueous media, the absorption spectrum is blue-shifted with almost no influence on the emission spectrum. This accounts for all the BAPTA PCT sensors in the **fura** (**35**) and **still** (**36**) series. The **indo** (**34**) series however displays a rather large shift in the emission spectrum as well, which is rather untypical as we learned earlier. The absorption and emission maxima in presence and absence of  $\text{Ca}^{2+}$  for the three described molecules is shown in table 04.

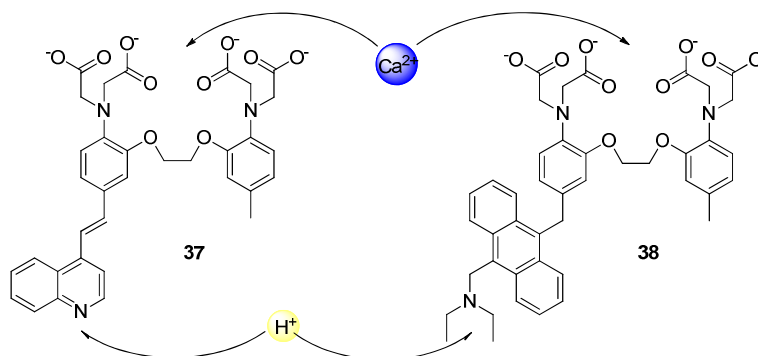
---

**Table 04:** Absorption and emission maxima of BAPTA PCT sensors in presence and absence of  $\text{Ca}^{2+}$ .

	Abs. max (nm) ( $-\text{Ca}^{2+}$ )	Abs. max (nm) ( $+\text{Ca}^{2+}$ )	Em. max (nm) ( $-\text{Ca}^{2+}$ )	Em. max (nm) ( $+\text{Ca}^{2+}$ )
<b>Indo-1 (34)</b>	349	331	485	410
<b>Fura-2 (35)</b>	362	335	512	505
<b>Still-1 (36)</b>	362	329	537	529

The same interpretation forwarded for the crown ethers applies here as well, meaning that the electron density of the aniline conjugated with the electron-withdrawing group of the fluorophore is reduced in the excited state and might become positively polarized which causes disruption between the cation and nitrogen binding. The possibility of photoejection in these molecules has not been examined yet. A study of the excited state revealed that the binding affinity of fura-2 (**35**) is three orders of magnitudes lower in the excited state.<sup>94</sup> As for the exception indo-1 (**34**), the PCT may not be sufficient to cause bond breaking between nitrogen and  $\text{Ca}^{2+}$ . This would explain the shorter wavelength of the fluorescence emission compared to the other PCT sensors, indicating a less polar charge-transfer state.

As a last example, two multiple addressable systems based on the BAPTA ionophore and a pH sensing unit are presented. In figure 29 a presentation of two multi-addressable systems is given.

**Figure 29:** Multi-addressable molecular systems based on an ion and proton binding unit linked to a fluorophore.

The multiple addressable system **37**<sup>95</sup> and **38**<sup>96</sup> described by McClenaghan and de Silva found applications as molecular logic gates. As for **37**, which consists of the a BAPTA fragment linked to a conjugated quinoline,  $\text{Ca}^{2+}$  addition leads to an hypsochromic shift of the absorption spectrum while the decrease of the pH lead to a bathochromic shift of the absorption spectrum. By monitoring the absorbance at a certain wavelength a two input logic

---

gate was designed. **38** displays as well the BAPTA fragment on one side and a diethyl amine on the other side of an anthracene fluorophore. In principle this system is addressable using the same ion / proton. When the PET is blocked on either side with  $H^+$  or  $Ca^{2+}$  characteristic anthracene emission can be observed yielding an AND logic gate when fluorescence is considered as an output. This is an example of the exploitation of PET for non-biological applications since most studies concerning these BAPTA based ion sensors involve the detection of cellular  $Ca^{2+}$ .<sup>97,98</sup>

Even though the field fluorescent ion sensing is rather old, research is still ongoing. Besides the continuous unravelling of the involvement of  $Ca^{2+}$  in biological processes,<sup>99</sup> there is an interest in further improving the existing systems in terms of accessibility and utility. More recent publication on the field of  $Ca^{2+}$  sensing include the modification of binding affinities by altering the core structure,<sup>100</sup> novel fluorionophores with improved emission wavelengths<sup>101</sup> and  $Ca^{2+}$  decaying agents with improved decaying properties<sup>102</sup> or alternative triggers.<sup>103</sup> A recently published example of a series of novel PET  $Ca^{2+}$ -sensor was developed by Collot *et.al.*<sup>101</sup> The molecular structure of the fluorionophores is shown in figure 30.

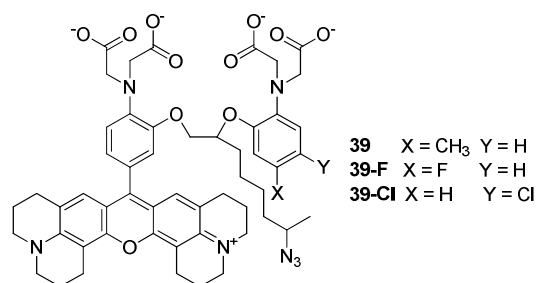


**Figure 30:** Red light emitting BAPTA based fluorionophore bearing a x-rhodamine fluorophore (**39**).

The unique feature in the molecular structure of these  $Ca^{2+}$ -sensors (**39**) is the presence of an aliphatic chain bearing an aromatic azide linked to the ethylene glycol part of the molecule. Like that the aromatic ring was free to tune the binding affinity of the BAPTA unit. Incorporating electron withdrawing groups like fluorine (**39-F**) and chlorine (**39-Cl**) decreased the binding affinity towards  $Ca^{2+}$  from 3  $\mu M$  (**39**) over 6  $\mu M$  (**39-F**) to 22  $\mu M$  (**39-Cl**). Fluorescence enhancement upon ion binding was in the range of 50-fold for the halogen derivatives and 60-fold for the parent molecule (**39**). The aliphatic azide chain had been subjected to “click”-chemistry in order to couple the ion sensor to substrates. The excitation

---

---

maximum at 586 nm and emission maximum 604 nm gives rise to applications in multicolour imaging. Recent advance in  $\text{Ca}^{2+}$  decaging agents will be discussed in chapter 3.

## 1.8 Biomimetic nanodomains and self-assembled cell mimicry

In order to study ion transfer in biomimetic nanodomains one needs to look at the cell mimicking assemblies that are available. This has been a vast field of research involving biologists and chemists in equal measure. Biologists, for example, have favoured a top-down approach by knocking out genes of an existing bacterium to obtain a cell with a minimum amount of genes in order to load them with synthetically created DNA.<sup>104</sup> Chemists on the other hand have been working on the bottom-up approach. Ever since the discovery that phospholipids are the major ingredient of the cell wall<sup>105,106</sup> they have been extensively studied for the mimicry of biomembranes.<sup>107</sup> Years later it was found that these phospholipids are not the only organic molecules which are able to self-assemble into vesicles containing a biomembrane mimicking bilayer. Synthetic amphiphiles have been found to form bilayered structures in aqueous media as well.<sup>108</sup> The contribution of polymer chemistry to the self-assembled vesicles field is more recent. In 1999 Discher *et al.*<sup>109</sup> found that block copolymers consisting of a hydrophilic and a hydrophobic polymers can self-assemble to form polymer bilayers. These types of vesicles were called polymersomes and have ever since been exploited for the preparation of cell mimicry applications such as synthetic red blood cell mimics<sup>110</sup> or where engineered to possess the adhesive properties of leucocytes.<sup>111</sup>

The three building blocks for cellular bilayer mimicry will be introduced in more detail in chapter 4. For now, it should be noted that there are vast selection of amphiphiles and polymers available to achieve the goal of cell mimicry and the subsequent biomimetic ion transfer studies in confined compartments.

## 1.9 Conclusion

The vast field of supramolecular chemistry holds the potential to impact a large variety of applications. The presented ion binding motifs in combination with photoactive groups like fluorescent dyes or photoswitchable groups give the opportunity to study ion transfer, which

---

can be measured by fluorescence spectroscopy and microscopy techniques. Supramolecular assemblies using lipids, amphiphiles and polymer deliver the building blocks for the creation of cell mimicry. By combining the aforementioned disciplines of chemistry, a novel approach to artificial cell mimicry can be envisaged.

---

## References:

- (1) Brodie, C.; Bak, A.; Shainberg, A.; Sampson, S. R. *J. Cell. Physiol.* **1987**, *130*, 191.
- (2) Alberts, A. J., A.; Lewis, J.; Raff, M.; Roberts, K.; Walter, P. **2007**.
- (3) Romani, A. *Arch. Biochem. Biophys.* **2007**, *458*, 90.
- (4) Permyakov, E. A.; Kretsinger, R. H. *Journal of Inorganic Biochemistry* **2009**, *103*, 77.
- (5) Frizzell, R. A. *J. Membr. Biol.* **1977**, *35*, 175.
- (6) Rall, T. W.; Sutherland, E. W. *J. Biol. Chem.* **1958**, *232*, 1065.
- (7) L.V., H. **1943**.
- (8) Ringer, S. *J. Physiol. (Lond.)* **1883**, *4*, 29.
- (9) Clapham, D. E. *Cell* **2007**, *131*, 1047.
- (10) Augustine, G. J.; Santamaria, F.; Tanaka, K. *Neuron* **2003**, *40*, 331.
- (11) Erlichma, J.; Rosenfel, R.; Rosen, O. M. *J. Biol. Chem.* **1974**, *249*, 5000.
- (12) Yang, C.; Jas, G. S.; Kuczera, K. *Biochimica Et Biophysica Acta-Proteins and Proteomics* **2004**, *1697*, 289.
- (13) Ellis-Davies, G. C. R. *Chem. Rev.* **2008**, *108*, 1603.
- (14) Marambaud, P.; Dreses-Werringloer, U.; Vingtdoux, V. *Mol. Neurodegener.* **2009**, *4*.
- (15) Hu, F.; Yang, S.; Zhao, D.; Zhu, S. Y.; Wang, Y. X.; Li, J. Y. *Biochem. Biophys. Res. Commun.* **2012**, *424*, 196.
- (16) Lehn, J. M. *Proc. Natl. Acad. Sci. U. S. A.* **2002**, *99*, 4763.
- (17) Steed, J. W. A., L. *Supramolecular Chemistry, John Wiley & Sons* **2009**.
- (18) Rose, L.; Jenkins, A. T. A. *Bioelectrochemistry* **2007**, *70*, 387.
- (19) Hunter, C. A. *Angew. Chem. Int. Ed.* **2004**, *43*, 5310.
- (20) Pedersen, C. J. *J. Am. Chem. Soc.* **1967**, *89*, 7017.
- (21) Pedersen, C. J. *J. Am. Chem. Soc.* **1967**, *89*, 2495.
- (22) Martell, A. E.; Hancock, R. D.; Motekaitis, R. J. *Coord. Chem. Rev.* **1994**, *133*, 39.
- (23) Johnson, R. D.; Bachas, L. G. *Anal. Bioanal. Chem.* **2003**, *376*, 328.
- (24) Buhlmann, P.; Pretsch, E.; Bakker, E. *Chem. Rev.* **1998**, *98*, 1593.
- (25) Shim, J. H.; Jeong, I. S.; Lee, M. H.; Hong, H. P.; On, J. H.; Kim, K. S.; Kim, H. S.; Kim, B. H.; Cha, G. S.; Nam, H. *Talanta* **2004**, *63*, 61.
- (26) Flora, S. J. S.; Pachauri, V. *Int. J. Environ. Res. Public. Health* **2010**, *7*, 2745.
- (27) Bers, D. M.; Patton, C. W.; Nuccitelli, R. In *Calcium in Living Cells*; Whitaker, M., Ed. 2010; Vol. 99, p 1.
- (28) Toescu, E. C.; Vreugdenhil, M. *Cell Calcium* **2010**, *47*, 158.
- (29) BenitezKing, G.; Rios, A.; Martinez, A.; AntonTay, F. *Biochim. Biophys. Acta-Gen. Subj.* **1996**, *1290*, 191.
- (30) Tsien, R. Y. *Biochemistry* **1980**, *19*, 2396.
- (31) Putney, J. W. *Taylor & Francis Group* **2006**, *Second edition*.
- (32) Ikeda, A.; Tsudera, T.; Shinkai, S. *J. Org. Chem.* **1997**, *62*, 3568.
- (33) Fabbriizzi, L.; Foti, F.; Patroni, S.; Pallavicini, P.; Taglietti, A. *Angew. Chem. Int. Ed.* **2004**, *43*, 5073.
- (34) Rodriguezubis, J. C.; Juanes, O.; Brunet, E. *Tetrahedron Lett.* **1994**, *35*, 1295.
- (35) Costero, A. M.; Andreu, C.; Monrabal, E.; Tortajada, A.; Ochando, L. E.; Amigo, J. M. *Tetrahedron* **1996**, *52*, 12499.
- (36) Coyle, J. D. *John Wiley & Sons Inc* **1988**.
- (37) Valeur, B. *Wiley-VCH Verlag GmbH* **2001**.

- 
- (38) Condon, E. *Physical Review* **1926**, *28*, 1182.
- (39) Franck, J. *Transactions of the Faraday Society* **1926**, *21*, 0536.
- (40) Birks, J. B. *Organic Molecular Photophysics*, Wiley-VCH **1975**.
- (41) Lakowicz, J. R. *Principles of Fluorescence Spectroscopy*, Plenum Press, New York **1983**.
- (42) Irie, M. *Chem. Rev.* **2000**, *100*, 1683.
- (43) Hamon, F.; Djedaini-Pilard, F.; Barbot, F.; Len, C. *Tetrahedron* **2009**, *65*, 10105.
- (44) Nguyen, T. T. T.; Turp, D.; Wang, D. P.; Nolscher, B.; Laquai, F.; Mullen, K. *J. Am. Chem. Soc.* **2011**, *133*, 11194.
- (45) Asakawa, M.; Ashton, P. R.; Balzani, V.; Brown, C. L.; Credi, A.; Matthews, O. A.; Newton, S. P.; Raymo, F. M.; Shipway, A. N.; Spencer, N.; Quick, A.; Stoddart, J. F.; White, A. J. P.; Williams, D. J. *Chemistry-a European Journal* **1999**, *5*, 860.
- (46) Tian, H.; Yang, S. J. *Chem. Soc. Rev.* **2004**, *33*, 85.
- (47) Matsuda, K.; Irie, M. *Journal of Photochemistry and Photobiology C-Photochemistry Reviews* **2004**, *5*, 169.
- (48) Katsonis, N.; Lubomska, M.; Pollard, M. M.; Feringa, B. L.; Rudolf, P. *Prog. Surf. Sci.* **2007**, *82*, 407.
- (49) Zhang, X.; Chen, Y. *ChemPhysChem* **2009**, *10*, 1993.
- (50) Shinkai, S.; Minami, T.; Kusano, Y.; Manabe, O. *J. Am. Chem. Soc.* **1983**, *105*, 1851.
- (51) Emond, M.; Sun, J.; Gregoire, J.; Maurin, S.; Tribet, C.; Jullien, L. *Phys. Chem. Chem. Phys.* **2011**, *13*, 6493.
- (52) Malval, J. P.; Gosse, I.; Morand, J. P.; Lapouyade, R. *J. Am. Chem. Soc.* **2002**, *124*, 904.
- (53) Bandara, H. M. D.; Walsh, T. P.; Burdette, S. C. *Chemistry-a European Journal* **2011**, *17*, 3932.
- (54) Gwizdala, C.; Basa, P. N.; MacDonald, J. C.; Burdette, S. C. *Inorg. Chem.* **2013**, *52*, 8483.
- (55) Mbatia, H. W.; Kennedy, D. P.; Burdette, S. C. *Photochem. Photobiol.* **2012**, *88*, 844.
- (56) Ciesinski, K. L.; Haas, K. L.; Dickens, M. G.; Tesema, Y. T.; Franz, K. J. *J. Am. Chem. Soc.* **2008**, *130*, 12246.
- (57) Iwabuchi, S.; Watanabe, T.; Kawahara, K. *Neurochem. Int.* **2013**, *62*, 1020.
- (58) Barrera, N. P.; Morales, B.; Villalon, M. *Biochem. Biophys. Res. Commun.* **2007**, *364*, 815.
- (59) Valeur, B.; Leray, I. *Coord. Chem. Rev.* **2000**, *205*, 3.
- (60) de Silva, A. P.; Gunaratne, H. Q. N.; Gunnlaugsson, T.; Huxley, A. J. M.; McCoy, C. P.; Rademacher, J. T.; Rice, T. E. *Chem. Rev.* **1997**, *97*, 1515.
- (61) Carafoli, E. K., C. B. *Calcium as a Cellular Regulator*, Oxford University Press, Inc. **1999**.
- (62) Ashokkumar, P.; Ramakrishnan, V. T.; Ramamurthy, P. *J. Phys. Chem. A* **2011**, *115*, 14292.
- (63) Hirayama, T.; Van de Bittner, G. C.; Gray, L. W.; Lutsenko, S.; Chang, C. J. *Proc. Natl. Acad. Sci. U. S. A.* **2012**, *109*, 2228.
- (64) Sung, K. S.; Fu, H. K.; Hong, S. H. *Journal of Fluorescence* **2007**, *17*, 383.
- (65) De Silva, A. P.; Desilva, S. A. *Journal of the Chemical Society-Chemical Communications* **1986**, 1709.
-

- 
- (66) Akkaya, E. U.; Huston, M. E.; Czarnik, A. W. *J. Am. Chem. Soc.* **1990**, *112*, 3590.
- (67) De Silva, A. P.; Gunaratne, H. Q. N. *Journal of the Chemical Society-Chemical Communications* **1990**, 186.
- (68) Czarnik, A. W. *Fluorescence Chemosensors of Ion and Molecule Recognition, Ed.; ACS Symp. Ser. 538 Washington DC* **1993**.
- (69) Gust, D.; Moore, T. A. *Top. Curr. Chem.* **1991**, *159*, 103.
- (70) Gust, D.; Moore, T. A.; Moore, A. L. *Acc. Chem. Res.* **1993**, *26*, 198.
- (71) Kollmannsberger, M.; Rurack, K.; Resch-Genger, U.; Rettig, W.; Daub, J. *Chem. Phys. Lett.* **2000**, *329*, 363.
- (72) Gee, K. R.; Rukavishnikov, A.; Rothe, A. *Comb. Chem. High Throughput Screening* **2003**, *6*, 363.
- (73) Minta, A.; Kao, J. P. Y.; Tsien, R. Y. *J. Biol. Chem.* **1989**, *264*, 8171.
- (74) Hyman, L. M.; Franz, K. J. *Coord. Chem. Rev.* **2012**, *256*, 2333.
- (75) Kamiya, M.; Johnsson, K. *Anal. Chem.* **2010**, *82*, 6472.
- (76) Su, W. Q.; Tong, J.; Yang, B. Q. *Chinese Journal of Organic Chemistry* **2013**, *33*, 982.
- (77) He, H. R.; Jenkins, K.; Lin, C. *Anal. Chim. Acta* **2008**, *611*, 197.
- (78) Gao, Y. D.; Zheng, J. W.; Li, P.; Cheng, M.; Yang, J. *J. Asthma* **2013**, *50*, 439.
- (79) De Silva, A. P.; Desilva, S. A.; Dissanayake, A. S.; Sandanayake, K. *Journal of the Chemical Society-Chemical Communications* **1989**, 1054.
- (80) Metivier, R.; Leray, I.; Valeur, B. *Chemistry-a European Journal* **2004**, *10*, 4480.
- (81) Marcus, R. A. *Angewandte Chemie-International Edition in English* **1993**, *32*, 1111.
- (82) Knibbe, H.; Rehm, D.; Weller, A. *Berichte Der Bunsen-Gesellschaft Fur Physikalische Chemie* **1968**, *72*, 257.
- (83) Knibbe, H.; Rehm, D.; Weller, A. *Berichte Der Bunsen-Gesellschaft Fur Physikalische Chemie* **1969**, *73*, 839.
- (84) Lord, S. J.; Conley, N. R.; Lee, H. L. D.; Liu, N.; Samuel, R.; Twieg, R. J.; Moerner, W. E. In *Reporters, Markers, Dyes, Nanoparticles, and Molecular Probes for Biomedical Applications*; Achilefu, S., Raghavachari, R., Eds. 2009; Vol. 7190.
- (85) Valeur, B. B., J.; Pouget, J.; Czarnik A.W. *Chemosensors of Ion and Molecule Recognition, ACS Symposium Series 538, Washington DC* **1993**.
- (86) Rettig, W. L., R.; Lakowicz, J.R. *Topics in Fluorescence Spectroscopy, vol 4, Plenum, New York* **1994**.
- (87) Kasner, S. E.; Ganz, M. B. *Am. J. Physiol.* **1992**, *262*, F462.
- (88) Minta, A.; Tsien, R. Y. *J. Biol. Chem.* **1989**, *264*, 19449.
- (89) Mateeva, N.; Enchev, V.; Antonov, L.; Deligeorgiev, T.; Mitewa, M. *J. Inclusion Phenom.* **1994**, *20*, 323.
- (90) Bourson, J.; Valeur, B. *J. Phys. Chem.* **1989**, *93*, 3871.
- (91) Martin, M. M.; Plaza, P.; Meyer, Y. H.; Badaoui, F.; Bourson, J.; Lefevre, J. P.; Valeur, B. *J. Phys. Chem.* **1996**, *100*, 6879.
- (92) Martin, M. M.; Plaza, P.; Hung, N. D.; Meyer, Y. H.; Bourson, J.; Valeur, B. *Chem. Phys. Lett.* **1993**, *202*, 425.
- (93) Tsien, R. Y.; Rink, T. J.; Poenie, M. *Cell Calcium* **1985**, *6*, 145.
- (94) Vandenbergh, V.; Boens, N.; Deschryver, F. C.; Ameloot, M.; Steels, P.; Gallay, J.; Vincent, M.; Kowalczyk, A. *Biophys. J.* **1995**, *68*, 1110.
- (95) de Silva, A. P.; McClenaghan, N. D. *J. Am. Chem. Soc.* **2000**, *122*, 3965.
-

- 
- (96) Callan, J. F.; de Silva, A. P.; McClenaghan, N. D. *Chem. Commun.* **2004**, 2048.
- (97) Tanase, C. E.; Sartoris, A.; Popa, M. I.; Verestiuc, L.; Unger, R. E.; Kirkpatrick, C. J. *Biomedical Materials* **2013**, 8.
- (98) Xu, Q. T.; Fan, H. Y.; Jiang, Z.; Zhou, Z. Q.; Yang, L.; Mei, F. Z.; Qu, L. H. *Acta Biol Hung* **2013**, 64, 328.
- (99) Luccardini, C.; Yakovlev, A. V.; Pasche, M.; Gaillard, S.; Li, D. D.; Rousseau, F.; Ly, R.; Becherer, U.; Mallet, J. M.; Feltz, A.; Oheim, M. *Cell Calcium* **2009**, 45, 275.
- (100) He, H. Z.; Lei, L.; Li, J. L.; Shi, Z. *Synth. Commun.* **2009**, 39, 2074.
- (101) Collot, M.; Loukou, C.; Yakovlev, A. V.; Wilms, C. D.; Li, D. D.; Evrard, A.; Zamaleeva, A.; Bourdieu, L.; Leger, J. F.; Ropert, N.; Eilers, J.; Oheim, M.; Feltz, A.; Mallet, J. M. *J. Am. Chem. Soc.* **2012**, 134, 14923.
- (102) Cui, J. X.; Gropeanu, R. A.; Stevens, D. R.; Rettig, J.; Campo, A. *J. Am. Chem. Soc.* **2012**, 134, 7733.
- (103) Bhattacharyya, K. X.; Boubekour-Lecaque, L.; Tapsoba, I.; Maisonhaute, E.; Schollhorn, B.; Amatore, C. *Chem. Commun.* **2011**, 47, 5199.
- (104) Gibson, D. G.; Glass, J. I.; Lartigue, C.; Noskov, V. N.; Chuang, R. Y.; Algire, M. A.; Benders, G. A.; Montague, M. G.; Ma, L.; Moodie, M. M.; Merryman, C.; Vashee, S.; Krishnakumar, R.; Assad-Garcia, N.; Andrews-Pfannkoch, C.; Denisova, E. A.; Young, L.; Qi, Z. Q.; Segall-Shapiro, T. H.; Calvey, C. H.; Parmar, P. P.; Hutchison, C. A.; Smith, H. O.; Venter, J. C. *Science* **2010**, 329, 52.
- (105) Bangham, A. D.; Glauert, A. M.; Horne, R. W.; Dingle, J. T.; Lucy, J. A. *Nature* **1962**, 196, 952.
- (106) Bangham, A. D.; Horne, R. W. *J. Mol. Biol.* **1964**, 8, 660.
- (107) Lee, J.; Lee, J. K.; Busnaina, A.; Park, B.; Lee, H. *J. Nanosci. Nanotechnol.* **2013**, 13, 144.
- (108) Kunitake, T.; Okahata, Y. *J. Am. Chem. Soc.* **1977**, 99, 3860.
- (109) Discher, B. M.; Won, Y. Y.; Ege, D. S.; Lee, J. C. M.; Bates, F. S.; Discher, D. E.; Hammer, D. A. *Science* **1999**, 284, 1143.
- (110) Kim, H. W.; Greenburg, A. G. *Artif Organs* **2004**, 28, 813.
- (111) Hammer, D. A.; Robbins, G. P.; Haun, J. B.; Lin, J. J.; Qi, W.; Smith, L. A.; Ghoroghchian, P. P.; Therien, M. J.; Bates, F. S. *Faraday Discuss.* **2008**, 139, 129.

---

---

---

---

---

## **2 F<sub>5</sub>-BODIPY for selective labeling, fluorescence studies and surface patterning**

---

---

## 2.1 Introduction

The **BoronDIPyrrromethene** (BODIPY) fluorophore was first synthesized in 1968 by German chemists, namely Alfred Treibs and Franz-Heinrich Kreuzer.<sup>1</sup> The unsubstituted BODIPY skeleton, which is responsible for the molecule's name, was however not synthesized until the year 2009 and different routes of the synthesis had been published by 3 different groups.<sup>2-4</sup> The structure of the core compound (**40**) is given in Figure 30.

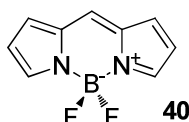
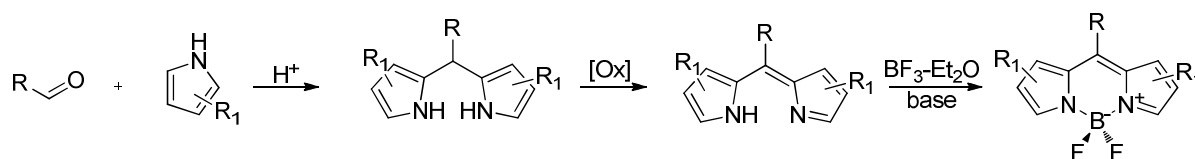


**Figure 31:** molecular structure of the BODIPY core compound (**40**)

The fluorescent properties of BODIPYs are generally defined by high quantum yields (0.2 – 1) and high extinction coefficients ranging from 30000 to 80000  $\text{cm}^{-1}\text{M}^{-1}$  depending on the substitution pattern.<sup>5</sup> Fluorescent emission occurs with a characteristic small Stokes shift and the dye displays a photostability which is often above those of frequently used fluorescence standards.

There are two main routes for the synthesis of BODIPY dyes which can be found in different variations throughout the literature. For the synthesis of symmetrical molecules a 3 step synthesis consists of the condensation of two pyrroles with an aldehyde leading to a dipyrromethane, which is subsequently oxidized to a dipyrromethene and complexed with  $\text{BF}_3$  as shown in scheme 02.

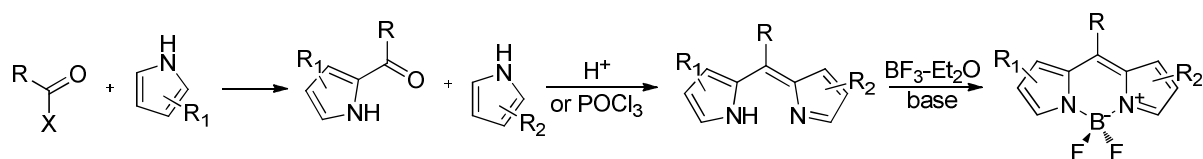


**Scheme 02:** Synthesis of symmetric substituted BODIPY dyes.

For non-symmetrical BODIPYs a different approach was used to synthesize the final compound. The synthesis starts by the condensation of a pyrrole with an acylium equivalent, for example an acid chloride, an anhydride or an orthoester, leading to an acylpyrrole.<sup>6,7</sup> This intermediate is usually not isolated due to side reactions with other pyrroles in solution under acidic conditions. In a subsequent step, the acylpyrrole is reacted with a second differently

---

substituted pyrrole to give the dipyrromethene and then complexed with boron trifluoride to form the asymmetric BODIPY. The synthesis is outlined in scheme 03.



**Scheme 03:** Synthesis of an asymmetric BODIPY

Because of their relatively high chemical stability BODIPYs can be post-modified in several different ways which make them available for applications in labeling of proteins<sup>8,9</sup> or tuning of the fluorescence properties.

### 2.1.1 Post-functionalization of the BODIPY core

There are numerous ways for post modification of the BODIPY chromophore, which are linked to the aromatic nature of the molecule and are exploited in the literature. In figure 32 the positions of modifications are highlighted.

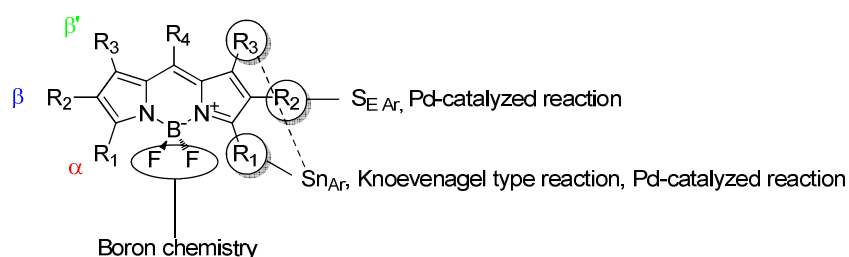
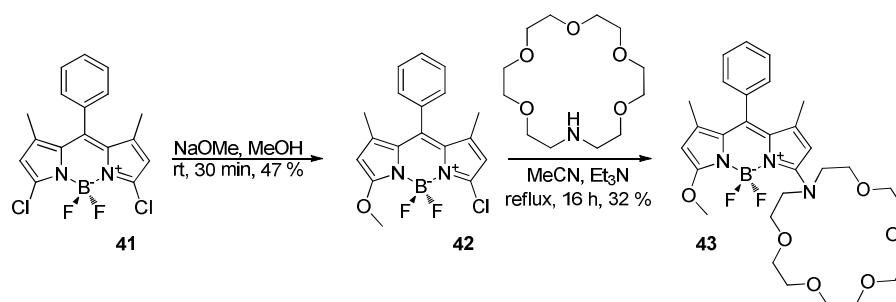


**Figure 32:** Possible post-functionalization of the BODIPY skeleton.

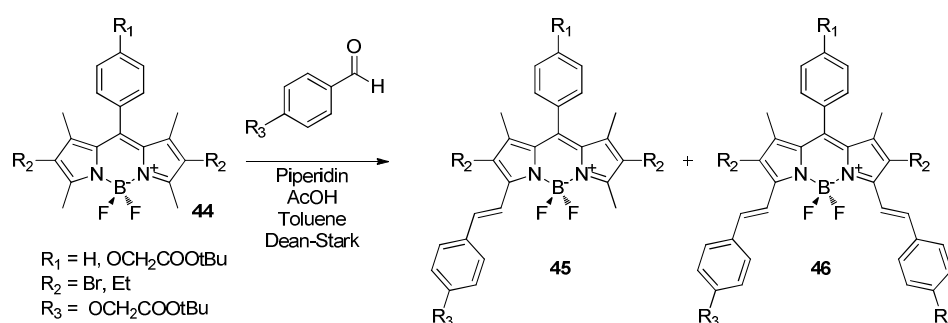
The  $\alpha$ -position is easily modified by nucleophilic aromatic substitution reactions due to the electron-withdrawing effect of the partially positively charged nitrogen in proximity. Monohalogenated derivatives had been synthesized by Dehaen and co-workers and were subsequently functionalized by different nucleophiles using Pd-catalyzed crosscoupling.<sup>10</sup> In this manner the fluorescent properties of the dye could be tuned with emission maxima ranging from 503 – 578 nm. In the same manner the  $\beta$ -position, substituted by an iodine, has been functionalized with conjugated aromatic groups, to change the spectral properties. Another example from the same group uses  $S_{N,Ar}$  of a chlorine in the  $\alpha$ -position of BODIPY

(41) first by a methoxylate (42) and subsequently by an azacrown ether to produce a ratiometric, fluorescent potassium sensor (43) as shown in scheme 04.<sup>11</sup>



**Scheme 04:** Preparation of a potassium sensor by  $S_{\text{N}}\text{Ar}$  on a chlorinated BODIPY fluorophore.

If the BODIPY  $\alpha$ -position bears a methyl-group (44) the protons are sufficiently acidic to undergo Knoevenagel condensations with aromatic aldehydes as shown in scheme 05. To date no example has been shown where an aliphatic aldehyde was used, which is due to the electron deficiency of aliphatic aldehydes. In general the yield of those reactions rarely surpasses 30 % and a mixture of mono- (45) and disubstituted (46) products are obtained. These elongated BODIPYs show red shifts in absorption and emission spectra leading to near infrared emitting dyes. The influence of the solvent polarity is also increased suggesting a more polar excited state of these structures<sup>12</sup>.



**Scheme 05:** Knoevenagel type reaction on a BODIPY bearing methyl groups in the  $\alpha$ -position.

The  $\beta$ -position is the most electron rich position of the fluorophore, which can be shown by the mesomeric structures. Therefore this position is susceptible to electrophilic aromatic substitution. The classical examples can be found in the literature namely sulfonation (48), nitration (49), formylation (50) and halogenations (51). While sulfonation is mostly applied to increase the water solubility of the dye while maintaining its spectral properties,<sup>13</sup> formylation<sup>14,15</sup> and halogenation<sup>16</sup> lead to intermediates which can be further modified.

Bromination of the BODIPY core showed a red-shift in absorption and emission spectra and fluorescent quantum yields were decreased due to the heavy atom effect. An overview of the  $S_{E,Ar}$  reactions is given in figure 33 showing a schematic representation of standard BODIPY (**47**) in the center.

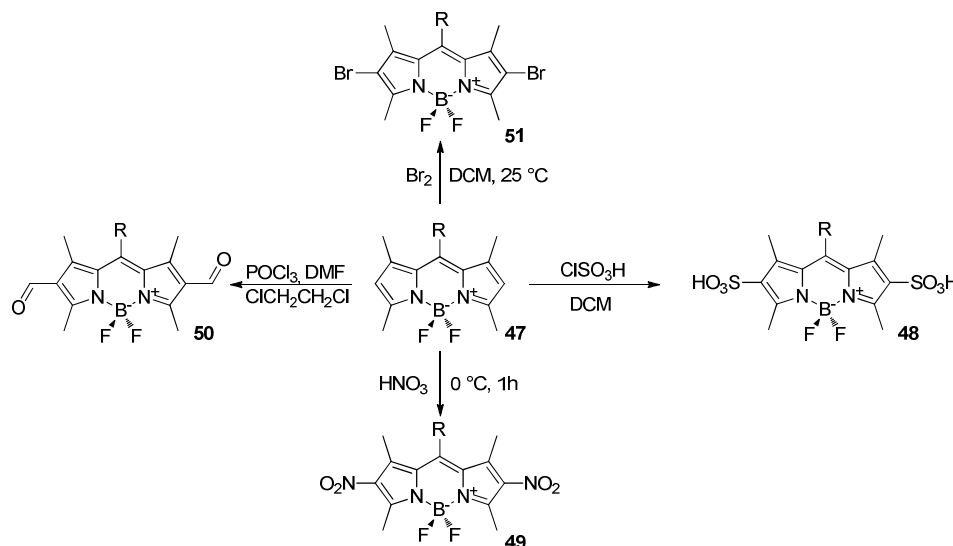
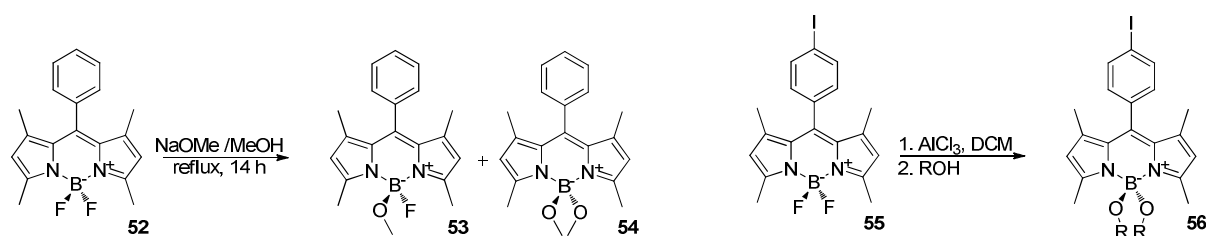


**Figure 33:** Examples for  $S_{E,Ar}$  in  $\beta$ -position of BODIPY

As a last example for post-synthetic modifications on the BODIPY skeleton, the chemistry on the boron atom is presented. BODIPY **52** and **55** serve as an example and reactions are highlighted in scheme 06. Essentially, there are two possibilities to substitute the fluorine atoms on the boron. First an attacking nucleophile is activated by a base, leading to mono- (**53**) or disubstituted products (**54**) when reaction times are prolonged and excess nucleophile is used.<sup>17</sup> The reaction yield decreases when more sterically hindered alcohols are used. The second way to make the boron react is the activation of the boron center itself by strong Lewis acids like  $AlCl_3$  leading to disubstituted reaction products (**56**).<sup>18</sup> Other examples include the use of organometallic compounds like organolithium or Grignard-type reactants.<sup>19</sup>



**Scheme 06:** Substitution of fluorine at the boron center. left: basic conditions, right: acidic conditions.

---

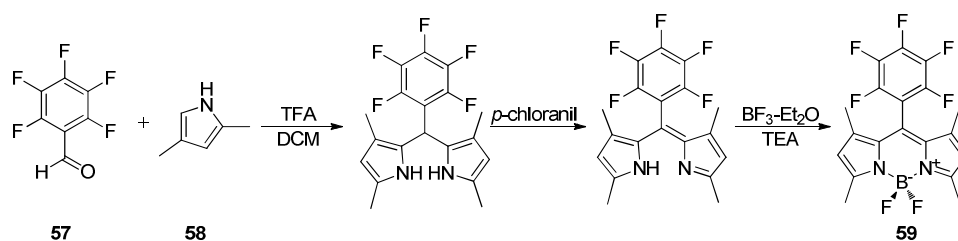
In next few pages a new BODIPY based chromophore is introduced with a new way to post functionalize the BODIPY skeleton based on the chemistry of a pentafluoro phenyl ring. Perfluorophenyl rings are known to undergo  $S_{N,Ar}$  reactions due to the electron withdrawing effect of the fluorine atoms. This chemistry has been extensively exploited for different application for example in post-modification of polymers or the facile introduction of side chains onto a porphyrin ring system.<sup>20,21</sup>

---

## 2.2 Synthesis and selective labeling of F<sub>5</sub>-BODIPY (**59**)

### 2.2.1 Synthesis and crystal structure of F<sub>5</sub>-BODIPY (**59**)

The synthesis of the chromophore was based on the previously mentioned procedure of symmetric BODIPYs. Commercially available pentafluorobenzaldehyde (**57**) was first reacted with 2,4-dimethylpyrrole (**58**) to afford a dipyrromethane intermediate, which was oxidized by *p*-chloranil to a dipyrromethene intermediate. This was then reacted with BF<sub>3</sub>-Et<sub>2</sub>O to yield the desired product in 33 % overall yield. The reaction sequence is shown in scheme 07 and the exact procedure can be found in the experimental section. It is noteworthy, that the purification of the compound had to be performed in two steps. Step one being purification by column chromatography with silica as the stationary phase and the second step being crystallization from chloroform. This proved to be necessary due to the instability of the title compound on the chromatography column. This instability can be explained by the unsubstituted β-position, which seems to be unstable under the slightly acidic conditions on the column. Derivatives with an ethyl group in this position were chemically more stable and are shown later on in this manuscript. A representation of the synthetic pathway is given in scheme 07. The overall reaction yield was 33 % with respect to the pentafluorobenzaldehyde (**57**).



**Scheme 07:** One-pot synthesis of F<sub>5</sub>-BODIPY (**59**).

Single crystals suitable for X-ray diffraction were obtained from chloroform. The formation of single crystals of BODIPYs has recently been reported from acetonitrile.<sup>22</sup>

The crystallographic structure of F<sub>5</sub>-BODIPY (**59**) shows a planar BODIPY moiety and the out of plane pentafluorinated phenyl ring. The phenyl ring is oriented in a 90.01° angle in the solid state with respect to the BODIPY plane, which is an important factor in assuring the high fluorescence of the molecule.

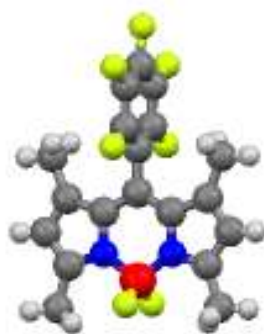


**Figure 34:** Ball and stick representation of the X-ray diffraction structure of F<sub>5</sub>-BODIPY (**59**)

The steric hindrance of the methyl groups along with the more bulky fluorine atoms compared to hydrogen atoms is the mainly the reason for the exact perpendicular orientation. On comparing with a related hydrocarbon analogue like a para bromophenyl-BODIPY where the fluorine atoms are replaced by hydrogen resulted in a decrease of the angle to 78.91° and the dimethylamino analogue showed an angle of 87.61°<sup>23</sup>.

### 2.2.2 S<sub>N</sub>Ar on the perfluorophenyl ring of F<sub>5</sub>-BODIPY (**59**) with thiol and amine conjugates

As described in the introduction, perfluorinated phenyl rings are susceptible to nucleophilic aromatic substitution,<sup>24</sup> offering an effective reaction pathway to C-C, C-S and C-N bond formation. This offers an alternative to metal-catalyzed S<sub>N</sub>2 reactions and introduces a new way of modification to the BODIPY core. The boron center of the BODIPY is in general also able to undergo those kind of modifications. However, as presented in the introduction, relatively harsh conditions need to be applied to make the boron react and activation of either the nucleophile or the boron centre itself is needed. S<sub>N</sub>Ar substitution reactions were tested at room temperature under mild conditions in DMF and advancement of the reaction was followed by HPLC. HPLC traces and reaction schemes are shown in figure 35. As a first trial ethane thiol was tested as a reactant representing a biologically interesting group in terms of labeling due to its presence in many proteins, containing the amino acid cysteine. The reaction took around 45 min at which time full conversion of the starting material was observed. HPLC traces revealed no side products during the reaction which was proven by <sup>19</sup>F-NMR spectroscopy of the crude reaction mixture. The parent molecule showed signals for the aromatic fluorine atoms at -161.9, -153.0 and -143.5 ppm while the substitution product displayed signals at -134.1 and -143.6 ppm. The retention time on the HPLC (cyclohexane /

ethyl acetate, 96 / 4, v/v) for the substitution product was slightly longer (7.7 min) compared to the parent molecule (6.3 min), indicating an increased polarity of **61**.

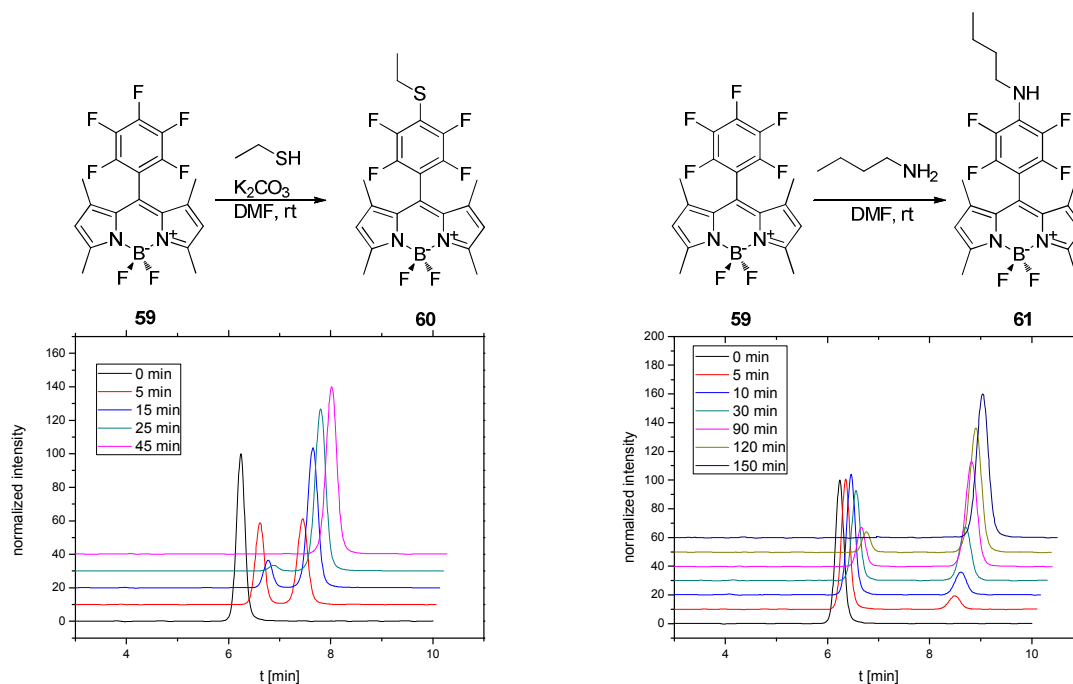


**Figure 35:** Reaction scheme and HPLC traces showing the conversion of F5-BODIPY (**59**) to EtS-BODIPY (**60**) (left) and to BuNH-BODIPY (**61**) (right) after different reaction times recording at 520 nm.

As a second example for a biologically interesting reactive functional group, a primary amine was chosen as a representative for amine bearing amino acids in proteins like lysine. As in the previous experiment, the reaction of **59** with an excess of butyl amine (8 fold) was monitored by means of HPLC. The reaction proved to be slower compared to the substitution with ethane thiol under basic conditions. Equally, no side products were observed. The retention time of the BuNH-BODIPY (**61**) was even longer (8.3 min) which is due to the free hydrogen in the secondary amine. Recording the <sup>19</sup>F-NMR spectrum of the crude reaction mixture displayed fluorine signals at -147.6 and -161.6 ppm indicating the clean substitution in the 4-position of **59**. The parent molecule did not react with diethyl amine at room temperature. Upon heating to 120 °C overnight and using 40 eq. of diethyl amine, the substitution in the *para*-position could be forced towards the substitution product Et<sub>2</sub>N-BODIPY (**62**). Unlike the case with a primary amine, side products were observed and careful purification by column chromatography and crystallization was necessary to obtain the pure product. A direct comparison of the reaction progression of F<sub>5</sub>-BODIPY (**59**) with amines and thiol as judged by the integrated peak areas in the HPLC chromatograms is depicted in figure 36, highlighting the increased reactivity of **59** towards thiols. The reaction of **59** in presence of

ethane thiol (5 eq.) and butylamine (8 eq.) gave quasi-exclusively the thiol product after only 5 min reaction time. This is due to the increased solubility of amine base in DMF compared to  $K_2CO_3$  and therefore more efficient deprotonation of the thiol as shown in figure 36 on the right side.

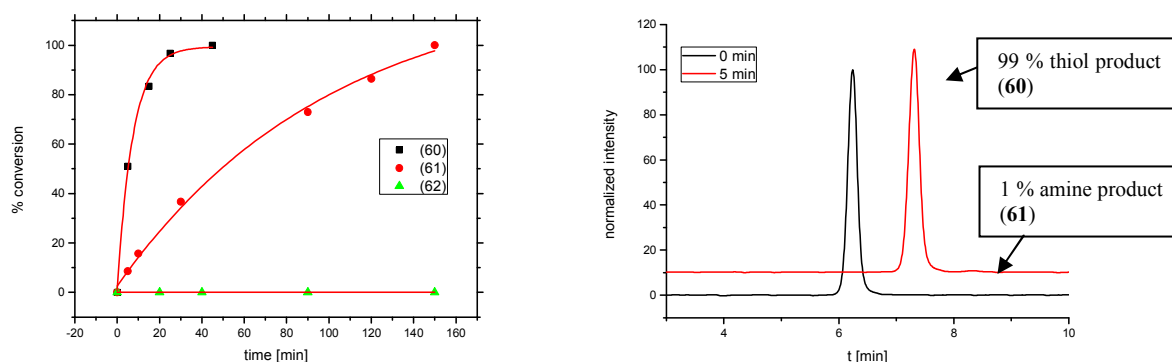


**Figure 36:** left: Direct comparison of the reactivities of F<sub>5</sub>-BODIPY (**59**) with thiol and amine conjugates; right: HPLC-trace of the reaction of **59** with a mixture of ethane thiol and butyl amine recorded at 520 nm.

The selectivity and high reactivity of thiols with the perfluorophenyl moiety under basic conditions has been demonstrated. The reaction of **59** with ethane thiol in DMF without adding a base is much more sluggish and gave a conversion of only 54 % after 5 days at room temperature. In a 1:1 (v/v) mixture of DMF in water conversion proved to be equally efficient regarding the selectivity of thiol over amine. In fact the amine conjugate seemed to be unreactive under these protic conditions. However the reaction proceeded much slower showing a total conversion of 89 % after 27 h. Reaction progression as judged by HPLC peak intensities is shown in figure 37.

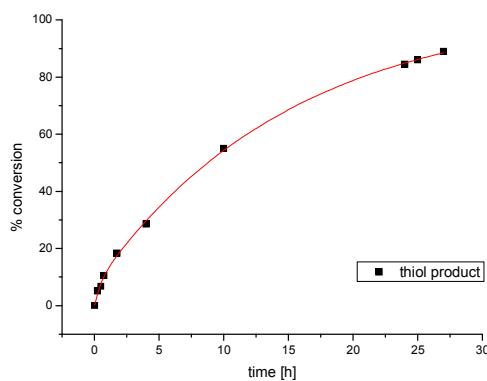


**Figure 37:** Progression of the reaction forming EtS-BODIPY (**60**) in a mixture of DMF:H<sub>2</sub>O (1:1, v/v) using 5 eq of ethane thiol and 8 eq of butyl amine.

In order to improve the reaction rate, additional charged groups like sulfonic acids or carboxylic acids could be incorporated into the BODIPY-skeleton to improve the water solubility, which might ultimately lead to a faster conversion.

### 2.3 Spectroscopical studies of F<sub>5</sub>-BODIPY (**59**) and its substitution products (**60**, **61** and **62**)

The spectral properties of parent BODIPY (**59**) and its substitution products (**60**, **61** and **62**) have been measured in air-equilibrated THF, a relatively polar solvent which efficiently solubilises all the chromophores. The parent molecule shows a high molar extinction coefficient as shown in figure 38. Emission following irradiation at 488 nm occurs with a small Stokes shift of 413 cm<sup>-1</sup>, which is typical for BODIPY fluorophores (ca. 400 cm<sup>-1</sup>). The quantum yield was determined by comparison to a reference standard which was chosen to be fluorescein in 0.1 M NaOH (aq.) with a quantum yield of 0.95.<sup>25</sup> The fluorescein was chosen as reference as it offered a similar absorption and emission range to the molecules under investigation. The quantum yield of BODIPY (**59**) was determined to be 0.98, reaching almost unity. The absorption and emission spectra (figure 38) of the *para*-position substituted BODIPYs are almost unchanging with respect to the parent molecule showing similarly high molar extinction coefficients for the lowest energy band and fluorescence quantum yields (0.90 – 0.96). For better comparison these results are listed in table 04.

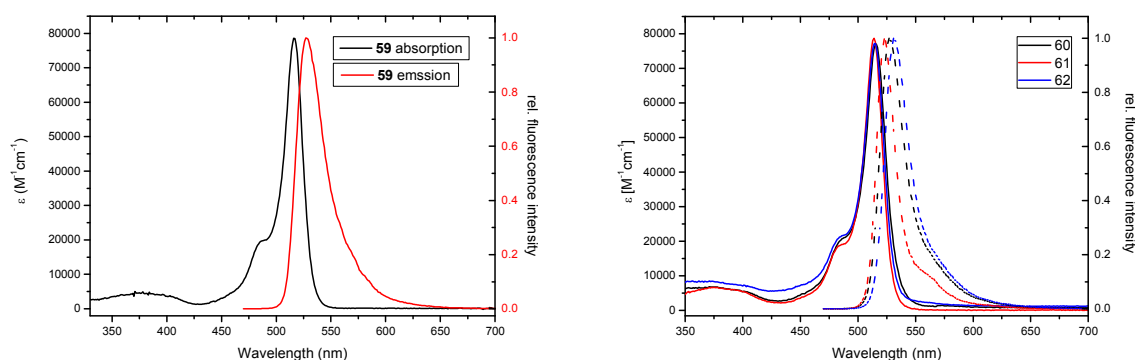


**Figure 38:** Absorption and emission spectra of F<sub>5</sub>-BODIPY (**59**) in air equilibrated THF (left) and of the substitution products EtS-BODIPY (**60**), BuNH-BODIPY (**61**) and Et<sub>2</sub>N-BODIPY (**62**) (right). Emission has been recorded upon irradiation at 465 nm.

The absorption spectra of these fluorophores are almost coincident with widely used argon ion laser, which emits at 514 nm and remote substitution has only a negligible effect on the absorption spectra, making this method for *ad hoc* introduction of the fluorophore a viable alternative to known methods like ester formation where the emission spectra and quantum yield is altered from the acid.<sup>26</sup> Relatively few fluorophores are perfectly adapted for this wavelength and are often expensive like commercially-available “Alexa Fluor 514”.

**Table 04:** Spectral properties of **59** – **62** in air equilibrated THF

Molecule	$\lambda_{\max}$ (nm)	$\epsilon$ ( $M^{-1}cm^{-1}$ )	$\lambda_{em}$ (nm)	$\Phi_f$	$\tau_{calc}$ (ns)	$\tau$ (ns)
<b>59</b>	516	78600	527	0.98	5.8	6.1
<b>60</b>	516	77000	527	0.90	5.4	5.9
<b>61</b>	514	78700	525	0.93	6.1	5.7
<b>62</b>	515	77200	523	0.96	6.0	5.7

Fluorescence lifetimes for molecule **59** – **62** were obtained by time-correlated single photon counting spectrometry. An example of emission from F<sub>5</sub>-BODIPY (**59**) is given in figure 39 showing the photon counting on the left and the fitting of the lifetime and distribution of residuals and the standard deviation on the right.

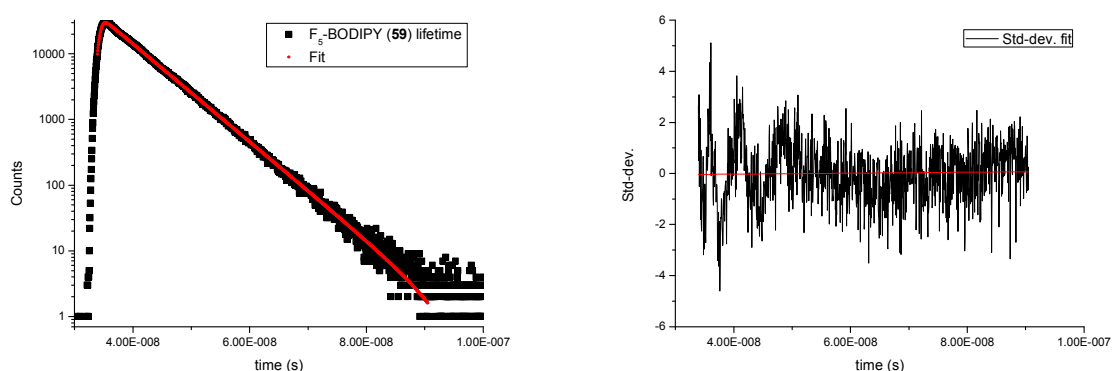


**Figure 39:** Time-correlated single photon counting spectrometry and fitting of the fluorescence lifetime for **59** (left). Residuals of fit in terms of standard deviation for the fitting of the lifetime (right, chi-square: 1.5).

The strongly allowed nature of the  $S_0 \rightarrow S_1$  transition, as denoted by the strong molar extinction coefficients allows estimation of the excited-state lifetime using a Strickler-Berg analysis as denoted in equation 07. In this equation  $n$  is the refractive index of the solvent (assumed to be the same in all spectral regions),  $\langle \nu_F^{-3} \rangle^{-1}$  is the reciprocal of the mean value of

---

the wavenumber ( $\nu^{-3}$ ) across the fluorescence spectrum,  $\epsilon$  is the molar absorptivity and the natural lifetime ( $\tau_{rad}$ ).<sup>27</sup>

$$\frac{1}{\tau_{rad}} = 2.88 \times 10^{-9} n^2 \langle \nu_F^{-3} \rangle^{-1} \int \frac{\epsilon(\nu)}{\nu} d\nu \quad \text{equation 07}$$

Substituting the reciprocal of the natural lifetime ( $k_r$ ) into equation 08 gives estimated fluorescence lifetimes on the nanosecond scale which are in good agreement with the measured values (table 04).

$$k_r = \frac{\phi_f}{\tau_0} \quad \text{equation 08}$$

This suggests that the excited parent and derivatives are all structurally reminiscent to that of the respective ground-state species and that solvent interactions are unchanging.

Fluorescence quantum yields and lifetimes have been measured in a mixture of H<sub>2</sub>O and DMF (75/25, v/v) to show the feasibility of labeling applications and fluorescence measurements in aqueous media. DMF needed to be added to increase the solubility of the test compounds. Similarly high quantum yields have been measured for BODIPY **59** and **60**, which have been determined to be 0.91 with a lifetime of 6.6 ns and 0.93 with a lifetime of 6.6 ns, respectively. Meanwhile, the amine derivative (**61**) exhibits a drastically reduced quantum yield of 1 % presumably due to hydrogen bonding enhanced vibrational quenching. This principle is exploited in BODIPY-based pH sensors carrying amines, for example.<sup>28</sup> Picosecond transient absorption spectroscopy has been employed to follow the evolution of the excited state of parent F<sub>5</sub>-BODIPY (**59**) to elucidate the presence of any dark-state, which could not be detected by classical fluorescence spectroscopy. Population of such a state would present an unwanted alternative to emissive deexcitation and could promote degradation of the molecule. The transient absorption spectrum of the excited state are plotted in figure 40, along with fluorescence and absorption spectra for comparison. The transient absorption spectrum (TRABS, black) resembles the fluorescence emission spectra (FLUO, green) with only minor intensity differences. Two positive transient absorption bands have been observed at 350 nm and 420 nm while a larger negative band appears at 525 nm. By subtracting the fluorescence emission spectra (green) and the absorption spectrum (ABS, red) from TRABS, the excited state spectrum shown in blue is obtained.

---

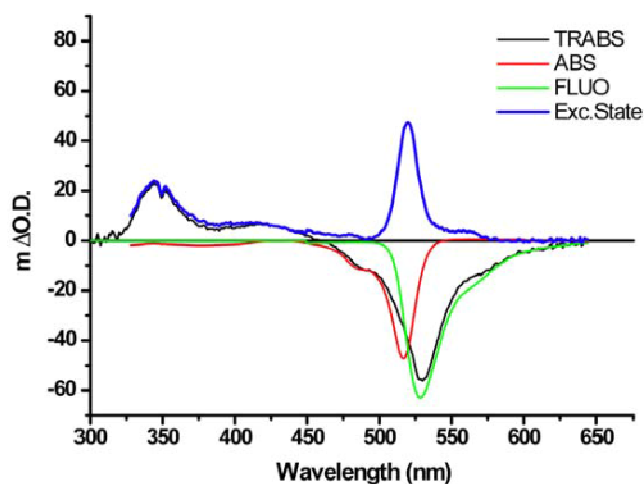


**Figure 40:** Measured transient absorption spectrum (TRABS, black) in THF. Steady-state ground state absorption (red) and steady state fluorescence (green). The excited state spectrum of **59** (blue) was obtained on subtracting absorption, fluorescence/stimulated emission contributions from TRABS ( $\lambda_{\text{exc}} = 510 \text{ nm}$ ).

A similar excited state absorption has been obtained for a multicomponent BODIPY-containing molecule<sup>29</sup>. The excited state spectrum, which is close to the ground state absorption spectrum leads to the conclusion that no significant population of states other than the emissive  $S_1$  state occur.

The quantum yield of photodegradation had been determined taking in account the reaction scheme presented in figure 41. It was assumed that all excited molecules relax to the ground state, as supported by the transient absorption measurements shown earlier, except a small population which is devoted to the quantum yield of photo degradation ( $Q_{\text{Photoproduct}}$ ).

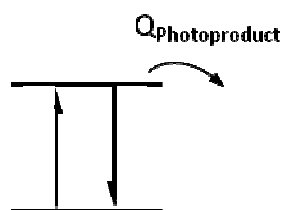


**Figure 41:** Reaction scheme for photodegradation.

As stated by the Stark-Einstein law, each photon absorbed by a chemical system, only one molecule is activated for a following reaction. According to this law of photo equivalence equation 09 can be formulated and shows that the number of molecules excited ( $N_{\text{exc}}$ ) equals the number of photons absorbed ( $K_{\text{abs}}$ ).  $K$  is the incident photon number and can be derived

---

from equation 10 where  $Wt$  is the energy dose in Joules meaning the power by second multiplied by the time. Dividing the energy dose by the Planck constant ( $h$ ) and the wavelength ( $\nu$ ),  $K$  can be obtained.

$$K_{abs} = K(1 - 10^{\epsilon c_0}) = N_{exc} \quad \text{equation 09}$$

$$K = \frac{Wt}{h\nu} \quad \text{equation 10}$$

According to our schematic representation of the reaction scheme (figure 41) a part of the molecules undergoes an irreversible photoreaction or photodegradation with a certain quantum yield ( $Q$ ). This photoreaction yields that the number of molecules which reach the ground state ( $N_{relax}$ ) are less than initially excited and can be expressed in equation 11 and 12

$$N_{relax} = N_{exc} (1 - Q) \quad \text{equation 11}$$

$$N_{relax} - N_{exc} = -N_{exc} Q \quad \text{equation 12}$$

By taking in account equation 12, the changes of the ground state population or the number of molecules in the ground state ( $N_g$ ) in time can be expressed as shown in equation 13. Substituting equation 09 in equation 13 and having in mind the photon flux from equation 10, one obtains for slowly varying steady-state absorption equation 14

$$\frac{dN_g}{dt} = -\frac{dN_{exc}}{dt} Q \quad \text{equation 13}$$

$$\frac{dN_g}{dt} = -K \left( 1 - 10^{-\frac{N_g \epsilon}{V}} \right) Q = -\frac{Wt}{h\nu} \left( 1 - 10^{-\frac{N_g \epsilon}{V}} \right) Q \quad \text{equation 14}$$

Initial condition is  $N_G = N$  at the beginning of the experiment ( $t=0$ ) and  $c_0 = \frac{\epsilon}{V}$  for 1 cm cell.

If the absorption ( $N_G \epsilon / V$ ) of initial solution is small, the exponent in the Taylor series can be developed

$$10^{ax} = e^{x \ln 10} = 1 + x \ln 10 + \dots \quad \text{equation 15}$$

and after insertion into equation 14, equation 16 can be formulated.

---

$$N_G = \exp\left(-\frac{W\varepsilon Q \ln 10}{h\nu V} t\right) \quad \text{equation 16}$$

That corresponds to an exponential relaxation of the ground state population or the steady state absorption with a time constant expressed in equation 17

$$r = \frac{h\nu V}{W\varepsilon Q \ln 10} \quad \text{equation 17}$$

Thus, the quantum yield of the irreversible photoreaction (photodegradation) can be found from the exponential kinetics of a steady state absorption decay upon irradiation as denoted in equation 18.

$$Q = \frac{h\nu V}{W\varepsilon \ln 10 r} \quad \text{equation 18}$$

The quantum yields of photodegradation for molecule **59** – **62** were then determined in air-equilibrated THF by irradiating a stirred solution of the molecule under continuous irradiation at 504 and 512 nm. Photodegradation graphs with corresponding fitting are depicted in figure 42.

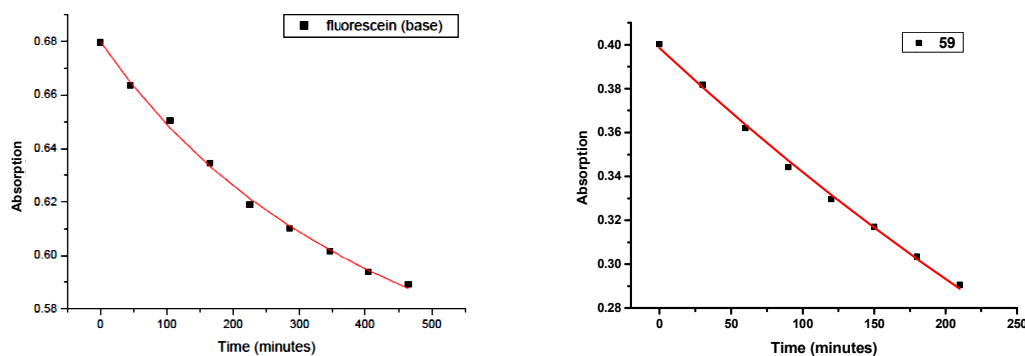


**Figure 42:** Left: Changing absorption at 464 nm accompanying the photodegradation of fluorescein in air-equilibrated ethanol as a function of irradiation time,  $\lambda_{\text{exc}} = 504$  nm. ( $P=3.5\text{mW}$ ). Right: Changing absorption at 515 nm accompanying the photodegradation of F<sub>5</sub>-BODIPY (**59**) in air-equilibrated acetonitrile as a function of irradiation time,  $\lambda_{\text{exc}} = 512$  nm ( $P=3.9$  mW).

The quantum yields for photodegradation ( $Q_{\text{photoproduct}}$ ) were determined to be  $7.5 \times 10^{-5}$  for fluorescein isocyanate which is in the same order of magnitude as a literature value in deoxygenated EtOH.<sup>30</sup> The  $Q_{\text{photoproduct}}$  for molecule **60** - **62** were estimated to be  $2.7 \times 10^{-5}$ ,

---

$4.1 \times 10^{-5}$  and  $2.7 \times 10^{-5}$ , respectively. In general it can be said that these BODIPY chromophores are 2 – 3 times more stable than the fluorescein standard, which makes them an attractive tool in microscopy experiments and eventually studies down to the single molecule level.

### 2.3.1 Single molecule studies of F<sub>5</sub>-BODIPY (**59**) in PMMA

In order to study single molecule emission of BODIPY **59**, it was dispersed in a polymethylenemethacrylate (PMMA) matrix by spin coating from solution onto a glass slide, dried and studied under a continuous flow of N<sub>2</sub> to ensure deoxygenated conditions. For more details about the experimental setup see chapter 7 (experimental). Point-measurements were performed on a single molecule after a first prescan of the sample to localize the molecules. Measuring in time-tagged time resolved (TTTR) mode, emission trajectories and decay times could be obtained. The total number of photons and emission duration before photobleaching, as well as the peak emission intensity of each single molecule after removing the contribution of the background, which consisted of a weak PMMA emission and instrumental background, were measured. Each fluorescence lifetime shown in figure 43 corresponds to the longest lifetime resulting from a biexponential decay.

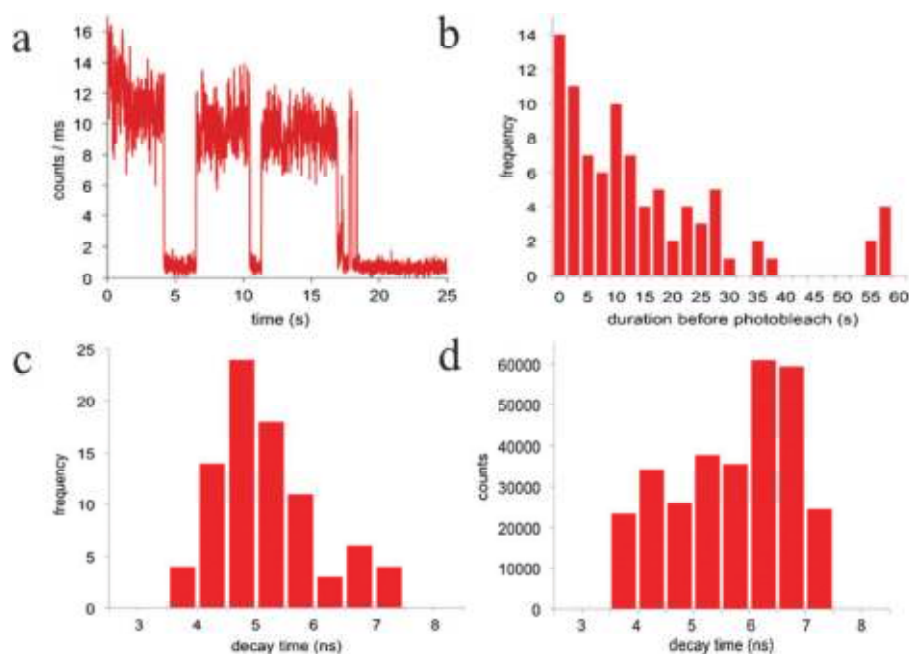


**Figure 43:** Single molecule emission of **59** in PMMA ( $\lambda_{\text{ex}}=488$  nm,  $\lambda_{\text{em}}> 500$  nm): (a) emission trajectory of a single molecule (number of photons detected per ms); (b–d) distribution for 82 single molecules of: the total duration of emission before photobleaching (b); the decay time (c); correlation between the decay time and the average number of counts emitted before photobleaching (d).

Measuring several PMMA sample and emission trajectories of **59** allowed the attribution of the short lifetime component to the PMMA film to residual emission, light scattering or Raman loss and the longest component to **59**. A linearly polarized laser at a standard wavelength of 488 nm ( $1.5 \text{ kWcm}^2$ ) was used. The emission trajectory of a single molecule (figure 43a) shows the blinking of a single molecule correlated to the singlet ON and OFF states. Unlike photobleaching, which is a light-induced chemical reaction and irreversible, blinking of an organic single molecule is reversible (in absence of photobleaching) and occurs in the timescale of several milliseconds to seconds. In the past this process has been attributed to non or low emissive states, such as triplet states,<sup>31</sup> photoisomers<sup>32</sup> or other metastable species (for example geminate radicals or species originating from proton or electron transfer).<sup>33-35</sup> For 50 % of 82 molecules of **1** the peak emission intensity reflecting the brightness was determined to be at least  $5.3 \times 10^3 \frac{\text{photons}}{\text{s}}$  and could reach values up to  $2.9 \times 10^4 \frac{\text{photons}}{\text{s}}$ . These values are in good agreement with an upper limit of  $2.9 \times 10^5 \frac{\text{photons}}{\text{s}}$ .<sup>36</sup> The lower values measured arise from the random orientation of the molecules relative to the excitation beam polarization and the instrumental detection efficiency. From 50 % of the molecules at least  $2.1 \times 10^4$  photons and in the best case up to  $2.4 \times 10^5$  photons have been emitted before photobleaching (figure 44).

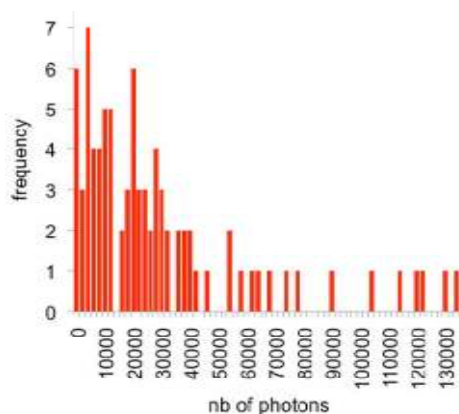


**Figure 44:** Histogram of the total number of photons collected before photobleaching for 82 molecules of F<sub>5</sub>-BODIPY (**59**).

Considering the limitations of system, as mentioned previously, the measured value of  $\frac{1}{Q_{\text{protodproduct}}} = 3.7 \times 10^4$  photons in solution reflects the results obtained in the single molecule studies and is in good agreement with known organic emitters.<sup>36</sup> The emission occurs within 11 seconds for 50 % of the molecules and the duration can reach up to one

---

minute (figure 43b). An exponential decrease in the duration of until photobleaching is observed from 0 to 45 seconds, while a second population of molecules is observed emitting photons longer (55 s – 60 s). The distribution of the decay times of **59** is highlighted in figure 43c. The average lifetime deduced from this experiment is 5.1 ns with a standard deviation of 0.9 ns and a peak at 4.9 ns. This is in accordance with the measured lifetime value of 5.8 ns in bulk solution but somewhat slightly shorter. This could result from an enhanced non-radiative deactivation of the excited states in the polymer environment. As in figure 43b, a second population of single molecules displaying a lifetime of 6.8 ns is observable. By plotting the number of photons emitted over the fluorescence lifetime (figure 43d) it becomes evident that a small number of molecules possessing a longer fluorescence lifetime also emit a higher average number of photons. In a previous study of single molecules in PMMA<sup>37</sup> the same observation has been made and the minor population of molecules had been attributed to molecules embedded in the more rigid micro-environments of PMMA. BODIPY **59** shows therefore some sensitivity to the environment and can respond with a change in fluorescence lifetime and the average number of photons emitted while preserving suitable emissive properties.

## 2.4 Conclusion

Selective functionalization of a perfluorophenyl bearing BODIPY (**59**) has been shown and selective labeling with thiols over amines has been accomplished via C-N and C-S bond formation. These photostable conjugates show strong absorption and emission in organic solvents. In aqueous mixtures, high selectivity for reaction with thiols conspires with a 90-fold higher quantum yield of the corresponding conjugate (EtS-BODIPY (**60**) cf. BuNH-BODIPY (**61**)), which makes the thiol conjugate especially attractive for the labeling of amino acids in proteins. Indeed, this corresponds to a circa  $10^4$  contrast on a  $-\text{NH}_2$  versus  $-\text{SH}$  site basis. In principle, perfluorophenyl chemistry can be exploited for other fluorophores in the same fashion it has been presented here. Another application could be the labeling of surface using the perfluorophenyl BODIPY **59** to introduce in a simple fashion functional groups, which can be used for example in surface patterning applications which is presented in the following section.

---

## 2.5 Perspectives and preliminary results of photoinduced surface patterning using an azide-BODIPY (**63**) and click chemistry

Due to the high photostability and unique reactivity of the F<sub>5</sub>-BODIPY (**59**) several applications can be envisaged. Here some preliminary results obtained for perfluorophenylazide-BODIPY based on the molecular structure of F<sub>5</sub>-BODIPY (**59**) in the application of photoinduced surface patterning are presented. Several click and click-like reactions are known to date. Here a short introduction to photoinduced click-like reactions and application in surface patterning is given. For example, in the group of Barner-Kowollik<sup>38</sup> the photoreaction between a maleimide unit and a 2-formyl-3-methylphenoxy (FMP) group has been exploited to immobilize a bromide-bearing maleimide derivative on silicon wafers functionalized with FMP. A photomask was applied so that a pattern was produced on the surface upon irradiation of a FMP surface at 320 nm in a solution containing the brominated maleimide. The most prominent example for click reactions is the cycloaddition of an azide to an alkyne which was developed in the groups of Sharpless<sup>39</sup> and Meldal<sup>40</sup>. The approach of an photoinduced generation of an Cu<sup>I</sup> using a photoinitiator to generate the cycloadduct with spatial resolution has been shown in the group of Bowman.<sup>41</sup> A Cu<sup>II</sup> pre-catalyst in a solution containing polyethylene glycol (PEG)-alkyne was irradiated in the UV in the presence of a photoinitiator on the surface of an azide-functionalized polypropylene on a silicon substrate. By using a photomask, spatial patterning of the cycloadduct was achieved. A schematic representation of the process is given in figure 45

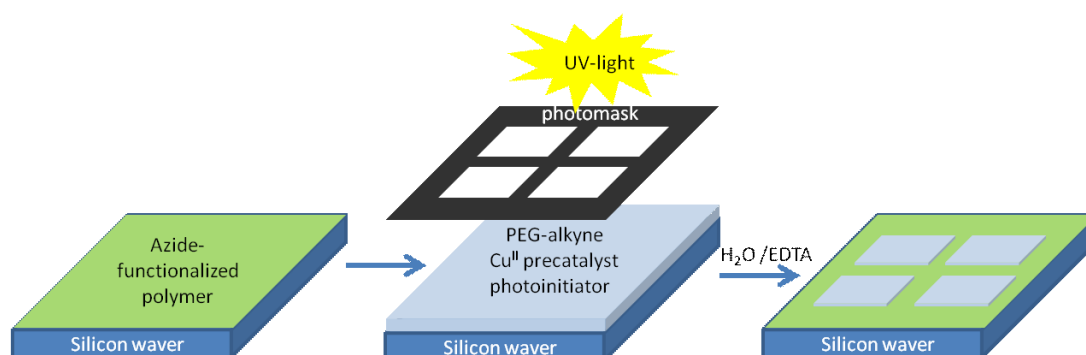


**Figure 45:** Photoinduced patterning of a PEG-based hydrogel onto an azide-functionalized polypropylene using a photomask.

Perfluorophenyl azides have also been used for the direct surface modification of polymer films.<sup>42</sup> Therefore the reactivity of the azide group, namely formation of a nitrene and incorporation into C-H bonds or addition to olefins upon irradiation was used to attach them

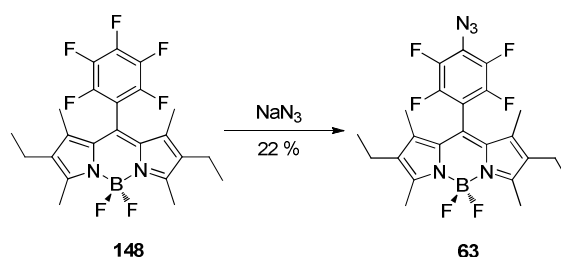
---

---

covalently to the polymer film. A last example which excludes the use of light but achieves the patterning of a surface without the use of a mask is shown in the group of Stoddart.<sup>43</sup> An atomic force microscopy tip was coated with copper and alkynes in a solution on top of an azide-functionalized surface was patterned by writing the desired pattern via moving the AFM needle over the surface. The approach taken in this preliminary study is a combination of the photoinduced click reaction on surfaces and the “writing” of a pattern on a surface.

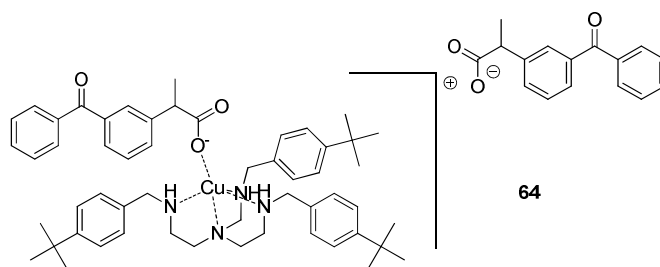
### 2.5.1 Chemistry of azide-BODIPY (**63**) and photoinduced click reaction in solution

The synthesis of the azide-BODIPY (**63**) was straightforward starting from the perfluorinated BODIPY intermediate (**148**) shown in chapter 5. The azide in the *para*-position of the perfluorophenyl ring was introduced by reacting **148** with a 3-fold excess of NaN<sub>3</sub> in DMF at room temperature as shown in scheme 08. The product was obtained after purification via column chromatography in 22 % yield. The reaction conditions were however not optimized.



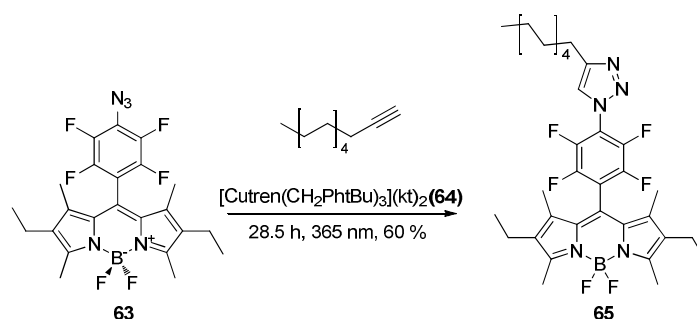
**Scheme 08:** Synthesis of azide-BODIPY (**63**)

The photoinduced click-reaction was tested using the photoreducible copper(II)-tren complex (**64**) developed in the group of Vincent and published in several papers by Harmand *et.al.*<sup>44,45</sup> The photolabile catalyst was kindly provided by the group and the molecular structure is shown in scheme 09. Upon irradiation in the UV the ketoprofenate provokes a monoelectronic oxidation of the ligand due to the quenching of the triplet state via charge transfer. The ligand abstracts then a proton from the solvent leading overall to an reduced metalcomplex, a protonated ligand and a hydroxyl radical. It has been shown that the catalyst can be activated by UV light and stopped by purging the reaction with oxygen leading to an oxidized metal center. The click-reaction could be restarted after depletion of oxygen upon irradiation in the UV.



**Scheme 09:** Molecular structure of the photoreducible copper(II)-tren complex [Cutren(CH<sub>2</sub>PhtBu)<sub>3</sub>](kt)<sub>2</sub>, **64**. kt = ketoprofenate.

In a first test, the reaction between azide-BODIPY (**63**) and dodec-1-yne was tested in solution using [Cutren(CH<sub>2</sub>PhtBu)<sub>3</sub>](kt)<sub>2</sub> (**64**) (see scheme 10). All reactants and the catalyst were dissolved in toluene, deoxygenated by argon bubbling and irradiated for 28.5 h at 365 nm using a classical TLC lamp. By that time the reaction had proceeded to 78 % completion, and was stopped and purified. The reaction product was obtained in 60 % yield after column chromatography. The reaction scheme leading to the click-product triazole-BODIPY (**65**) is shown in scheme 10. The reaction proceeded rather slow most likely due to the larger extinction coefficient of the BODIPY fluorophore ( $52\,000\text{ cm}^{-1}\text{M}^{-1}$ )<sup>46</sup> and therefore much less incident light reaches the catalyst.



**Scheme 10:** Click-reaction between azide-BODIPY (**63**) and dodec-1-yne catalysed by photolabile copper catalyst [Cutren(CH<sub>2</sub>PhtBu)<sub>3</sub>](kt)<sub>2</sub> (**64**).

In principle it has been shown that the cycloaddition between azide-BODIPY (**63**) and a terminal alkyne can be catalysed by [Cutren(CH<sub>2</sub>PhtBu)<sub>3</sub>](kt)<sub>2</sub> (**64**). The reaction yield was sufficient for some proof-of-principle experiments to pattern the azide bearing BODIPY onto alkyne-functionalized surfaces. In order to verify that the click product is still fluorescent and at an observable wavelength range, electronic absorption and emission spectra of **65** were recorded in ethanol and the graphs are shown in figure 46.

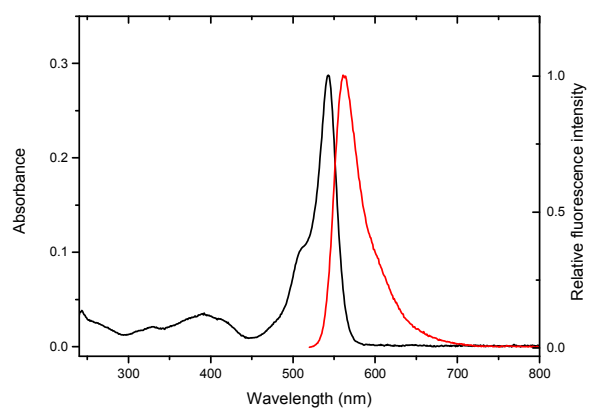


**Figure 46:** Absorption and emission spectra of the click-product in THF ( $\lambda_{\text{exc}} = 510 \text{ nm}$ ) (**65**).

The absorption maximum can be found at 543 nm and the emission occurs with a typically small Stokes shift of BODIPY fluorophores at 561 nm. An extinction coefficient of  $57\,000 \text{ M}^{-1} \text{ cm}^{-1}$  has been measured and is only a little lower than previously mentioned BODIPY dyes (**59 – 62**).

---

## 2.5.2 Surface patterning using azide-BODIPY (**63**) and [Cutren(CH<sub>2</sub>PhtBu)<sub>3</sub>](kt)<sub>2</sub> (**64**)

A precise description of the confocal fluorescence microscope setup used for the experiment is given in the experimental section. Low density (LD, 10<sup>9</sup> – 10<sup>10</sup> alkynes/cm<sup>2</sup>) and high density (HD, 10<sup>14</sup> alkynes/cm<sup>2</sup>) on polyethylene glycol coated glass surfaces were purchased from Micro Surface Inc. (<http://www.proteinslides.com>) and used as bought. The surface patterning process is described in figure 47.

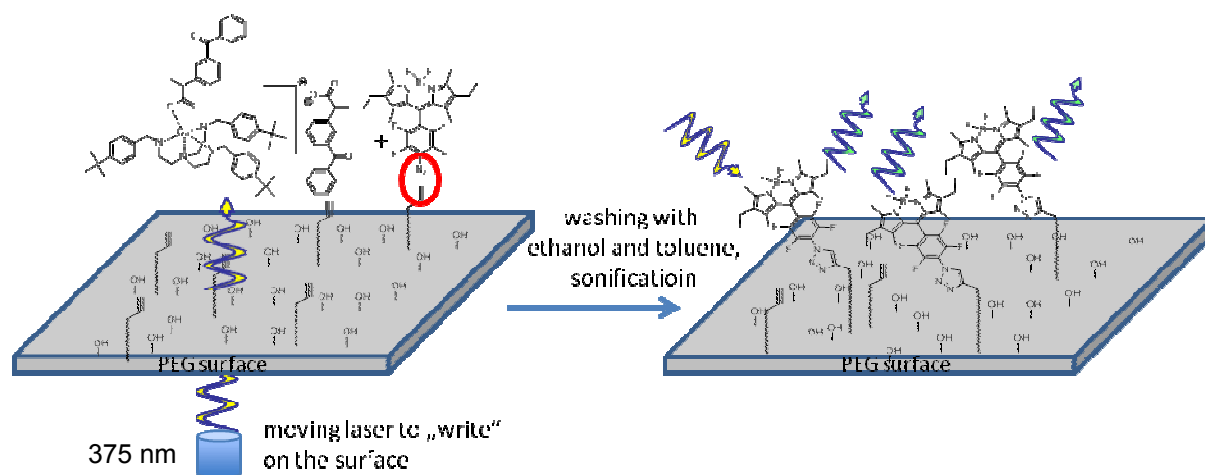


**Figure 47:** Schematic representation of the surface patterning procedure using a solution containing 50 mM azide-BODIPY (**63**) and 1 mM [Cutren(CH<sub>2</sub>PhtBu)<sub>3</sub>](kt)<sub>2</sub> (**64**) in toluene.

A solution containing 50 mM azide-BODIPY (**63**) and 1 mM [Cutren(CH<sub>2</sub>PhtBu)<sub>3</sub>](kt)<sub>2</sub> (**64**) in toluene was placed on top of the alkyne-coated surface. Irradiation was performed from the bottom of the coated glass cover slide with a 375 nm laser source. After irradiation the solution containing the azide (**63**) and the catalyst (**64**) were removed and the coated glass cover slide was cleaned via 3 cycles of sonication in ethanol using a classical ultrasound bath. Subsequently, the process was repeated in toluene. The now BODIPY (**63**) - functionalized fluorescent glass surface was observed via confocal microscopy using the observation setup described in figure 48.

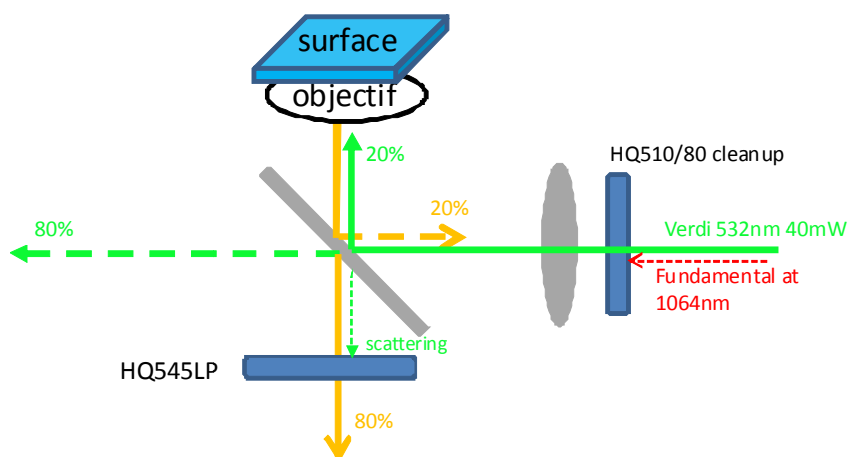


**Figure 48:** Scheme of the confocal microscopy setup used to observe the surfaces.

A frequency doubled 1064 nm CW-laser was used to obtain the 532 nm excitation. In order to cut the fundamental wavelength at 1064 nm a G70-550 bandpass filter was used to let only incident 532 nm light pass. The laser was directed to a dichroic mirror, which reflects 20 % of the light towards the sample objective. 80 % of the emitted light from the sample was passed through a HQ545 long-pass filter, which cuts off the scattered light from the irradiation beam.

The first experiment conducted was the irradiation of a low density surface covered with the previously mentioned solution containing 50 mM azide-BODIPY (**63**) and 1 mM [Cutren(CH<sub>2</sub>PhtBu)<sub>3</sub>](kt)<sub>2</sub> (**64**) in toluene. A photomask was applied over half the surface and the sample was irradiated for 1 h at 365 nm using a TLC lamp. After cleaning the surface according to the described procedure the LD-surface was observed in the confocal microscope. The obtained image was compared to a LD-surface untreated directly from the stock (figure 49).

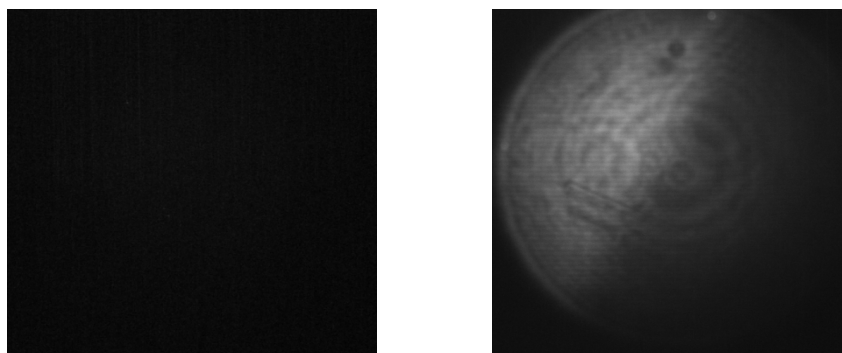


**Figure 49:** Left: Confocal microscopy image (800 x 800 μm, 10x objective) of the alkyne- functionalized surface (LD) fresh from the box. Right: Confocal microscopy image of the cleaned surface after irradiating at

365 nm in the presence of azide-BODIPY (**63**) and [Cutren(CH<sub>2</sub>PhtBu)<sub>3</sub>](kt)<sub>2</sub> (**64**) in toluene while covering half the surface with a photomask.

The first observation is that the fresh LD-surfaces show almost no fluorescence background resulting from impurities or defects on the surface, see figure 49 left. However, the LD-surface that was subjected to irradiation shows a clear stepwise increase of the intensity with higher fluorescence on the irradiated side and a side with lower fluorescence corresponding to the position of the photomask. It should be noted that a certain fluorescence intensity is also seen on the non-irradiated part of the surface due to the incubation with fluorophore. The difference in fluorescence is nevertheless specific.

In following step a new LD-surface was used and covered with a toluene solution of azide (**63**) and catalyst (**64**). In figure 50 the conducted experiment is described on the left side and the obtained fluorescence lifetime imaging microscopy (FLIM) image is shown on the right. A laser beam at 375 nm with a power of 400 au (corresponding to nW +/- 5%) was used to “write” squares with a size of 20 x 20 μm, on the surface. Four patterns were produced by scanning the same area several times with the same constant speed of 1.2 ms/pixel of 100 mm of a constant CW power of 400 nW. The scanning pattern is shown in figure 50 The brighter corners correspond to scanner parking. The FLIM images on the right side of figure 50 show the fluorescence intensity in terms of brightness as well as the fluorescence lifetime of the emitted light. First it is seen that an increased the number of passages results in a brighter fluorescence emission with a maximum at 3 passages.

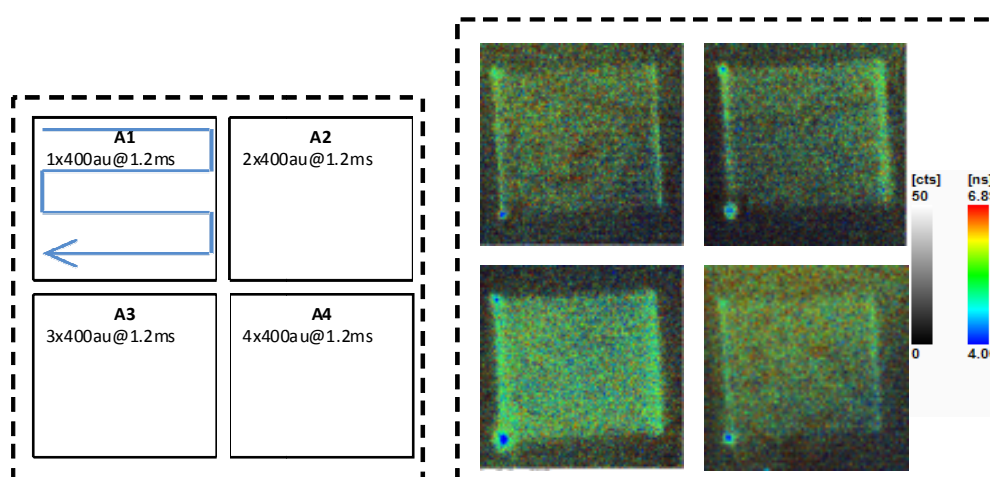


**Figure 50:** Left: A summary of the experiment conducted, indicating the number of passages, laser power and duration of irradiation time per/pixel at 375 nm. Right: Confocal microscopy image of the conducted experiment after washing (LD surface). Images obtained by scanning the surface with the observation setup shown in figure 48 with a speed of 1.248 ms/pixel.

An additional passage seems not to further increase the fluorescence emission even though that needs to be considered with care since some non-coplanarity of the substrate vs scanner leads to a loss in intensity as well. The fluorescence lifetime is in the range of 5 ns as expected of BODIPY fluorophores. At the point where the irradiation started a shorter lifetime of around 4 ns is observed with much higher intensity, which will be discussed later on.

A similar experiment was conducted using the high-density alkyne functionalized surface (HD-surface) mentioned above. Again 4 squares ( $20\ \mu\text{m} \times 20\ \mu\text{m}$ ) were patterned on the surface using a confocal laser beam at 375 nm. In addition to the 4 squares, a series of 8 points with increasing irradiation times per point were patterned with a laser power of 400 nW (left to right) and 10000 nW (top to bottom) as described in figure 51 (left). The obtained image showing intensity and fluorescence lifetime is depicted in figure 51 (right). Unlike in the previous experiment, the laser power was varied for the squares rather than the number of passages. 400 nW (top left), 1000 nW (top right), 5000 nW (bottom left) and 10000 nW (bottom right) were used to prepare the squares with a passage time of 1.2 ms/pixel at 375 nm. After the described washing procedure the surface was observed under the confocal microscope.

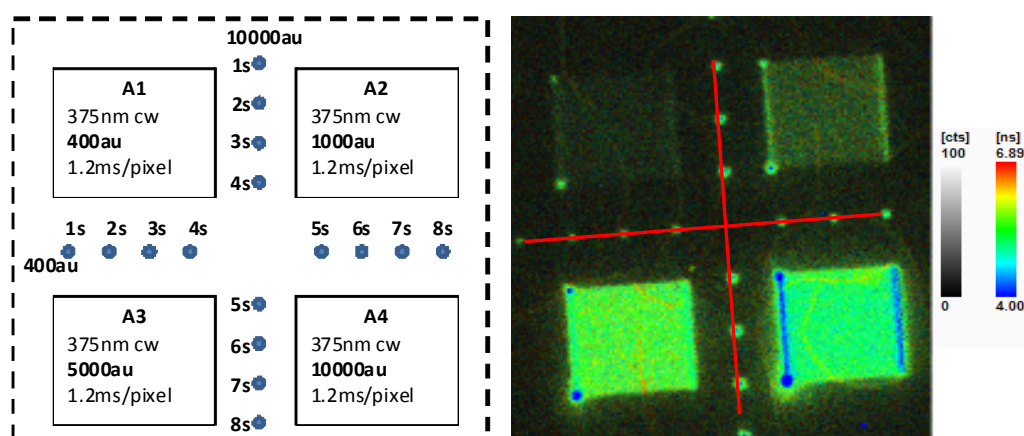


**Figure 51:** Left: A summary of the experiment conducted indicating laser power, wavelength and duration of irradiation time per/pixel. Right: Confocal FLIM image of the conducted experiment after washing (HD surface). Images obtained by scanning the surface with the observation setup shown in figure 48 with a speed of 0.600 ms/pixel.

In the fluorescence image it is visible that the increasing laser power yields an increase in fluorescence on the HD-surface. Laser powers between 5000 and 10000 nW yield very bright squares with respect to the background. The square produced with a laser power of 1000 nW shows a brighter fluorescence at the edges of the square where the laser changed its direction and therefore stayed longer in place. The characteristic shortening of the lifetime in the corner where the irradiation started is present on the HD-surfaces as well. The square produced with 10000 a.u. even shows the shorting of the lifetime along the whole edge. A explanation could be a secondary photoreaction which occurs in places with longer irradiation times which is not surprising since the perfluorophenyl azide unit is photoactive on its own and forms reactive nitrenes upon irradiation.<sup>47</sup> Analysis of the fluorescence intensity of the point series with 400 and 10000 nW and increasing irradiation times is given in figure 52.

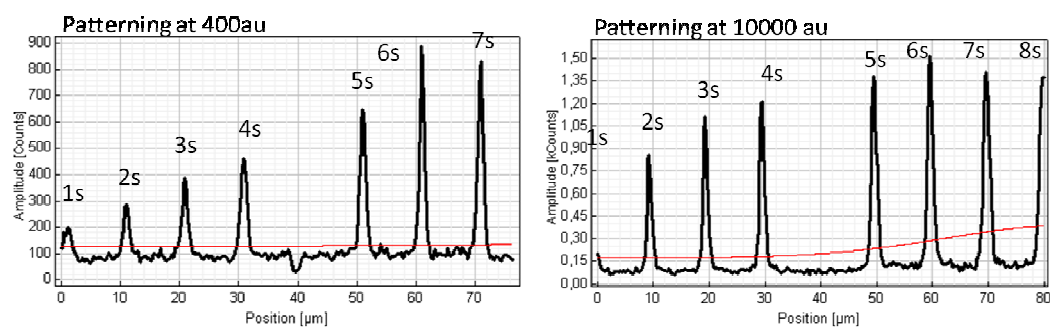


**Figure 52:** Left: Fluorescence intensities of points created with 400 nW laser power. Right: Fluorescence intensities of points created with 10000 nW laser power. Image obtained by scanning the surface with the observation setup shown in figure 48 with a speed of 0.600 ms/pixel.

For the points prepared with 400 nW, 375 nm irradiation the fluorescence intensity increases almost linearly with increasing irradiation times. No further signal increase is noted for the point at 7 s. The dots prepared with 10000 nW. show an increase until 6 s of irradiation, where they reach saturation and no further increase is noted anymore.

Since the spatial resolution of the surface patterning should involve the diffusion of catalyst (**64**) and azide, a solution of 50 mM azide-BODIPY (**63**) and 1 mM [Cutren(CH<sub>2</sub>PhtBu)<sub>3</sub>](kt)<sub>2</sub> (**64**) was prepared in cyclohexanol which is a rather viscous solvent (41.07 mPa.s). The experiment was then conducted using the previously described procedure, covering the HD-surface with the azide / catalyst mixture and preparing squares and points via irradiation at 375 nm in the confocal volume. The plan of the experiment is shown in figure 53 on the left.

The laser power was varied for the 4 squares using 400 nW (top left), 1000 nW (top right), 5000 nW (bottom left) and 10000 nW (bottom right). All squares were prepared by scanning the laser at 375 nm over the square area with a speed of 1.2 ms/pixel. In between the squares several points have been patterned using 400 nW (top line from left to right) increasing the irradiation time from 1 to 13 s, 1000 nW (bottom from left to right) increasing the irradiation time from 1 to 13 s and 5000 nW (top to bottom) increasing the irradiation time from 1 to 12 s. The obtained image after the washing procedure is shown in the middle for figure 53. The obtained image was, despite the higher viscosity of the solvent, unexpectedly rather blurry. The square obtained with 400 nW is not visible in this experiment. Between the square obtained at 1000 nW and 5000 nW an increase in fluorescence intensity is noted along with a shorter lifetime at the corner of the square. The square obtained with 10000 nW irradiation shows a shortened lifetime for the whole square area and a reduced fluorescence intensity.

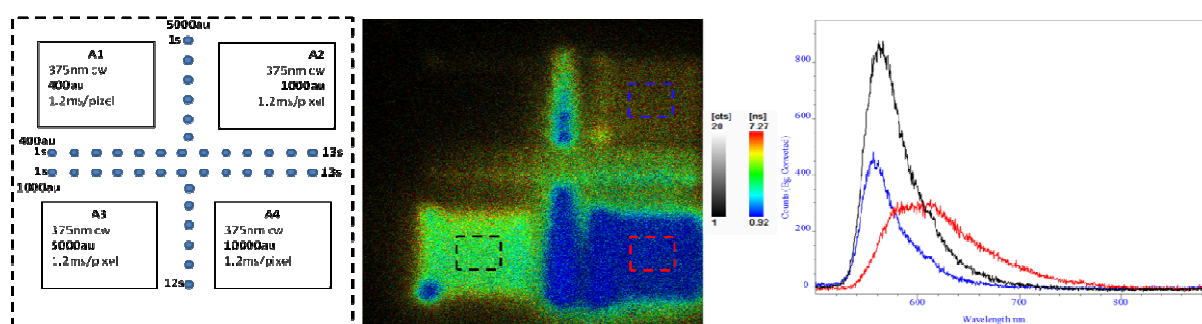


**Figure 53:** Left: A summary of the experiment conducted indicating laser power, wavelength and duration of irradiation time per/pixel. Middle: Confocal fluorescence microscopy image of the conducted experiment after washing (HD surface). Right: Fluorescence emission spectra obtained from surface top right, bottom left and bottom right. The colours of the curve correspond to the colours of the squares shown in the image.

The points in this experiment are not sufficiently well-resolved to allow a single analysis by intensity profiles. The points obtained from top to bottom using a laser power of 5000 nW show a shortening of the lifetime between approximately 3 and 4 s irradiation time. The fluorescence emission spectra of the square obtained with 1000 and 5000 nW show the unaltered emission spectra of the BODIPY (65). The emission spectra of the square obtained with 10000 nW irradiation, where the lifetime is tremendously shortened also shows a different emission spectra with a non-negligible red shift, which supports the hypothesis that the shortening of lifetime correlates to the formation of a photoproduct or the growth of a second band. Overall it can be said that the resolution of the pattern become worse in

---

cyclohexanol and the fluorescence intensity decreases with increase in irradiation time, which is the opposite effect as observed in toluene.

## 2.6 Summary

In summary, an application for the perfluorinated BODIPY fluorophore has been shown harnessing the facile introduction of an azide group in para-position of the perfluorophenyl ring. Proof-of-principle results have been obtained for surface patterning by means of photolithography using this azido-BODIPY dye (**63**) in concert with a photoactivatable Cu(II)-precatalyst (**64**). The straightforward micrometre-resolution patterning on the surface using confocal laser excitation without recourse to a photomask shows a distinct advantage over many known systems.

The system depends on many parameters. Increasing viscosity seems to decrease the resolution while the increase of the excitation power leads to more intense labeling in toluene and to photobleaching in cyclohexanol. Longer irradiation times lead to more patterning in toluene but to photobleaching in cyclohexanol, leading to the assumption that the diffusion parameter is indeed not yet understood and further studies need to be conducted. The presence of oxygen is another factor which seems to inhibit the patterning process completely (experiment not shown).

---

## References

- (1) Treibs, A.; Kreuzer, F. H. *Annalen Der Chemie-Justus Liebig* **1968**, *718*, 208.
- (2) Schmitt, A.; Hinkeldey, B.; Wild, M.; Jung, G. *Journal of Fluorescence* **2009**, *19*, 755.
- (3) Tram, K.; Yan, H. B.; Jenkins, H. A.; Vassiliev, S.; Brucec, D. *Dyes Pigm.* **2009**, *82*, 392.
- (4) Arroyo, I. J.; Hu, R. R.; Merino, G.; Tang, B. Z.; Pena-Cabrera, E. *J. Org. Chem.* **2009**, *74*, 5719.
- (5) Loudet, A.; Burgess, K. *Chem. Rev.* **2007**, *107*, 4891.
- (6) Boyer, J. H.; Haag, A. M.; Sathyamoorthi, G.; Soong, M. L.; Thangaraj, K.; Pavlopoulos, T. G. *Heteroat. Chem.* **1993**, *4*, 39.
- (7) Li, Z. G.; Mintzer, E.; Bittman, R. *J. Org. Chem.* **2006**, *71*, 1718.
- (8) Lee, J. J.; Lee, S. C.; Zhai, D. T.; Ahn, Y. H.; Yeo, H. Y.; Tan, Y. L.; Chang, Y. T. *Chem. Commun.* **2011**, *47*, 4508.
- (9) Niu, S. L.; Massif, C.; Ulrich, G.; Ziessel, R.; Renard, P. Y.; Romieu, A. *Org. Biomol. Chem.* **2011**, *9*, 66.
- (10) Leen, V.; Leemans, T.; Boens, N.; Dehaen, W. *Eur. J. Org. Chem.* **2011**, 4386.
- (11) Baruah, M.; Qin, W. W.; Vallee, R. A. L.; Beljonne, D.; Rohand, T.; Dehaen, W.; Boens, N. *Org. Lett.* **2005**, *7*, 4377.
- (12) Dost, Z.; Atilgan, S.; Akkaya, E. U. *Tetrahedron* **2006**, *62*, 8484.
- (13) Worries, H. J.; Koek, J. H.; Lodder, G.; Lugtenburg, J.; Fokkens, R.; Driessen, O.; Mohn, G. R. *Recueil Des Travaux Chimiques Des Pays-Bas-Journal of the Royal Netherlands Chemical Society* **1985**, *104*, 288.
- (14) Jiao, L. J.; Yu, C. J.; Li, J. L.; Wang, Z. Y.; Wu, M.; Hao, E. H. *J. Org. Chem.* **2009**, *74*, 7525.
- (15) Zhu, S. L.; Bi, J. H.; Vegesna, G.; Zhang, J. T.; Luo, F. T.; Valenzano, L.; Liu, H. Y. *Rsc Advances* **2013**, *3*, 4793.
- (16) Shah, M.; Thangaraj, K.; Soong, M.-L.; Wolford, L. T.; Boyer, J. H.; Politzer, I. R.; Pavlopoulos, T. G. *Heteroat. Chem.* **1990**, *1*, 389.
- (17) Rousseau, T.; Cravino, A.; Ripaud, E.; Leriche, P.; Rihn, S.; De Nicola, A.; Ziessel, R.; Roncali, J. *Chem. Commun.* **2010**, *46*, 5082.
- (18) Tahtaoui, C.; Thomas, C.; Rohmer, F.; Klotz, P.; Duportail, G.; Mely, Y.; Bonnet, D.; Hibert, M. *J. Org. Chem.* **2007**, *72*, 269.
- (19) Goze, C.; Ulrich, G.; Mallon, L. J.; Allen, B. D.; Harriman, A.; Ziessel, R. *J. Am. Chem. Soc.* **2006**, *128*, 10231.
- (20) Kempe, K.; Krieg, A.; Becer, C. R.; Schubert, U. S. *Chem. Soc. Rev.* **2012**, *41*, 176.
- (21) Hori, T.; Osuka, A. *Eur. J. Org. Chem.* **2010**, 2379.
- (22) Zhou, X. F. *Acta Crystallographica Section E-Structure Reports Online* **2010**, *66*, O757.
- (23) Wang, D. C.; He, C.; Fan, J. L.; Huang, W. W.; Peng, X. J. *Acta Crystallographica Section E-Structure Reports Online* **2007**, *63*, O2900.
- (24) Becer, C. R.; Hoogenboom, R.; Schubert, U. S. *Angew. Chem. Int. Ed.* **2009**, *48*, 4900.
- (25) Brannon, J. H.; Magde, D. *J. Phys. Chem.* **1978**, *82*, 705.
- (26) Song, A. M.; Zhang, J. H.; Zhang, M. H.; Shen, T.; Tang, J. A. *Colloids and Surfaces a-Physicochemical and Engineering Aspects* **2000**, *167*, 253.
- (27) Strickler, S. J.; Berg, R. A. *J. Chem. Phys.* **1962**, *37*, 814.

- 
- (28) Qi, X.; Kim, S. K.; Jun, E. J.; Xu, L.; Kim, S. J.; Yoon, J. *Bull. Korean Chem. Soc.* **2007**, *28*, 2231.
- (29) Puntoriero, F.; Nastasi, F.; Campagna, S.; Bura, T.; Ziessel, R. *Chemistry-a European Journal* **2010**, *16*, 8832.
- (30) Meallier, P.; Guittonneau, S.; Emmelin, C.; Konstantinova, T. *Dyes Pigm.* **1999**, *40*, 95.
- (31) Yip, W. T.; Hu, D. H.; Yu, J.; Vanden Bout, D. A.; Barbara, P. F. *J. Phys. Chem. A* **1998**, *102*, 7564.
- (32) Peterman, E. J. G.; Brasselet, S.; Moerner, W. E. *J. Phys. Chem. A* **1999**, *103*, 10553.
- (33) Zondervan, R.; Kulzer, F.; Orlinskii, S. B.; Orrit, M. *J. Phys. Chem. A* **2003**, *107*, 6770.
- (34) Liu, R. C.; Holman, M. W.; Zang, L.; Adams, D. M. *J. Phys. Chem. A* **2003**, *107*, 6522.
- (35) Holman, M. W.; Liu, R. C.; Adams, D. M. *J. Am. Chem. Soc.* **2003**, *125*, 12649.
- (36) Moerner, W. E.; Fromm, D. P. *Rev. Sci. Instrum.* **2003**, *74*, 3597.
- (37) Hou, Y. W.; Bardo, A. M.; Martinez, C.; Higgins, D. A. *J. Phys. Chem. B* **2000**, *104*, 212.
- (38) Pauloehrl, T.; Delaittre, G.; Winkler, V.; Welle, A.; Bruns, M.; Borner, H. G.; Greiner, A. M.; Bastmeyer, M.; Barner-Kowollik, C. *Angew. Chem. Int. Ed.* **2012**, *51*, 1071.
- (39) Rostovtsev, V. V.; Green, L. G.; Fokin, V. V.; Sharpless, K. B. *Angew. Chem. Int. Ed.* **2002**, *41*, 2596.
- (40) Tornøe, C. W.; Christensen, C.; Meldal, M. *J. Org. Chem.* **2002**, *67*, 3057.
- (41) Adzima, B. J.; Tao, Y. H.; Kloxin, C. J.; DeForest, C. A.; Anseth, K. S.; Bowman, C. N. *Nature Chemistry* **2011**, *3*, 256.
- (42) Yan, M. D.; Ren, J. *Chem. Mater.* **2004**, *16*, 1627.
- (43) Paxton, W. F.; Spruell, J. M.; Stoddart, J. F. *J. Am. Chem. Soc.* **2009**, *131*, 6692.
- (44) Harmand, L.; Lescure, M. H.; Candelon, N.; Duttine, M.; Lastecoueres, D.; Vincent, J. M. *Tetrahedron Lett.* **2012**, *53*, 1417.
- (45) Harmand, L.; Cadet, S.; Kauffmann, B.; Scarpantonio, L.; Batat, P.; Jonusauskas, G.; McClenaghan, N. D.; Lastecoueres, D.; Vincent, J. M. *Angew. Chem. Int. Ed.* **2012**, *51*, 7137.
- (46) Galangau, O.; Dumas-Verdes, C.; Meallet-Renault, R.; Clavier, G. *Org. Biomol. Chem.* **2010**, *8*, 4546.
- (47) Liu, L. H.; Yan, M. D. *Acc. Chem. Res.* **2010**, *43*, 1434.
-

---

---

---

---

---

### **3 Synthesis and characterisation of fluorescent $\text{Ca}^{2+}$ - sensors and photolabile $\text{Ca}^{2+}$ -decaging agents**

---

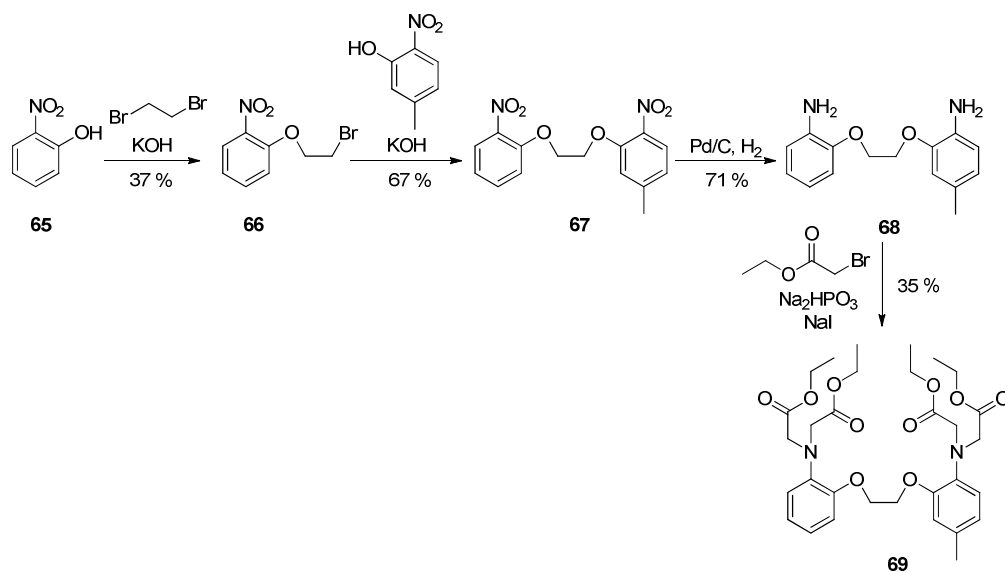
---

As previously outlined, one final goal of the project is the demonstration of ion transfer between nano-objects in confined compartment to mimic rudimentary cellular communication. In the general introduction some fluorescent ion sensors and photolabile ion ejectors were described. In chapter 1 the properties of BODIPY fluorophores were discussed and a novel fluorophore based on a perfluorophenyl moiety bearing BODIPY has been introduced. In this chapter the focus lies on the design of a fluorescent ion switch based on a BODIPY fluorophore, harnessing the unique spectral properties of this molecular unit and combining it with an ion-sensor. Equally, the design of amphiphilic photo-decaging molecules is presented using a  $\text{Ca}^{2+}$ -chelator and subsequently, on combining these functional molecules ion transfer is established under pseudo physiological conditions with micromolar concentrations of calcium.

### 3.1 Synthesis and spectral studies of water soluble $\text{Ca}^{2+}$ -sensors based on BAPTA and BODIPY

#### 3.1.1 Synthesis of BAPTA-BODIPYs (**72** and **76**)

The BAPTA binding unit was chosen for its high affinity constant and selectivity towards  $\text{Ca}^{2+}$  over  $\text{Mg}^{2+}$  under physiological conditions of ionic strength and pH. In this receptor, which comprises aniline units rather than the aliphatic amines in EGTA, shows less pH-sensitivity in the physiological pH range (6.5 - 7.5) due to the conjugation of the aniline electron pair with the benzene ring. Equally this unit, with an accessible oxidation potential can be exploited for photoinduced electron transfer processes, for example as a means to switch the fluorescence of an adjacent fluorophores via reductive quenching offering the means to develop selective fluoroionophores. The multi-step synthesis of the BAPTA receptor, which would subsequently serve as a synthon in the elaboration of more functional molecules, was carried out according to a published procedure by the group of Tsien.<sup>1</sup> The synthesis is presented in scheme 11

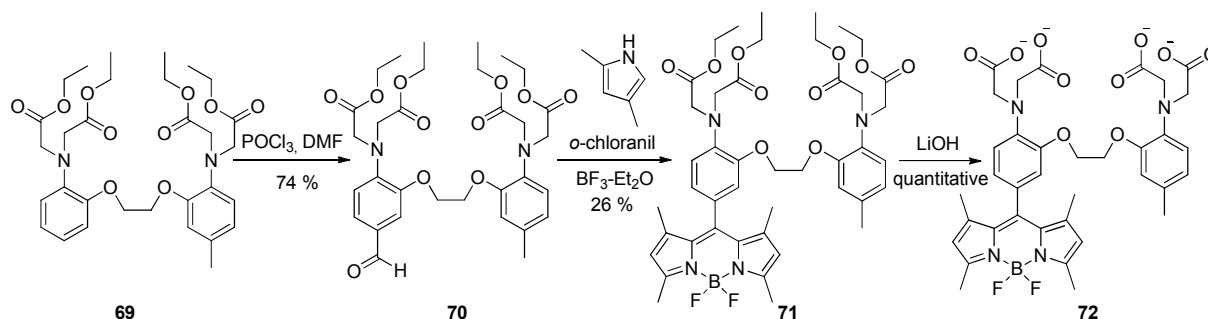


**Scheme 11:** Synthesis of methyl-BAPTA precursor (**69**).

The potassium salt of *o*-nitrophenol (**65**) was formed in methanol using potassium hydroxide and subsequently reacted with a large excess (10 eq) of 1,2-dibromoethane to obtain the mono-substituted bromoethane (**66**) with a yield of 37 %. Generally, the yield for this reaction rarely surpasses 45 % due to the formation of disubstituted product even while working with a high excess of reactants and upon slow addition of **65** as well as a possible elimination reaction. In order to obtain a BAPTA derivative which is susceptible to reactions only on one of the two aromatic rings, **66** was reacted with an *o*-nitrophenol carrying a methyl group in the para-position with respect to the nitro-group. Thus the potassium salt of 5-methyl-2-nitrophenol was formed with KOH in MeOH and was then subsequently reacted with intermediate **66** to form the dinitro intermediate (**67**) with a yield of 67 %. A Pd/C catalysed hydrogenation led to the diamine intermediate (**68**) with a yield of 71 % and subsequent alkylation of the amines, using ethyl bromoacetate under basic conditions in acetonitrile with sodium iodide as catalyst, formed the methyl-BAPTA precursor (**69**) (35 % yield). The unoptimized reaction yield was rather low due to the short reaction time which was used during the procedure which could otherwise lead to more product, for example on adding periodically multiple aliquots of the ethyl bromoacetate.

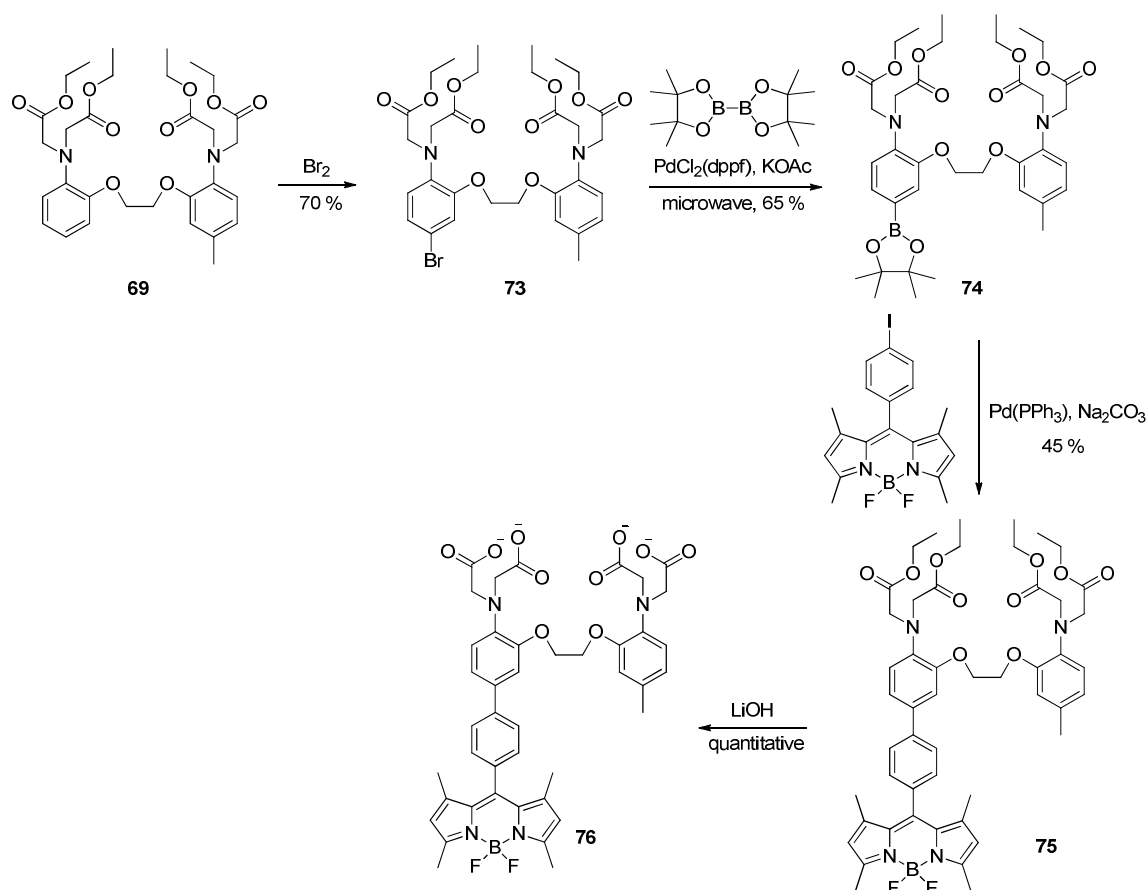
Starting from methyl-BAPTA (**69**), the synthesis of two different water soluble BAPTA-BODIPY fluorescent ion sensors was envisaged. The synthesis is outlined in scheme 12 for BAPTA-BODIPY (**72**) and scheme 13 for BAPTA-PH-BODIPY (**76**) bearing a phenyl linker between ionophore and fluorophore. The phenyl spacer is anticipated to better separate the

discrete molecular subunits thus affording a greater degree of predictability in the behaviour of complexation and switching, while the molecule where the molecular subunits are directly connected case could give a more dramatic switching performance.



**Scheme 12:** Synthesis of BAPTA-BODIPY (72)

Methyl-BAPTA (**69**) was formylated using a Vilsmeier-Haack procedure<sup>1</sup> using POCl<sub>3</sub> and DMF. Following a mild hydrolysis, the resulting aldehyde (**70**) could be obtained in a good isolated yield (74 %). The ester protected BAPTA-BODIPY (**71**) was obtained following a known three step, one-pot procedure.<sup>2,3</sup> Aldehyde (**70**) was reacted with 2,4-dimethyl pyrrole to afford the dipyrromethane intermediate, which was subsequently oxidized to dipyrromethene using *p*-chloranil. Complexation with BF<sub>3</sub>-Et<sub>2</sub>O lead to the desired product (**71**), after column chromatography and subsequent crystallization from ethanol with a yield of 26 %. The saponification of the esters under mild conditions, using an excess of LiOH, yielded the ion sensitive BAPTA-BODIPY fluorescent switch (**72**).



**Scheme 13:** Synthesis of BAPTA-PH-BODIPY (**76**)

For BAPTA-PH-BODIPY (**76**) a different synthetic approach was adopted. The synthesis started from the methyl-BAPTA precursor (**69**) and the reactive aromatic ring was brominated in the para position of the aniline using  $\text{Br}_2$ .<sup>4</sup> The brominated BAPTA intermediate (**73**) was obtained with a yield of 70 % after purification. Reaction at the bromine-bearing carbon of **73** allowed conversion into a boronic ester following the Miyaura methodology.<sup>5</sup> The BAPTA boronic ester intermediate (**74**) was obtained reacting the bromine (**73**) with bis(pinacolato)diboron under microwave conditions employing a  $\text{PdCl}_2(\text{dppf})$  ([1,1-bis(diphenylphosphino)ferrocene]-dichloro palladium) catalyst and potassium acetate as base with a yield of 65 %. Indeed, this intermediate was intended to serve as a starting compound for the facile introduction of different fluorophores and small molecules via mild C–C bond formation harnessing Suzuki coupling. Following this idea, 4-iodo-BODIPY which was available in the laboratory was introduced using  $\text{Pd}(\text{PPh}_3)_4$  and  $\text{Na}_2\text{CO}_3$  to yield the ester-protected BAPTA-PH-BODIPY (**75**) with 45 % yield. Hydrolysis was achieved using  $\text{LiOH}$  following the same procedure as mentioned earlier to obtain the final BAPTA-PH-BODIPY (**76**). Due to the mild saponification procedure, products of satisfactory purity could be

---

obtained after rinsing of the products with organic solvents, without further purification. Because esters or activated ester are employed in biological studies to cross the cell membrane,<sup>6</sup> studies were performed on the esters (**71** and **75**) and the free acids (**72** and **76**).

### 3.1.2 Single crystal X-ray diffraction studies of ester protected BAPTA-BODIPYs (**71** and **75**)

A structural factor which is important for high fluorescence in BODIPY fluorophores, which are meso-substituted with phenyl rings, is the orthogonal orientation of the ring with respect to the dipyrromethene unit.<sup>7</sup> This orthogonality can be partly achieved through the incorporation of methyl groups in the  $\alpha$ -position of the BODIPY fluorophore, which was for example used in the F<sub>5</sub>-BODIPY (**59**) introduced in chapter 2. The nature of the phenyl ring in the meso-position also plays an important role in the orientation. A 4-bromophenyl BODIPY, for example, showed an angle between phenyl ring and diazaindecene unit of 78.9°,<sup>8</sup> whereas a 4-dimethylaminophenyl ring had an determined angle of 87.8° between planes.<sup>9</sup> On incorporating a bulky perfluorophenyl ring in the meso-position the angle becomes 90.01°, as shown in chapter 2.<sup>3</sup> A survey of over thirty related structures in the Cambridge Crystallographic Data Center (CCDC) revealed that the average angle between the two planes is 81.26° and can be as little as 70.7° as the least twisted<sup>10</sup> and essentially orthogonal with an angle of 89.85°.<sup>11</sup> The average deviation from the ideal planarity is 0.054 Å with a maximal deviation of 0.219 Å.

Single crystal X-ray diffraction samples of molecules **71** and **75** had been obtained from ethanol and the determined structures are shown in figure 54. The crystal structure confirms the orthogonal arrangement of phenyl plane in the ester protected fluorionophores **71** and **75** which is imposed by the substituents of the BODIPY subunit. The dihedral angle between BODIPY and phenyl fragment planes is 87.2° for **71** and 85.8° for **75**, respectively. The phenyl rings in the biphenyl unit of BAPTA-PH-BODIPY ester (**75**) are slightly tilted with a dihedral angle of 28.0°.

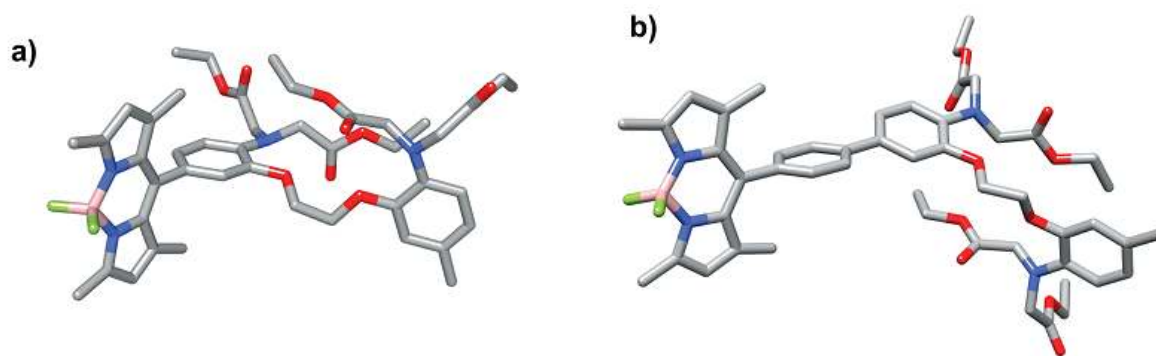


**Figure 54:** Stick representation of the single crystal X-ray structures of BAPTA-BODIPY ester (**71**) (a) and BAPTA-PH\_BODIPY ester (**75**) (b), whose crystals were obtained from ethanol. Atoms and corresponding colours are: carbon (grey), oxygen (red), nitrogen (blue), boron (pink) and fluorine (green).

The diazaindacene part of the molecule is essentially planar showing a maximum deviation from the least squares mean plane of the 12 atoms of the indacene of 0.087 Å For **71** and 0.089 Å for **75**. The bond distances for the indacene, with an average value for B–N of 1.54 Å and for B–F of 1.39 Å, are in good agreement with similar systems in the literature.<sup>12,13</sup>

### 3.1.3 Quantum chemical calculations of model compounds for BAPTA-BODIPYs (**72** and **76**)

Quantum chemical calculations were performed using the MOPAC2007 (PM6 Hamiltonian, COSMO salvation model for acetonitrile).<sup>14</sup> In order to simplify the calculations, an aniline with a methoxy group in ortho-position was used as a representative for the BAPTA moiety, while the BODIPY fluorophore was taken in its entirety. Molecular orbitals which are potentially involved in an electron transfer reaction are highlighted in Figure 55. In both representatives (**72** and **76**) the HOMO-1 and the LUMO are located on the BODIPY fluorophore and show the molecular orbitals which are involved in the lowest gap optically-active transition. As shown in the crystal structure, the phenyl group in meso-position to the indacene is almost perpendicular due to the steric hindrance caused by the  $\alpha$ -methyl groups. The angle between indacene and the phenyl ring was calculated to be 88°, which resembles the values obtained from the single crystal X-ray diffraction experiment.

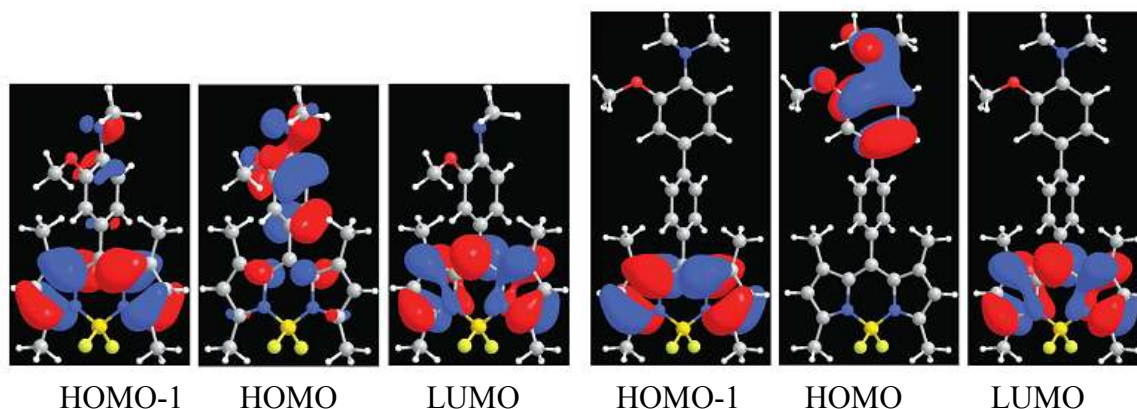


**Figure 55:** HOMO-1, HOMO and LUMO orbitals of model compounds for molecules **72** (left) and **76** (right) calculated by MOPAC 2007.

Regarding the HOMO for the model of BAPTA-BODIPY (**72**), it can be seen that even though almost perfect orthogonality between the planes is given, the adjacent  $\pi$ -system is not completely decoupled. Therefore some electronic communication between the planes is possible and could give rise to some spectral modifications to varying extents in different solvents, for example. On the other hand the model for BAPTA-PH-BODIPY (**76**) shows complete deconjugation of the BAPTA and the BODIPY part (figure 55, right) for HOMO-1, HOMO and LUMO levels. Thus the HOMO located on the BAPTA fragment is not affected by the transition  $\text{LUMO} \leftarrow \text{HOMO-1}$  and participates as the electron donating orbital in the charge separation reaction. The twist angle here between the indacene and the phenyl spacer is estimated at  $89^\circ$ , which resembles the angle measured in the single crystal X-ray structure. However, the angle between phenyl spacer and BAPTA fragment is modelled at  $51^\circ$  which is somewhat larger than the angle measured in the crystal structure ( $28^\circ$ ). Overall, while a similar alkoxyanilino moiety and fluorophore is present in both molecules, the absence of a phenyl spacer between both fragments leads to a more intimate coupling in the case of BAPTA-BODIPY (**72**), which may ultimately influence the rate of charge separation, efficiency of fluorescence enhancement upon ion binding and emission, whilst a more straightforward case may be anticipated for BAPTA-PH-BODIPY (**76**) which conforms more to the successful “receptor-spacer-fluorophore” concept.<sup>15</sup>

---

### 3.1.4 Spectral characterization of BAPTA-BODIPY (**72** and **76**) and their corresponding esters (**71** and **75**)

The ester-protected BAPTA-BODIPY molecules (**71** and **75**) were studied in air equilibrated THF by steady-state electronic absorption and emission spectroscopy. The spectral data obtained are summarised in table 05.

**Table 05:** Summary of the spectral characterization of BAPTA-BODIPYs and esters.

	$\lambda_{\max}$	$\epsilon$ ( $M^{-1}cm^{-1}$ )	$\lambda_{em}$	$\Phi_{em}$
<b>71</b>	501	79500	514	0.01
<b>75</b>	501	82800	512	0.04
<b>72</b>	498		508	0.0003
<b>76</b>	497		507	0.004

The absorption spectra for the BAPTA-BODIPY esters **71** and **75** show similarly high extinction coefficients with a maximum at 501 nm, while the value for ester **75** is slightly higher due to the increased conjugated system carrying an extra phenyl ring. The band shape is characteristic for BODIPY derivatives as shown in chapter 2 and in the literature.<sup>16</sup> The emission spectra display a maximum at 514 nm (**71**) and 512 nm (**75**) with a typically small Stokes shift ( $\Delta\omega = 500\text{ cm}^{-1}$  and  $430\text{ cm}^{-1}$ , respectively) which are similarly low for the acids **72** and **76** ( $\Delta\omega = 400\text{ cm}^{-1}$  and  $440\text{ cm}^{-1}$ , respectively). Ester **71** has a low fluorescence quantum yield of 0.01 which is only 4 times higher for ester **75** (0.04). Those quantum yields are much lower compared to native BODIPY fluorophores and can be explained by efficient quenching via photoinduced electron transfer from the aniline to the fluorophore or charge transfer processes similar to the ones described for a BODIPY-crown ether derivative or a dimethylanilino-BODIPY.<sup>17,18</sup> Having a closer look into the emission spectra of the dimethylanilino-BODIPY it should be noted that a dual emission occurs in some solvents, among them THF, where the charge transfer emission is 47 times that of the locally excited emission. In the case of the BAPTA-BODIPY ester (**71**) a dual emission in THF could be observed as well, however this is not the case for the BAPTA-PH-BODIPY (**75**) with an additional phenyl linker. The emission spectra in THF are depicted in figure 56 for comparison.

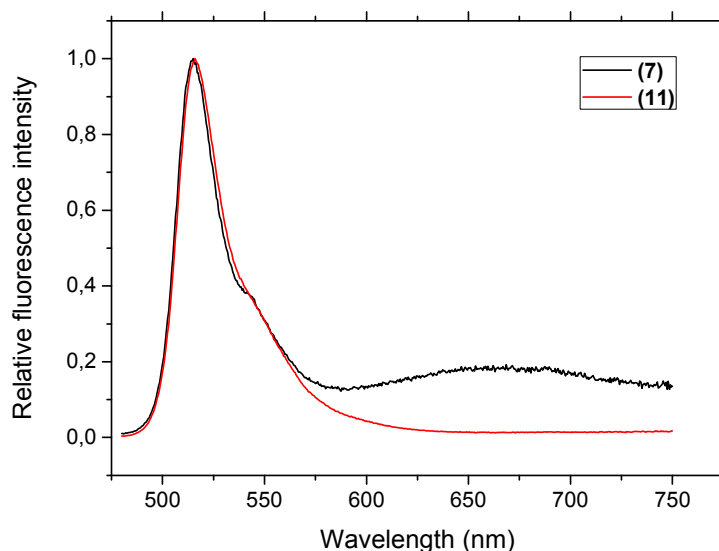


**Figure 56:** Emission spectra of BAPTA-BODIPY ester (**71**) and BAPTA-PH-BODIPY ester (**75**) in air equilibrated THF ( $\lambda_{\text{exc}} = 475 \text{ nm}$ ).

The contribution of the charge transfer emission ( $\tau = 950 \text{ ps}$ ) to the total emission could be estimated to be circa 100 times less than the locally excited emission. This second emission band disappeared in more polar acetonitrile and was not anticipated in an aqueous mixture, which will be the solvent for the calcium binding studies. The dimethylamino BODIPY by Rurack<sup>17</sup> showed a charge transfer band which displayed almost the same intensity as the initial  $S_0 \leftarrow S_1$  emission in THF with an even higher contribution in acetonitrile.

### 3.1.5 $\text{Ca}^{2+}$ complexation studies of BAPTA-BODIPYs (**72** and **76**)

The effective dissociation constants ( $K_d$ ) of the calcium complexes of fluorionophores **72** and **76** were determined in an aqueous buffer under pseudo-intracellular conditions (30 mM MOPS (3-[N-morpholino]propanesulfonic acid), 100 mM KCl at pH 7.2) by UV-Vis and fluorescence spectroscopy as a function of  $\text{Ca}^{2+}$ . The precise titration procedure can be found in the experimental section. In short, a solution containing 1-10  $\mu\text{M}$  of  $\text{Ca}^{2+}$ -sensor **72** or **76** were prepared in the mentioned pseudo intracellular buffer and the concentration of  $\text{Ca}^{2+}$  was adjusted using 10 mM EGTA in one buffer to result in a  $\text{Ca}^{2+}$ -free solution since all free  $\text{Ca}^{2+}$ -impurities from glassware and present in water are bound to EGTA and 10 mM CaEGTA to obtain a solution with a free  $\text{Ca}^{2+}$  concentration of 39  $\mu\text{M}$ . By mixing these two fluoroionophore containing buffers, the free  $\text{Ca}^{2+}$  concentration was adjusted to the values given in figure 57 and figure 58 as described by Tsien.<sup>1,4</sup>

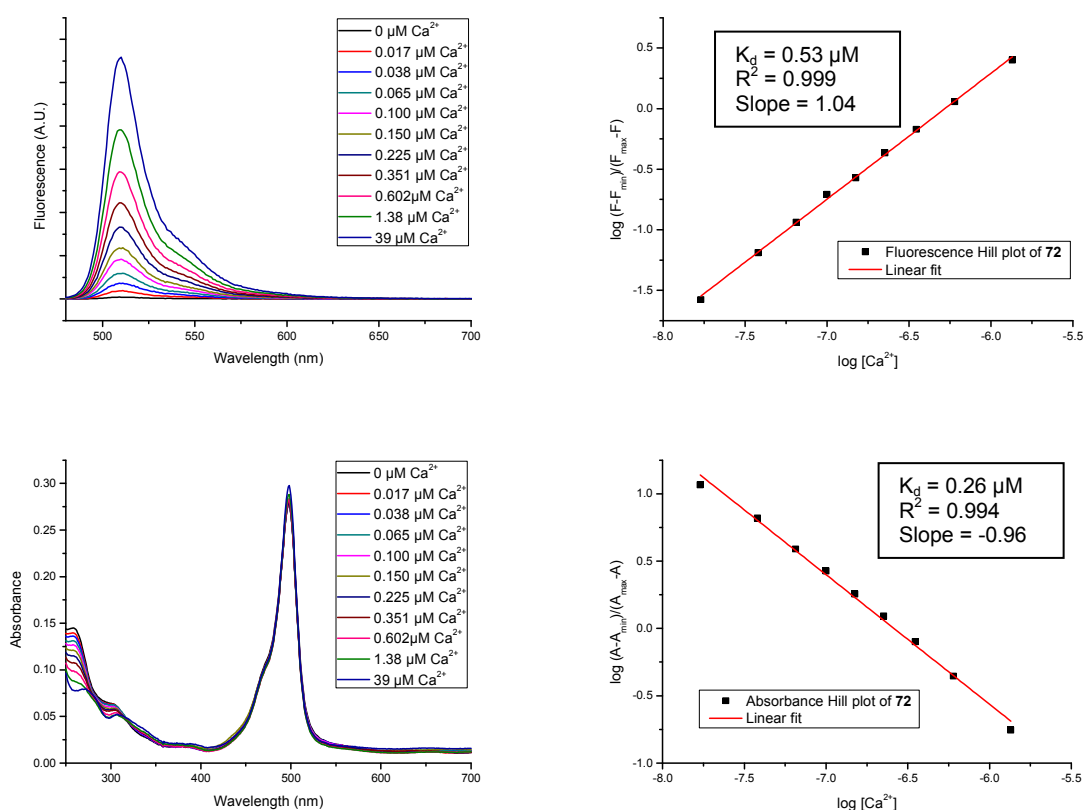


**Figure 57:** Fluorescence emission spectra of BAPTA-BOIDPY **72** upon  $\text{Ca}^{2+}$ -addition in pseudo intracellular buffer ( $\lambda_{\text{exc}} = 476 \text{ nm}$ ) (top left). Hill plot for the spectral change in fluorescence emission at 515 nm (top right). Electronic absorption spectra of **72** upon  $\text{Ca}^{2+}$ -addition in pseudo intracellular buffer (bottom left). Hill plot for the spectral change in electronic absorption at 260 nm (bottom right).

For both molecules there is only a small change in the visible region of the spectra upon addition of  $\text{Ca}^{2+}$ . Significant changes were observed in the UV-region of BAPTA-BODIPY (**72**), due to the perturbation of the alkoxyanilino moiety upon complexation, with a maximal change at 260 nm. BAPTA-PH-BODIPY (**76**) shows two significant bands which alter upon  $\text{Ca}^{2+}$  addition with a maximal change at around 260 nm and a second band with a maximal change at 316 nm. The second band is attributed to the presence of the additional phenyl spacer between fluorophore and the BAPTA fragment. These spectral variations allowed the calculation of the ground-state dissociation constant ( $K_d$ ). Linear fitting of the spectral change via Hill plot (figure 57 and 58 bottom right) which is the logarithm of the spectral change plotted over the logarithm of the free  $\text{Ca}^{2+}$  concentration, yields a straight line for mono-ionic binding. The slope of the resulting linear fitting indicates the order of the complex.

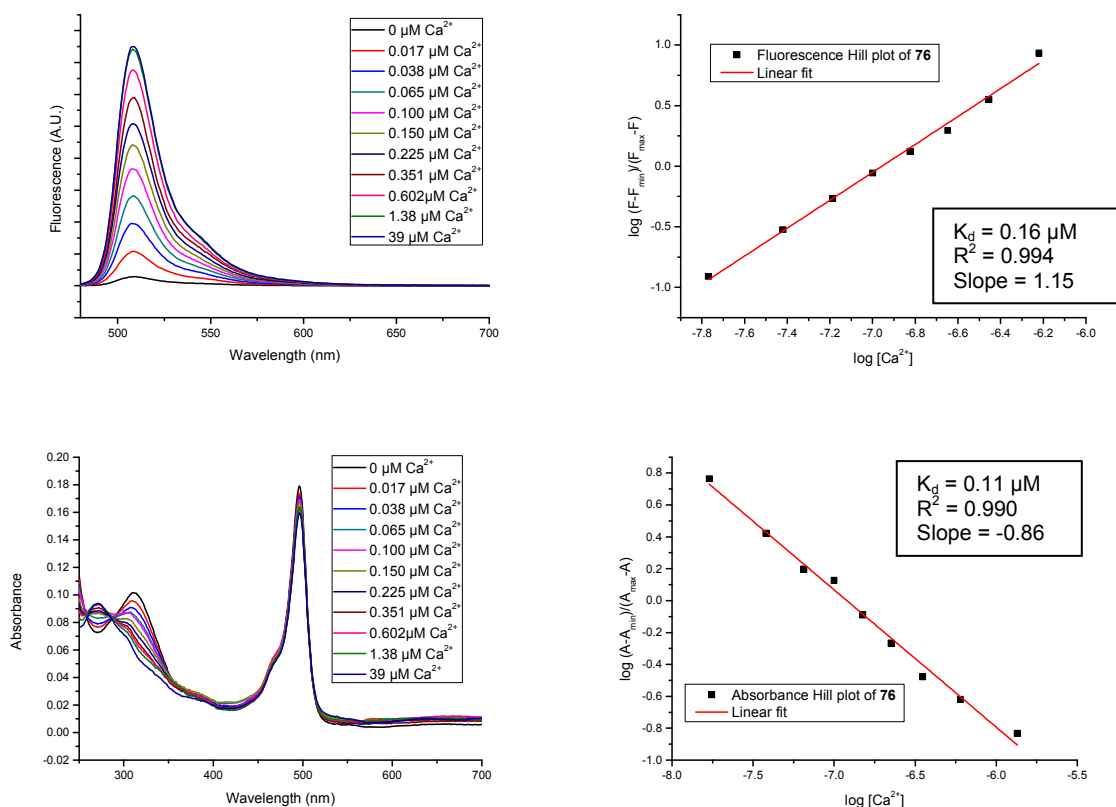


**Figure 58:** Fluorescence emission spectra of BAPTA-PH-BODIPY (**76**) upon  $\text{Ca}^{2+}$ -addition in pseudo intracellular buffer ( $\lambda_{\text{exc}} = 476 \text{ nm}$ ) (top left). Hill plot for the spectral change in fluorescence emission at 509 nm (top right). Electronic absorption spectra of **76** upon  $\text{Ca}^{2+}$ -addition (bottom left). Hill plot for the spectral change in electronic absorption at 316 nm (bottom right).

While a slope of 1 means a 1:1 binding, a slope smaller than 1 indicates negative cooperative binding and a slope larger than one indicates positive cooperative binding. The x-intercept of the graph yields  $\text{pK}_d$  of the system and  $K_d$  can be extracted. The ground-state dissociation constants of BAPTA-BODIPYs **72** and **76** were determined to be  $0.26 \mu\text{M}$  and  $0.11 \mu\text{M}$  respectively. These values are in the range of known BAPTA ionophores bearing different types of functional groups in the para-position of the aniline (e.g. BAPTA =  $0.59 \mu\text{M}$ , 5,5'-dimethyl-BAPTA =  $0.16 \mu\text{M}$ ).<sup>19</sup> Concerning the fluorescence emission spectra, similar titrations were performed and are depicted in figure 57 and 58 on the top. The fluorescence quantum yields for fluoroionophores **72** and **76** in the  $\text{Ca}^{2+}$ -free sample were very low with values of 0.0003 and 0.004, respectively. This low emission, and hence strong quenching, with respect to the parent fluorophore is consistent with a thermodynamically-allowed photoinduced electron transfer process. However, the quantum yield of BAPTA-PH-BODIPY (**76**) is about 10-fold higher than the one of BAPTA-BODIPY (**72**) which might be explained

by the longer distance between BAPTA and BODIPY induced by the phenyl linker and therefore a loss in efficiency of the electron transfer process. Upon addition of  $\text{Ca}^{2+}$  a larger increase of the fluorescence intensity and hence the quantum yield was observed in both cases without a shift of the emission maxima. Since the lone electron pair of the amino group of the BAPTA moiety is known to be involved in the binding of  $\text{Ca}^{2+}$ , calcium coordination partially blocks the PET process and yields an increased fluorescence. The fluorescence enhancement factors were determined to be 122 for **72** and 23 for **76** respectively. The smaller increase in fluorescence emission for phenyl linker bearing BAPTA-BODIPY (**76**) again shows a more intimate donor-acceptor interaction. The fluorescence quantum yields measured against a fluorescein standard for the  $\text{Ca}^{2+}$ -complexes of BAPTA-BODIPYs **72** and **76** gave 0.04 and 0.09, respectively. The data obtained by fluorometric titrations for the ion sensors **72** and **76** are summarized in table 06.

**Table 06:** Summary of the absorption, emission and complexation characteristics of BAPTA-BODIPYs.

	$\lambda_{\text{max}}$	$\lambda_{\text{em}}$	$\Phi_{\text{em}}$	$\text{p}K_{\text{d}}$	$F_{\text{max}}/F_{\text{min}}$
<b>72</b>	498	508	0.0003		
<b>76</b>	497	507	0.004		
<b>72</b> + $\text{Ca}^{2+}$	498	508	0.04	6.3	122
<b>76</b> + $\text{Ca}^{2+}$	497	507	0.09	6.8	23

The calcium dissociation constants ( $K_{\text{d}}$ ) were established to be  $0.53 \mu\text{M}$  for BAPTA-BODIPY (**72**) and  $0.16 \mu\text{M}$  for BAPTA-PH-BODIPY (**76**), showing a similar trend to spectrophotometrically-determined values. However, it is noteworthy that even though the binding constants for fluorionophore **76** are in good agreement with each other there is a bigger difference in the values obtained for  $\text{Ca}^{2+}$ -sensor **72** and corresponds more to the value of an unsubstituted BAPTA. The difference in the determined  $K_{\text{d}}$  values from fluorescence and UV-Vis measurements for BAPTA-BODIPY (**72**) is most likely based on the a polar excited state of the molecule which is supported by the appearance of an charge transfer band in the emission spectra seen for the ester (**71**) in THF. The excited state has a lowered electron density on the aromatic ring which leads to a lower binding affinity.

### 3.1.6 Time-resolved transient absorption studies of BAPTA-BODIPYs (**72** and **76**)

Transient absorption spectroscopy provides the possibility to follow the evolution of the excited state of a molecule in the first few pico to nanoseconds after excitation. Since the

BODIPY triplet absorption spectra of BODIPY has been reported recently<sup>20,21</sup> and the spectroelectrochemical study of the BODIPY radical anion formation has been carried out,<sup>22</sup> it is now possible to disentangle the electron transfer pathway. The transient absorption measurements have been carried out in collaboration with the department of physics at the university of Bordeaux. The obtained results are shown in great detail in the thesis of Dr. Batat.<sup>23</sup> A short summary with essential results is described in the following pages.

Transient absorption spectra for the free acids (**72** and **76**) in buffered aqueous solution are given in figure 59 and 60. On short timescales there is a short-lived wide positive band which appears in the spectra of both molecules. This band was attributed to non-linear phenomena in the solvent and was not further investigated. By fitting the gain band at 530 nm, the relaxation time of singlets was calculated to be 300 fs for BAPTA-BODIPY (**72**) and while the gain band disappears new characteristic absorption bands rise at 420 nm and 570 nm, which were attributed to anion radical absorption bands of the BODIPY fluorophore which corresponds to literature data on BODIPY fluorophores.<sup>21,22</sup>

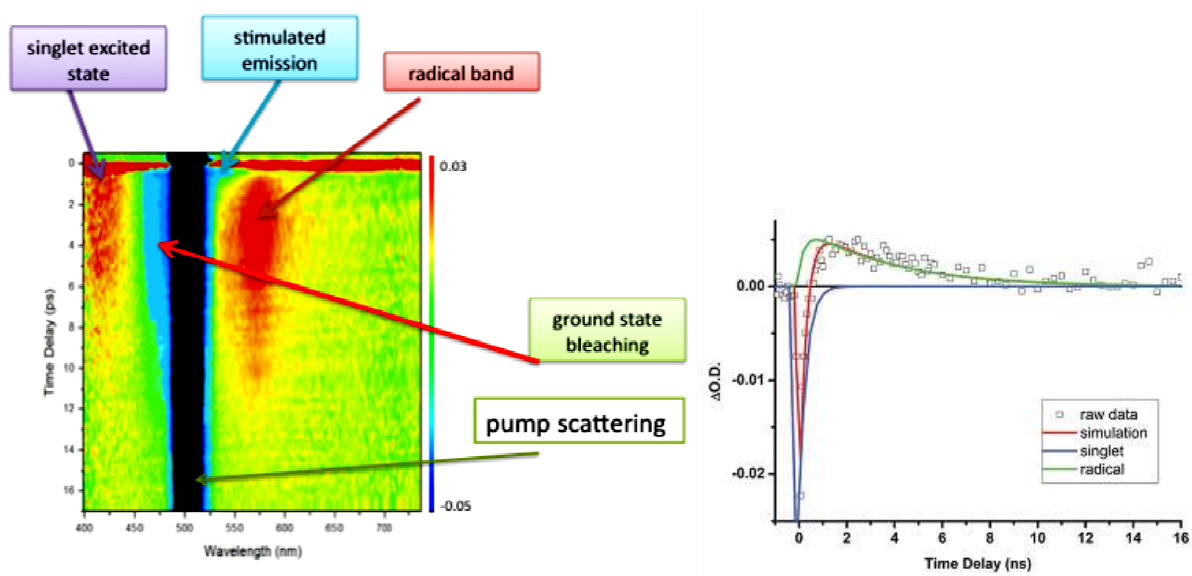


**Figure 59:** Transient absorption map for BAPTA-BODIPY (**72**) in buffered water ( $\lambda_{\text{exc}} = 500$  nm) and kinetics at 540 nm of radical grow-in from excited singlet (right).

BAPTA-BODIPY (**72**) shows a singlet state population which decays to give rise to radical pairs and relax in 3.8 ps. However, no evidence of triplet population from the short-lived radicals was measured in aqueous buffer. The initial non-linear effects on the transient absorption spectrum for BAPTA-PH-BODIPY (**76**) are stronger and overlapped with the excited singlet state absorption band as can be seen in figure 60. The excited singlet state absorption band at 425 nm relaxes in 1.2 ps as deduced from ground state bleaching and

stimulated emission signal. After a fast relaxation, anion radical absorption band of the BODIPY part still remain at 425 nm and between 600-800 nm with a decay rate of 21 ps. Much in the way of BAPTA-BODIPY (**72**) no triplet states were observed for BAPTA-PH-BODIPY (**76**) in aqueous buffer.

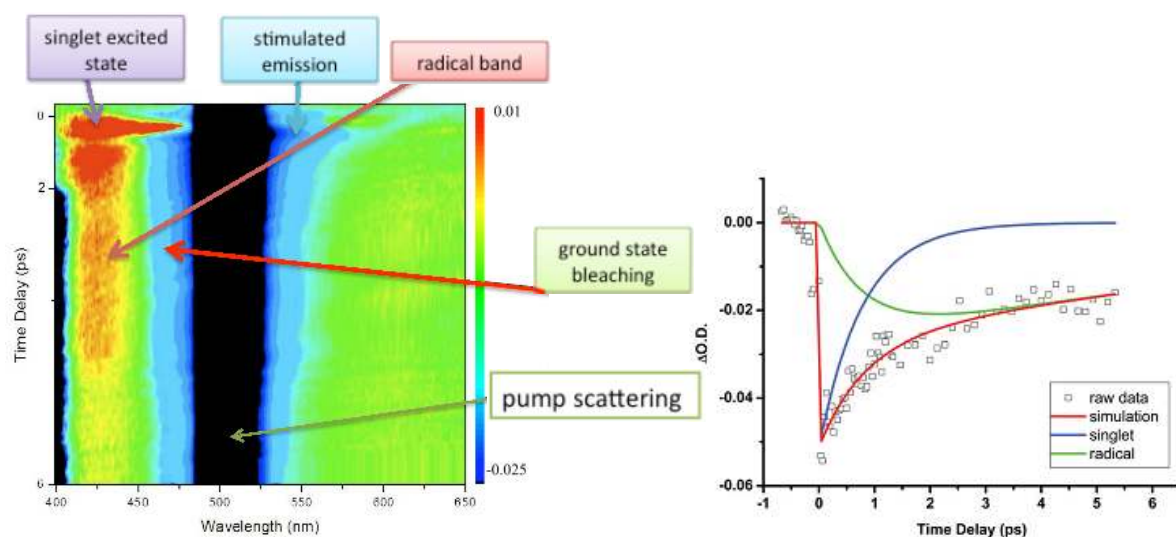


**Figure 60:** Transient absorption map for molecule BAPTA-PH-BODIPY (**76**) in buffered water ( $\lambda_{exc} = 500$  nm) and kinetics of radical grow-in from excited singlet (right) at 540 nm.

Upon binding  $Ca^{2+}$  the oxidation potential of the receptor changes and the PET becomes energetically unfavourable. This blocks the radical formation thus restoring the fluorescence emission. The steady state emission behavior is in good agreement with this observation as denoted in figure 57 and figure 58. The transient absorption spectra obtained in the presence of  $Ca^{2+}$  resemble the spectra obtained in THF in the presence of acid (data not shown) for both ion sensors, showing that charge separation does not occur but the fluorescence increases instead (figure 61). For BAPTA-BODIPY (**72**) in presence of  $Ca^{2+}$  the stimulated emission decay with  $\tau = 600$  ps while BAPTA-PH-BODIPY (**76**) in presence of  $Ca^{2+}$  shows a slightly longer time constant  $\tau = 760$  ps. In order to obtain an estimation of the radiative rate constant, the fluorescence quantum yields given in table 06 were divided by the apparent lifetime obtained from stimulated emission decays.

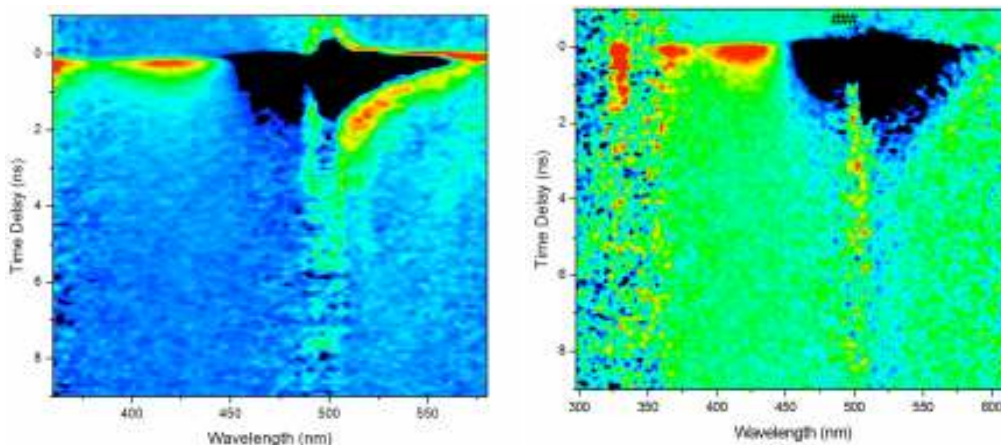


**Figure 61:** Transient absorption maps for BAPTA-BODIPY (**72**) (left) and BAPTA-PH-BODIPY (**76**) (right) in the presence of  $\text{Ca}^{2+}$  in aqueous buffer ( $\lambda_{\text{exc}} = 500 \text{ nm}$ ).

Consequently, radiative rate constants of  $6.7 \times 10^7 \text{ s}^{-1}$  and  $1.2 \times 10^8 \text{ s}^{-1}$  for **72** and **76** were obtained, respectively. These values are in good agreement to literature values for BODIPY fluorophores,<sup>24</sup> which are in general around  $2 \times 10^8 \text{ s}^{-1}$ . Corresponding non-radiative rate constants are similar at  $1.7 \times 10^9 \text{ s}^{-1}$  and  $1.3 \times 10^9 \text{ s}^{-1}$ , respectively. The rate of charge separation ( $k_{\text{ET}}$ ) has been calculated using equation 19 where  $1/\tau_{\text{free}}$  corresponds to the rate of deexcitation in absence of  $\text{Ca}^{2+}$  and  $1/\tau_{\text{Ca}^{2+}}$  equals the rate of deexcitation in the presence of the ion, taking the assumption that other rate parameters are not significantly disturbed by the presence of  $\text{Ca}^{2+}$ .

$$k_{\text{ET}} = \frac{1}{\tau_{\text{free}}} - \frac{1}{\tau_{\text{Ca}^{2+}}} \quad \text{equation 19}$$

Electron transfer rates were calculated to be  $3.3 \times 10^{12} \text{ s}^{-1}$  for BAPTA-BODIPY (**72**) and  $8.3 \times 10^{11} \text{ s}^{-1}$  for BAPTA-PH-BODIPY (**76**) in aqueous buffer based on stimulated emission decays.

---

### 3.1.7 Intermediate conclusion

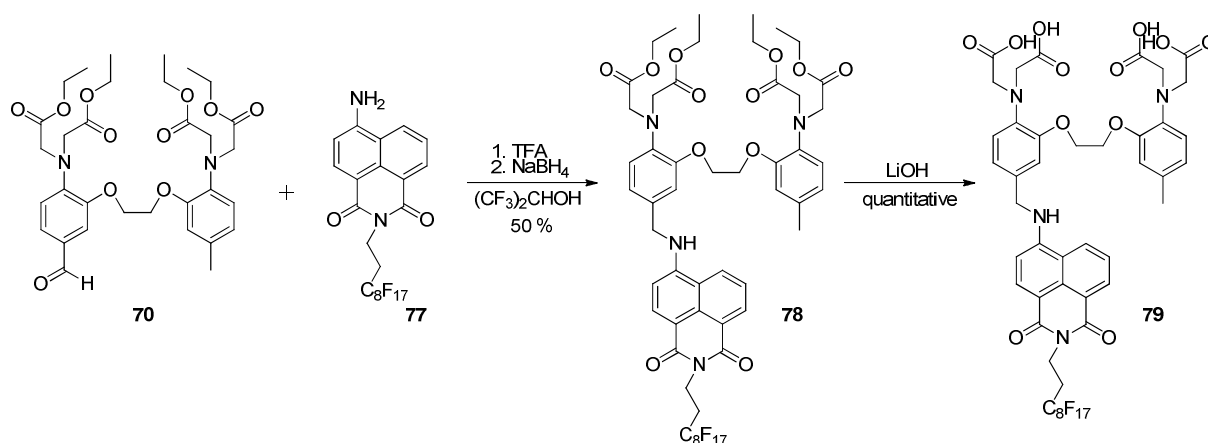
In conclusion, two novel BAPTA-BODIPY conjugates have been developed with efficient  $\text{Ca}^{2+}$  binding-induced fluorescence enhancement. A different behavior could be observed in aprotic solvents like THF compared to protic water. The electron transfer is several times faster in water and unlike in the organic solvent, no triplet formation from the charge-separated state has been obtained. As a result of the ion-binding induced blocking of the PET fluorescence enhancements of 122 and 23 fold are measured for BAPTA-BODIPY (**72**) and BAPTA-PH-BODIPY (**76**) respectively making them effective fluorescent chemosensors. The receptor-spacer-fluorophore construction of **76** gives a better predictability of the behavior but ultimately the direct linkage of ionophore and fluorophore yields a more efficient switch, which will be used in following ion transfer experiments under pseudo-intracellular conditions in the following section.

## 3.2 Synthesis and spectral characterization of amphiphilic $\text{Ca}^{2+}$ -sensors

After the introduction of a novel water-soluble ion-sensor these properties needed to be transferred to the membrane of self-assembled vesicles. To that end, amphiphilic chemosensors based on the BAPTA ionophore were designed. This section describes the synthesis and the spectral properties of three such amphiphilic ion sensors.

### 3.2.1 Synthesis of BAPTA based amphiphilic fluorionophores bearing naphthalimide (**79**), BODIPY (**82**) and furan (**97**) fluorophores

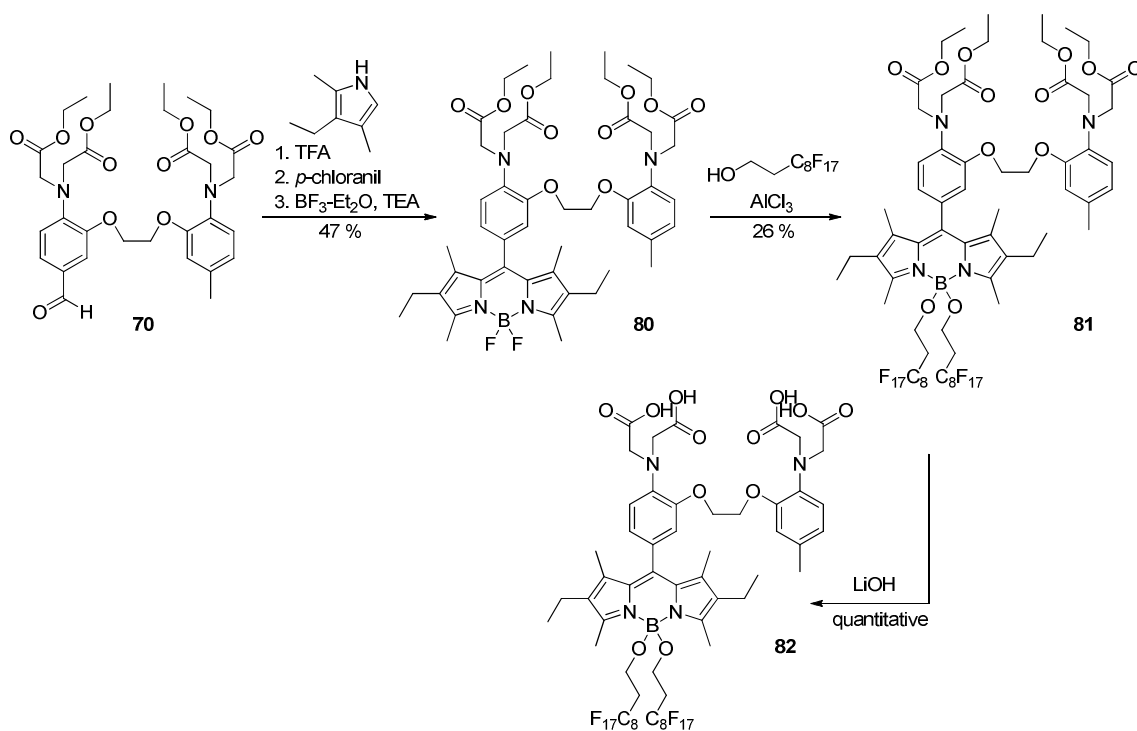
The first amphiphilic  $\text{Ca}^{2+}$ -sensor that was synthesized was a BAPTA-naphthalimide derivative. A previous project in the laboratory concerned the preparation of water-soluble and amphiphilic naphthalimide based ion sensors and therefore intermediates were available in the laboratory. The synthesis of fluorinated BAPTA-naphthalimide (BANIF, **79**) is depicted in scheme 14. Starting from the BAPTA-aldehyde intermediate, described in the previous section, **79** was synthesized in a two step, one pot synthesis. The initial aldehyde was reacted with an amine-functionalized naphthalimide chromophore which carries an aliphatic chain on the imide functionality (**77**).



**Scheme 14:** Synthesis of amphiphilic Ca<sup>2+</sup>-chemosensor **79**.

The defining feature of the aliphatic chain is the C<sub>8</sub>F<sub>17</sub> fragment, which affords the opportunity to incorporate the resulting compound into the membrane of fluorinated vesicles. More information about the incorporation of amphiphile molecules into fluorinated vesicle membranes is given in the following chapters. The reaction mixture containing BAPTA-aldehyde (**70**) and fluorinated naphthalimide (**77**) was acidified by adding TFA in order to form an imine, which was subsequently reduced with NaBH<sub>4</sub> to obtain the ester protected BANIF (**78**). In order to increase the reactivity, hexafluoroisopropanol was chosen as solvent to give the desired amphiphilic fluorescent ion-sensor in 50 % yield. The reaction rate increasing effect of fluorinated solvents in reductive aminations had been shown by Tajbakhsh *et. al.*<sup>25</sup> In that fashion a novel fluorescent ion-switch was designed harnessing the ionophore-spacer-fluorophore format. The hydrolysis of **78** was achieved under mild conditions using LiOH in a methanol/THF mixture, which yielded the free acid (**79**) in sufficient purity such that after washing no further purification was needed.

The design of the second amphiphilic ion sensor is based on the previously studied BAPTA-BODIPY chemosensor. Some minor modifications had been applied to the core structure in order to render the molecule more chemically stable. The reactive β-protons which are responsible for a certain instability on silica columns and under acidic conditions were replaced by ethyl groups which have only a small effect on the absorption and emission spectra but results in a chemically more robust compound. The synthesis is shown in scheme 15.



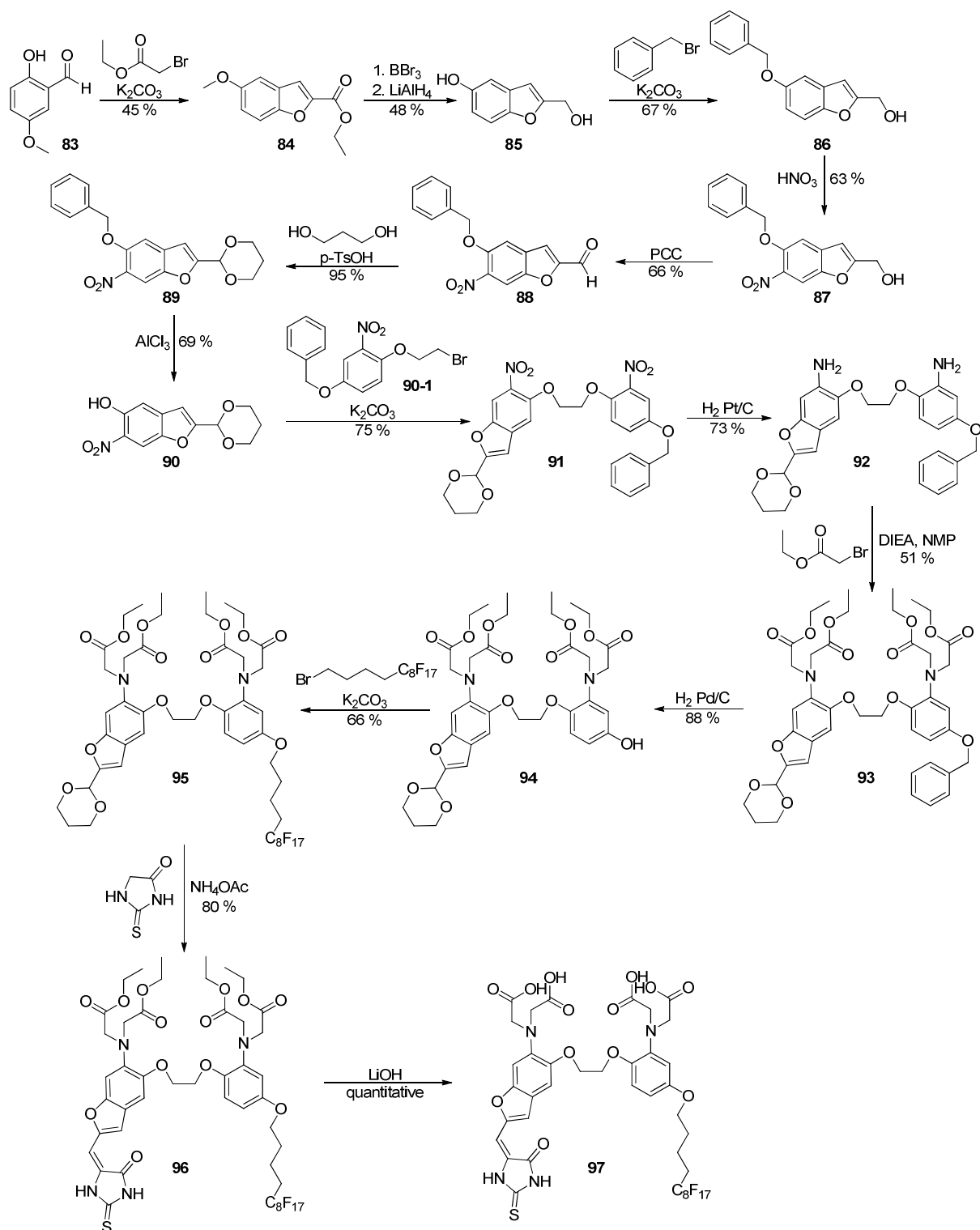
**Scheme 15:** Synthesis of amphiphilic BAPTA-BODIPY (**82**)

BAPTA-BODIPY2 (**80**) was synthesized according to the classical three step, one pot synthesis which was introduced in the previous section. Briefly, kryptopyrrole was reacted with BAPTA-aldehyde (**70**) using TFA as the reaction catalyst to form the dipyrromethane, which was subsequently oxidized to the dipyrromethene using *p*-chloranil. Complexation with boron trifluoride-diethyletherate was accomplished under basic conditions by adding TEA to the reaction mixture. The BAPTA-BODIPY2 intermediate (**80**) was obtained in 47 % yield which is almost double the reaction yield of the BAPTA-BODIPY (**72**) bearing reactive hydrogens in the  $\beta$ -position. The increase in reaction yield is mostly attributed to the much simpler purification since no additional crystallization is needed. The fluorinated chains were introduced following a procedure of Tahtaoui.<sup>26</sup> The boron center of the BODIPY fragment is activated using  $\text{AlCl}_3$  and subsequently reacted with an alcohol. In that fashion we introduced  $\text{C}_8\text{F}_{17}$ -ethanol onto the boron by substituting the fluorine atoms. The ester protected  $\text{C}_8\text{F}_{17}$ -BAPTA-BODIPY (**81**) was obtained in 26 % yield which is lower than the reaction yields reported in the paper due to partial hydrolysis of the esters judged by TLC. The final molecule (**82**) was then obtained quantitatively after ester hydrolysis via LiOH in a MeOH / THF mixture after a simple washing with organic solvents.

---

Having designed two fluorescent ion sensors which show an increase in their fluorescence intensity upon ion binding (i.e. off/on switching) a third fluorescent ion switch was envisaged with ratiometric properties. The advantage of such ion sensors is that they are unaffected by photobleaching, loading quantity or optical path length to estimate the  $\text{Ca}^{2+}$ -concentration. The design was based on the known furan derivative called “fura red” (invitrogen) which shows fluorescence emission in the visible region. The synthesis of the fura red ion-sensor was already published and patented<sup>27</sup> but in order to make an amphiphilic version harnessing the same properties, namely ratiometric ion binding response, the synthesis route needed to be altered in several places. The altered synthesis route is depicted in scheme 16.

2-methoxy-5-hydroxy benzaldehyde (**83**) was reacted with ethyl bromoacetate under basic conditions. Sufficiently long reaction times allowed the two step reaction, first nucleophilic addition and second cyclisation to yield ethyl 5-methoxybenzofuran-2-carboxylate (**84**) in 45 % yield.<sup>28</sup> Deprotection of the methoxy group to yield the free alcohol and subsequent reduction of the ester group were achieved in one pot without intermediate purification of the compound to give 2-(hydroxymethyl)benzofuran-5-ol (**85**) in 48 % over two steps. In the next step the benzyl protecting group was introduced due to a better orthogonality since it could be removed under mild conditions, more precisely catalytic hydrogenation later on in the synthesis. To that end, **85** was reacted with benzylbromide under basic conditions to give the desired protected furan (**86**) in 67 % yield. Introduction of the nitro group in ortho-position of the protected phenol was achieved by adding  $\text{HNO}_3$  (65 %) to a cooled solution of **86** in DCM. Other approaches like classical  $\text{HNO}_3$  / acetic acid gave predominantly the substitution in the 3-position of the benzofuran, whereas substitution in the 6-position dominated at low temperatures yielding the desired (5-(benzyloxy)-6-nitrobenzofuran-2-yl)methanol (**87**) in 63 % yield. Pyridinium chlorochromate was used to oxidize the free benzylic alcohol to an aldehyde following a procedure published by Dauben *et. al.*<sup>29</sup>. The corresponding aldehyde (**88**) was obtained in 66 % yield. In order to protect the aldehyde from the following catalytic deprotection of the benzyl group, it was reacted with 1,3-propanediol to obtain a six-ring acetal which is easier to hydrolyse than a 5-membered acetal. **88** was reacted with an excess of the diol in the presence of p-toluenesulfonic acid to obtain the benzofuran acetal (**89**) in almost quantitative yield (95 %).



**Scheme 16:** Synthesis route for the amphiphilic ratiometric  $\text{Ca}^{2+}$ -sensor (**97**).

Having protected the aldehyde, the benzyl group could be removed using  $\text{AlCl}_3$ . The free phenol (**90**) was obtained in 69% yield and could be reacted with 4-(benzyloxy)-1-(2-bromoethoxy)-2-nitrobenzene under basic conditions to yield a classical BAPTA precursor (**91**) already bearing the dinitrophenoxyethane fragment. Selective reduction of the nitro

---

groups in presence of a benzyl protecting group has been shown by Gryniewicz *et. al.*<sup>1</sup> amongst others. Therefore a platinum catalyst on charcoal was employed under hydrogen atmosphere to yield the selectively reduced diamine intermediate (**92**) with a reaction yield of 73 %. Several different methods have been employed to alkylate the diamine in order to introduce the ester protected carboxylic acid functions. The diamine intermediate proved to be unstable under reaction conditions involving inorganic salts like  $K_2CO_3$  and  $Na_2HPO_4$ . Decomposition of the compound could be observed after 2 – 3 hours reaction time in acetonitrile. Upon switching to a non-nucleophilic amine as a base only to the dialkylated product could be isolated. The introduction of a catalytic amount of NaI to increase the reactivity of the ethyl bromoacetate improved the alkylation slightly and the triple substituted product could be isolated, while the addition of an inorganic salt led to a non-negligible amount of decomposition. In order to drive the reaction to the quadruply alkylated diamine the solvent was changed to NMP and the all-inorganic salts were omitted. In that fashion, the BAPTA intermediate (**93**) was obtained with a reaction yield of 51 %. From here on the reactions proceeded quite smoothly. Deprotection of the benzyl group in **93** with  $H_2$  in the presence of Pd/C gave the BAPTA-phenol intermediate (**94**) in 88 % yield and subsequent introduction of the fluorinated aliphatic chain via  $C_8F_{17}$ -butyl bromide gave the amphiphilic ester-protected BAPTA intermediate (**95**) in 66 % yield. The formation of the actual chromophore was achieved by a two step, one pot reaction, namely the deprotection of the aldehyde and the subsequent introduction of the 2-thiohydantoin via a nucleophilic addition. The reaction yielded **96** in 80 % which was then hydrolyzed under mild conditions using LiOH to obtain the final molecule **97** which was named Furared- $C_8F_{17}$ . Having designed three different fluorescent ion sensors their spectral properties and binding needed to be compared.

### 3.2.2 $Ca^{2+}$ -complexation studies and spectral characterization of BANIF (**79**), $C_8F_{17}$ -BAPTA-BODIPY (**82**) and $C_8F_{17}$ -fura red (**97**)

The calcium complexation studies of **79**, **82**, and **97** was performed under pseudo intracellular conditions (100 mM KCl, 30 mM MOPS, pH 7.2), similar to those used for the water-soluble BAPTA-BODIPYs (**72** and **76**) described in the previous chapter, following the same titration procedure. The naphthalimide-based fluorescent  $Ca^{2+}$ -switch (**79**) displays an increase in the fluorescence emission upon complexation of  $Ca^{2+}$ . The emission maximum shifts from 550 nm in absence of the ion to 575 nm in presence of  $Ca^{2+}$ . This is due to the polar excited state which exhibits a larger dipole moment than the ground state of the

naphtalimide fluorophore, which leads to a sensing of the polarity of its environment. This effect has been studied and exploited in the literature to prepare, for example, ratiometric ion sensors or as a dye in cell imaging.<sup>30,31</sup> The red-shift of the fluorescence emission indicates an increase in the polarity of the environment which corresponds to the increasing free  $\text{Ca}^{2+}$  concentration during the titration. Linearising the data via Hill plot yields a dissociation constant ( $K_d$ ) of  $0.185 \mu\text{M}$  and a slope of 1.05 matches the 1:1 stoichiometry of the BAPTA unit to a divalent ion. The electronic absorption spectra of BANIF (**79**) upon  $\text{Ca}^{2+}$  addition show a much smaller ion-induced change (figure 62). The lowest energy absorption band only decreases slightly and no shift of the maximum absorption wavelength is observed, indicating the lower dipole moment of the ground state of the naphtalimide fluorophore. The maximum change in the absorption spectrum is observed at 245 nm. Plotting the spectral change via the Hill procedure leads to a  $K_d$  of  $0.117 \mu\text{M}$ , which corresponds well to the dissociation constant obtained from the fluorescence titration and is within the experimental error.

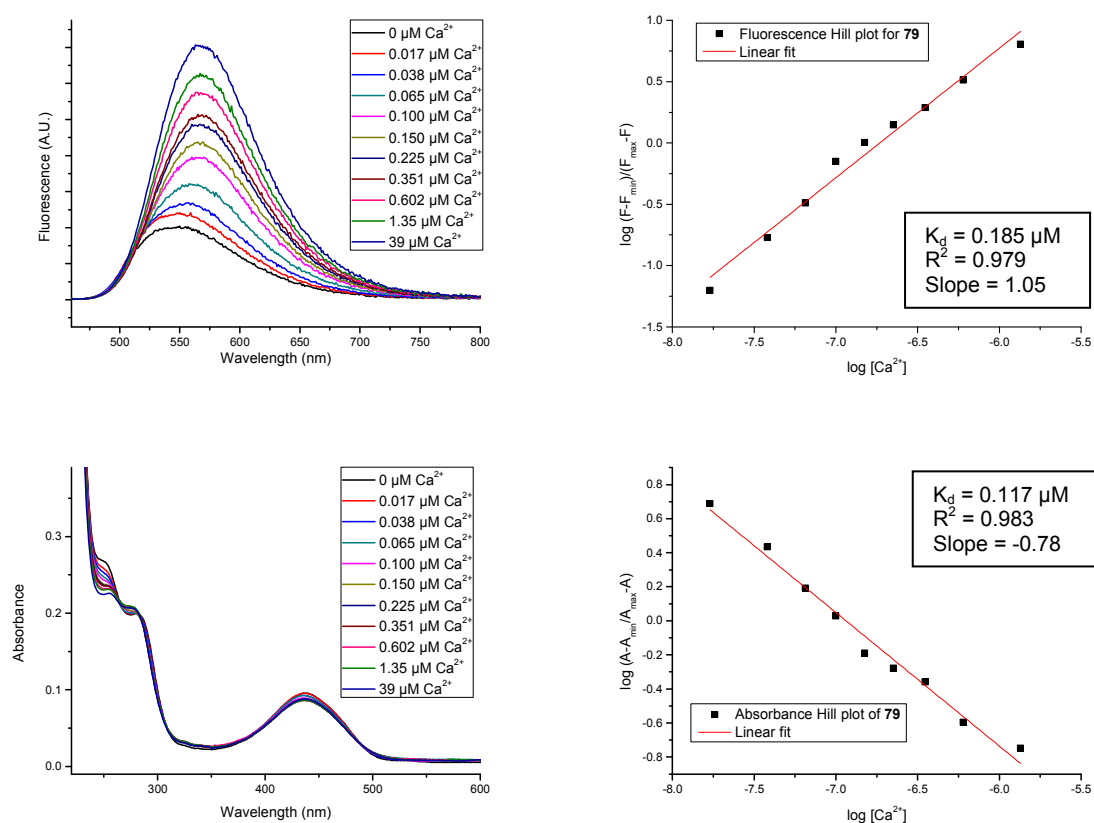


**Figure 62:** Fluorescence emission spectra of BANIF (**79**) upon  $\text{Ca}^{2+}$ -addition in pseudo-intracellular buffer ( $\lambda_{\text{exc}} = 450 \text{ nm}$ ) (top left). Hill plot for the spectral change in fluorescence emission at 575 nm (top right). Electronic absorption spectra of **79** upon  $\text{Ca}^{2+}$ -addition (bottom left). Hill plot for the spectral change in electronic absorption at 245 nm (bottom right).

---

The Stokes shift of the fluorinated BAPTA-naphthalimide (**79**) in presence of  $\text{Ca}^{2+}$  was determined to be  $5170\text{ cm}^{-1}$  and is much larger than that of the BAPTA-BODIPYs (**72** and **76**) presented in the previous section. Fluorescence quantum yields of **79** were determined in the presence of  $\text{Ca}^{2+}$  ( $\Phi_{\text{em}} = 0.026$ ) and in its absence ( $\Phi_{\text{em}} = 0.006$ ). In absence of  $\text{Ca}^{2+}$  the quantum yield is comparably low to the one measured for BAPTA-BODIPYs **72** and **76**. However, the increase in fluorescence emission upon ion complexation is lower, which was attributed to the aliphatic chain in the molecule, creating a tendency to aggregate in aqueous solution. A similarly low increase in the fluorescence emission upon  $\text{Ca}^{2+}$  complexation is also expected for the amphiphilic BAPTA-BODIPY ion sensor (**82**).

The amphiphilic BAPTA-BODIPY derivative (**82**) was titrated with  $\text{Ca}^{2+}$  under pseudo-intracellular conditions using EGTA to control the free  $\text{Ca}^{2+}$  concentration. Electronic absorption and fluorescence emission spectra were red-shifted ( $\lambda_{\text{abs}} = 529\text{ nm}$ ,  $\lambda_{\text{em}} = 542\text{ nm}$ ) in comparison with **72** and **76** due to the additional ethyl groups in the  $\alpha$ -position of the BODIPY fluorophore rendering it more electron rich (figure 63, left top and bottom). Besides the red-shifted absorption and emission, properties are reminiscent of the hydrosoluble BAPTA-BODIPYs with a Stokes shift of  $460\text{ cm}^{-1}$  and large extinction coefficient ( $\epsilon_{\text{max}} = 56800$ ). The maximum change in the fluorescence emission is obtained at  $542\text{ nm}$  and **82** displays a low fluorescence quantum yield in the absence of  $\text{Ca}^{2+}$  ( $\Phi_{\text{em}} = 0.001$ ), which is comparable to BAPTA-BODIPY (**72**) and BAPTA-PH-BODIPY (**76**) in absence of the ion. The fluorescence enhancement factor upon  $\text{Ca}^{2+}$  addition was determined to be 4, calculated from the fluorescence quantum yield, which is rather low compared to its water soluble counterparts. This effect was attributed to the formation of the aggregates of this amphiphilic fluorescent switch, leading to self quenching of the fluorescence.

After linearizing the spectral change via Hill plot, a 1:1 binding with a  $K_{\text{d}}$  of  $0.724\text{ }\mu\text{M}$  has been revealed. This value is only slightly higher than the  $K_{\text{d}}$  value obtained for BAPTA-BODIPY (**72**). The electronic absorption spectra of amphiphilic BAPTA-BODIPY (**82**) shows the typical shape of a BODIPY fluorophore. The maximum change in the absorption spectrum was observed at  $265\text{ nm}$ . The dissociation constant, obtained via Hill plot from the absorption spectra at  $265\text{ nm}$ , yield a  $K_{\text{d}}$  of  $0.467\text{ }\mu\text{M}$  under pseudo intracellular conditions. This value is slightly lower than the  $K_{\text{d}}$  of  $0.724$  obtained from the fluorescence titration. The same observation concerning the binding affinity obtained from fluorescence and electronic absorption spectra has been made for the water soluble parent BAPTA-BODIPY (**72**). The

---

third ion switch (**97**) was based on the ratiometric fluorescent sensor fura red (commercially available from Invitrogen). Unlike the amphiphilic fluorescent sensors **79** and **82**, the fluorescence emission decreases upon  $\text{Ca}^{2+}$  addition which results from a slightly lower quantum yield of the  $\text{Ca}^{2+}$ -complex ( $\Phi_{\text{em}} = 0.004$ ) as compared to the non complexed form ( $\Phi_{\text{em}} = 0.006$ ).

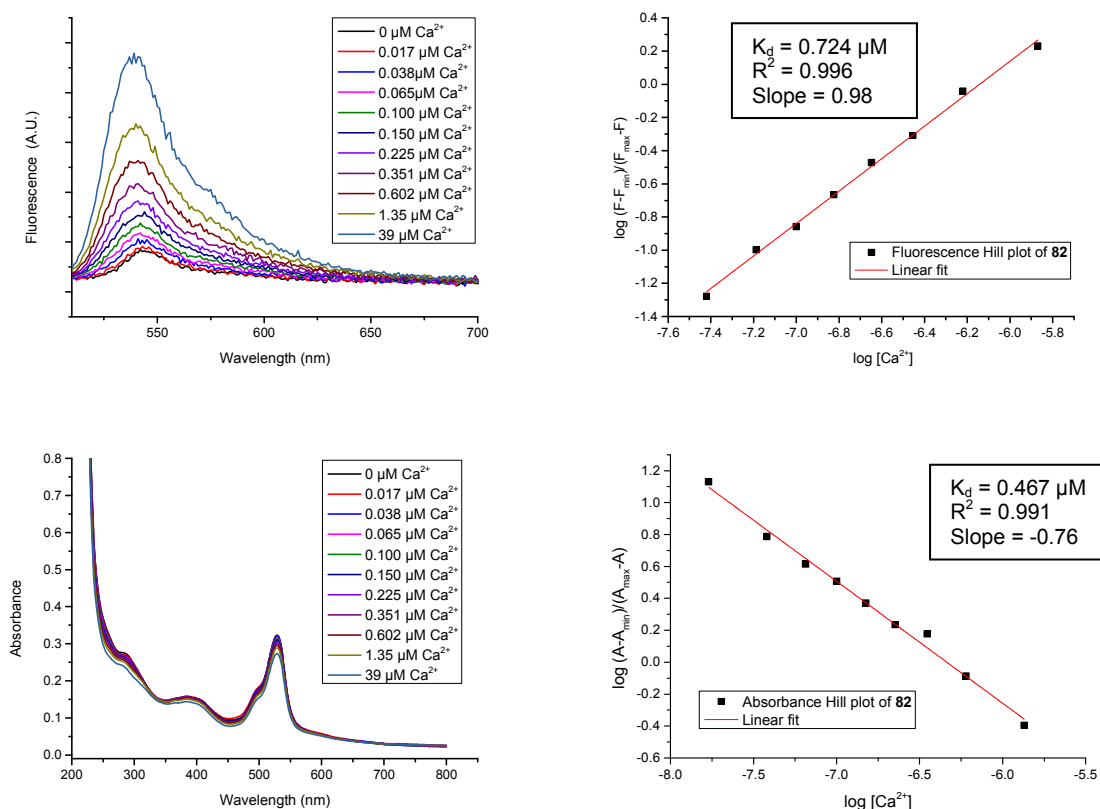


**Figure 63:** Fluorescence emission spectra of amphiphilic BAPTA-BODIPY (**82**) upon  $\text{Ca}^{2+}$ -addition in pseudo intracellular buffer ( $\lambda_{\text{exc}} = 496 \text{ nm}$ ) (top left). Hill plot for the spectral change in fluorescence emission at 542 nm (top right). Electronic absorption spectra of **82** upon  $\text{Ca}^{2+}$ -addition (bottom left). Hill plot for the spectral change in electronic absorption at 265 nm (bottom right).

Electronic absorption and emission spectra upon  $\text{Ca}^{2+}$  addition in aqueous buffer are depicted in figure 64. Fluorescence emission is observed with a rather large Stokes shift of  $6790 \text{ cm}^{-1}$  in the complexed and  $8820 \text{ cm}^{-1}$  in the non-complexed form. The emission band is broad, from 580 nm to almost 800 nm with a maximum emission at 672 nm. Linearising the spectral change at 680 nm via a Hill plot (shown in figure 64, top right) results in a  $K_d$  of  $0.076 \mu\text{M}$ . Due to the additional oxygen at the BAPTA moiety, the ionophore is more electron rich and a higher binding affinity and hence a lower dissociation constant is measured for amphiphilic

fura red (**97**). The slope of the Hill plot indicates also in this case a classical 1:1 binding towards  $\text{Ca}^{2+}$ .

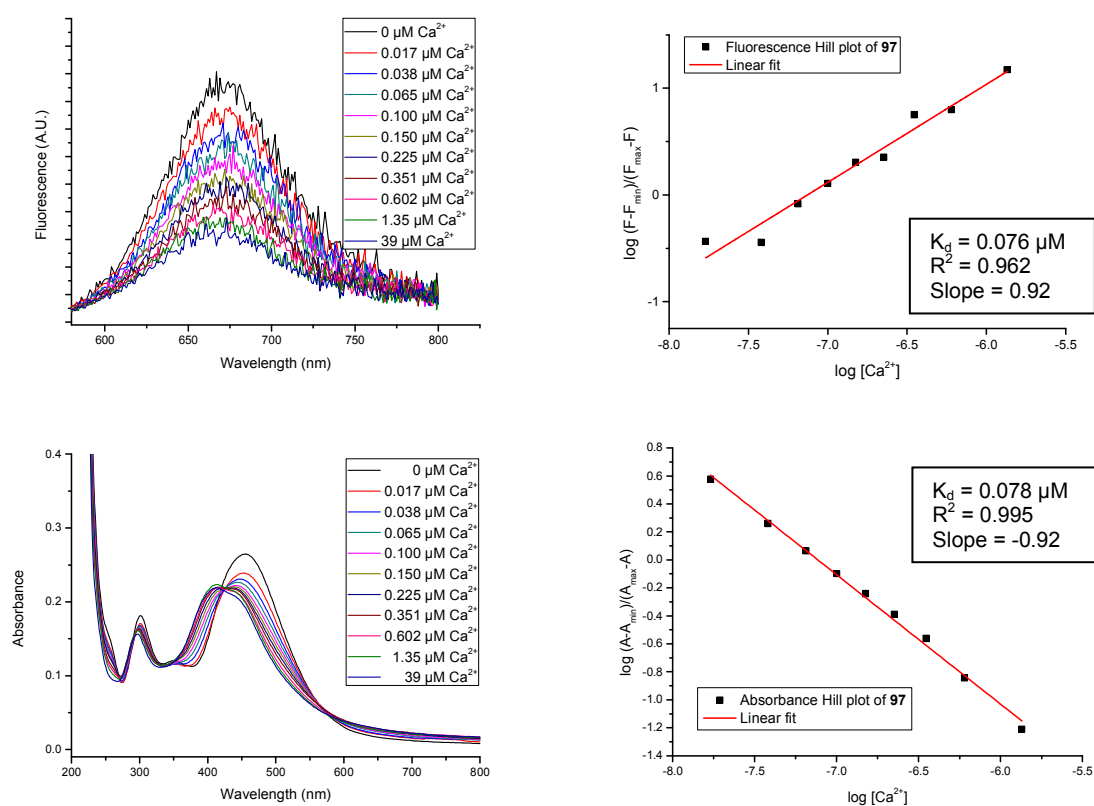


**Figure 64:** Fluorescence emission spectra of  $\text{C}_8\text{F}_{17}$ -fura red (**97**) upon  $\text{Ca}^{2+}$ -addition in pseudo intracellular buffer ( $\lambda_{\text{exc}} = 496 \text{ nm}$ ) (top left). Hill plot for the spectral change in fluorescence emission at 680 nm (top right). Electronic absorption spectra of **97** upon  $\text{Ca}^{2+}$ -addition (bottom left). Hill plot for the spectral change in electronic absorption at 496 nm (bottom right).

The second reason for the decrease and the stronger contribution to the emission decrease is the change in the UV-Vis spectrum. Unlike for the other amphiphilic molecules the major change upon  $\text{Ca}^{2+}$ -binding is observed in the electronic absorption spectrum. The absorption maximum for amphiphilic fura red (**97**) can be found at 456 nm and undergoes a hypsochromic shift to 413 nm accompanied by a decrease of the initial extinction coefficient of  $30700 \text{ M}^{-1}\text{cm}^{-1}$  upon  $\text{Ca}^{2+}$  binding due to internal charge transfer. The absorption spectra show five isosbestic points at 575 nm, 425 nm, 350 nm, 295 nm and at 270 nm. Due to these changes the ion sensor can be used ratiometrically, irradiating at two different wavelengths and comparing the fluorescence emission ratio between these two irradiation wavelengths at different  $\text{Ca}^{2+}$  concentrations. The Hill plot of the spectral change at 496 nm yields a  $K_d$  of  $0.078 \mu\text{M}$ , which is in good agreement with the value obtained from the fluorescence titration.

A summary of the obtained spectral data for amphiphilic fluorionophores **79**, **82** and **97** is depicted in table 07 for better comparison.

**Table 07:** Summary of the spectral characterization of amphiphilic fluorescent ion switches.

Sample	$\epsilon$ ( $M^{-1}cm^{-1}$ )	$\lambda_{abs}$	$\lambda_{em}$	$\Phi_{fluorescence}$	$F_{Ca}/F$
<b>79</b>	17300	436	550	0.006	
<b>79</b> +Ca <sup>2+</sup>		436	575	0.026	4.3
<b>82</b>	56800	529	542	0.001	
<b>82</b> +Ca <sup>2+</sup>		529	542	0.004	4
<b>97</b>	30700	456	672	0.006	
<b>97</b> +Ca <sup>2+</sup>		413	672	0.004	0.6

All three amphiphilic fluorescent Ca<sup>2+</sup>-sensors possess interesting properties and could be appropriate sensors for the envisaged ion transfer studies in vesicles. However, before studying the ion transfer in nanodomains, photoactive Ca<sup>2+</sup>-decaging agents need to be chosen for the ion transfer in solution and later on in nanodomains.

### 3.3 Water soluble and amphiphilic nitrobenzyl-based Ca<sup>2+</sup>-decaging agents

In the general introduction ion binding motives and triggered ion movement / release has been discussed. In this section specific Ca<sup>2+</sup>-decaging agents are introduced and the synthesis and photochemistry of selected Ca<sup>2+</sup>-decaging molecules, appropriate for the following ion transfer experiments are discussed. Many different photolabile Ca<sup>2+</sup>-decaging agents are now known, showing different decaging mechanisms and bearing different photoactive groups. A selection of photoactive molecules described in the literature is given in table 08 and compared to their non-photocleavable molecular counterpart. The nitrobenzyl chromophore is a widely used photo-decaging group and is used, for example, to study ATP-dependent processes in biological systems.<sup>32</sup> This photoactive system has widely been exploited also for sophisticated decaging mechanisms like the simultaneous decaging of a substrate and a reporter molecule via a self-immolated cascade reaction shown in the group of Jullien.<sup>33</sup> The nitrobenzyl moiety was then later on exploited for the photoinduced release of divalent ions such as Ca<sup>2+</sup>. A first example was synthesized by Ellis-Davis *et.al.*<sup>34</sup> using an EDTA-based

binding unit. The molecular structure of this Ca<sup>2+</sup>-decaging agent and its photoproduct is shown in Figure 65.

**Table 08:** Properties of photolabile Ca<sup>2+</sup>-cages and Ca<sup>2+</sup>-chelators.

	K <sub>d</sub> (Ca <sup>2+</sup> ) (μM)	K <sub>d</sub> (prod.) (μM)	Affinity change	K <sub>d</sub> (Mg) (μM)	Quantum yield (Φ)	ε (cm <sup>-1</sup> M <sup>-1</sup> )
<b>EDTA</b>	0.032			5		
<b>EGTA</b>	0.150			12 000		
<b>BAPTA</b>	0.110			17 000		
<b>DM-nitrophen</b>	0.005	3 x 10 <sup>3</sup>	600 000	2.5	0.18	4 300
<b>NP-EGTA</b>	0.080	1 x 10 <sup>3</sup>	12 500	9 000	0.2-0.23	975
<b>DMNPE-4</b>	0.048	2 x 10 <sup>3</sup>	40 000	10 000	0.09	5 120
<b>nitr-5</b>	0.145	6.3	54	8 500	0.012-0.035	5 500
<b>azid-1</b>	0.230	0.12 x 10 <sup>3</sup>	520	8 000	1.0	33 000

An EDTA (**8**) based Ca<sup>2+</sup>-decaging agent has, however, the drawback that the binding affinities for Ca<sup>2+</sup> and Mg<sup>2+</sup> are both rather high. Since the cellular concentration of Mg<sup>2+</sup> is between 3 – 4 orders of magnitudes higher than that of Ca<sup>2+</sup>. A set of more selective decaging agents has been developed in the group of Ellis-Davies in 1998.<sup>35</sup> Here the Ca<sup>2+</sup> binding unit is based on EGTA (**9**), which has a binding affinity difference for the two divalent cations of more than 10<sup>4</sup>. The most notably and widely used derivative is DMNPE-4 (**99**) which is also depicted in figure 65. The difference in binding affinity before and after photolysis of these decaging-agents is rather high, with an affinity change of 600000 and 40000 being published in the literature as denoted in table 08.<sup>36</sup> This rather large change is based on the cleavage of the ion binding unit which leads to two molecules with tremendously lowered binding affinity. The mechanism for nitrobenzyl- based photocleavage is highlighted in scheme 17. Other photoactive Ca<sup>2+</sup>-ejectors are based on BAPTA (**10**) which is a derivative of EGTA (**9**) bearing anilines in place of aliphatic amines. This gives rise to a slightly improved binding affinity towards Ca<sup>2+</sup> due to the higher electron density and an slightly improved affinity for Ca<sup>2+</sup> over Mg<sup>2+</sup> 155000 K<sub>Mg</sub>/K<sub>Ca</sub> (BAPTA, **10**) and 80000 (EGTA, **9**). Since the electron pair of the aniline is included in the conjugation of the aromatic ring processes like photoinduced electron transfer and it can be harnessed to create fluorescent ion switches as described in the previous section. A second advantage is the relative insensitivity of the binding affinity under

physiological conditions due to the lower pK<sub>a</sub> of the anilines (pK<sub>a</sub> = 4 – 6) compared to the amines in EGTA (**9**) (pK<sub>a</sub> = 10).

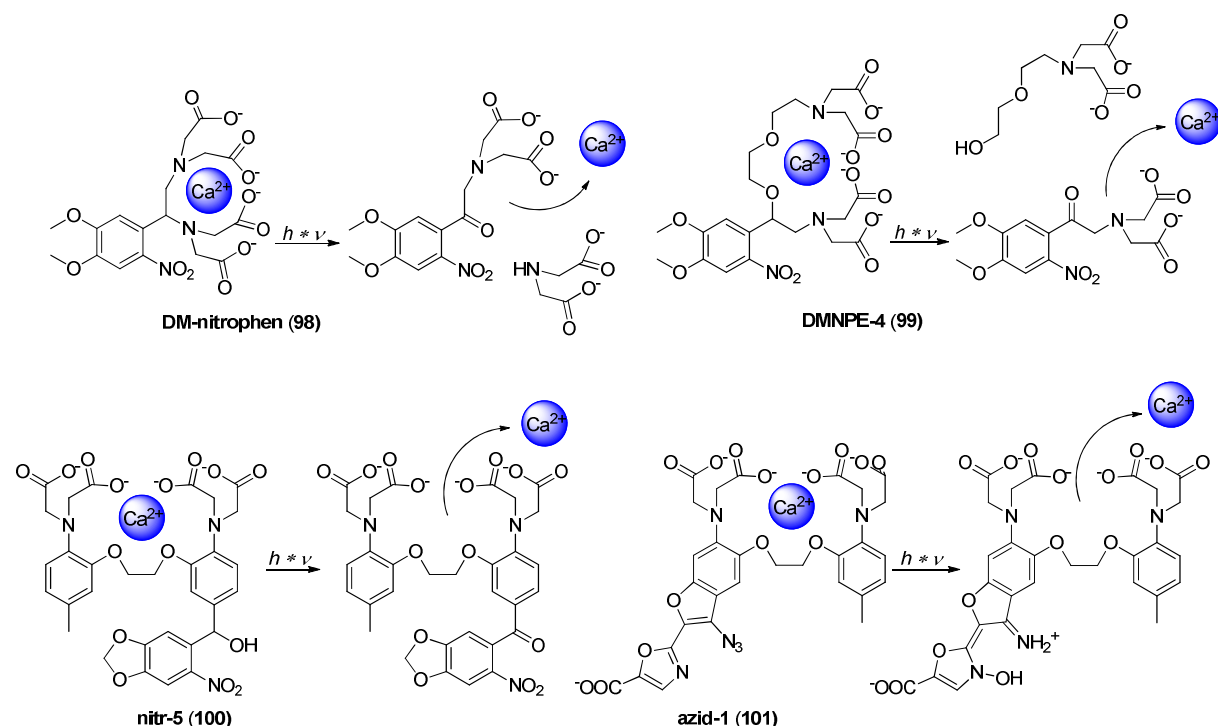
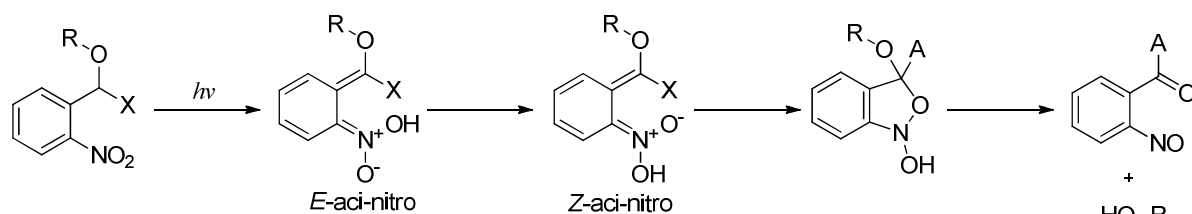


**Figure 65** : Structural formulas of photolabile EDTA, EGTA and BAPTA-based Ca<sup>2+</sup>-cages and their respective photoproducts resulting in a decrease in binding affinity and a release of Ca<sup>2+</sup>-ions.

In terms of Ca<sup>2+</sup>-decaging of BAPTA derivatives, most mechanisms include the lowering of the electron density in the aromatic ring and thus a decrease in the binding affinity. “nitr” derivatives carry a *o*-nitrobenzhydryl unit as an extension to one of the aromatic rings. Upon irradiation in the UV, the nitrobenzyl moiety undergoes the same reaction mechanism displayed in scheme 17. Instead of cleaving a part of the binding unit as in the case of DMNPE-4 (**99**), the “nitr” compounds liberate H<sub>2</sub>O while forming a ketone.



**Scheme 17**: Mechanism of the nitrobenzyl photoreaction carrying different substituents.

This increases the conjugation of the system to the nitrobenzyl fragment which was previously separated. Due to the electron deficient nature of the nitrobenzyl chromophore, the electron density of the aniline is lowered and the molecule experiences a decrease in binding

---

affinity from 0.145  $\mu\text{M}$  to 6.3  $\mu\text{M}$ , which is a 54-fold decrease. The side product during the photo-reaction is only water which makes that molecule suitable for biological studies. Tsien and Zucker used these compounds as early as 1986 to control cytoplasmic calcium with light.<sup>38</sup> The quantum yield for the photoreaction is rather low (0.012 – 0.015) which renders this type of photo-decaging molecule inconvenient, since long irradiation times or high irradiation power is needed to release sufficient  $\text{Ca}^{2+}$  which can provoke photodegradation. The BAPTA derivative azid-1 (**101**) shown in figure 65 (bottom right) tackles these problems.<sup>39</sup> The  $\text{Ca}^{2+}$ -decaging agent carries a benzofuran fluorophore on one side of the molecule much like its parent molecule fura-2 (**35**) which is commercially available. In the 3-position of the benzofuran ring azid-1 (**101**), however, bears an aromatic azide. Aromatic azides undergo nitrene formation upon irradiation which can lead to a variety of products. The major photoproduct is also shown in figure 65. Passing through the nitrene state the reaction evolves towards an imminium product which carries a positive charge yielding as only side product only  $\text{N}_2$  in the reaction pathway. This positive charge is responsible for an enormous decrease in binding affinity due to conjugation to the aniline part of the molecule. The change in binding affinity was determined to be 520-fold from 0.230  $\mu\text{M}$  to essentially 120  $\mu\text{M}$ . The quantum yield for the photoreaction was measured to be slightly higher than one which was attributed to the experimental error of the set up.

In recent years some progress has been made in terms of new  $\text{Ca}^{2+}$ -decaging molecules. Main goal is always to create molecules with a large difference in binding affinity or a increased sensitivity towards a trigger like light which results in a higher decaging yield. In the group of del Campo  $\text{Ca}^{2+}$ -decaging molecule has been developed based on the design of nitr-5 (**100**).<sup>40</sup> The photolabile molecule bears two photodecaging groups in the para-position to the aniline namely *o*-nitrobenzhydryl groups. Upon irradiation the photosensitive group undergoes photoconversion to the 4-amino-2'-nitrosobenzophenone which has an electron withdrawing effect on the BAPTA unit. The change in binding affinity was measured to be 3000-fold compared to 40-fold in the presence of only one photodecaging group. The incorporation of two photolabile groups simultaneously increased the  $\text{Ca}^{2+}$  decaging tremendously but EGTA based decaging agents still give higher affinity changes. The advantage is though that a relatively high release rate is combined with the pH insensitivity of BAPTA based  $\text{Ca}^{2+}$ -binders.

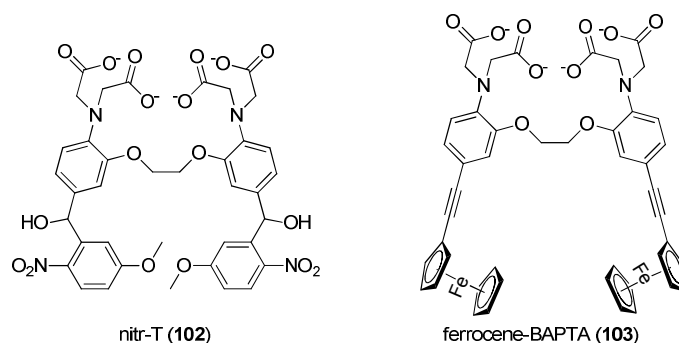


**Figure 66:** Recent developments in the  $\text{Ca}^{2+}$ -decaging field. Left: nitr-T (**102**) a photolabile decaging agent with a binding affinity change of 3000-fold. Right: A redox triggered  $\text{Ca}^{2+}$ -decaging agent based on ferrocene (**103**).

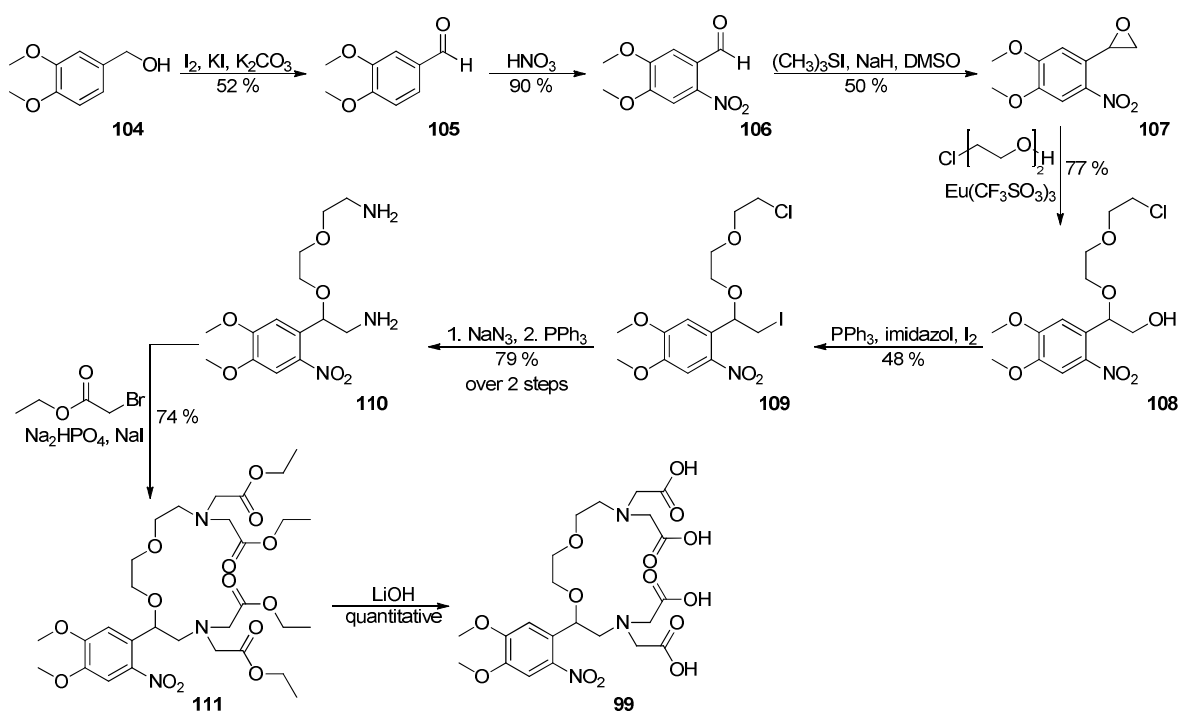
A redoxactive  $\text{Ca}^{2+}$ -chelator (**103**) has been designed by Bhattacharyya *et.al.*<sup>41</sup> The BAPTA based binding unit is substituted in the para position of both aromatic rings with a ferrocenyl-ethynyl-unit (see figure 66, right). First electrochemical tests have been performed which revealed a different behavior in terms of the oxidation of the aniline in presence and absence of the ion. The preliminary results of the study encouraged further investigation in electrochemical release measurements which have yet to be carried out.

However, the goal of the project was light triggered ion transfer with focus on the photoactive decaging agents. Irradiation of DM-nitrophen (**98**) shows a big change in binding affinity but only a rather low selectivity for  $\text{Ca}^{2+}$  over  $\text{Mg}^{2+}$ . While the change in binding affinity for nitr-5 (**100**) and its derivatives only show a moderate difference with rather low photolysis quantum yields and nitr-T was not known at the beginning of this work, the choice for the building block of the photolabile  $\text{Ca}^{2+}$ -decaging agent fell to azid-1 and DMNPE-4 (**99**). First tests with azid-1 (**101**) in the laboratory showed that the photochemical quantum yield of azid-1 ( $\phi = 1$ ) actually proved problematic since light needed to be omitted entirely. Photolysis occurred already during the transport of a azid-1 (**101**) sample from one room to another. Due to the high change in  $\text{Ca}^{2+}$ -affinity, while retaining a high selectivity for  $\text{Ca}^{2+}$  over  $\text{Mg}^{2+}$  DMNPE-4 (**99**) was chosen as building block for the following  $\text{Ca}^{2+}$ -decaging molecules in this study, even though the photochemical quantum yield was much lower than the one for azid-1 ( $\phi = 0.09$ ).

### 3.3.1 Synthesis of Ca<sup>2+</sup>-decaging agents DMNPE-4 (**99**) and amphiphilic DMNPE-4 (**122** and **124**)

#### 3.3.1.1 Synthesis of DMNPE-4 (**99**)

The synthetic pathway largely followed the procedure published by Ellis-Davies.<sup>35</sup> Experimental details however were not available and therefore the synthesis was altered in several places. Reaction conditions and yields are depicted in scheme 18. The first reaction in the 8 step synthesis to the DMNPE-4 Ca<sup>2+</sup>-decaging agent started from commercially available (3,4-dimethoxyphenyl)methanol (**104**), which was oxidized using iodine under basic conditions to yield the 3,4-dimethoxybenzaldehyde (**105**) in 52 % yield. The nitro group in the 2-position of the phenyl ring was introduced using a mild nitration procedure using HNO<sub>3</sub> in DCM at 0 °C. This reaction lead to the photoactive core, a functionalized nitrobenzyl unit, in 90 % reaction yield. The sodium methylsulfonylmethylide reagent was prepared with trimethylsulfonyl iodide and NaH in DMSO. The



**Scheme 18:** Synthetic route for the water soluble photo-labile Ca<sup>2+</sup> decaging agent DMNPE-4 (**99**).

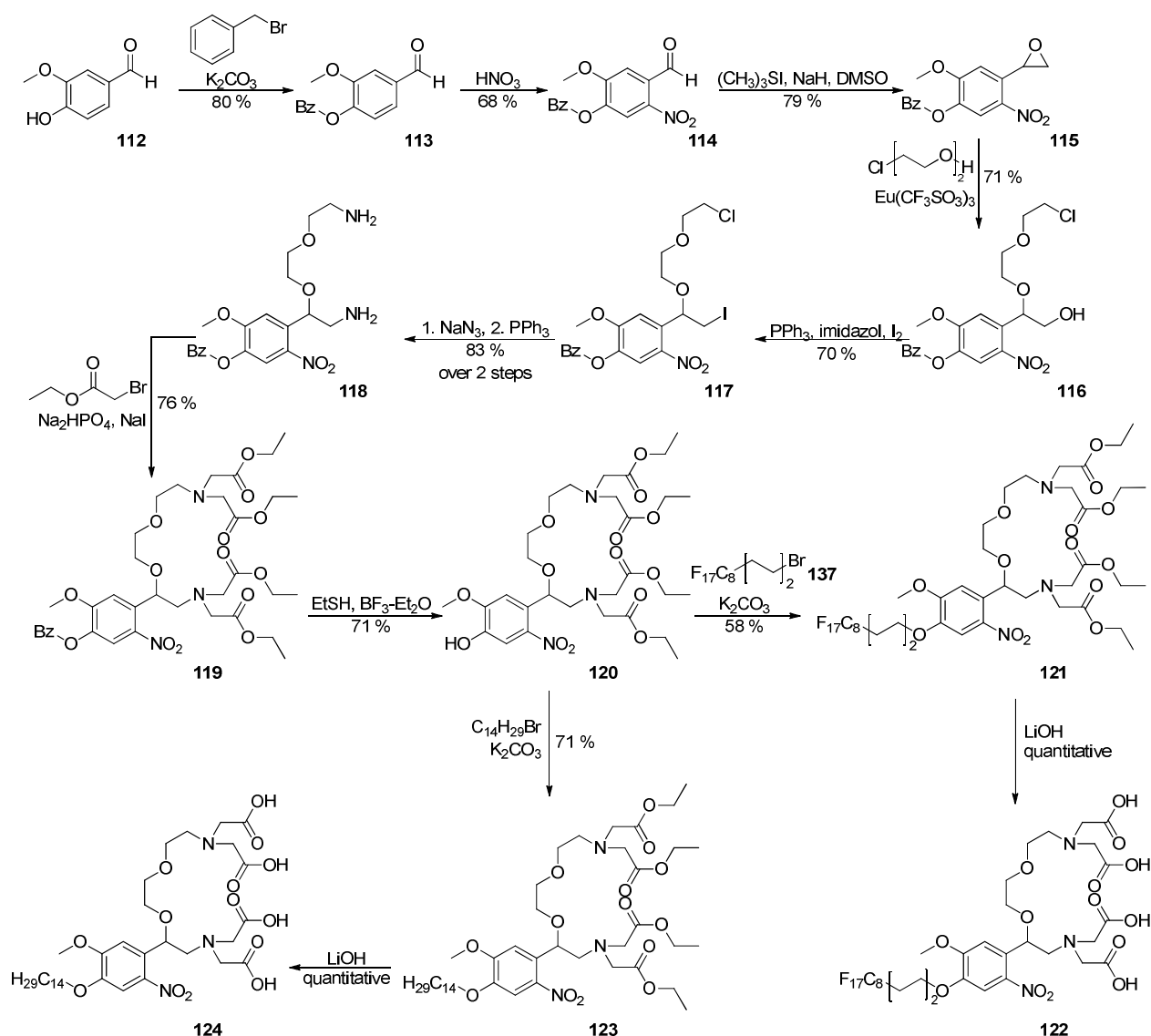
After addition of 2,4-dimethoxy-2-nitrobenzaldehyde (**106**) to the solution the 2-(4,5-dimethoxy-2-nitrophenyl)oxirane (**107**) was obtained with a reaction yield of 50 %. **107** was subsequently reacted with 2-(2-chloroethoxy)ethanol in presence of europium triflate as catalyst to obtain the photolabile intermediate **108** in 77 % yield. The hydroxyl group was then effectively replaced by an iodide in order to show the same reactivity as the chlorine

---

using triphenylphosphine in the presence of imidazole and I<sub>2</sub>. Intermediate **109** was obtained with 48 % yield and subsequently subjected to a two step reaction replacing the two halogens. **110** was obtained by first replacing the halogens with azides using NaN<sub>3</sub> in DMF and after the reaction was complete triphenylphosphine was added to reduce the azides to their corresponding amines. The reaction proceeded smoothly and the diamine intermediate (**110**) was obtained in 79 % yield over the two steps. Classical conditions known from the BAPTA syntheses were employed to yield the ester protected DMNPE-4 (**111**), namely the reaction of the diamine under basic conditions with ethyl bromoacetate using Na<sub>2</sub>HPO<sub>4</sub> as a base and KI as a catalyst. The reaction yield was 74 % and after hydrolysis of the ester using the mild LiOH based procedure the water soluble DMNPE-4 Ca<sup>2+</sup>-ejector (**99**) was obtained quasi-quantitatively without further purification.

### 3.3.1.2 Synthesis of amphiphilic DMNPE-4 (122 and 124)

The synthesis of the amphiphilic versions of the DMNPE-4 Ca<sup>2+</sup>-photo decaging agent (**124**) was performed adapting the successful steps developed in the synthesis described for the water soluble decaging molecule (**99**). However, the synthesis started with the benzyl protection of commercially available vanillin (**112**) using benzyl bromide under basic conditions to yield **113** (80 %). The synthesis route is shown in scheme 19. The benzyl protected vanillin was then directly subjected to nitration with HNO<sub>3</sub> in an organic solvent to obtain the 4-(benzyloxy)-5-methoxy-2-nitrobenzaldehyde (**114**). **115** to **119** were obtained using the same set of reactions as described previously for DMNPE-4. Reaction yields were either in the same range as previously recorded or slightly improved showing the same reactivity of the corresponding intermediates. The benzyl and ester protected DMNPE-4 intermediate (**119**) was selectively benzyl deprotected using ethane thiol in the presence of boron trifluoride diethyletherate complex to yield an ester protected DMNPE-4 intermediate bearing a free OH group (**120**). **120** is an important intermediate since different aliphatic chains or different chain lengths can be introduced following a simple nucleophilic substitution reaction under basic conditions. In our study we will focus on fluorinated self-assembled amphiphilic vesicles and therefore an aliphatic chain bearing a C<sub>8</sub>F<sub>17</sub>-unit was envisaged. To that end, HO-DMNPE-4 **120** was reacted with C<sub>8</sub>F<sub>17</sub>-butyl bromide (**137**) in the presence of K<sub>2</sub>CO<sub>3</sub> to obtain the ester-protected C<sub>8</sub>F<sub>17</sub>-DMNPE-4 (**121**). Again the hydrolysis using LiOH led to the final product (**122**) quasi-quantitatively and was used without further purification.



**Scheme 19:** Synthesis route for the amphiphilic photo-labile  $\text{Ca}^{2+}$ -decaging agent based on DMNPE-4 (**53**).

**124** was synthesized on reacting intermediate **120** with tetradecyl bromide under basic conditions to yield **123** in 71% yield and subsequent hydrolysis of the esters was performed using  $\text{LiOH}$  to obtain  $\text{C}_{14}\text{H}_{29}$ -DMNPE-4 (**124**) quasi-quantitatively.

### 3.3.2 Spectral characterization and $\text{Ca}^{2+}$ binding studies of DMNPE-4 (**99**) and $\text{C}_{14}\text{H}_{29}$ -DMNPE-4 (**124**)

Amphiphilic  $\text{Ca}^{2+}$ -decaging agent (**124**) was studied as a representative example of amphiphilic DMNPE-4 based decaging agents. Due to the obtained results the assumption was made, that the fluorinated analog possesses the same spectral properties. The electronic

absorption bands of **99** and **124** have essentially the same shape with similar absorption maxima at 345 nm and 346 nm, respectively. Indeed, the difference of 1 nm falls within the error of the machine. Absorption maxima and extinction coefficients correspond well to the reported values of 350 nm and  $5100 \text{ cm}^{-1}\text{M}^{-1}$ .<sup>36</sup> Values for DMNPE-4 (**99**) and C<sub>14</sub>H<sub>29</sub>-DMNPE-4 (**124**) are  $5110 \text{ cm}^{-1}\text{M}^{-1}$  and  $5150 \text{ cm}^{-1}\text{M}^{-1}$  respectively as reported in table 09.

**Table 09:** Spectral properties of DMNPE-4 (**99**) and C<sub>14</sub>H<sub>29</sub>-DMNPE-4 (**122**).

	Abs. max	$\epsilon \text{ (cm}^{-1}\text{M}^{-1}\text{)}$	$\Phi_{\text{photocleavage}}$	$K_d \text{ (}\mu\text{M)}$
<b>99</b>	345	5110	0.09	0.057
<b>124</b>	346	5150	0.1	0.032

Since the absorption spectra of the Ca<sup>2+</sup>-cages are very flat around the maximum, a small deviation from the literature data is not surprising. Upon irradiation at 365 nm both compounds undergo the photoinduced cleavage of the substituent in the benzyl position. After the initial photochemical reaction, which is the abstraction of an proton in the benzyl position leading to the *aci-nitro* intermediate as shown in the reaction mechanism for nitrobenzyl protected compounds in scheme 17, deexcitation occurs via bond rupture in benzyl position and reorganization of the  $\pi$ -electron system.<sup>42</sup> If the molecules carry an oxygen on the benzylic carbon the reaction results in the formation of a carbonyl group as shown. The formation of the resulting new compound can be monitored by means of electronic absorption spectroscopy.

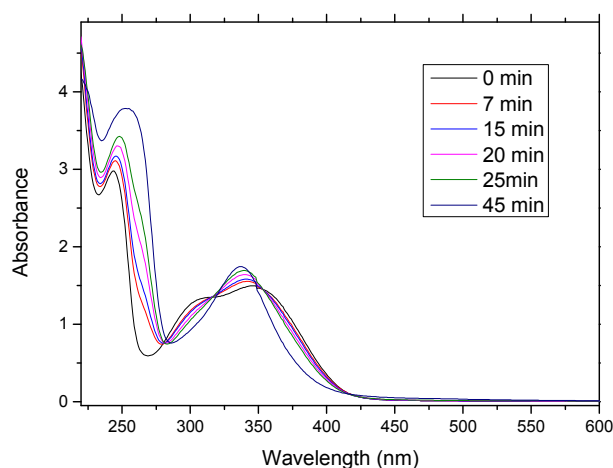


**Figure 67:** Spectral changes in the electronic absorption spectrum of **99** upon irradiation at 365 nm for 0, 7, 15, 20, 25 and 45 min using a mercury lamp with monochromator (see experimental section).

---

The photocleavage of **99** is observed in figure 67 and is representative for both molecules since they bear the same photoactive group. In fact no evident difference could be observed between **99** and **124**. Upon irradiation at 365 nm, the absorption maximum shows a hypsochromic shift towards 336 nm. Isosbestic points at 282, 315 and 355 nm indicate the clean conversion into the ketone with no other absorbing side products present. Photochemical quantum yields have been determined using a ferrioxalate actinometer (see experimental section for precise procedure).<sup>43</sup> Briefly, a sample containing ferrioxalate was irradiated at 365 nm and subsequently the Fe<sup>2+</sup>-ions produced during irradiation were complexed with 1,10-phenanthroline (phen) to obtain the colored Fe(phen)<sub>3</sub><sup>2+</sup> complex. Knowing the quantum yield for the photoreaction of ferrioxalate and the irradiation time, the amount of produced Fe<sup>2+</sup> per time unit and therefore the amount of incident photons per unit time could be determined by measuring the absorption of the lowest lying Metal-to-Ligand Charge Transfer absorption band of the Fe(phen)<sub>3</sub><sup>2+</sup> complex, whose molar extinction coefficient is known. Thus samples of DMNPE-4 (**99**) and C<sub>14</sub>H<sub>29</sub>-DMNPE-4 (**124**) were irradiated and the conversion into the ketone was checked via UV-Vis spectroscopy. The photochemical quantum yield was then calculated to be 0.09 (**99**) and 0.1 (**124**). The value for DMNPE-4 (**99**) is the same as that measured in the literature, while the quantum yield for **124** is slightly higher, which falls within the error in the measurement and may be considered essentially the same.

Ca<sup>2+</sup>-binding affinities could not be determined by direct titration as for the BAPTA-based fluorescent switches. Since there is no conjugation between the EGTA binding unit and the benzene ring, no discernible optical changes concomitant with complexation were observed. In order to overcome this problem an indirect determination of the K<sub>d</sub> was performed. To that end, a more concentrated solution of Ca<sup>2+</sup>-ejector was prepared in pseudo-intracellular buffer (100 mM KCl, 30 mM MOPS, pH 7.2) and CaCl<sub>2</sub> was been added stepwise. The change in free Ca<sup>2+</sup> concentration was then monitored via a competition experiment with a fluorescent ion sensor with a known binding affinity. BAPTA-BODIPY (**72**) was used as the reference.<sup>3</sup> In figure 68 (left) the fluorescence emission spectra of a solution containing 0.80 mM of DMNPE-4 (**99**) and 6 μM of BAPTA-BODIPY (**72**) in the presence of varying amounts of CaCl<sub>2</sub> is shown. The data can then be linearised using a Scatchard-type analysis shown in figure 68 (right).

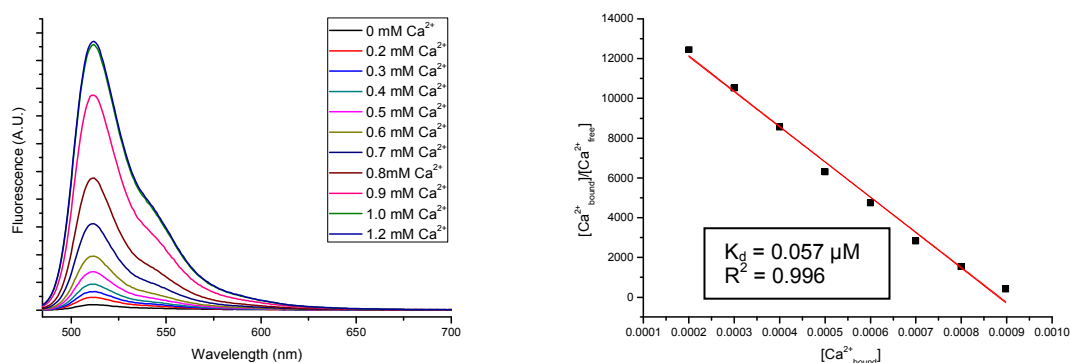


**Figure 68:** Fluorescence emission spectra of a solution containing 0.80 mM of DMNPE-4 (**99**) and 6  $\mu\text{M}$  of BAPTA-BODIPY (**72**) in the presence of varying amounts of  $\text{Ca}^{2+}$  in pseudo intracellular buffer ( $\lambda_{\text{exc}} = 476 \text{ nm}$ ) (left). Scatchard plot of the  $\text{Ca}^{2+}$ -titration (right).

In the Scatchard plot the concentration of bound  $\text{Ca}^{2+}$  divided by the concentration of free  $\text{Ca}^{2+}$  is plotted over the concentration of free  $\text{Ca}^{2+}$ . The slope of the graph yields the negative association constant of the studied molecule. BAPTA-BODIPY (**72**) is in this case a sensor for the free  $\text{Ca}^{2+}$ -concentration. The obtained  $K_d$  value for DMNPE-4 (**99**) was determined to be 0.057  $\mu\text{M}$  which is in good agreement with the published data ( $K_d = 0.048 \mu\text{M}$ ) as shown in table 09. This is not only a verification that the synthesized ion-ejector (**99**) is the targeted molecule but also that the determined  $K_d$  values for BAPTA-BODIPY (**72**) is correct.

The  $\text{Ca}^{2+}$ -dissociation constant ( $K_d$ ) of  $\text{C}_{14}\text{H}_{29}$ -DMNPE-4 (**124**) was determined in the same fashion. A solution of 0.62 mM  $\text{C}_{14}\text{H}_{29}$ -DMNPE-4 (**124**) and 5.2  $\mu\text{M}$  BAPTA-BODIPY (**72**) was prepared in a pseudo-intracellular buffer (100 mM KCl, 30 mM MOPS, pH 7.2) and the fluorescence emission spectra were recorded as above in the presence of varying concentrations of  $\text{CaCl}_2$ . The fluorescence emission spectra of the titration are given in figure 69 on the left side and the corresponding Scatchard plot is shown in the same figure on the right side.

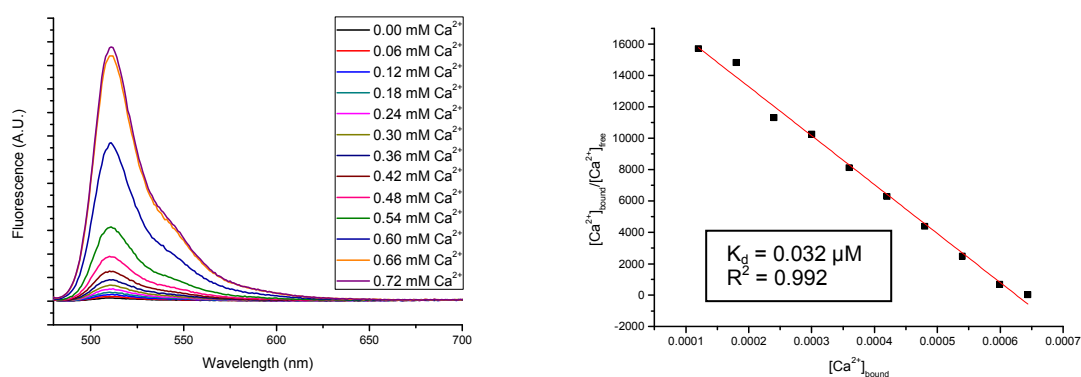


**Figure 69:** Fluorescence emission spectra of a solution containing 0.62 mM of  $C_{14}H_{29}$ -DMNPE-4 (**124**) and 5.2  $\mu$ M of BAPTA-BODIPY (**72**) in the presence of varying amounts of  $Ca^{2+}$  in pseudo intracellular buffer ( $\lambda_{exc} = 476$  nm) (left). Scatchard plot of the  $Ca^{2+}$ -titration (right).

The  $K_d$  value obtained from the linear fitting of the Scatchard plot gave a dissociation constant of  $K_d = 0.032 \mu$ M which is slightly lower, but in good agreement with, the  $K_d$  value of the parent molecule. Since the binding affinity for DMNPE-4 (**99**) and  $C_{14}H_{29}$ -DMNPE-4 (**124**) are similar it can be assumed that the change in binding affinity is equally similar upon photo-cleaving the  $Ca^{2+}$ -recognition unit. However, the experiments have not been performed due to the lack of a  $Ca^{2+}$ -sensitive electrode in the laboratory.

### 3.4 $Ca^{2+}$ -transfer between DMNPE-4 (**99**) and BAPTA-BODIPY (**72**) under pseudo intracellular conditions

Ion transfer between photolabile ion-ejectors and a water soluble ion-acceptor has been shown in the literature for several different molecules. In most of the cases the ion transfer was used to show the actual release from a newly synthesized decaging agent. One example is the ZnClev-2 published in the group of Burdette.<sup>44</sup> The molecule consists of a  $Zn^{2+}$  binding unit using TPEN (N,N,N',N'-tetrakis(2-pyridylmethyl)-ethylenediamine) and a nitrobenzyl chromophore much like in the case of DMNPE-4 (**99**). Upon irradiation at 350 nm the  $Zn^{2+}$  was released and the ion was taken up by a fluorescent  $Zn^{2+}$ -switch thus increasing the fluorescence emission of the solution.  $Ca^{2+}$ -transfer was shown in the group of Ellis-Davis using DMNPE-4 (**99**) and commercially-available Ca-orange-5N as ion detector.<sup>36</sup> In the following experiments the optimization of the ion transfer conditions will be carried out and

---

the ion transfer between DMNPE-4 (**99**) and BAPTA-BODIPY (**72**) will be studied in aqueous solution in order to apply these conditions for the ion transfer between vesicles.

The ideal ratio between  $\text{Ca}^{2+}$ -ejector (**99**) and fluorescent  $\text{Ca}^{2+}$ -acceptor (**72**) was determined by means of fluorescence titration. A solution containing  $5\ \mu\text{M}$  of BAPTA-BODIPY (**72**) and  $5\ \mu\text{M}$   $\text{CaCl}_2$ , in order to turn on the fluorescence, in pseudo-intracellular buffer was prepared and 1 to 10 equivalents of DMNPE-4 (**99**) were added yielding the curve (black squares) in figure 70. The same titration was performed using **99** after photolysis at 365 nm. Adding 1 to 10 equivalents of this photolysed solution to the same BAPTA-BODIPY (**72**) containing buffer yielded the curve shown in red dots in figure 70.

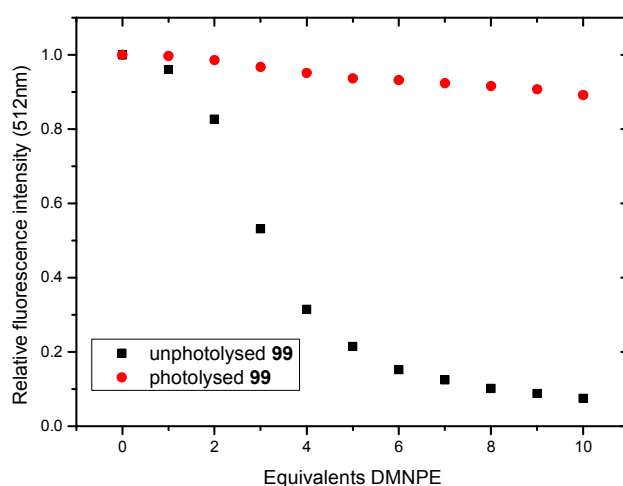


**Figure 70:** Fluorescence titration ( $\lambda_{\text{exc}} = 476\ \text{nm}$ ) of a solution containing  $5\ \mu\text{M}$  BAPTA-BODIPY (**72**) and  $5\ \mu\text{M}$   $\text{CaCl}_2$  in pseudo intracellular buffer (100 mM KCl, 30 mM MOPS, pH 7.2) with unphotolysed (black squares) and photolysed (red dots) DMNPE-4 (**99**).

The titration curve using unphotolysed **99** describes a sigmoid shape due to the equilibrium between the two  $\text{Ca}^{2+}$  binding species in solution. The titration with photolysed **42** shows only a small decline in fluorescence intensity with about 90 % of its initial fluorescence after the addition of 10 equivalent of photolysed ion ejector. This shows that even though the binding affinity towards  $\text{Ca}^{2+}$  is greatly reduced, a certain binding of the ions remains even in the photolysed form. Between 8 and 10 equivalent of DMNPE-4 (**99**) the difference in fluorescence intensity is maximal. Thus, for the following ion transfer experiment 10 eq of **99** with respect to BAPTA-BODIPY (**72**) were used.

The photoinduced ion transfer experiment was performed in pseudo-intracellular buffer and the fluorescence emission of the BAPTA-BODIPY (**72**) is shown in figure 71. The first part of the experiment is the addition of  $\text{Ca}^{2+}$  in the form of  $\text{CaCl}_2$  to a solution  $5 \mu\text{M}$  BAPTA-BODIPY (**72**) and is shown in black. The fluorescence intensity is already quite elevated (80 %) at the beginning of the experiment, which can be attributed to the impurities of  $\text{Ca}^{2+}$  in the glassware and the buffer solution. The addition of  $5 \mu\text{M}$   $\text{Ca}^{2+}$  increases the fluorescence emission to its maximum due to the uptake of the free  $\text{Ca}^{2+}$  by the fluorescent ion sensor (**72**). The addition of another equivalent does not increase the fluorescence any further.

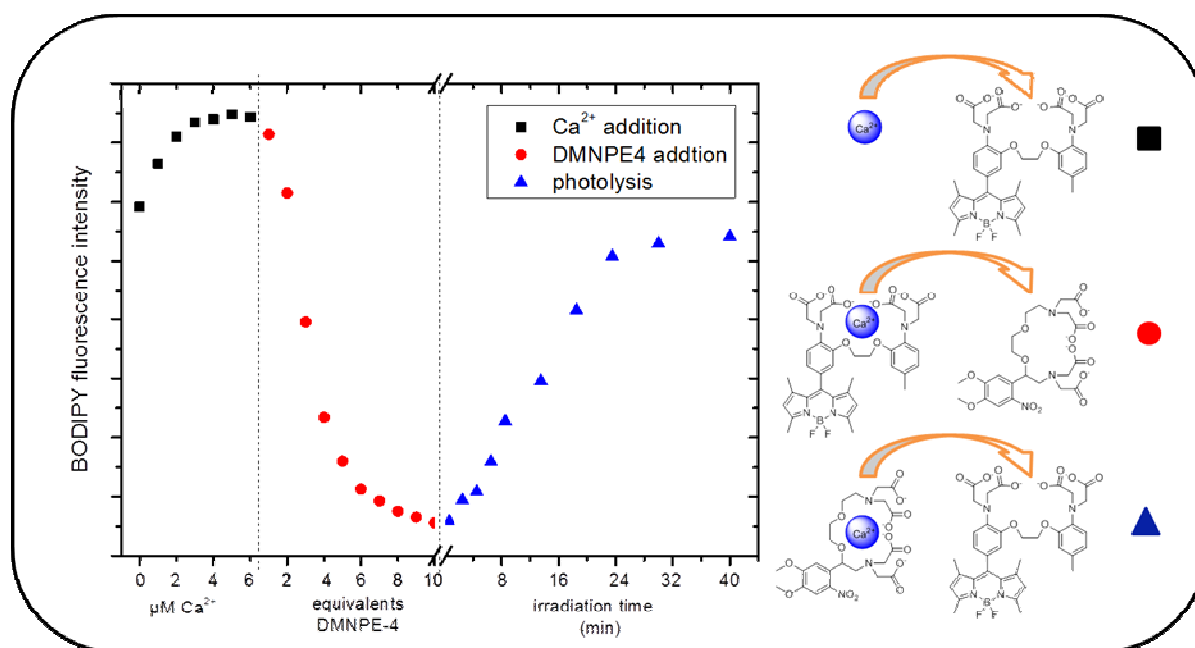


**Figure 71:** Fluorescence intensity at 512 nm of BAPTA-BODIPY (**72**) ( $\lambda_{\text{exc}} = 476 \text{ nm}$ ) upon addition of  $\text{CaCl}_2$  (black), DMNPE-4 (**99**) and upon irradiation at 365 nm (blue) using a mercury lamp with monochromator on an irradiation bench with 15 cm distance between sample and lamp.

The second part of the experiment consists of the addition of the water soluble photolabile  $\text{Ca}^{2+}$ -decaging agent (**99**). Similarly to the experiment shown in figure 70, the fluorescence intensity decreases in a sigmoidal fashion due to the equilibrium between the two species until it reaches almost its minimum after the addition of 10 eq DMNPE-4 (**99**), at which point the  $\text{Ca}^{2+}$  ion can be considered as transferred to the ejector. The last part of the experiment is shown in blue and consists of the irradiation of the solution at 365 nm in order to cleave the decaging agent (**99**) and transfer the  $\text{Ca}^{2+}$  in a photo-controlled fashion back to the ion sensor (**72**). It is shown in figure 71, that on increasing the irradiation time more fluorescence is restored resulting from the photocleavage of **42** and the ion transfer to the ion sensor (**72**). The maximum fluorescence emission is attained after 30 min and further irradiation does not

---

increase the fluorescence emission any more. The maximum emission corresponds to 75 % of the overall emission in the experiment which is due to the binding affinity of the photoproducts of Ca<sup>2+</sup>-decaging agent (**99**) and the induced photobleaching of the fluorophore. The ion-sensor itself absorbs at 365 nm and the rather long irradiation time could explain the lowered maximum fluorescence emission observed.

### 3.5 Conclusion

In addition to the water soluble Ca<sup>2+</sup> which have been concluded earlier, three novel amphiphilic Ca<sup>2+</sup>-ion sensors have been synthesized and show efficient binding under pseudo-intracellular conditions of pH and ionic strength. Ca<sup>2+</sup>-dissociation constants of 0.185 μM for BANIF (**79**), 0.724 μM for C<sub>8</sub>F<sub>17</sub>-BAPTA-BODIPY (**82**) and 0.076 μM for C<sub>8</sub>F<sub>17</sub>-fura red (**97**) had been determined via fluorescence titrations. The obtained values are in good agreement with known Ca<sup>2+</sup>-sensors in the literature and commercially available. The fluorescence enhancement of BANIF (**79**) (4.3-fold) and C<sub>8</sub>F<sub>17</sub>-BAPTA-BODIPY (**82**) (4-fold) is somewhat diminished due to their amphiphilic nature and the aggregation of the molecules in aqueous media. C<sub>8</sub>F<sub>17</sub>-fura red (**97**) shows ratiometric behaviour in the absorption spectrum upon Ca<sup>2+</sup> binding which can be exploited for ratiometric measurements of Ca<sup>2+</sup> concentration in solution. In addition water soluble (**99**) and amphiphilic Ca<sup>2+</sup>-decaging agents bearing a hydrocarbon (**122**) and a fluorocarbon chain (**124**) have been synthesized which show a high affinity towards Ca<sup>2+</sup> (0.057 μM and 0.032 μM respectively). Upon irradiation and photocleavage of the Ca<sup>2+</sup>-binding site the binding affinity of these molecules decreases. Finally the Ca<sup>2+</sup>-based ion transfer between DMNPE-4 (**99**) and BAPTA-BODIPY (**72**) has been established under pseudo-intracellular conditions determining the molecular ratio of ion-ejector and ion-sensor for the following experiments in self-assembled systems.

---

## References

- (1) Gryniewicz, G.; Poenie, M.; Tsien, R. Y. *J. Biol. Chem.* **1985**, *260*, 3440.
- (2) Singh-Rachford, T. N.; Haefele, A.; Ziessel, R.; Castellano, F. N. *J. Am. Chem. Soc.* **2008**, *130*, 16164.
- (3) Vives, G.; Giansante, C.; Bofinger, R.; Raffy, G.; Del Guerzo, A.; Kauffmann, B.; Batat, P.; Jonusauskas, G.; McClenaghan, N. D. *Chem. Commun.* **2011**, *47*, 10425.
- (4) Tsien, R. Y. *Biochemistry* **1980**, *19*, 2396.
- (5) Tahtaoui, C.; Demailly, A.; Guidemann, C.; Joyeux, C.; Schneider, P. *J. Org. Chem.* **2010**, *75*, 3781.
- (6) Rotman, B.; Papermas. *Bw Proc. Natl. Acad. Sci. U. S. A.* **1966**, *55*, 134.
- (7) Kee, H. L.; Kirmaier, C.; Yu, L. H.; Thamyongkit, P.; Youngblood, W. J.; Calder, M. E.; Ramos, L.; Noll, B. C.; Bocian, D. F.; Scheidt, W. R.; Birge, R. R.; Lindsey, J. S.; Holten, D. *J. Phys. Chem. B* **2005**, *109*, 20433.
- (8) Wang, D. C.; He, C.; Fan, J. L.; Huang, W. W.; Peng, X. J. *Acta Crystallographica Section E-Structure Reports Online* **2007**, *63*, O2900.
- (9) Yu, Y. H.; Shen, Z.; Xu, H. Y.; Wang, Y. W.; Okujima, T.; Ono, N.; Li, Y. Z.; You, X. Z. *J. Mol. Struct.* **2007**, *827*, 130.
- (10) Yin, X. D.; Li, Y. J.; Zhu, Y. L.; Jing, X. A.; Li, Y. L.; Zhu, D. B. *Dalton Trans.* **2010**, *39*, 9929.
- (11) Huh, J. O.; Do, Y.; Lee, M. H. *Organometallics* **2008**, *27*, 1022.
- (12) Wan, C. W.; Burghart, A.; Chen, J.; Bergstrom, F.; Johansson, L. B. A.; Wolford, M. F.; Kim, T. G.; Topp, M. R.; Hochstrasser, R. M.; Burgess, K. *Chemistry-a European Journal* **2003**, *9*, 4430.
- (13) Shen, Z.; Rohr, H.; Rurack, K.; Uno, H.; Spieles, M.; Schulz, B.; Reck, G.; Ono, N. *Chemistry-a European Journal* **2004**, *10*, 4853.
- (14) Stewart, J. J. P. *Journal of Molecular Modeling* **2007**, *13*, 1173.
- (15) de Silva, A. P.; Gunaratne, H. Q. N.; Gunnlaugsson, T.; Huxley, A. J. M.; McCoy, C. P.; Rademacher, J. T.; Rice, T. E. *Chem. Rev.* **1997**, *97*, 1515.
- (16) Ulrich, G.; Ziessel, R.; Harriman, A. *Angew. Chem. Int. Ed.* **2008**, *47*, 1184.
- (17) Kollmannsberger, M.; Rurack, K.; Resch-Genger, U.; Daub, J. *J. Phys. Chem. A* **1998**, *102*, 10211.
- (18) Hu, R. R.; Lager, E.; Aguilar-Aguilar, A.; Liu, J. Z.; Lam, J. W. Y.; Sung, H. H. Y.; Williams, I. D.; Zhong, Y. C.; Wong, K. S.; Pena-Cabrera, E.; Tang, B. Z. *J. Phys. Chem. C* **2009**, *113*, 15845.
- (19) Pethig, R.; Kuhn, M.; Payne, R.; Adler, E.; Chen, T. H.; Jaffe, L. F. *Cell Calcium* **1989**, *10*, 491.
- (20) Galletta, M.; Campagna, S.; Quesada, M.; Ulrich, G.; Ziessel, R. *Chem. Commun.* **2005**, 4222.
- (21) Galletta, M.; Puntoriero, F.; Campagna, S.; Chiorboli, C.; Quesada, M.; Goeb, S.; Ziessel, R. *J. Phys. Chem. A* **2006**, *110*, 4348.
- (22) Richards, V. J.; Gower, A. L.; Smith, J.; Davies, E. S.; Lahaye, D.; Slater, A. G.; Lewis, W.; Blake, A. J.; Champness, N. R.; Kays, D. L. *Chem. Commun.* **2012**, *48*, 1751.
- (23) Batat, P. *Communication moleculaire photo-ionique: les etudes ultrarapides de composé supramoleculaire, thesis université Bordeaux I* **2011**.
- (24) Karolin, J.; Johansson, L. B. A.; Strandberg, L.; Ny, T. *J. Am. Chem. Soc.* **1994**, *116*, 7801.

- 
- (25) Tajbakhsh, M.; Hosseinzadeh, R.; Alinezhad, H.; Ghahari, S.; Heydari, A.; Khaksar, S. *Synthesis-Stuttgart* **2011**, 490.
- (26) Tahtaoui, C.; Thomas, C.; Rohmer, F.; Klotz, P.; Duportail, G.; Mely, Y.; Bonnet, D.; Hibert, M. *J. Org. Chem.* **2007**, 72, 269.
- (27) DeMarinis R. M., K. H. E., Muirhead K. A. *US Patent* **1989**, US4849362 A.
- (28) Korthals, K. A.; Wulff, W. D. *J. Am. Chem. Soc.* **2008**, 130, 2898.
- (29) Dauben, W. G.; Michno, D. M. *J. Org. Chem.* **1977**, 42, 682.
- (30) Xu, Z. C.; Yoon, J.; Spring, D. R. *Chem. Commun.* **2010**, 46, 2563.
- (31) Lin, H. H.; Chan, Y. C.; Chen, J. W.; Chang, C. C. *J. Mater. Chem.* **2011**, 21, 3170.
- (32) Kaplan, J. H.; Hollis, R. J. *Nature* **1980**, 288, 587.
- (33) Labruere, R.; Alouane, A.; Le Saux, T.; Aujard, I.; Pelupessy, P.; Gautier, A.; Dubruille, S.; Schmidt, F.; Jullien, L. *Angew. Chem. Int. Ed.* **2012**, 51, 9344.
- (34) Ellisdavies, G. C. R.; Kaplan, J. H. *Proc. Natl. Acad. Sci. U. S. A.* **1994**, 91, 187.
- (35) Ellis-Davies, G. C. R. *Tetrahedron Lett.* **1998**, 39, 953.
- (36) Ellis-Davies, G. C. R.; Barsotti, R. J. *Cell Calcium* **2006**, 39, 75.
- (37) Il'ichev, Y. V.; Schworer, M. A.; Wirz, J. *J. Am. Chem. Soc.* **2004**, 126, 4581.
- (38) Tsien, R. Y.; Zucker, R. S. *Biophys. J.* **1986**, 50, 843.
- (39) Adams, S. R.; LevRam, V.; Tsien, R. Y. *Chem. Biol.* **1997**, 4, 867.
- (40) Cui, J. X.; Gropeanu, R. A.; Stevens, D. R.; Rettig, J.; Campo, A. *J. Am. Chem. Soc.* **2012**, 134, 7733.
- (41) Bhattacharyya, K. X.; Boubekur-Lecaque, L.; Tapsoba, I.; Maisonhaute, E.; Schollhorn, B.; Amatore, C. *Dalton Trans.* **2012**, 41, 14257.
- (42) Pelliccioli, A. P.; Wirz, J. *Photochem. Photobiol. Sci.* **2002**, 1, 441.
- (43) Montalti, M. C., A.; Prodi, L.; Gandolfi, M. T. *Handbook of photochemistry, Taylor and Francis* p601-604.
- (44) Bandara, H. M. D.; Walsh, T. P.; Burdette, S. C. *Chemistry-a European Journal* **2011**, 17, 3932.

---

---

---

## **4 $\text{Ca}^{2+}$ -transfer between self-assembled synthetic vesicles and in microcompartments**

---

## 4.1 Introduction

A wide range of techniques and molecules are known to form spontaneous organized supramolecular architectures such as micelles and vesicles. In this thesis the focus lies on amphiphilic structures consisting of molecules bearing a polar head group and a hydrophobic tail. These amphiphiles can self-assemble spontaneously into different structures depending on concentration, environment and temperature. Since the goal of the project is the formation of multicompartmentalized systems and the ion transfer between nano-objects inside, only persistent vesicle-forming amphiphiles are discussed in detail.

### 4.1.1 Amphiphiles and liposome formation

Amphiphilic molecules dissolve in water at very low concentration but above a certain, amphiphile-specific concentration (the CMC or critical micellar concentration) they self-assemble in order to minimise unfavourable hydrophobic chain – water interactions and are held together by hydrophobic interactions. The type of assembly formed by amphiphiles depends partly on the molecular structure of the amphiphile or the surfactant packing parameter ( $S$ ) which is defined by equation 20,

$$S = \frac{V}{l \times a_0} \quad \text{equation 20}$$

where  $V$  is the volume of the hydrophobic part of the molecule,  $l$  is the length of the hydrocarbon chain and  $a_0$  is the effective area per headgroup.<sup>1,2</sup> These parameters give information on the geometrical shape of the amphiphile and thus about the tendency to form certain structures. By convention  $S$  is smaller than 1 when the hydrophilic head is curved around the hydrophobic chain and bigger than 1 when the hydrophobic part is curved around the hydrophilic head. The second case is called a reversed aggregate while the former is referred to as a normal aggregate or phase. A  $S$  value of 1 corresponds to a planar bilayer, while a value of around 1/3 indicates the formation of micelles and between 1/2 and 1 the formation of curved bilayers is possible. An example is given in figure 72.

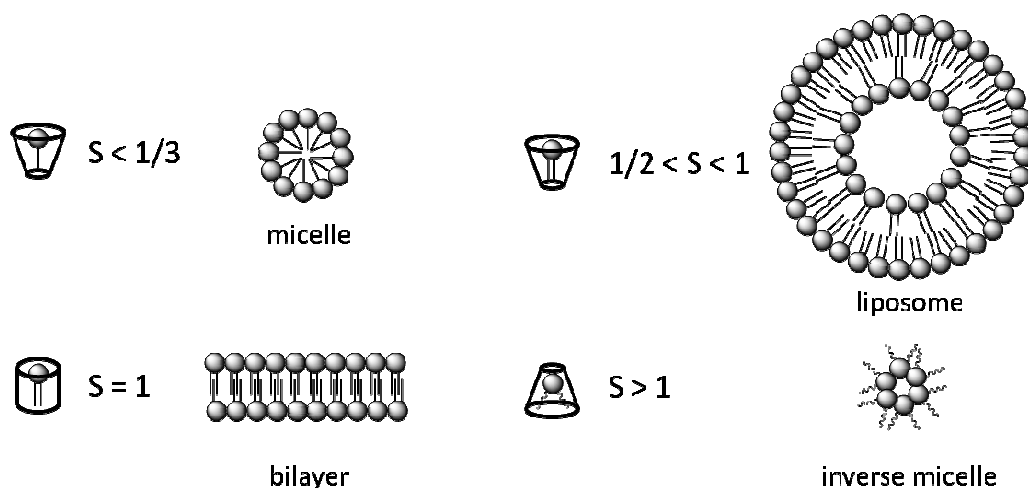


**Figure 72:** Possible self-assembled structures depended on the surfactant packing parameter (S).

The first biomimetic vesicular structure was discovered in 1964 by Bangham and Horne by hydrating lipids on surfaces.<sup>3,4</sup> The resulting liposomes consisted of a lipid bilayer with a thickness of around 4 nm encapsulating an aqueous core. The most popular example for liposomes are the ones consisting of a bilayer made of glycerophospholipid shown in figure 73. Ever since their discovery, liposomes have been studied extensively for their properties due to their resemblance to biological membranes which consist largely of phospholipids (see figure 73, **125**).<sup>5</sup> The unique property of these capsules is the confinement of water-soluble molecules in their aqueous interior or incorporation of hydrophobic molecules in the lipid bilayer which resulted in many applications as drug delivery agents or for example as micro-reactors.<sup>6,7</sup> Even though they are part of the cell membrane, phospholipids are not the only amphiphiles which have a tendency to self-assembly into bilayer-vesicles.

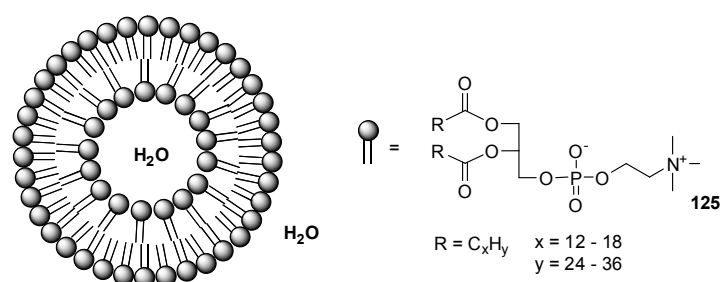


**Figure 73:** Schematic representation of a phospholipid liposome in aqueous media.

Kinitake showed in his study that a dispersion of di-*n*-dodecylammonium bromide (DDAB, **126**) in an aqueous medium forms uni- and multilamellar vesicles with a bilayer thickness around 3 nm.<sup>8</sup> From there on it became clear that a wide range of synthetic amphiphiles

posses the ability to form bilayers or liposome-like structures, see examples in figure 74. These amphiphiles can be cationic like DDAB (**126**), di-*n*-octadecylammonium bromide (DOAB, **127**) and gemini amphiphiles with two ammonium headgroups or anionic like di-*n*-dodecyl phosphate (DDP, **129**) and di-*n*-hexadecyl phosphate (DHP, **130**). Uncharged amphiphiles like polyglycerol (PGE, **128**) or zwitterionic species like the phospholipid 1,2-dimyristoyl-*sn*-glycero-3-phosphocholine (DMPC, **131**) belong to this family as well.

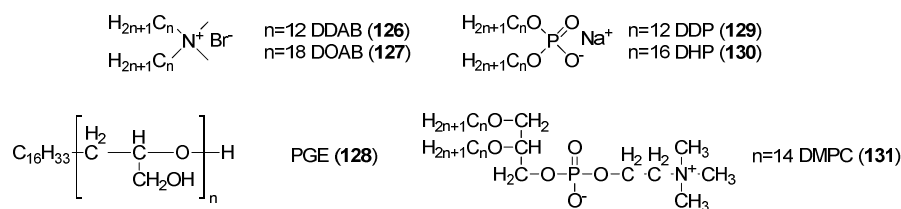


**Figure 74:** Molecular structures of some vesicle-forming synthetic amphiphiles.

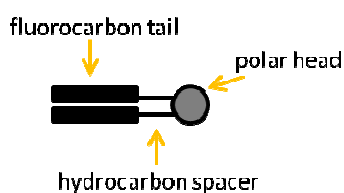
Vesicle membranes made of synthetic amphiphiles can be, much like liposomes, unilamellar or multilamellar. The aqueous interior typically varies between 20 – 100 nm.<sup>9</sup> Polymerisable amphiphiles and vesicles containing polymers have been introduced in recent years and will be discussed later on.<sup>10</sup>

#### 4.1.2 Fluorinated amphiphiles and vesicles

Fluorinated amphiphiles have several advantages over their hydrocarbon analogues when it comes to vesicle formation. These amphiphiles consist of a polar headgroup, such as phosphocholine or ammonium, and a hydrophobic fluorocarbon tail. A schematic representation is given in figure 75. The formation of vesicles by amphiphiles is based on the hydrophobic interaction of the hydrocarbon tail as mentioned earlier. In fluorocarbon amphiphiles this effect is increased due to the higher hydrophobicity of the fluorocarbon chain and therefore exhibits a stronger character to self-organize to avoid interactions with the surrounding medium so that even single chained phosphocholines are able to form vesicles.<sup>11</sup> A second property which needs to be highlighted is the lipophobicity of these structures leading to a minimization of the repulsion between hydrocarbon and fluorocarbon segments.<sup>12</sup> Vesicles can be formed using classical methods for the preparation of liposomes. The resulting vesicles are characterized by a fluorinated core and a lipophilic shell surrounded by polar headgroups facing the aqueous medium as shown in figure 75.

---

### Fluorinated amphiphile



### Fluorinated vesicle

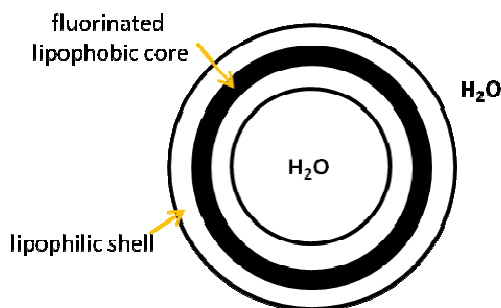


**Figure 75** Schematic representation of fluorinated amphiphiles and fluorinated vesicles.

Most of the fluorinated amphiphiles are based on the structure of phospholipids and have been extensively studied. Compared to their non-fluorinated counterparts, vesicles formed by fluorinated amphiphiles tend to display higher phase transition temperatures ( $T_c$ ) at which the change from the liquid crystalline to the fluid state occurs.<sup>13</sup> Other characteristics are the stability during autoclaving without significant size changes, increased long term shelf stability, lowered permeability of the membrane and increased stability in biological media.<sup>14,15</sup> Fluorinated vesicles have also prepared from synthetic amphiphile-based structures. In the group of Oda gemini-based semi-fluorinated amphiphiles had been prepared and compared to their hydrocarbon analogous.<sup>16</sup> Similarly to the phosphocholine-based fluorinated amphiphiles the gemini-based fluorinated amphiphiles showed an increased aggregation behavior and were found to form vesicles while the hydrocarbon analogue formed entangled micelles. Another type of self-assembled structure with increased stability are vesicles consisting of block-copolymer units which will be described in the next section.

#### 4.1.3 Polymersomes

The term "polymersome" was coined in 1999 by Discher *et.al.*<sup>17</sup> and described vesicles made of a block copolymer. The block copolymers used to form those polymeric vesicles need to be of amphiphilic nature much like their low molecular weight counterparts. The length of each subunit in block copolymers is crucial for the formation of bilayers since many other structures like micelles or worm like structures are possible.<sup>18</sup> The properties of the copolymer-containing bilayer can be easily tuned in terms of stability and permeability simply by changing the molecular weight of the polymer used.<sup>19</sup> More recently polymersomes consisting of a triblock-copolymer (poly(2-methyloxazoline)-*block*-poly(dimethylsiloxane)-*block*-poly-(2-methyloxazoline)) with two hydrophilic and one hydrophobic part have been

---

---

prepared and shown to form vesicles under certain conditions.<sup>20</sup> A schematic representation for the structure of a classical polymersome consisting of a diblock copolymer is given in figure 76.

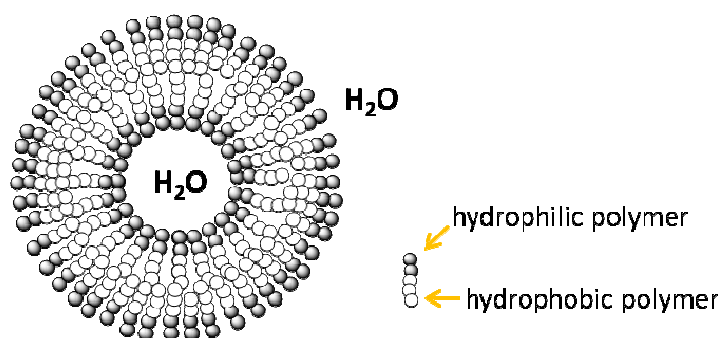


**Figure 76:** Schematic representation of a vesicle formed by a block copolymer (polymersome).

Since their discovery, polymersomes, like liposomes years before, have gained considerable interest in drug delivery applications due to their ability to encapsulate different molecules like drugs, DNA or siRNA in their aqueous core or hydrophobic molecules in their membrane.<sup>21,22</sup> Additionally their circulation time in the human body is increased compared to liposomes and an increased stability results from a thicker membrane (3 – 4 nm).<sup>23</sup> Even though a lot of different methods for the preparation of polymeric vesicles are known and resemble those of liposomes, they follow mostly two main routes. The first is analogous to liposome formation via the hydration of a dried thin film with aqueous buffer yielding a polydisperse solution of different vesicles sizes. The second is the solvent switching method where the polymer is first dissolved in an organic solvent and the injected into an aqueous phase.<sup>24,25</sup>

The stability and the mode of preparation give rise to some interesting applications in terms of multicompartmentalization since bigger and more stable vesicles can be formed.

#### 4.1.4 Multicompartmentalized systems

Multilamellar vesicles can be considered as multicompartmentalized systems. However, it proved to impossible to do this multicompartmentalization in a controlled fashion or even with different bilayers until the year 1997. The first controlled multicompartmentalized system was reported by Zasadzinski and co-workers which he named vesosomes and they consisted of small liposomes with a size of 100 nm in the aqueous interior of a big liposome with a size around 400 nm.<sup>26</sup> A schematic representation of the preparation process is given in figure 77.

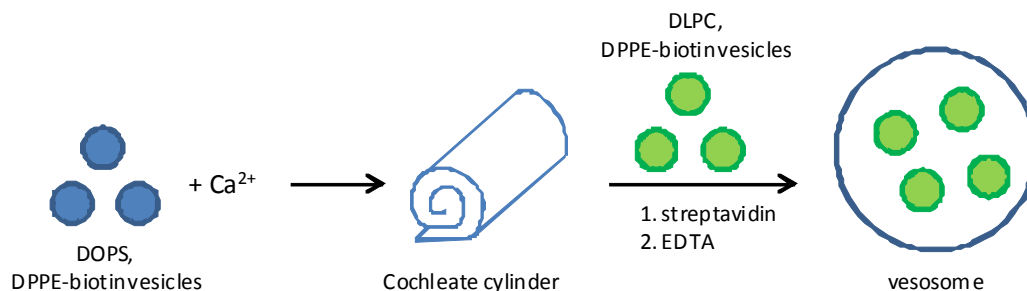


**Figure 77:** Schematic representation of the first preparation of a multicompartimentalized liposomes in a liposome (vesosome).

Negatively charged unilamellar dioleoylphosphatidylserine (DOPS) vesicles doped with biotinylated 1,2-dipalmitoyl-*sn*-glycero-3-phosphoethanolamine (DPPE-biotin) were turned into a cochleate cylinder in the presence of Ca<sup>2+</sup>. A batch of 1,2-dilauroyl-*sn*-glycero-3-phosphocholine (DLPC) vesicles doped with DPPE-biotin were added to this solution in the presence of streptavidin. The streptavidin had two effects, first it clustered the DLPC liposomes together and second it attached these liposomes to the surface of the cochleate cylinder. By adding EDTA the Ca<sup>2+</sup> was complexed and the cylinder was unrolled to form a single bilayer around the DLPC vesicles. This system showed several advantages in terms of cargo leakage compared to their unilamellar counterparts. In serum ciproflaxin retention was reported to increase from less than 10 min for unilamellar vesicles to over 6 h in vesosomes.<sup>27</sup> In the group of Bolinger, vesosomes have been prepared simply by hydrating a thin film with preformed liposomes.<sup>28</sup> The incorporation of liposomes with different phase transition temperatures lead to the construction of a vesosomic nano-reactor which was controlled by heating the sample above the phase transition temperature of the inner small unilamellar vesicles (SUV) to release their payload into the aqueous interior of the surrounding large unilamellar vesicle. This approach can be considered as a first example for a mimicry of cell activity.

Much effort has been invested into the fledgling field of polymeric multicompartimentalized systems, due to their higher mechanical stability<sup>29</sup> and their lower permeability.<sup>30</sup> The first multicompartimentalized system based on polymers was demonstrated by McPhail *et al.*<sup>31</sup> In this study a hybrid polymer lipid vesicle was encapsulated in the interior of an egg phosphatidylcholine liposome. A fully polymeric system was described by Chiu *et al.*<sup>32</sup> who used a double emulsion technique to produce polymersomes in polymersomes. Poly(acrylic acid-*co*-distearin acrylate) (poly(AAc-*co*-DSA)) were formed by double emulsion in

---

THF/CHCl<sub>3</sub> as organic phase and buffered water. The primary inverted emulsion was first emulsified and subsequently added to an excess water phase, which yielded the multicompartmentalized vesicles after evaporation of the organic solvent. In the group of Lecommandoux a process which was initially invented for the almost quantitative loading of giant liposomes<sup>33</sup> namely emulsion centrifugation was used to prepare polymersomes in polymersomes.<sup>34</sup> Therefore a first set of polymersomes had been prepared using poly(trimethylene carbonate)-*b*-poly(L-glutamic acid) (PTMC-*b*-PGA) via nanoprecipitation. The aqueous solution of (PTMC-*b*-PGA) polymersomes was then emulsified in an organic phase via polybutadiene-*b*-poly(ethylene oxide) (PB-*b*-PEO) and was poured over an aqueous phase. At the interface excess PB-*b*-PEO formed a monolayer and after centrifugation PTMC-*b*-PGA polymersomes in larger PB-*b*-PEO polymersomes were obtained.

In the following study the system used by Lecommandoux and co-workers will be used to create a new kind of multicompartmentalized assembly.

## 4.2 Ion transfer between synthetic vesicles

This chapter will focus on ion transfer between synthetic fluorinated vesicles in the aqueous interior of a giant polymersome. Each type of vesicle (Ca<sup>2+</sup>-decaging and Ca<sup>2+</sup>-sensing) vesicles will be discussed separately and preliminary test in terms of ion transfer between vesicles will be shown.

### 4.2.1 Ca<sup>2+</sup>-decaging hydrocarbon vesicles preparation and ion release

Liposomes with amphiphilic photolabile Ca<sup>2+</sup> decaging agent (**124**) incorporated into the liposomal bilayer have been prepared using DOPC (1,2-di-(9Z-octadecenoyl)-*sn*-glycero-3-phosphocholine). A thin film of amphiphilic DMNPE-4 (**124**) and DOPC was prepared by mixing the two components in a mixture of chloroform and methanol and slowly evaporating the solvent until a thin film was formed. Rehydration with pseudo-intracellular buffer (100 mM KCl, 30 mM MOPS, pH 7.2) yielded vesicles with the Ca<sup>2+</sup>-decaging agent (**124**) in their membrane with a final concentration of 1.5 mM DOPC and 50 μM amphiphilic DMNPE-4 (**124**) (formulation A). A more precise description of the experimental procedure for the vesicle preparation can be found in the experimental section. A preliminary test was

carried out in order to prove that  $\text{Ca}^{2+}$  can be ejected upon irradiation at 365 nm. To that end, the aforementioned formulation was doped with 5  $\mu\text{M}$  water soluble BAPTA-BODIPY and 5  $\mu\text{M}$   $\text{CaCl}_2$  in order to reproduce the ion transfer conditions determined in the previous chapter.

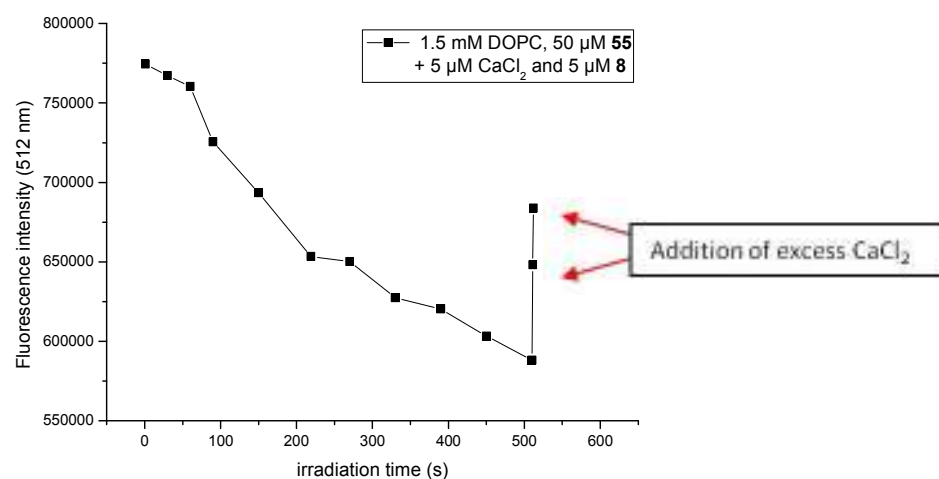


**Figure 78:** Fluorescence emission at 512 nm ( $\lambda_{\text{exc}} = 475$  nm) of a solution containing formulation A, 5  $\mu\text{M}$  of BAPTA-BODIPY (**72**) and  $\text{CaCl}_2$  respectively upon irradiation at 365 nm using a classical TLC lamp.

The fluorescence emission of the selectively-excited BAPTA-BODIPY (**72**) after different irradiation times at 365 nm is shown in figure 78. Instead of the expected increase in the fluorescence emission due to  $\text{Ca}^{2+}$  transfer from the  $\text{Ca}^{2+}$ -ejecting vesicles (formulation A), a continuous decrease in fluorescence emission is observed between 1 – 500 s irradiation time. Addition of an excess of  $\text{Ca}^{2+}$  at the end of the experiment showed however that the fluorescent sensor (**72**) is capable of detecting an increase in the  $\text{Ca}^{2+}$  concentration. The observed effect is most likely based on two things, first is the binding affinity of phospholipids to  $\text{Ca}^{2+}$  due to the presence of an ionized phosphate group and second is the destabilisation of the lipid bilayer induced by the UV-irradiation as proposed by Uda *et.al.*<sup>35,36</sup> Upon irradiation the phospholipid bilayer gets destabilized and breaks in several places, which gives  $\text{Ca}^{2+}$  easier access to the phosphate group resulting in an decrease of free  $\text{Ca}^{2+}$  and a decrease in fluorescence intensity.

After this preliminary result a different amphiphile was used for the formation of  $\text{Ca}^{2+}$ -decaging vesicles, namely di-tetradecylammonium bromide (DTDAB ()), structure shown in figure 79). Using the same preparation method as previously mentioned, formulation B has been prepared containing vesicles made of 1.5 mM DDAB, 50  $\mu\text{M}$  amphiphilic DMNPE-4 (99) in pseudo intracellular buffer. The polydisperse vesicle solution has been observed with an optical microscope equipped with an irradiation source and filters for different wavelengths. The images taken of formulation B are shown in figure 79.

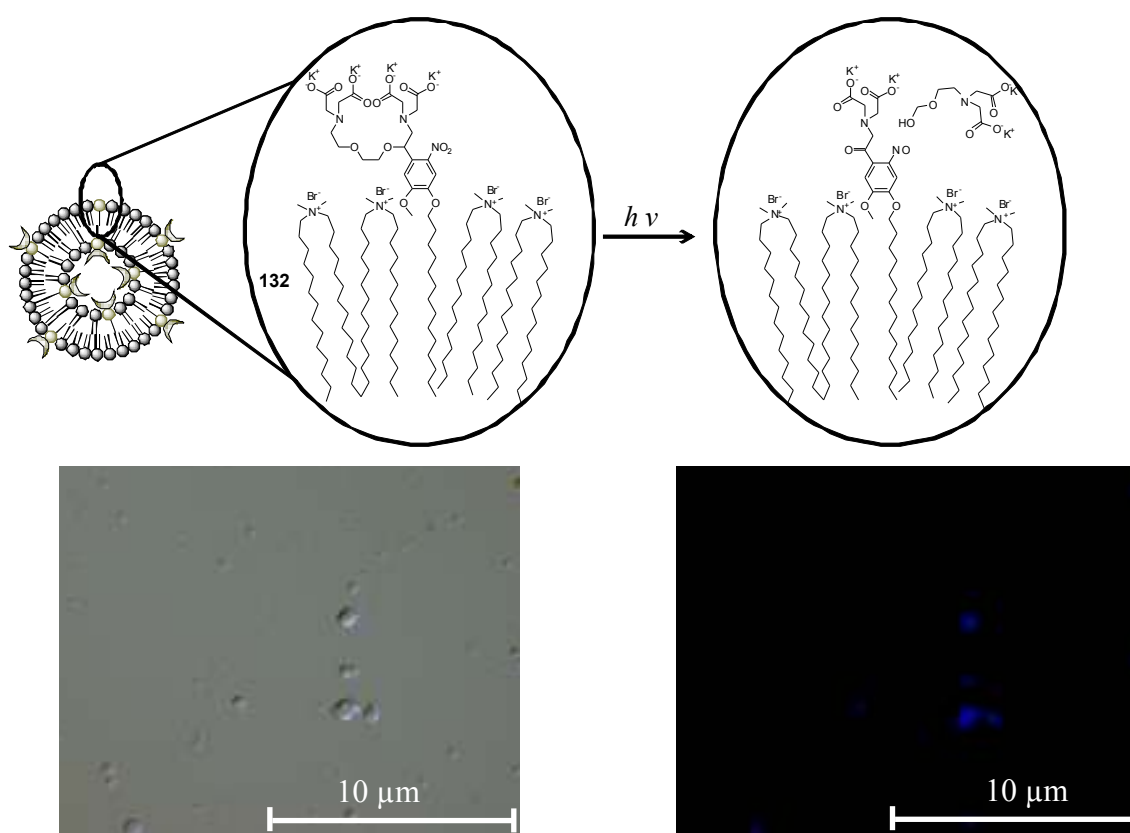


**Figure 79:** optical microscope image of formulation B (left) x 40 magnification. Epifluorescence image of the same region ( $\lambda_{\text{exc}} = 330 - 380 \text{ nm}$ )

Polydisperse vesicles with a diameter between 200 nm and 2  $\mu\text{M}$  can be observed and display a well-defined membrane without additional features. Upon irradiation between 330 and 380 nm vesicles become fluorescent after several seconds of irradiation. The appearance of fluorescence is linked to the photo-decaging of the  $\text{Ca}^{2+}$  binding unit, since the resulting ketone exhibits weak fluorescence in the blue region. This experiment proves that the amphiphilic  $\text{Ca}^{2+}$  decaging agent is in fact located in the membrane of the vesicles and the irradiation with UV-light does not disrupt the membrane.

In order to test the ion ejection from formulation B 5  $\mu\text{M}$  BAPTA-BODIPY (**72**) and 5  $\mu\text{M}$   $\text{CaCl}_2$  were added and the sample was irradiated at 365 nm and the fluorescence emission of the ion sensor (**72**) was measured after different irradiation times. The result of this experiment is plotted in figure 80. Conversely to the ion ejection experiment for formulation A,  $\text{Ca}^{2+}$  ejection upon irradiation yields an increase in the BAPTA-BODIPY (**72**) fluorescence intensity, indicating that the ion is effectively liberated from the surface of the vesicle and transferred to the ion acceptor in solution. In the amphiphile used no phosphate is present and the polar head is made of a quaternary ammonium salt so that no competitive binding can occur.

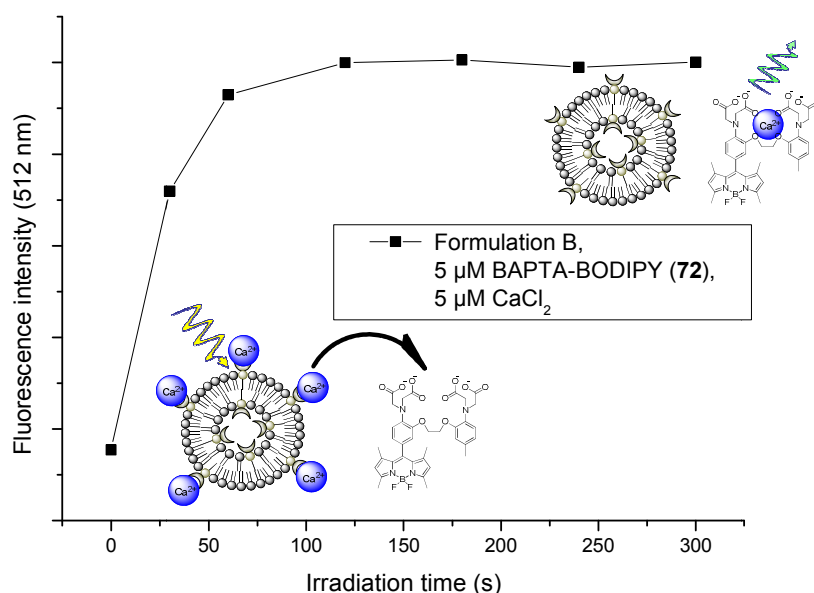


**Figure 80:** Fluorescence emission at 512 nm ( $\lambda_{\text{exc}} = 475$  nm) of a solution containing formulation B, 5  $\mu\text{M}$  of BAPTA-BODIPY (**72**) and  $\text{CaCl}_2$  respectively upon irradiation at 365 nm using a classical TLC lamp.

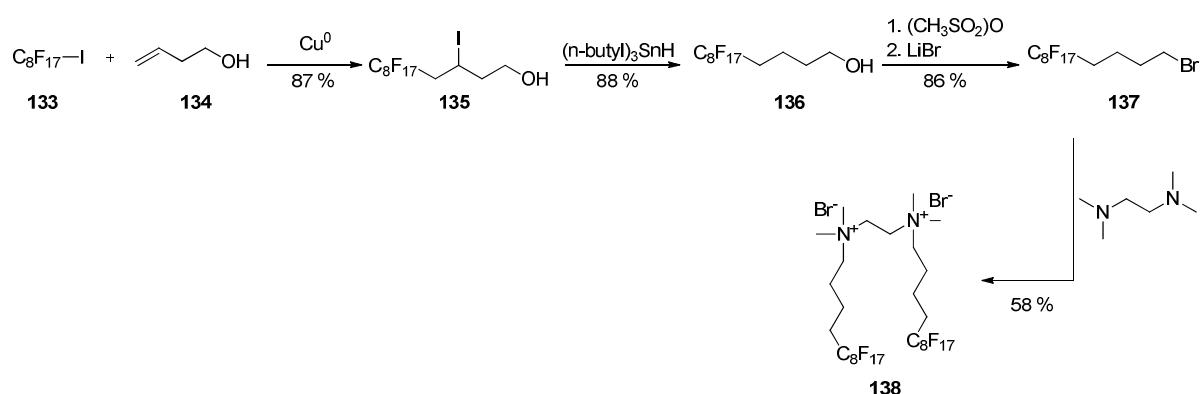
After approximately 100 s irradiation time with a classical TLC lamp at 365 nm enough  $\text{Ca}^{2+}$  is released to completely switch on the fluorescence of the ion sensor (**72**).

## 4.2.2 Ca<sup>2+</sup>-sensing fluorinated vesicles preparation and spectral properties

Before the preparation and characterization of Ca<sup>2+</sup>-sensing vesicles will be introduced, the synthesis of the semi-fluorinated amphiphile is discussed. This type of amphiphile was chosen since amphiphilic cationic surfactants show an immiscibility with cationic semi-fluorinated supramolecular structures as shown by Oda *et.al.*<sup>16</sup>

### 4.2.2.1 Synthesis of a semi-fluorinated gemini surfactant (138)

The synthesis of amphiphilic semi-fluorinated gemini surfactants was performed according to mentioned publication. The synthesis is shown in scheme 20. The first reaction included the radical addition of commercially-available 1-iodoperfluorooctane (**133**) to 3-buten-1-ol (**134**) in the presence of fine copper powder in absence of any solvent. The resulting heptadecafluoro-3-iododecan-1-ol (**135**), which was obtained in 87 % yield, was reacted with tributyltin hydride to replace the iodine for a hydrogen, resulting in heptadecafluorododecan-1-ol (**136**) with a reaction yield of 88 %.



**Scheme 20:** Synthetic route for semi-fluorinated cationic gemini surfactant **138**.

The substitution of the hydroxyl group was achieved in two steps without intermediate purification. The alcohol was first activated with methylsulfonic anhydride to produce an efficient leaving group and was subsequently reacted with lithium bromide to yield the heptadecafluoro-1-bromo dodecane (**137**) in 86 %. To obtain the final semi-fluorinated surfactant (**138**), heptadecafluoro-1-bromo dodecane (**137**) dissolved in acetonitrile in the presence of TMEDA (N,N,N',N'-Tetramethyl-1,2-ethanediamine) was stirred in a pressure tube for more than 3 days at 5 °C above the boiling point of the solvent. The surfactant (**61**) was obtained in 58 % yield after a double recrystallisation from a mixture of chloroform and acetone.

4.2.2.2  $\text{Ca}^{2+}$  binding affinities of fluorinated vesicles bearing 79, 82 and 97 in the bilayer  
 In order to see if there is a membrane-induced effect on the binding affinity,  $\text{Ca}^{2+}$ -titrations were performed for amphiphilic  $\text{Ca}^{2+}$ -sensors incorporated in the vesicle membrane made of the fluorinated gemini (**138**). To that end, three formulations of vesicles were prepared which are summarized in table 10.

**Table 10:** Overview of formulation C - D

	Gemini conc.	$\text{Ca}^{2+}$ -sensor conc.	$\text{Ca}^{2+}$ -sensor	Average size DLS
<b>Formulation C</b>	1.5 mM	12.5 $\mu\text{M}$	BANIF ( <b>79</b> )	138 nm
<b>Formulation D</b>	1.5 mM	10.1 $\mu\text{M}$	$\text{C}_8\text{F}_{17}$ -BAPTA-BODIPY ( <b>82</b> )	134 nm
<b>Formulation E</b>	1.5 mM	9.9 $\mu\text{M}$	$\text{C}_8\text{F}_{17}$ -Fura red ( <b>97</b> )	132 nm

Formulations C – E were prepared via the thin film hydration method previously described. A mixture of amphiphilic  $\text{Ca}^{2+}$  sensor (**79**, **82** or **97**) and fluorinated gemini (**138**) in a chloroform / methanol mixture was slowly evaporated and the thin film rehydrated with pseudo-intracellular buffer containing either 10 mM HEEDTA (N-(2-hydroxyethyl)ethylenediamine-N,N',N'-triacetic acid) or 10 mM CaHEEDTA. HEEDTA was chosen for the determination of the  $\text{Ca}^{2+}$ -dissociation constants due to its lower binding affinity towards  $\text{Ca}^{2+}$  (5.55 at pH 7.24)<sup>37</sup> compared to EGTA and therefore a wider range of  $\text{Ca}^{2+}$  concentrations. The fluorescence titration at different concentration of  $\text{Ca}^{2+}$  for formulation C is shown in figure 81. The emission maximum shifts from 523 nm to 530 nm with increasing amount of  $\text{Ca}^{2+}$  which is somewhat smaller than the shift measured for the molecule in solution (550  $\rightarrow$  575 nm). Also the emission maximum can be found at shorter wavelengths. This is due to the incorporation of the vesicle membrane into the hydrophobic environment which therefore leads to a blue shift of the emission wavelength. Linearization via a Hill plot as previously described yields a straight line with a slope of almost 1 indicating a 1:1 binding of  $\text{Ca}^{2+}$  to the ion-sensing vesicle. The  $\text{Ca}^{2+}$  dissociation constant ( $K_d$ ) was found to be 3.0  $\mu\text{M}$ , which is about one order of magnitude higher than in free solution. The cationic head groups of the gemini vesicles are responsible for lowering the binding affinity since the divalent cation  $\text{Ca}^{2+}$  experiences partial repulsion from the vesicle surface.

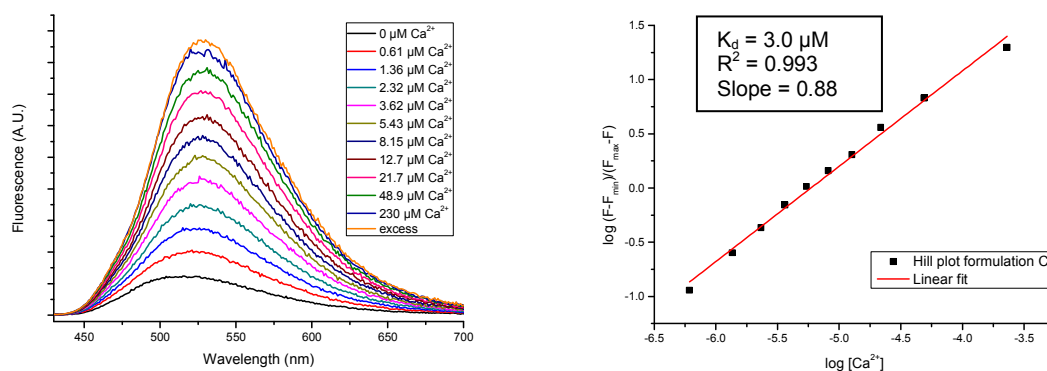


**Figure 81:** Fluorescence emission of formulation C ( $\lambda_{\text{exc}} = 425 \text{ nm}$ ) upon  $\text{Ca}^{2+}$ -addition (left). Hill plot for the spectral change in fluorescence emission at 530 nm (right).

Similar observations have been made for formulation D bearing the amphiphilic BODIPY  $\text{Ca}^{2+}$  sensor (**82**) in the membrane. Fluorescence emission spectra of formulation D in the presence of different concentrations of free  $\text{Ca}^{2+}$  are plotted in figure 82. The fluorescence intensity increases significantly between 48.9  $\mu\text{M}$  and 230  $\mu\text{M}$  free  $\text{Ca}^{2+}$ . This is an indication for a drastically-lowered binding affinity towards the ion. In fact the titration needed to be continued up to 1.05 mM free  $\text{Ca}^{2+}$  in order to come close to saturation. The Hill plot of the titration shown in figure 82 on the right side revealed a  $K_d$  value of 77  $\mu\text{M}$  which is two orders of magnitude lower than the one observed in free solution (0.724  $\mu\text{M}$ ) with a slope of 0.82 indicating 1:1 binding of  $\text{Ca}^{2+}$  by the ion sensor. As in formulation C, the repulsion of the cation from the cationic surface from the vesicles leads to a decrease in binding affinity.

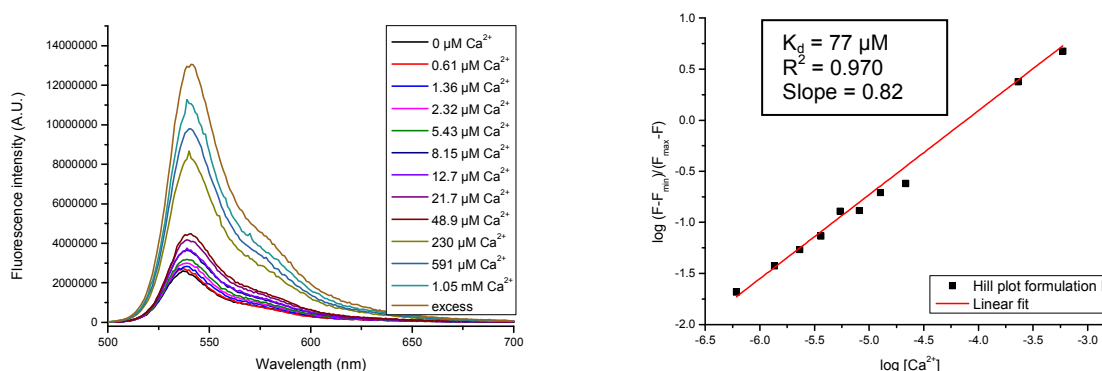


**Figure 82:** Fluorescence emission of formulation D ( $\lambda_{\text{exc}} = 485 \text{ nm}$ ) upon  $\text{Ca}^{2+}$ -addition (left). Hill plot for the spectral change in fluorescence emission at 545 nm (right).

Due to the different structure of amphiphilic BAPTA-BODIPY (**82**) and BANIF (**79**) the effect has a different impact. C<sub>8</sub>F<sub>17</sub>-BAPTA-BODIPY (**82**) could be less advantageously orientated on the surface and therefore display a larger decrease in binding affinity. Formulation E has been titrated in the same fashion but the spectral change was observed in the electronic absorption spectrum due to the ratiometric nature of C<sub>8</sub>F<sub>17</sub>-furared (**97**). The absorption spectra in the presence of varying amounts of free Ca<sup>2+</sup> are shown in figure 83.

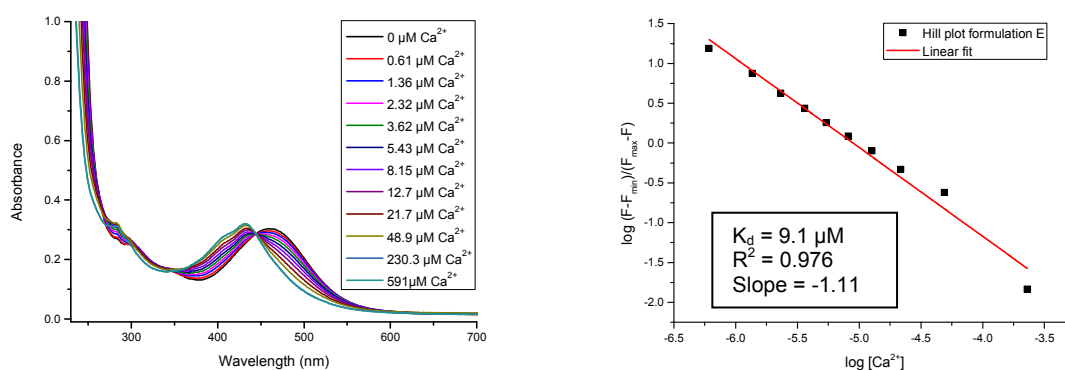


**Figure 83:** Electronic absorption spectra of formulation E upon Ca<sup>2+</sup>-addition (left). Hill plot for the spectral change in the absorption spectra at 476 nm (right).

The absorption spectra show an isosbestic point at 445 nm with a decreasing absorption above 445 nm and an increase between 350 and 445 nm. The spectral change at 476 nm was linearised via Hill plot, which yielded a straight line with a slope of -1.1 indicating 1:1 binding of host and guest. The extracted Ca<sup>2+</sup> dissociation constant (K<sub>d</sub>) was 9.1 μM, which is also two orders of magnitude higher than in free solution (K<sub>d</sub> = 0.076 μM). Much like the amphiphilic BAPTA-BODIPY sensor (**82**), the amphiphilic furared (**33**) bears the fluorinated chain rather close to the BAPTA fragment of the molecule which locates the binding site closer to the vesicle surface and decreases the binding affinity more than for the BANIF (**79**) ion sensor. The change of binding affinity of Ca<sup>2+</sup>-sensors in liposomal membranes has already been reported for DOPC vesicles.<sup>38</sup>

Fluorescence quantum yields have been determined for formulation C – E by comparison to fluorescein.<sup>39</sup> The results of the analysis are summarized in table 11. The determination of the fluorescence quantum yields in the vesicles shows that the previously mentioned low quantum yields are in fact due to aggregation of the amphiphilic Ca<sup>2+</sup>-sensors. In all cases the fluorescence quantum yield increases in the presence and absence of Ca<sup>2+</sup>. However, the

increase in emission upon  $\text{Ca}^{2+}$  complexation stays rather low. The fluorescence enhancement factor calculated from the quantum yields is 1.6 for formulation C and formulation D, respectively. As observed in solution, the fluorescence quantum yield for formulation E decreases slightly upon  $\text{Ca}^{2+}$  binding which can be exploited by irradiation after the isosbestic point, in that case a decrease in fluorescence intensity is caused by a lower quantum yield and a decrease in the absorption spectrum.

**Table 11:** binding affinities and quantum yields of formulation C – D and **79**, **82**, **97** in aqueous solution.

	Form. C	BANIF ( <b>79</b> )	Form. D	$\text{C}_8\text{F}_{17}$ -BAPTA- BODIPY ( <b>82</b> )	Form E	$\text{C}_8\text{F}_{17}$ -furared ( <b>97</b> )
$K_d$	3.0	0.117	77.6	0.724	9.1	0.076
$\Phi_{em} (+\text{Ca}^{2+})$	0.28	0.026	0.43	0.004	0.05	0.004
$\Phi_{em} (-\text{Ca}^{2+})$	0.17	0.006	0.26	0.001	0.08	0.006

Even though fluorescence increase is low, specific  $\text{Ca}^{2+}$ -sensing supramolecular assemblies have been designed with a detectable change in fluorescence intensity. Those will be used for ion transfer experiments in the following section.

#### 4.2.3 Photoinduced $\text{Ca}^{2+}$ transfer between hydrocarbon and fluorocarbon vesicles

After having prepared  $\text{Ca}^{2+}$ -decaging vesicles and fluorescent  $\text{Ca}^{2+}$ -sensing vesicles, ion transfer between these two populations needed to be tested. As a representative example a formulation of BANIF (**79**) in fluorinated gemini (**138**) has been prepared. Because of the following experiments and the preparation of multicompartimentalized systems a concentration of 130 mg/ml of sucrose needed to be present in the buffer. Therefore formulation F contained 5  $\mu\text{M}$  BANIF (**79**) in the membrane of 1.5 mM fluorinated gemini (**138**) vesicles in a pseudo-intracellular sucrose buffer (100 mM KCl, 30 mM MOPS, 130 mg/ml sucrose, pH 7.2). The fluorescence emission of this solution was then measured at 526 nm upon the addition of water-soluble DMNPE-4 (**99**) and subsequent irradiation at 365 nm. The resulting curve is plotted in Figure 84.

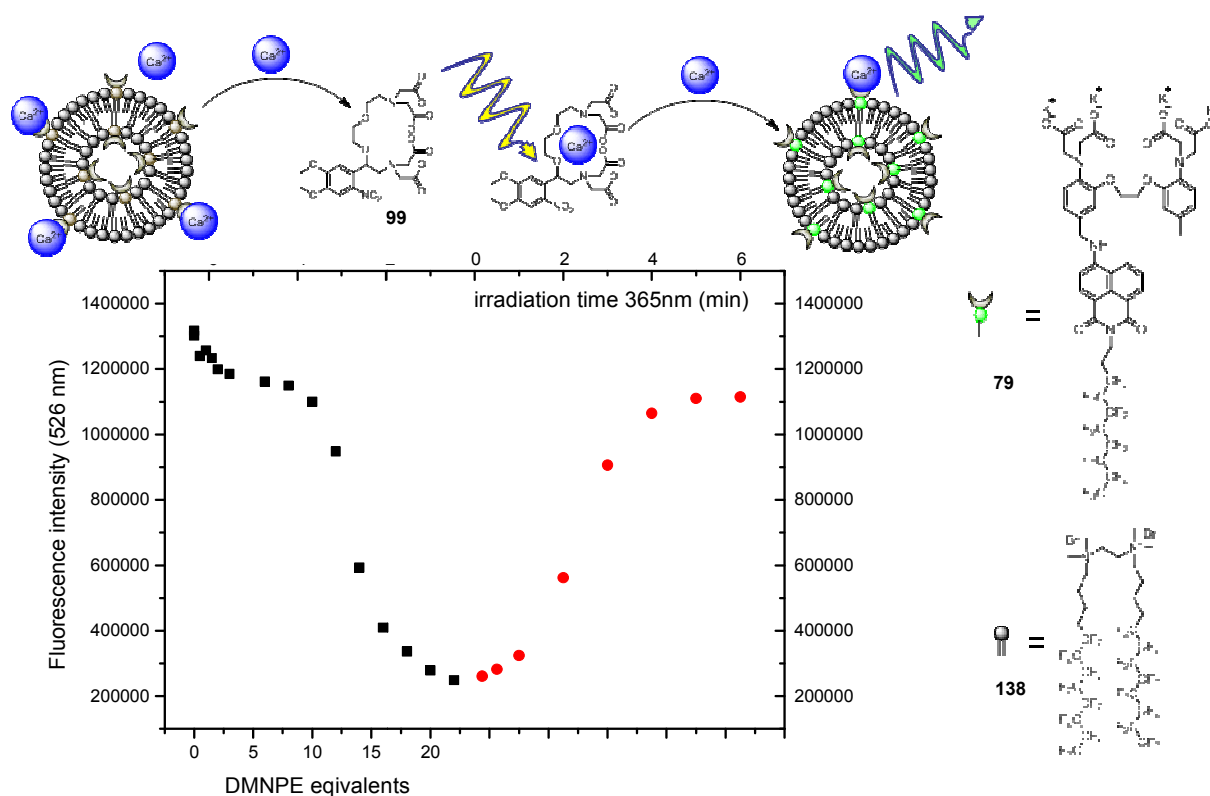


**Figure 84:** Fluorescence emission of formulation F at 526 nm ( $\lambda_{\text{exc}} = 425 \text{ nm}$ ) upon addition of DMNPE-4 (**99**) (black). Fluorescence emission of the same solution after 0 to 6 min of irradiation at 365 nm using a TLC lamp.

The first thing to note is a slight decrease in the fluorescence emission upon addition of DMNPE-4 (**99**). However, a larger decrease in the fluorescence intensity is only noted after the addition of 10 equivalents of DMNPE-4 with respect to the ion sensor (**79**) in the vesicle membrane. The fluorescence keeps decreasing until 22 equivalents of the  $\text{Ca}^{2+}$ -decaging agent (**99**) was added. Compared to the ion transfer experiment in solution, twice as much ion-decaging agent was needed to decrease the fluorescence efficiently. Since a large amount of sucrose is employed in the buffer it is probable that there is a large amount of  $\text{Ca}^{2+}$  impurities present in the sample in addition to the impurities coming from the glassware and the water. This observation needs to be taken in account for the preparation of  $\text{Ca}^{2+}$ -decaging vesicles later on. In the second part of the experiment the sample was irradiated at 365 nm after the addition of DMNPE-4 (**99**). The fluorescence emission keeps increasing continuously up to 5 min. No further increase is measured upon longer irradiation. Due to the photoinduced decaging from the water-soluble ion ejector (**99**), the  $\text{Ca}^{2+}$  ion are effectively transferred to the ion sensing vesicle formulation (formulation F). Based on the obtained results, a 3 times more concentrated  $\text{Ca}^{2+}$ -decaging vesicle formulation needed to be envisaged. The ratio between the amphiphilic  $\text{Ca}^{2+}$ -decaging agent (**124**) and a final concentration of  $150 \mu\text{M}$  amphiphilic

DMNPE-4 (**99**) incorporated in the membrane of the vesicles with an amphiphile concentration of 4.5 mM in pseudo-intracellular sucrose buffer has been prepared (formulation G). Formulation F and formulation G were mixed in equal volume ratio and 5  $\mu\text{M}$   $\text{CaCl}_2$  was added, then the fluorescence emission of formulation F was recorded at 526 nm. The obtained graph is shown in Figure 84. The fluorescence intensity emitted from formulation F is low at the beginning of the experiment due to the presence of formulation G, which binds most of the free  $\text{Ca}^{2+}$ -ions. Upon irradiating at 365 nm the fluorescence increases first slightly up to 60 s. A large jump in fluorescence intensity is observed between 60 and 200 s of irradiation. The reason for the slow increase in fluorescence is the excess of amphiphilic DMNPE-4 (**55**) present in the membrane of the vesicles in formulation G. Upon irradiation part of the photolabile decaging degrades and releases the  $\text{Ca}^{2+}$ -ion, which is directly taken up by another still unphotolysed DMNPE-4 (**55**).

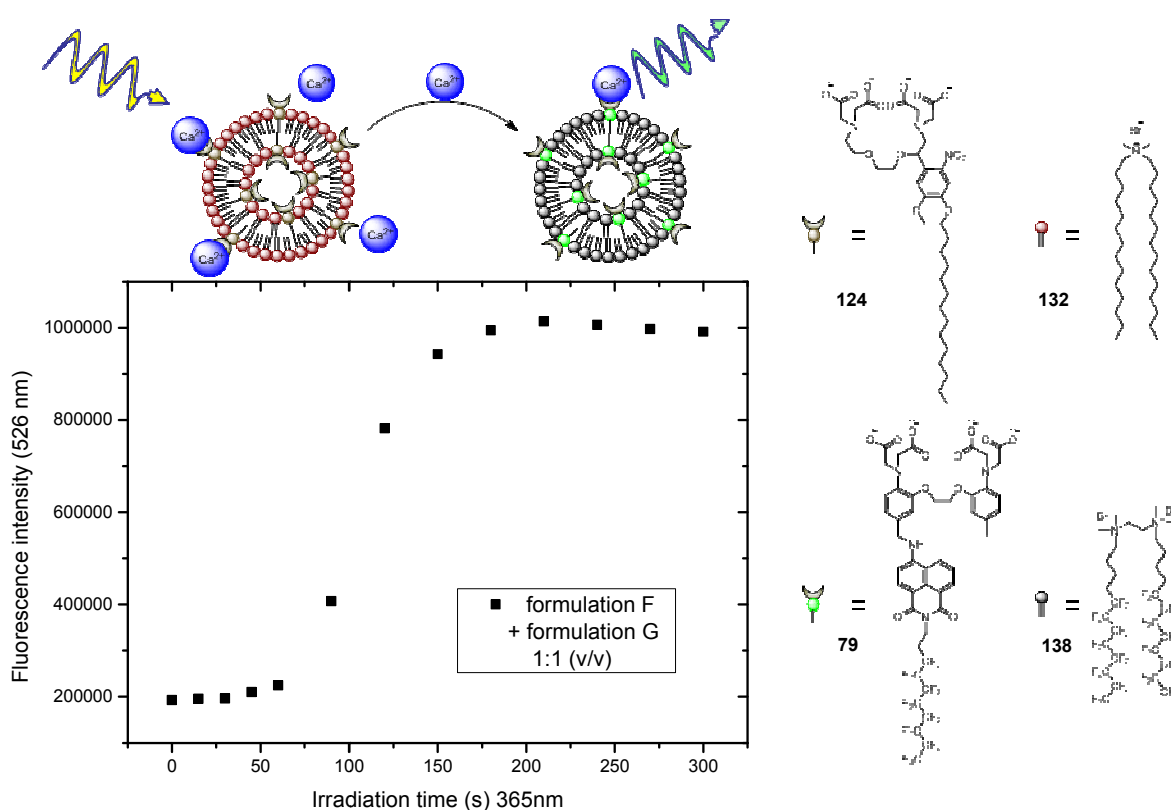


**Figure 84:** Schematic representation of the ion transfer between formulation G and F (top). Fluorescence emission of a 1:1 mixture of formulation F and G in the presence of 5  $\mu\text{M}$   $\text{CaCl}_2$  at 526 nm ( $\lambda_{\text{exc}} = 425$  nm) after increasing irradiation times at 365 nm using a TLC lamp.

---

After a sufficient amount of decaging agents are photolysed, a large increase in fluorescence intensity is noted due to the now more effective ion transfer from the ejecting vesicles (formulation G) to the accepting vesicles (formulation F). Above 200 s irradiation a slight decrease in fluorescence emission is observed due to photobleaching or other photo-decomposition processes since the amphiphilic  $\text{Ca}^{2+}$ -sensor in the membrane of the vesicles in formulation F also absorbs at 365 nm). In summary, the effective ion transfer from one vesicle formulation to the other has been shown and the ion transfer can be detected by means of fluorescence spectroscopy. This leads now to some first tests of multicompartmentalization.

---

### 4.3 Multicompartmentalization of fluorocarbon and hydrocarbon vesicles in PB-*b*-PEO polymersomes

In a next step the prepared vesicle formulations needed to be incorporated into the aqueous interior of a giant polymersome. To that end the procedure published in the group of Lecommandoux<sup>34</sup> has been adapted for the vesicle system previously described. The multicompartmentalization process is described in figure 85. A formulation of liposomes in pseudo-intracellular buffer loaded with 130 mg/ml sucrose which equals an osmotic pressure of 380 mOsm is emulsified in toluene using poly(butadiene)<sub>46</sub>-*b*-poly(ethylene oxide)<sub>30</sub> (PB-*b*-PEO). The polymer is known to form micelles and polymersomes and has been exploited for several studies in the literature.<sup>40,41</sup> Gentle shaking produced rather big droplets of the water-in-oil emulsion (top left, figure 85).

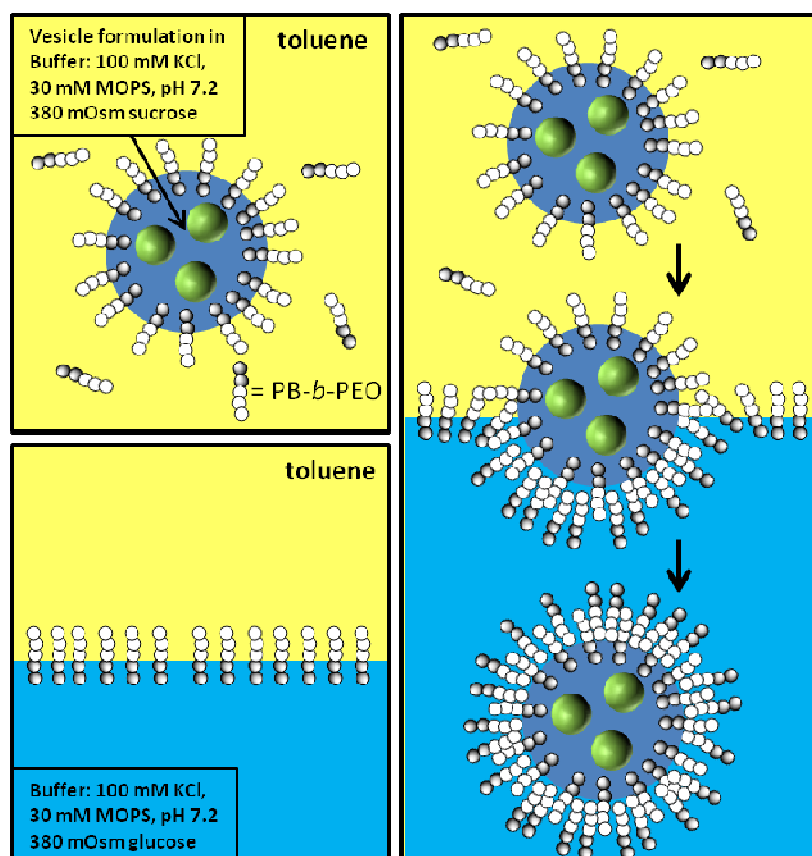


**Figure 85:** Multicompartmentalization of synthetic amphiphile-based vesicles in the interior of giant polymersomes.

The emulsion was then set on top of an aqueous pseudo intracellular buffer containing 380 mOsm of glucose in order to keep the final osmotic pressure equal after centrifugation. The excess PB-*b*-PEO is found at the interface between toluene and the aqueous buffer,

forming a monolayer of block copolymer with the hydrophobic part of the molecule pointing towards the oil phase (bottom left, figure 85). In a last step, the biphasic system was centrifuged. Due to the density difference of the emulsified droplets containing 380 mOsm sucrose compared to the density of the aqueous buffer containing 380 mOsm of glucose, the emulsified droplets pass downwards through the monolayer made of PB-*b*-PEO. During the passage through the monolayer a second layer of polymer is enwrapped around the emulsified droplets and thus forms a bilayer, yielding giant polymersomes with the prepared vesicle solution in the aqueous interior.

In order to test the process, vesicle formulations bearing a fluorescent dye in the membrane have been prepared. Formulation H was prepared via thin film hydration using the pseudo-intracellular sucrose buffer to yield vesicles bearing 5  $\mu\text{M}$   $\text{C}_8\text{F}_{17}$ -BODIPY (**149**) in the bilayer with an amphiphile concentration of 1.5 mM. The synthesis of the BODIPY (**149**) will be reported later on. The molecular structure of the vesicle formulations is depicted in figure 86.

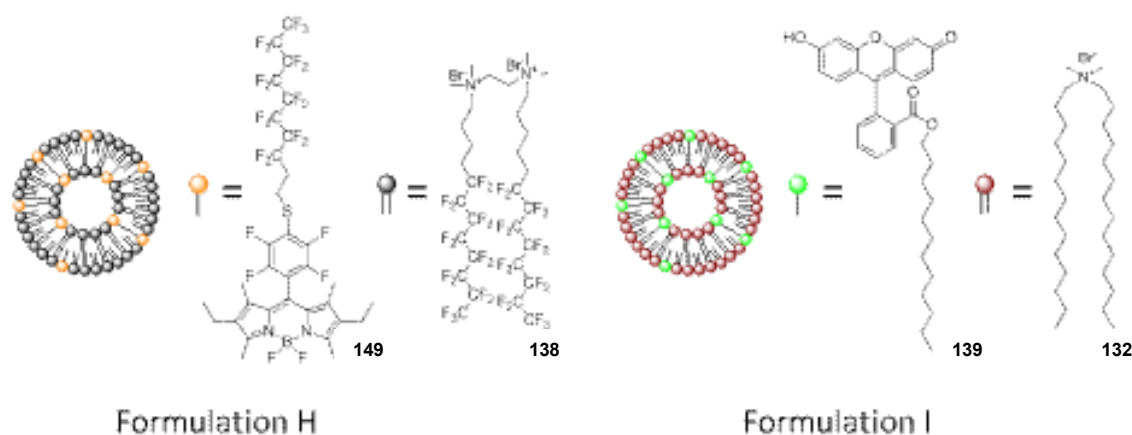


**Figure 86:** Schematic representation of the molecular composition of formulation H containing  $\text{C}_8\text{F}_{17}$ -BODIPY (**150**) and formulation I bearing dodecyl fluorescein in the bilayer.

Formulation I is the hydrocarbon analogue to formulation H and was prepared in the same fashion using the pseudo-intracellular sucrose buffer. Commercially available dodecyl fluorescein (**139**, 5  $\mu\text{M}$ ) was incorporated in the bilayer of hydrocarbon vesicles with an amphiphile concentration of 1.5 mM. Both formulations were extruded through a 800 nm membrane to get rid of large vesicles or aggregates. The resulting polydisperse formulations, with an average size of 308 nm (formulation H) and 398 nm (formulation I) were then used for the multicompartmentalization process and each step was followed via confocal

---

fluorescence microscopy. Bright field and fluorescence images of the emulsion of formulation H in water droplets stabilized by PB-*b*-PEO are depicted in figure 87.

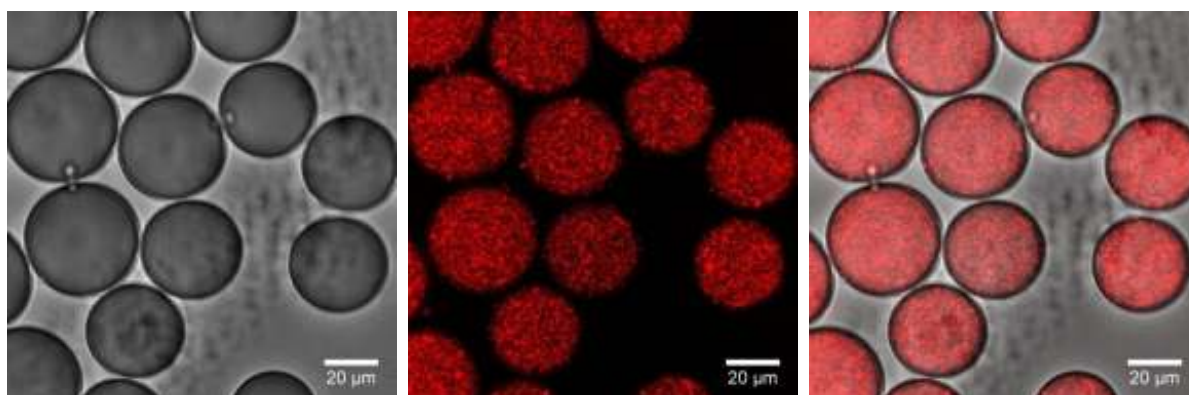


**Figure 87:** Bright field (left), fluorescence (middle) and overlay of bright field and fluorescence image (right) of a formulation H in a water in oil emulsion via PB-*b*-PEO.

In the bright field image the emulsified water droplets are clearly visible with a diameter ranging from 20 to 60  $\mu\text{m}$  in this image. The fluorescence image reveals the presence of the fluorinated vesicles in nanometer scale doped with the orange-red emitting BODIPY dye (**150**). The fluorescence and bright field overlay show that the fluorescent vesicles are well-incorporated in the interior of the water droplets. No fluorescence is observed in the toluene phase indicating the stability of the vesicles under these conditions.

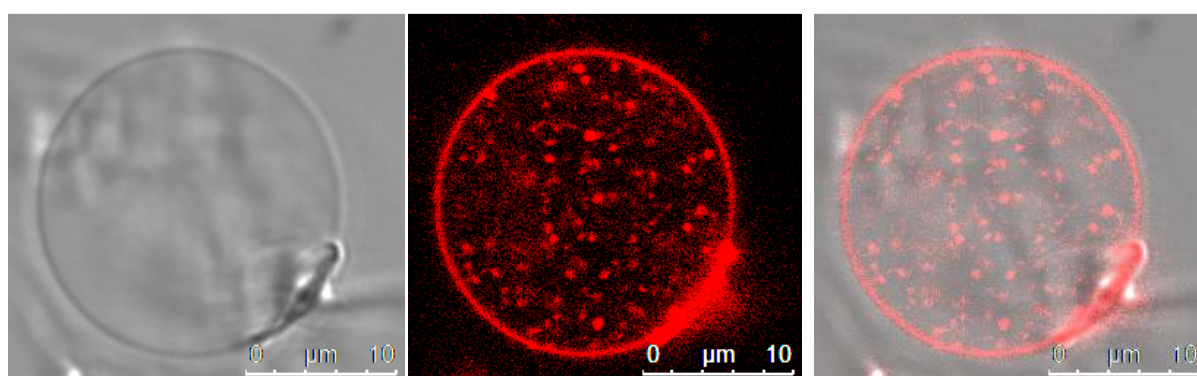


**Figure 88:** Bright field (left), fluorescence (middle) and overlay of bright field and fluorescence image (right) of a formulation H in the aqueous interior of a PB-*b*-PEO polymersome.

After extrusion of the emulsion over the aqueous layer containing pseudo-intracellular buffer and 380 mOsm glucose, polymersome with a bilayer made of the PB-*b*-PEO are obtained. Confocal microscopy images of a representative polymersome are shown in figure 88. The bright field image shows a polymersome with a diameter of 20  $\mu\text{m}$ . The fluorescence image

---

---

reveals the fluorescent vesicles in the interior of the aqueous compartment. It needs to be pointed out that a non-negligible amount of fluorescence is also observed in the polymer bilayer of the giant polymersome. This is due to the fusion of some vesicles with the polymer membrane during the preparation process. The rather high concentration of vesicles in formulation H might also support the incorporation of the some vesicles into the polymer bilayer. The bright field and fluorescence overlay on the right side shows as well that the vesicles are well-incorporated in the polymersome interior. The size of the vesicles reflects well the polydispersity of the formulation with some large vesicles with a size over a 1  $\mu\text{m}$  but also a lot of smaller ones.

The same experiment was conducted for the green fluorophore-labelled hydrocarbon analogue (formulation I). The emulsion-centrifugation procedure as described before was used to incorporate the hydrocarbon vesicles in the aqueous compartment of the polymersomes. The structures obtained during the process are given in figure 89 and compared to the fluorescence image of formulation I.

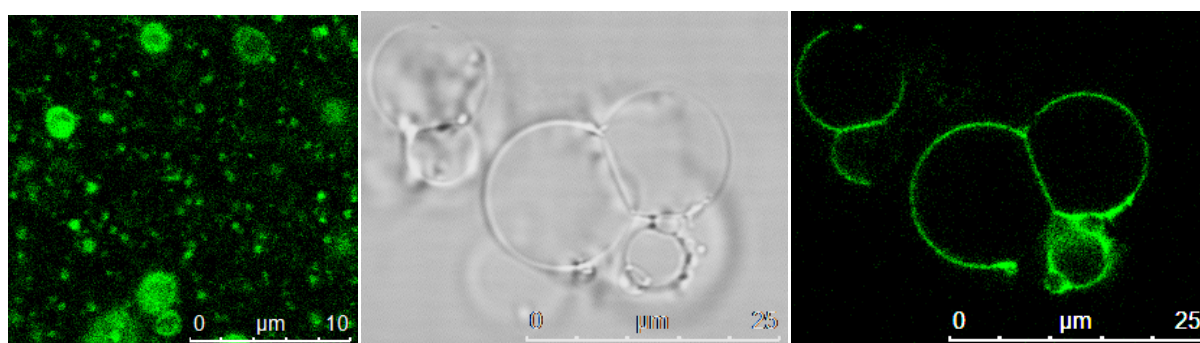


**Figure 89:** Fluorescence image of formulation I (left), Bright field (middle) and fluorescence image (right) ( $\lambda_{\text{exc}} = 476 \text{ nm}$ ) of a formulation I after the emulsion centrifugation procedure with PB-*b*-PEO.

In the left figure a fluorescence image of formulation I is shown, where the polydisperse hydrocarbon vesicles are clearly visible. The images obtained after the emulsion centrifugation process are shown in the middle and on the right side. The bright field image shows polymersome structures which are somewhat less well-defined than for formulation H with a diameter of 10 to 25  $\mu\text{m}$ . The fluorescence image of the same polymersome reveals that there are no vesicles present in the aqueous interior but all the fluorescence and therefore all the amphiphile can be found in the polymer bilayer. In fact the structures formed during the emulsion-centrifugation process are not pure polymersomes but polymer amphiphile

---

hybrid vesicles. One characteristic of these types of structures are areas of higher and lower amphiphile content which can be seen in areas with no apparent fluorescence in the bilayer (figure 89, right). This observation has been made previously in the literature for lipid polymer hybrid vesicles.<sup>42</sup> Although this was a negative result in terms of coencapsulation of the two different types of vesicle formulations these structures have a certain interest for studies of the membrane permeability which will not be further discussed here.

Because of the higher stability of the fluorinated vesicles<sup>14</sup> it was assumed that two different formulations of fluorinated vesicles could coexist at the same time in the interior of the polymersome and therefore another formulation bearing a green emitting fluorescein based dye (**152**) in the membrane has been prepared. The synthesis of this dye is shown in chapter 5. A schematic representation of the molecular composition of formulation J is shown in figure 89.

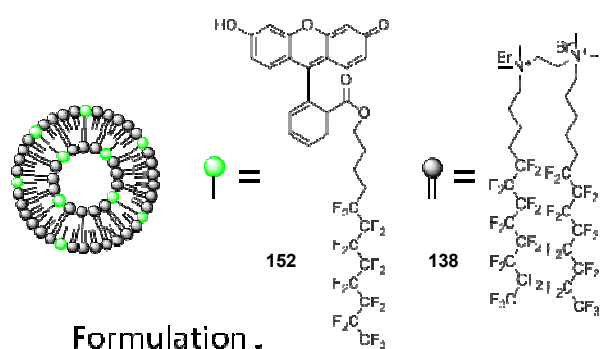


**Figure 89:** Schematic representation of the molecular composition of formulation J containing C<sub>8</sub>F<sub>17</sub>-fluorescein (**152**) in the bilayer.

Formulation J containing 5 μM C<sub>8</sub>F<sub>17</sub>-fluorescein (**150**) in the bilayer of fluorinated vesicles with an amphiphile concentration of 1.5 mM in pseudo-intracellular sucrose buffer was extruded through a 800 nm membrane to obtain vesicles with an average diameter of 396 nm. Formulation J and formulation H were then mixed in equal volume ratios. The obtained mixture was subsequently used in the emulsion-centrifugation procedure used for the previous results. In figure 90 confocal fluorescence microscope images are depicted of the obtained emulsion and the polymersomes after centrifugation.

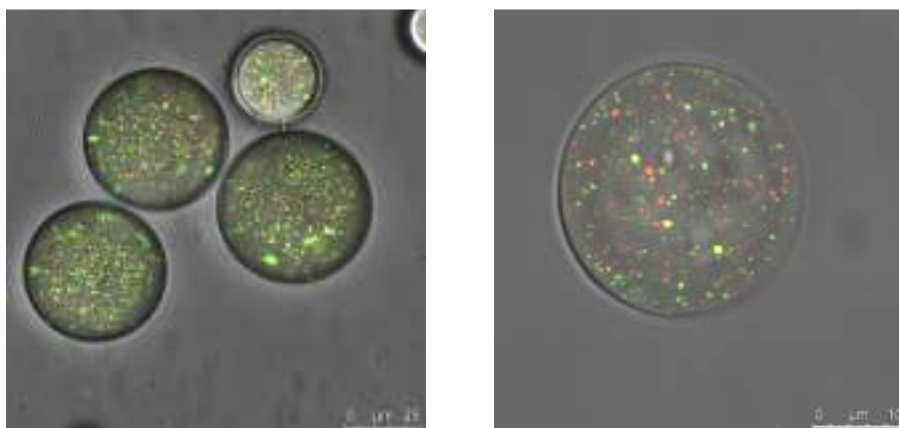


**Figure 90:** Bright field and fluorescence overlay images of the emulsion containing formulation H and J at the same time in the PB-b-PEO stabilized droplets (left). Bright field and fluorescence overlay image of the resulting polymersome after emulsion-centrifugation (right)

Already the bright field and fluorescence overlay image of the emulsion shows that two types of vesicles are present in the aqueous droplet. It seems that no overlay fluorescence is detected meaning no vesicles exhibiting green and red fluorescence are seen simultaneously. On the second picture a representative polymersome obtained after centrifugation is shown. The size of the polymer vesicle is around 20  $\mu\text{m}$  and vesicles deriving from formulation H and J are seen in the interior. The bright field and fluorescence overlay also reveals a much lower content of fluorophore in the polymer membrane. Ultimately it can be said, that the coencapsulation of two different types of vesicle formulations based on semi-fluorinated gemini amphiphiles (**138**) can be achieved, and to our knowledge it is the first time such a system has been reported.

#### 4.4 Molecular ion transfer in the aqueous compartment of PB-b-PEO vesicles.

In order to test the ion transfer in the aqueous compartment of the giant polymersomes a solution containing 5  $\mu\text{M}$  water soluble BAPTA-BODIPY (**72**), 5  $\mu\text{M}$   $\text{CaCl}_2$  and 75  $\mu\text{M}$  water soluble DMNPE-4 (**99**) in pseudo-intracellular sucrose buffer has been prepared.  $\text{Ca}^{2+}$ -decaging agents have already been used to phototrigger the formation of hydrogels in alginate solutions<sup>43</sup> but the ion transfer in confined polymer compartments has not been studied. Polymersomes containing the  $\text{Ca}^{2+}$ -decaging agent and the fluorescent ion sensor in the aqueous compartment have been prepared via the emulsion-centrifugation procedure replacing the vesicle containing aqueous solution with the ion-transfer system containing ion

---

sensor **72** and ion decaging agent **99**. A schematic representation of the resulting polymersome is given in figure 91.

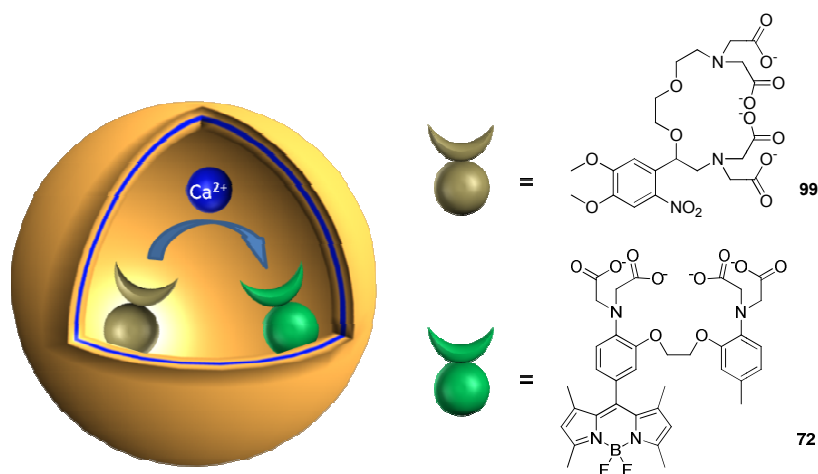


**Figure 91:** Schematic representation of the system prepared for the ion transfer between water-soluble molecules in PB-*b*-PEO vesicles.

The fluorescence emission was recorded between 510 and 650 nm while exciting the system at 405 nm. During the excitation in the UV range, photodecaging of the  $\text{Ca}^{2+}$  occurs and the ion is transferred to the fluorescent ion sensor (**72**). As a consequence the fluorescence intensity rises with prolonged irradiation. In figure 92 a set of the prepared polymersomes are shown at different irradiation times.

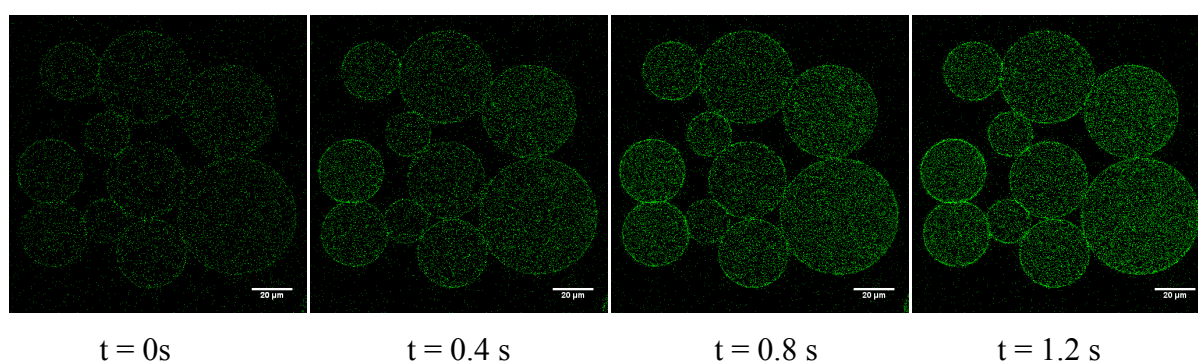


**Figure 92:** Confocal fluorescence images of polymersomes containing  $\text{Ca}^{2+}$ -decaging agent (**42**)  $5\ \mu\text{M}$   $\text{CaCl}_2$  and  $5\ \mu\text{M}$   $\text{Ca}^{2+}$ -sensor (**8**) in the aqueous lumen of the polymersome.

It can be clearly seen that the fluorescence emission at  $t = 0\text{ s}$  is rather low. The fluorescence emission increases progressively up to  $1.2\text{ s}$  at which point the maximum is reached and therefore the ion sensor received a maximum  $\text{Ca}^{2+}$ -ions. Like this a visible proof is given, that the ion transfer in the confined compartment occurs. In a second experiment the same

---

polymersome preparation was taken and a fluorescence recovery after photobleaching (FRAP) experiment was conducted. The fluorescence emission in the interior of 12 polymersome was recorded upon irradiating at 488 nm so that the  $\text{Ca}^{2+}$ -decaging agent remains untouched. After 800 ms a light pulse at 405 nm with maximal laser intensity was applied for 200 ms and the irradiation of the system at 488 nm was continued. The obtained graph from this experiment is plotted in figure 93. The fluorescence intensity in the beginning of the experiment is low due to the binding of  $\text{Ca}^{2+}$ -to the decaging agent (**99**) and the fluorescence emission does not increase until the laser pulse at 405 nm is given.

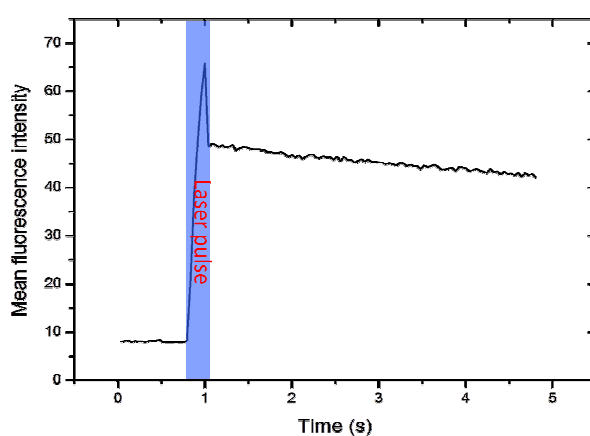


**Figure 93:** Average fluorescence emission of 12 independent polymersomes containing  $\text{Ca}^{2+}$ -decaging agent (**99**)  $5\ \mu\text{M}$   $\text{CaCl}_2$  and  $5\ \mu\text{M}$   $\text{Ca}^{2+}$ -sensor (**72**) in the aqueous interior of the polymersome. Continuous irradiation at 488 nm and a short laser pulse at 405 nm were applied and the fluorescence intensity recorded over time between 510 and 650 nm.

During the 200 ms laser pulse at 405 nm the fluorescence intensity increases sharply. The fluorescence enhancement is about 5 times its initial intensity. After the ions were transferred to the ion sensor (**72**) during the laser pulse, the fluorescence keeps decreasing slowly, which is due to photobleaching of the BAPTA-BODIPY ion sensor (**72**). However this experiment is more advantageous than the continuous irradiation at 405 nm due to the use of a less strong laser for the continuous irradiation. Also the  $\text{Ca}^{2+}$ -ions can be released “on demand” at any given moment during the experiment. After it was shown that the ion transfer in confined compartment is indeed possible the ion transfer between vesicles in the aqueous interior of the polymersome was studied.

#### 4.4.1 $\text{Ca}^{2+}$ sensing vesicles in the confocal microscope

Three formulations of  $\text{Ca}^{2+}$ -sensing vesicles have been prepared in order to find the most appropriate formulation for studies with the confocal microscope.

Formulation K consisted of 5  $\mu\text{M}$  BANIF (**79**) and 1.5 mM fluorinated amphiphile (**138**). The vesicles were prepared via thin film hydration using a pseudo-intracellular sucrose buffer and 10 mM EGTA. The sample was extruded through a 800 nm membrane to omit large multilamellar structures. After the preparation the sample was split in two and the  $\text{CaCl}_2$  was added to one part to obtain a free  $\text{Ca}^{2+}$  concentration of 39  $\mu\text{M}$ . In figure 94 the composition of formulation K and the fluorescence emission spectra in solution and the fluorescence emission obtained via confocal microscopy were compared. While the formulation K in the presence of  $\text{Ca}^{2+}$  is clearly more fluorescent regarding the emission spectra measured in a spectrofluorometer in this case is more complicated while observing the sample via confocal microscopy (figure 94, bottom right). Here the fluorescence emission shows the expected difference in fluorescence emission only in the beginning of the experiment.

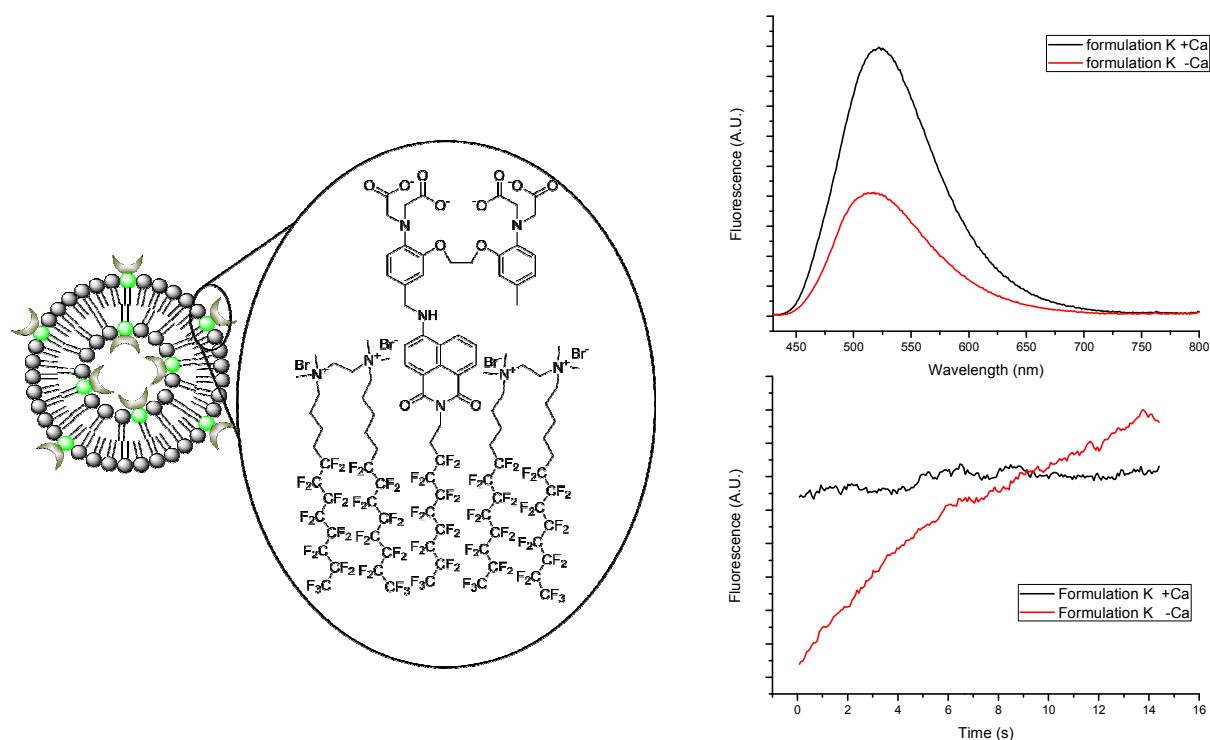


**Figure 94:** Schematic representation of formulation K (left). Fluorescence emission spectra of formulation K in presence and absence of  $\text{Ca}^{2+}$  ( $\lambda_{\text{em}} = 488 \text{ nm}$ ) (top right). Fluorescence emission between 510 and 650 nm measured via confocal microscopy ( $\lambda_{\text{em}} = 488 \text{ nm}$ ) (bottom right).

During the time course of 14 s the fluorescence of the  $\text{Ca}^{2+}$  free sample keeps increasing until it reaches and even surpasses the emission intensity of the  $\text{Ca}^{2+}$  containing sample. This might

be explained by the formation of a photoreactive species during excitation and the oxidation of the BAPTA unit during the excitation, since naphthalimides carrying an amine group in the 4 position are efficient pH-sensors,<sup>44,45</sup> and the fluorescence lifetime of these fluorophores are rather long (around 8 ns).<sup>46</sup> The oxidation of the BAPTA unit would lead to a permanent quenching of the PET process. This hypothesis is supported by the results obtained for the other two formulations. Formulation L was prepared under similar conditions as formulation K. The fluorinated vesicles consisting of 1.5 mM fluorinated gemini (**138**) were loaded with 5  $\mu$ M C<sub>8</sub>F<sub>17</sub>-BAPTA-BODIPY (**82**) with 10 mM EGTA present in the pseudo-intracellular sucrose buffer. The formulation was split in two and CaCl<sub>2</sub> was added to one part to reach a Ca<sup>2+</sup>-concentration of 39  $\mu$ M. Molecular composition and fluorescence emission spectra along with the fluorescence intensity of the formulation in presence and absence of Ca<sup>2+</sup> are shown in figure 95.

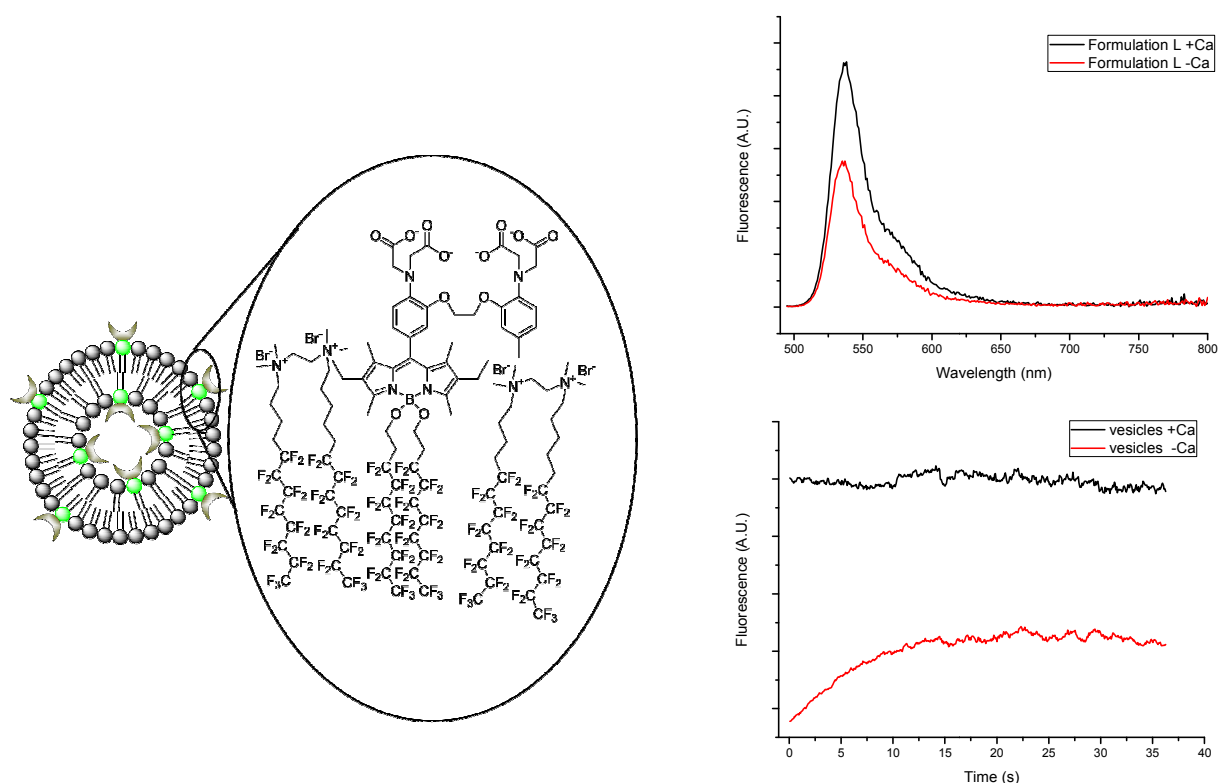


**Figure 95:** Schematic representation of formulation L (left). Fluorescence emission spectra of formulation L in presence and absence of Ca<sup>2+</sup> ( $\lambda_{em} = 488$  nm) (top right). Fluorescence emission between 510 and 650 nm measured via confocal fluorescence microscopy ( $\lambda_{em} = 488$  nm) (bottom left).

Again the fluorescence emission spectra obtained via a classical spectrofluorometer shows a characteristic difference in the fluorescence emission in the presence and absence of Ca<sup>2+</sup>. Regarding the fluorescence intensity measured via confocal microscopy a slight increase in

the emission intensity is observed between 0 and 10 s. In contrary to vesicle formulation K the fluorescence intensity stabilizes itself well below the fluorescence emission of formulation L in presence of  $\text{Ca}^{2+}$ . This formulation is therefore a suitable candidate for the studies via confocal fluorescence microscopy. The incident increase in fluorescence emission might be explained by low levels of impurities in the preparation of formulation L or a partial photoreaction. However a photoreaction would probably consume all molecules and can therefore be excluded. The last formulation which was studied was formulation M, which was prepared according to the previous two containing  $5\ \mu\text{M}$   $\text{C}_8\text{F}_{17}$ -furared (**97**) in the bilayer consisting of  $1.5\ \text{mM}$  fluorinated gemini (**138**) in pseudo-intracellular sucrose-containing buffer loaded with  $10\ \text{mM}$  EGTA.

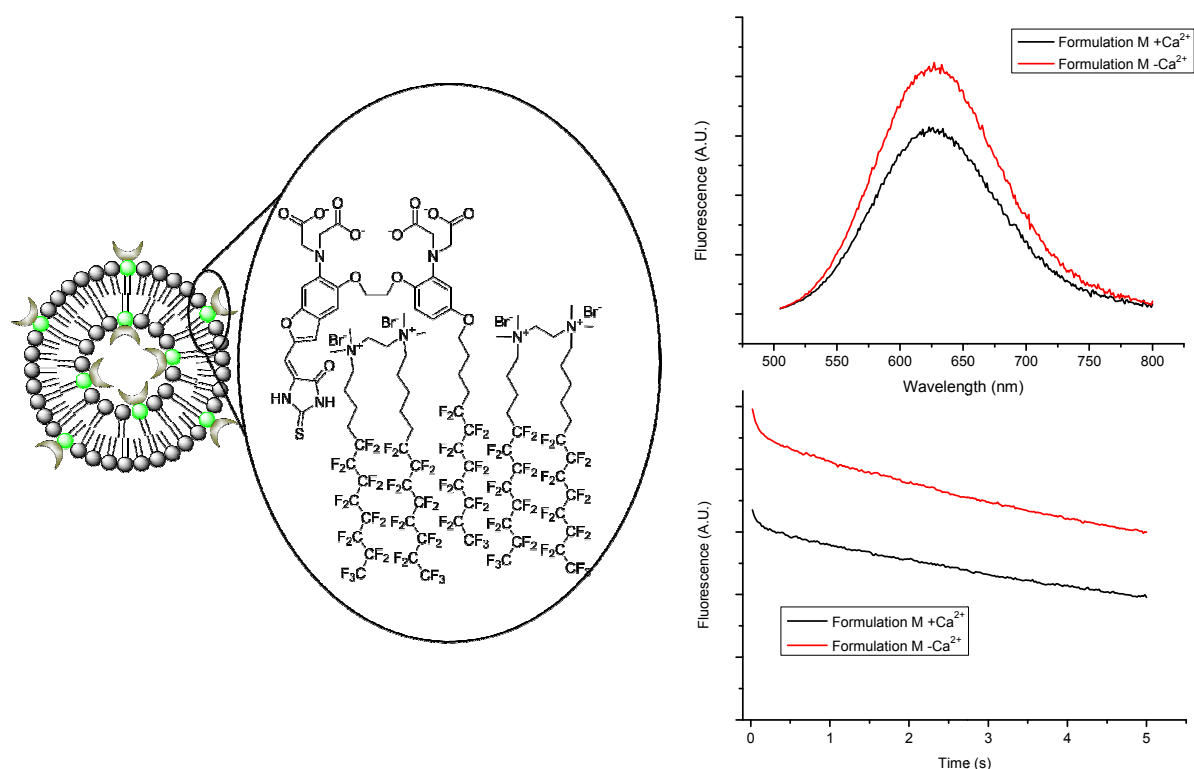


**Figure 96:** Schematic representation of formulation M (left). Fluorescence emission spectra of formulation M in presence and absence of  $\text{Ca}^{2+}$  ( $\lambda_{\text{em}} = 488\ \text{nm}$ ) (top right). Fluorescence emission between 510 and 810 nm measured via confocal microscopy ( $\lambda_{\text{em}} = 488\ \text{nm}$ ) (bottom left).

Molecular composition of formulation M, the emission spectra observed via a spectrofluorometer and the fluorescence intensity over time measured under a confocal fluorescence microscope are shown in figure 96. The fluorescence emission spectra also show a clear difference in the emission intensity in presence and absence of  $\text{Ca}^{2+}$ . It is noteworthy that in this formulation the emission intensity in presence of  $\text{Ca}^{2+}$  is lower than in the absence,

---

which is due to the lower quantum yield as shown before and the change in the absorption spectra which results in a lower absorption intensity at 488 nm upon  $\text{Ca}^{2+}$  binding. The photobleaching is non-negligible in this experiment (10 % in 5 s) due to the increased laser power which was needed due to the lower quantum yield of the  $\text{C}_8\text{F}_{17}$ -fura red ion sensor (**97**). Unlike the other two cases there is only a very small decrease in fluorescence between 0 and 0.5 s noted until a similar decrease in emission due to photobleaching is noted. With formulation M there is a second suitable candidate for ion transfer studies between vesicles. The formulation of choice, however, is formulation L due to a higher quantum yield which means the usage of lower laser powers and a slightly bigger difference in fluorescence enhancement (formulation L = 1.6, formulation M = 1.2). In the next section a formulation based on formulation L will be prepared and the ion transfer between a  $\text{Ca}^{2+}$ -decaging formulation of vesicles and a  $\text{Ca}^{2+}$ -sensing formulation will be studied in the aqueous compartment of a PB-*b*-PEO polymersome.

#### 4.4.2 Ion transfer between fluorocarbon vesicles in PB-*b*-PEO polymersomes

In order to test the ion transfer with  $\text{Ca}^{2+}$ -sensing vesicles in confined polymer compartment, a formulation of  $\text{C}_8\text{F}_{17}$ -BAPTA-BODIPY (**82**) bearing vesicles has been prepared (formulation N). The concentration of  $\text{C}_8\text{F}_{17}$ -BAPTA-BODIPY (**82**) was 5  $\mu\text{M}$  and the fluorinated amphiphile 1.5 mM in pseudo-intracellular sucrose-containing buffer. The formulation was extruded through a 800 nm membrane to omit large multilamellar structures. Water soluble DMNPE-4 (**99**) was added until a final concentration of 75  $\mu\text{M}$  of the  $\text{Ca}^{2+}$ -decaging agent was reached and subsequently 5  $\mu\text{M}$  of  $\text{CaCl}_2$ . This mixture was then subjected to the emulsion-centrifugation procedure using PB-*b*-PEO copolymer to obtain polymersomes with formulation N and DMNPE-4 (**99**) in the aqueous interior. A schematic representation of the system is given in figure 97. The fluorescence of these polymersomes was been recorded via confocal fluorescence microscopy. The fluorescence emission of 10 independent polymersomes with approximately the same size has been observed between 510 – 650 nm upon exciting the system at 488 nm. After 420 ms a laser pulse of 40 ms with maximum intensity at 405 nm was sent in order to photo-decage the bound  $\text{Ca}^{2+}$ . The observation made is plotted in figure 98 (black).

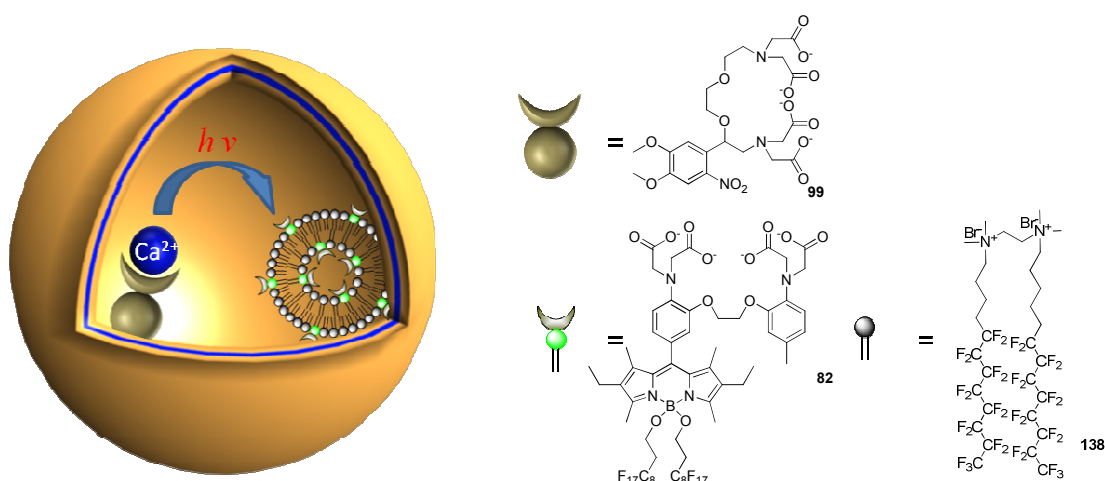


**Figure 97:** Schematic representation of the ion transfer in the interior of a giant PB-*b*-PEO polymersome between water-soluble DMNPE-4 (**99**) and vesicle formulation N bearing C<sub>8</sub>F<sub>17</sub>-BAPTA-BODIPY (**82**) in the bilayer of the fluorinated vesicles.

As a control experiment the same experiment has been conducted but the laser pulse was applied at 488 nm where no photo-decaging can occur due to the absence of absorption in the spectrum of DMNPE-4 (**42**). The recorded fluorescence intensity is plotted in the same graph in figure 98 (red). As we saw in the previous section the fluorescence enhancement in the vesicles is rather limited, therefore the difference in fluorescence intensity cannot be distinguished by observing the images. The observed fluorescence shown in the figure was normalized as shown in equation 21. Where  $FI_N$  is the normalized fluorescence intensity,  $FI(t)$  is the fluorescence intensity at a certain time and  $FI(t_0)$  is the fluorescence intensity at time 0.

$$FI_N = \frac{FI(t)}{FI(t_0)} \quad \text{equation 21}$$

Regarding figure 98 a clear difference in the fluorescence intensities can be seen. While the irradiation at 405 nm breaks the Ca<sup>2+</sup>-cage (**99**) and increases the fluorescence intensity to 1.25 times its initial intensity, the pulse at 488 nm has no effect on the fluorescence intensity.

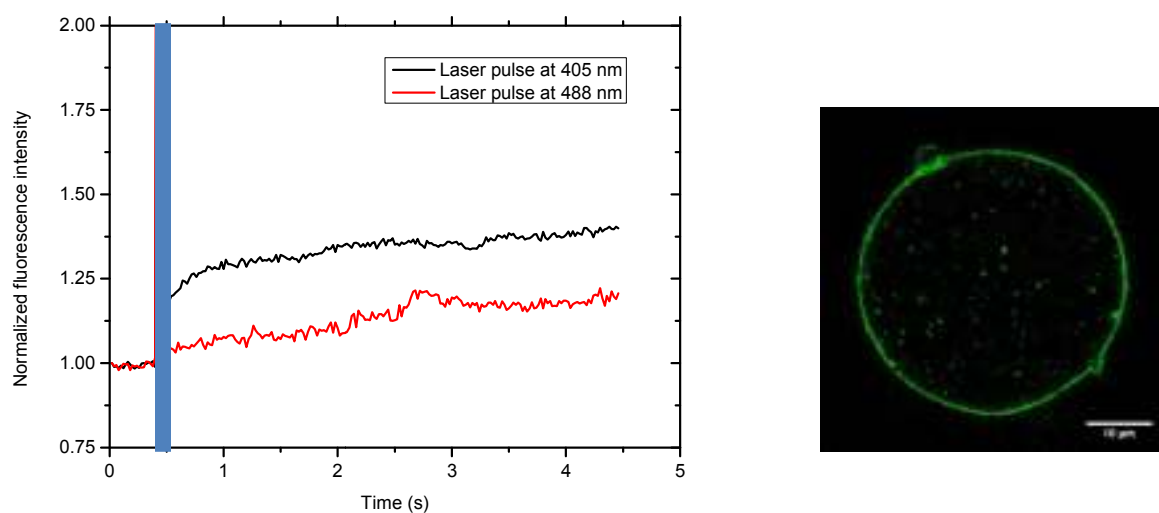


**Figure 98:** Fluorescence intensities over time (left) for a solution containing formulation N, 75  $\mu\text{M}$  DMNPE-4 (**42**) and 5  $\mu\text{M}$   $\text{CaCl}_2$  ( $\lambda_{\text{exc}} = 488 \text{ nm}$ ). A short laser pulse (40 ms) was applied after 420 ms observation either at 405 nm (black) or at 488 nm (red). Confocal fluorescence image of a formulation N containing PB-*b*-PEO polymersome (right).

It should be noted that the fluorescence increases slightly over time. This is the same observation which was made in formulation K in the previous section and is independent from the  $\text{Ca}^{2+}$ -transfer. It was shown that the ion transfer from water solubilized  $\text{Ca}^{2+}$  decaging agent occurs in the polymersome lumen. The subsequent step was the preparation of the  $\text{Ca}^{2+}$  decaging vesicles and to coencapsulate them with formulation N.

$\text{Ca}^{2+}$ -decaging vesicles were prepared via thin film hydration as mentioned before. Amphiphilic  $\text{Ca}^{2+}$ -decaging agent (**122**) with a final concentration of 150  $\mu\text{M}$  in the membrane of fluorinated vesicles consisting of 4.5 mM fluorinated gemini (**138**) were prepared in pseudo-intracellular sucrose buffer (formulation O). In order to make these vesicles visible in the confocal microscope they were loaded with 5  $\mu\text{M}$  BODIPYred (**150**). The synthesis of the red fluorescent dye will be shown in the next chapter. The vesicle-containing solution was extruded through a 800 nm membrane to get rid of larger vesicles and structures. Formulation O was then mixed in a ratio 1:1 and 3:1 with formulation N in the presence of 5  $\mu\text{M}$   $\text{CaCl}_2$  and subjected to the emulsion centrifugation procedure using PB-*b*-PEO. A schematic representation of the obtained system is given in figure 99

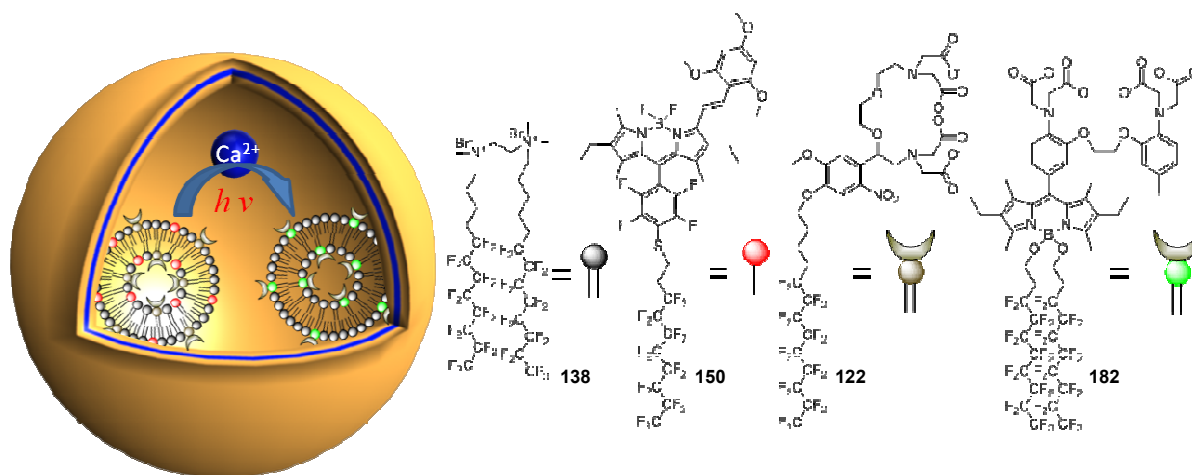


**Figure 99:** Schematic representation of the prepared PB-*b*-PEO polymersome containing formulation O and formulation N simultaneously in the aqueous compartment. The light-induced ion transfer is highlighted in the interior of the polymersome and the molecular composition is shown on the right side.

The obtained results for the two mixtures of formulation N and formulation O are shown in figure 100. The previously described FRAP experiment was used to observe the transfer behavior between the two vesicle formulations in a confined compartment. Briefly, after 400 ms recording the fluorescence intensity a laser pulse at 405 nm was applied (FWHM = 40 ms) to release the  $\text{Ca}^{2+}$  from the ejector vesicles (formulation O), while the fluorescence intensity was recorded on continuously exciting at 488 nm. The observed fluorescence was normalized as shown before and the average fluorescence of 10 polymersomes has been taken to obtain the curves depicted in figure 100. The 1:1 mixture of formulation N and O yielded a curve where the fluorescence intensity after the laser pulse at 405 nm is in fact smaller than the initial intensity. This is due to ratio between ion transferred and photobleaching, which is unfavorable in this case. However, the fluorescence intensity increases slightly after the laser pulse, which indicates that at least partial  $\text{Ca}^{2+}$  transfer is occurring.

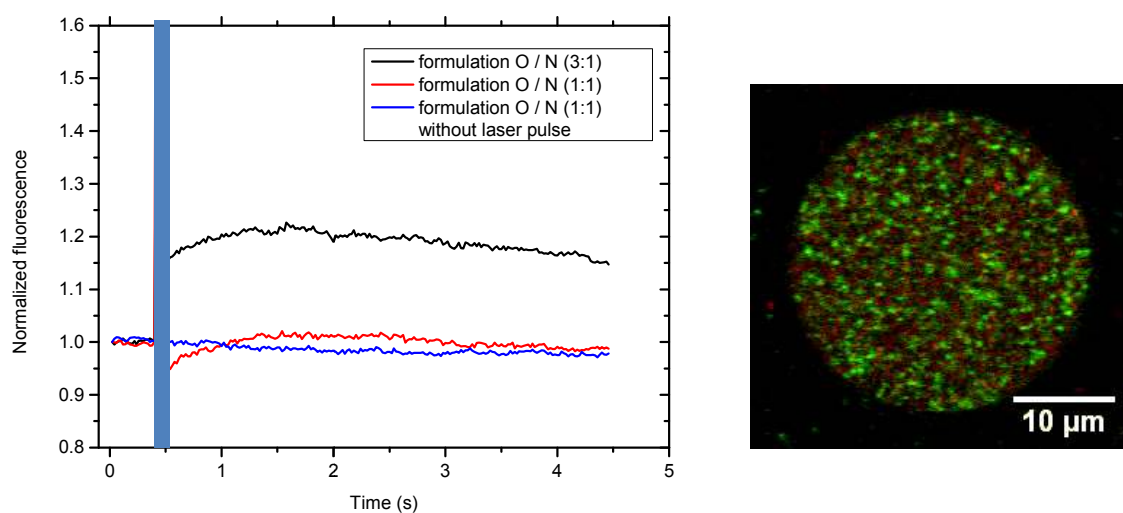


**Figure 100:** Left: Fluorescence intensities as a function of time recorded via confocal fluorescence microscopy of 10 polymersomes ( $\lambda_{\text{exc}} = 488 \text{ nm}$ ). A laser pulse at 405 nm (blue bare) to release  $\text{Ca}^{2+}$  is applied. Mixtures of formulation O and N (3:1, black and 1:1 red) were studied and compared to a 1:1 mixture of formulation O and N without laser pulse at 405 nm. Right: confocal fluorescence microscopy image of a characteristic polymersome containing formulation O and N.

The 3:1 mixture of formulation O and N gives a different picture. The fluorescence intensity after the laser pulse at 405 nm is elevated by a factor of 1.2 as previously observed for the  $\text{Ca}^{2+}$ -transfer experiment between water soluble DMNPE-4 (**99**) and formulation N. The final concentrations of amphiphile and  $\text{Ca}^{2+}$ -decaging agent are 3.37 mM fluorinated gemini (**138**) and 112  $\mu\text{M}$  amphiphilic DMNPE-4 (**122**) in formulation O and 0.38 mM fluorinated gemini (**138**) and 1.25  $\mu\text{M}$   $\text{C}_8\text{F}_{17}$ -BAPTA-BODIPY (**82**) in formulation N. With this ratio between  $\text{Ca}^{2+}$ -decaging vesicles and  $\text{Ca}^{2+}$ -sensing vesicles the ion transfer seems to work efficiently. It needs to be noted that the precise control of the  $\text{Ca}^{2+}$  concentration is rather difficult since it depends on several parameters including the  $\text{Ca}^{2+}$  impurities in the glassware, the purity of the water which can vary easily in terms of  $\text{Ca}^{2+}$  and the ion impurities in the reagents used. Therefore, a rather elevated concentration of  $\text{Ca}^{2+}$ -decaging vesicles were required. Additionally, the decrease in binding affinity once incorporated in the vesicles membrane which was determined for  $\text{Ca}^{2+}$ -sensing ion acceptors (**79**, **82** and **97**) in cationic fluorinated vesicles, most likely affects the amphiphilic DMNPE-4 (**122**) in the vesicle membrane as well. To that end, a higher concentration of decaging agent is needed to liberate the same amount of free  $\text{Ca}^{2+}$ . In a final experiment the rise of the fluorescence after the laser pulse at 405 nm was investigated in order to attribute the kinetics to either ion transfer or a decaging

process. For this experiment the same ratio between formulation O and formulation N was used as in the previous experiment but the laser pulse was kept as short as possible (20 ms) in order to see a maximum of the kinetics.

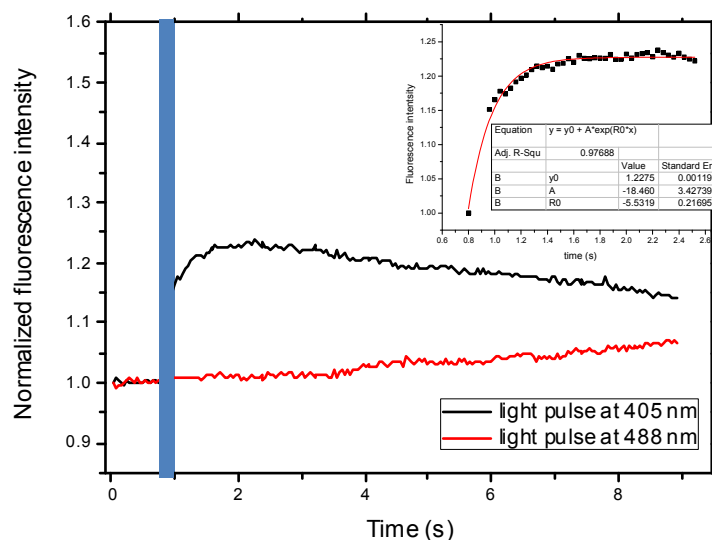


**Figure 101:** Fluorescence intensities between 510 and 650 nm as a function of time recorded via confocal fluorescence microscopy of 10 polymersomes ( $\lambda_{\text{exc}} = 488 \text{ nm}$ ) of a mixture of formulation O and N (3:1). A laser pulse at 405 nm (blue bare) to release  $\text{Ca}^{2+}$  is applied (black) and compared to the same sample with a laser pulse at 488 nm (blue bare). The fitting of the first 2.4 s of the experiment is shown (inlet).

The obtained normalized average fluorescence intensities of 10 polymersomes over time are plotted in figure 101. The ion transfer seems to work effectively also with the shortened laser pulse as can be seen in the rise of fluorescence after the laser pulse at 405 nm (black). A similar laser pulse at 488 nm where formulation O does not absorb light is unaffected (red). The slow photobleaching process after the laser pulse and continuous irradiation at 488 nm are similar to previous experiments. Mono-exponential fitting of the first 2.4 s after applying the laser pulse and extrapolating the 20 ms during the pulse to the initial intensity, gave a rate constant of  $5.53 \text{ s}^{-1}$ . This corresponds in the order of magnitude to the slow  $\text{Ca}^{2+}$ -decaying component measured in the group of Ellis-Davies for DMNPE-4 derivative ( $1.5 \text{ s}^{-1}$ ).<sup>47</sup> Assuming that the obtained rate constant is in fact connected to slow decaying of  $\text{Ca}^{2+}$  from DMNPE-4 based cages, it needs to be concluded that the incorporation in the vesicle membrane and the incorporation in the highly viscous aqueous compartment of the PB-*b*-PEO polymersomes somewhat slows the decaying process down. By applying the same fitting to the experiment conducted between water soluble DMNPE-4 (99) and formulation N a rate

---

constant of  $5.83 \text{ s}^{-1}$  was obtained. The later rate constant must be taken with care due to the rather long laser pulse and therefore a rather large part of the curve was extrapolated. Despite that, the rate constant is almost similar indicating that the slower release process is indeed due to the confinement in the aqueous interior of the polymersomes.

## 4.5 Conclusion

A new type of multicompartimentalized system has been designed, namely fluorinated cationic vesicles in polymersomes. Amphiphilic  $\text{Ca}^{2+}$ -decaging agents (**122**) and amphiphilic  $\text{Ca}^{2+}$ -fluorescent sensors (**79**, **82** and **97**) have been successfully incorporated in the membrane of fluorinated gemini based vesicles and their binding affinity towards  $\text{Ca}^{2+}$  determined, which showed a 1 – 2 order of magnitudes lower binding than water soluble parent molecules due to the cationic environment. These ion ejecting and sensing vesicles have been successfully introduced in the aqueous PB-*b*-PEO polymersome compartment and the ion transfer in the aqueous interior has been achieved in a photocontrolled fashion. Fitting of the fluorescence increase during ion transfer revealed a slower decaging rate compared to literature values. In summary a new photocontrolled ion transfer system has been designed which could be the basis for photocontrolled  $\text{Ca}^{2+}$ -triggered enzymatic reactions in confined microcompartments where compartmentalization is needed. This also gives the basis to photocontrolled cascade reactions in confined compartments. For example, the transfer of one type of ion to an intermediate vesicle which triggers the release of another ion which can be sensed in a third instance.

---

## References

- (1) Israelachvili, J. N.; Mitchell, D. J.; Ninham, B. W. *Journal of the Chemical Society-Faraday Transactions Li* **1976**, *72*, 1525.
- (2) Israelachvili, J. N.; Mitchell, D. J.; Ninham, B. W. *Biochim. Biophys. Acta* **1977**, *470*, 185.
- (3) Bangham, A. D.; Glauert, A. M.; Horne, R. W.; Dingle, J. T.; Lucy, J. A. *Nature* **1962**, *196*, 952.
- (4) Bangham, A. D.; Horne, R. W. *J. Mol. Biol.* **1964**, *8*, 660.
- (5) D.D., L. *Elsevier, Amsterdam.* **1993**.
- (6) Torchilin, V. P. *Nat. Rev. Drug Discovery* **2005**, *4*, 145.
- (7) Christensen, S. M.; Stamou, D. *Soft Matter* **2007**, *3*, 828.
- (8) Kunitake, T.; Okahata, Y. *J. Am. Chem. Soc.* **1977**, *99*, 3860.
- (9) Engberts, J.; Hoekstra, D. *Biochimica Et Biophysica Acta-Reviews on Biomembranes* **1995**, *1241*, 323.
- (10) Laschewsky, A.; Ringsdorf, H.; Schmidt, G.; Schneider, J. *J. Am. Chem. Soc.* **1987**, *109*, 788.
- (11) Riess, J. G.; Krafft, M. P. *Chem. Phys. Lipids* **1995**, *75*, 1.
- (12) Mukerjee, P.; Handa, T. *J. Phys. Chem.* **1981**, *85*, 2298.
- (13) Vierling, P.; Santaella, C.; Greiner, J. *J. Fluorine Chem.* **2001**, *107*, 337.
- (14) Frezard, F.; Santaella, C.; Montisci, M. J.; Vierling, P.; Riess, J. G. *Biochimica Et Biophysica Acta-Biomembranes* **1994**, *1194*, 61.
- (15) Ravily, V.; Santaella, C.; Vierling, P.; Gulik, A. *Biochimica Et Biophysica Acta-Biomembranes* **1997**, *1324*, 1.
- (16) Oda, R.; Huc, I.; Danino, D.; Talmon, Y. *Langmuir* **2000**, *16*, 9759.
- (17) Discher, B. M.; Won, Y. Y.; Ege, D. S.; Lee, J. C. M.; Bates, F. S.; Discher, D. E.; Hammer, D. A. *Science* **1999**, *284*, 1143.
- (18) van Dongen, S. F. M.; de Hoog, H. P. M.; Peters, R.; Nallani, M.; Nolte, R. J. M.; van Hest, J. C. M. *Chem. Rev.* **2009**, *109*, 6212.
- (19) Bermudez, H.; Brannan, A. K.; Hammer, D. A.; Bates, F. S.; Discher, D. E. *Macromolecules* **2002**, *35*, 8203.
- (20) Nardin, C.; Hirt, T.; Leukel, J.; Meier, W. *Langmuir* **2000**, *16*, 1035.
- (21) Lomas, H.; Canton, I.; MacNeil, S.; Du, J.; Armes, S. P.; Ryan, A. J.; Lewis, A. L.; Battaglia, G. *Advanced Materials* **2007**, *19*, 4238.
- (22) Christian, D. A.; Cai, S.; Bowen, D. M.; Kim, Y.; Pajerowski, J. D.; Discher, D. E. *Eur J Pharm Biopharm* **2009**, *71*, 463.
- (23) Discher, D. E.; Eisenberg, A. *Science* **2002**, *297*, 967.
- (24) Du, J. Z.; O'Reilly, R. K. *Soft Matter* **2009**, *5*, 3544.
- (25) Kita-Tokarczyk, K.; Grumelard, J.; Haeefe, T.; Meier, W. *Polymer* **2005**, *46*, 3540.
- (26) Walker, S. A.; Kennedy, M. T.; Zasadzinski, J. A. *Nature* **1997**, *387*, 61.
- (27) Wong, B.; Boyer, C.; Steinbeck, C.; Peters, D.; Schmidt, J.; van Zanten, R.; Chmelka, B.; Zasadzinski, J. A. *Advanced Materials* **2011**, *23*, 2320.
- (28) Bolinger, P. Y.; Stamou, D.; Vogel, H. *Angew. Chem. Int. Ed.* **2008**, *47*, 5544.
- (29) Kamat, N. P.; Katz, J. S.; Hammer, D. A. *Journal of Physical Chemistry Letters* **2011**, *2*, 1612.
- (30) Ahmed, F.; Photos, P. J.; Discher, D. E. *Drug Dev. Res.* **2006**, *67*, 4.
- (31) McPhail, D.; Tetley, L.; Dufes, C.; Uchegbu, I. F. *Int. J. Pharm.* **2000**, *200*, 73.
- (32) Chiu, H. C.; Lin, Y. W.; Huang, Y. F.; Chuang, C. K.; Chern, C. S. *Angew. Chem. Int. Ed.* **2008**, *47*, 1875.

- 
- (33) Pautot, S.; Frisken, B. J.; Weitz, D. A. *Langmuir* **2003**, *19*, 2870.
- (34) Marguet, M.; Edembe, L.; Lecommandoux, S. *Angew. Chem. Int. Ed.* **2012**, *51*, 1173.
- (35) Hauser, H.; Dawson, R. M. C. *Eur. J. Biochem.* **1967**, *1*, 61.
- (36) Uda, R. M.; Yamashita, D.; Sakurai, Y.; Kimura, K. *Langmuir* **2007**, *23*, 7936.
- (37) Adams, S. R.; Kao, J. P. Y.; Tsien, R. Y. *J. Am. Chem. Soc.* **1989**, *111*, 7957.
- (38) Lloyd, Q. P.; Kuhn, M. A.; Gay, C. V. *J. Biol. Chem.* **1995**, *270*, 22445.
- (39) Brannon, J. H.; Magde, D. *J. Phys. Chem.* **1978**, *82*, 705.
- (40) Carlsen, A.; Glaser, N.; Le Meins, J. F.; Lecommandoux, S. *Langmuir* **2011**, *27*, 4884.
- (41) Li, S. L.; Byrne, B.; Welsh, J.; Palmer, A. F. *Biotechnol. Prog.* **2007**, *23*, 278.
- (42) Chemin, M.; Brun, P. M.; Lecommandoux, S.; Sandre, O.; Le Meins, J. F. *Soft Matter* **2012**, *8*, 2867.
- (43) Cui, J. X.; Wang, M.; Zheng, Y. J.; Muniz, G. M. R.; del Campo, A. *Biomacromolecules* **2013**, *14*, 1251.
- (44) Cui, D. W.; Qian, X. H.; Liu, F. Y.; Zhang, R. *Org. Lett.* **2004**, *6*, 2757.
- (45) Tian, Y. Q.; Su, F. Y.; Weber, W.; Nandakumar, V.; Shumway, B. R.; Jin, Y. G.; Zhou, X. F.; Holl, M. R.; Johnson, R. H.; Meldrum, D. R. *Biomaterials* **2010**, *31*, 7411.
- (46) Ramachandram, B.; Saroja, G.; Sankaran, N. B.; Samanta, A. *J. Phys. Chem. B* **2000**, *104*, 11824.
- (47) Ellis-Davies, G. C. R.; Barsotti, R. J. *Cell Calcium* **2006**, *39*, 75.

---

---

---

## **5 White light emitting multicompartmentalized supramolecular assemblies**

---

---

## 5.1 Introduction

Before Newton conducted his famous prism experiment it was believed that white light is essentially colourless. Nowadays we know that white light consists of a whole spectrum of wavelength. In order to detect light comprising a range of different wavelengths, the human eye consists of two different types of light receptors. There are rods, which have a higher sensitivity but perceive light only in a small wavelength range, with a peak around 541 nm and the cones. Cones are the receptors responsible for the colour perception of the human eye but they are less sensitive, which is the reason why colours cannot be seen at night. They can be divided into three different types namely  $\rho$ ,  $\tau$  and  $\beta$  cones because they display three different sensitivity maxima at 590 nm (orange-red), 540 nm (green) and 440nm (blue). The colour matching functions (CMF) representing their spectral sensitivity were determined in two independent experiments conducted by Wright<sup>1</sup> and Guild<sup>2</sup>. As such, white light as recognised by the human, could be expressed through a mathematical formalism. These CMF showed some negative values and were therefore transformed in a way that only positive values appear. The standard observer based on these experiments was then defined by the Commission Internationale de l'Éclairage, CIE in 1931 and a graphical representation of these colour matching functions  $\bar{x}(\lambda)$ ,  $\bar{y}(\lambda)$  and  $\bar{z}(\lambda)$  for the standard observer are given in figure 102.

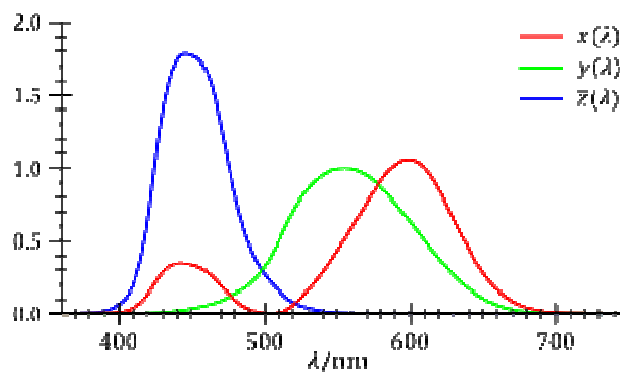


**Figure 102:** Colour matching functions for the standard observer according to CIE1931.

With these CMF the tristimulus values X, Y and Z can be calculated using equations 22. Where  $I(\lambda)$  is the emission spectrum of interest and  $\bar{x}(\lambda)$ ,  $\bar{y}(\lambda)$  and  $\bar{z}(\lambda)$  the normalized CMF. The CIE modulated tristimulus value Y to be an expression of luminosity or the brightness of the light source. That means at a given luminosity Y all chromaticities can be expressed by X

and Z. This states for example that the colour grey has the same chromaticity as the colour white but with less intensity.

$$X = \int_{380}^{780} I(\lambda) \bar{x}(\lambda) d\lambda \quad Y = \int_{380}^{780} I(\lambda) \bar{y}(\lambda) d\lambda \quad Z = \int_{380}^{780} I(\lambda) \bar{z}(\lambda) d\lambda \quad \text{equation 22}$$

The CIE1931 colour space can then be derived from equation xx.

$$x = \frac{X}{X+Y+Z} \quad y = \frac{Y}{X+Y+Z} \quad z = \frac{Z}{X+Y+Z} = 1 - x - y \quad \text{equation 23}$$

The CIE1931 is essentially a three dimensional space with the chromaticity in the x-y plane and the brightness in z. The graph has the shape of a horse shoe where monochromatic light can be found at the edges of the colour space. All other possible colours are mixtures of different wavelength and are located in the inner area of the horse shoe. White light emission can be found in the middle of the diagram shown in figure 103.

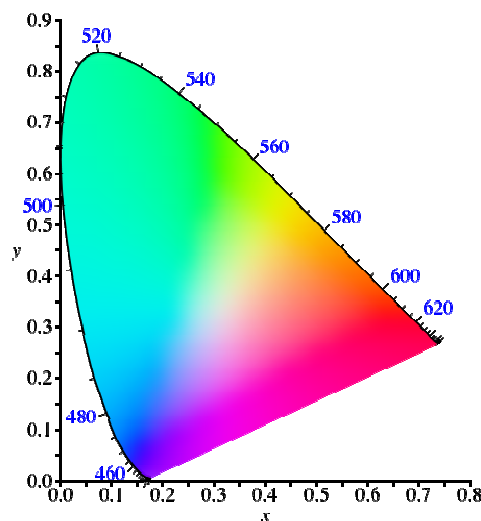


**Figure 103:** The x-y plane of the CIE 1931 Chromaticity Diagram or colour space. The monochromatic colours with wavelength (nm) are indicated.

White light is not defined as one specific coordinate in the chromaticity diagram but there are several different white light standards available. The most widely used white light standard is certainly the D65 mid daylight standard since it is used to define the white light in ordinary televisions. A list of coordinates in the CIE1931 colour space of white light standards of the

---

D-series is given in table 12. As one can see the definition of white light is rather broad and a wide range of coordinates can be perceived as white light.

**Table 12:** Coordinates of common white light illuminants<sup>3</sup>.

<b>Illuminant</b>	<b>X</b>	<b>Y</b>	<b>description</b>
<b>D50</b>	0.34567	0.35850	Horizon Light
<b>D55</b>	0.33242	0.34743	Mid-morning / Mid-afternoon Daylight
<b>D65</b>	0.31271	0.32902	Noon Daylight, Television
<b>D75</b>	0.29902	0.31485	North sky Daylight

### 5.1.1 White light emission in supramolecular chemistry

White light emission in supramolecular assemblies has gained considerable interest in the last few years due to their use in lighting and displays<sup>4</sup>. Many different approaches had been shown towards white light emission in these systems, most of the time this is achieved by combination of red, green and blue emitting dyes. When different chromophores are located close in space as one may anticipate in a discrete supramolecular assembly, Förster energy transfer often occurs between donor and acceptor fluorophores, which participates in defining the output colour and thus in obtaining white light.

The Förster resonance energy transfer theory<sup>5</sup> is based on dipole-dipole interactions between two molecules, one which is the donor and one which is the acceptor. This radiationless transfer of energy occurs between molecules which are in close proximity (10-100 Å)<sup>6</sup>, have a spectral overlap of the donor emission spectrum and the absorption spectrum of the acceptor and lead to an decrease in fluorescence intensity and a decrease in the fluorescence lifetime of the donor. The rate of energy transfer from one fluorophore to another is dependent on the sixth power of the distance between them due to the dipole-dipole nature of the electronic excitation and can be expressed with equation 24.

$$E = \frac{1}{1 + \left(\frac{r}{R_0}\right)^6} \quad \text{equation 24}$$

$E$  represents the efficiency of the Förster energy transfer,  $R_0$  the Förster radius and  $r$  is the distance between the fluorophores. The Förster distance can be calculated regarding the spectral characteristics of the fluorophores and be expressed with equation 25.

---


$$R_0 = 0.2108[\kappa^2\phi_0 n^{-4}J]^{\frac{1}{6}} \quad \text{equation 25}$$

Where  $\Phi_0$  is the quantum yield of the donor in absence of the acceptor,  $K$  is the dipole orientation factor,  $n$  the refractive index of the solvent and  $J$  the spectral overlap (Figure 104). The spectral overlap of the emission spectrum of the donor and the absorption spectra of the acceptor can be calculated according to equation 26

$$J(\lambda) \equiv \int_0^\infty \epsilon_A(\lambda)\lambda F_D(\lambda)d\lambda \quad \text{equation 26}$$

In this formula  $\epsilon_A$  stands for the extinction coefficient of the acceptor in  $M^{-1}cm^{-1}$ ,  $F_D$  is the normalized intensity of the donor emission spectrum and  $d\lambda$  is the wavelength range of the overlap.

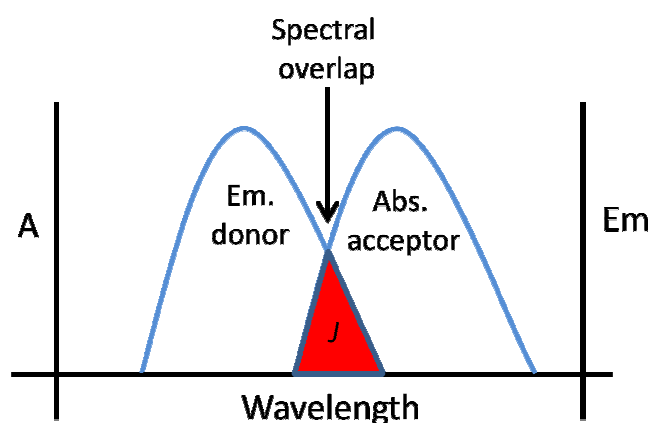


**Figure 104:** Schematic representation of the spectral overlap of fluorescence emission of a donor and the absorption spectrum of an acceptor.

By remodelling these formulas the distance between two fluorophores can be calculated by measuring the Förster energy transfer. Vice versa knowing the distance between two fluorophores the efficiency of the energy transfer can be calculated.

One approach to obtain white light emitting polymers and polymer films has been presented by Ego *et al.*<sup>7</sup>. They report that by either endcapping, copolymerisation or covalently crosslinking the polyfluorenes with perylene fluorophores, the colour and the emission spectra of these polymers can be tuned by changing the substitution/polymer ratio. This is an example where energy transfer between two light emitting molecules is exploited to tune the emission

of the system. The first preparation of white light emitting organogels has been accomplished by Ajayaghosh and co-workers<sup>8</sup> (see figure 105).

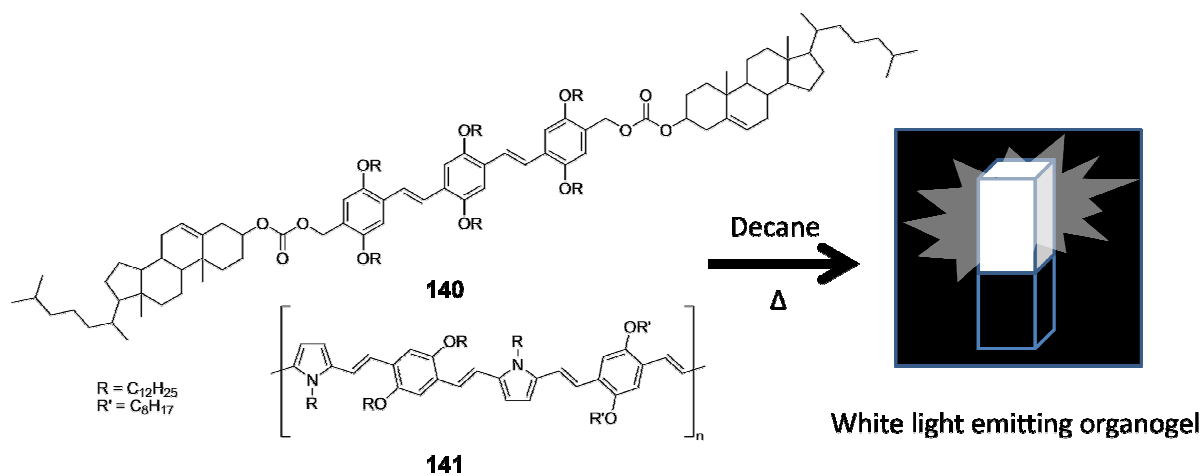


**Figure 105:** Molecular structure and schematic representation of the formation of white light emitting organogels<sup>8</sup>.

Oligo(*p*-phenylenevinylene)s (**141**) had been co-gelated in decane with a red light emitting acceptor in varying percentage (**140**). As mentioned previously, partial Förster energy transfer occurred and was exploited to optimize the spectra for white light emission. In the group of Del Guerzo, white light emitting nano-fibres have been prepared<sup>9</sup>. Alkyl chain functionalized anthracene, tetracene and rubrene derivatives were mixed and their fluorescence studied. While in solution almost complete energy transfer occurs and only the red emission of the rubrene derivative is observable, white light emitting nano-fibres had been obtained after gelation from hot DMSO. Inside the nano-fibres only partial energy transfer occurs and a white light emission could be obtained. Later on, white light emitting organic liquids have been prepared in the group of Ajayaghosh<sup>10</sup>. A schematic representation for the preparation of those liquids is depicted in figure 106. Choosing a liquid oligo(*p*-phenylenevinylene) (**142**) and blending it with rubrene (**144**) as red emitting dye and tris(8-hydroxyquinolino)aluminium (Alq<sub>3</sub>, **143**) as green emitting dye, white light emission could be achieved. This is a very facile approach towards white light emission since the components are soluble in the organic liquid and the white light emitting ink can be obtained under completely solvent-free conditions.

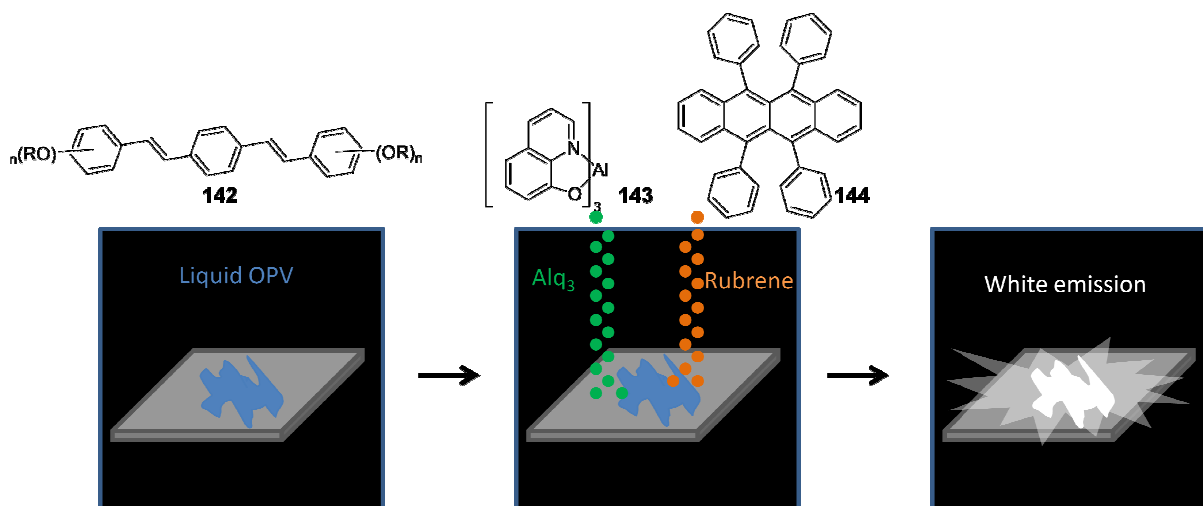


**Figure 106:** Preparation process of white light emitting ink using a liquid OPV and blending it with green emitting Alq<sub>3</sub> and red emitting rubrene.

While the previous examples made use of energy transfer between fluorophores to achieve white light emission another approach is the usage of a single white light emitting fluorophore. An example of the three different white light emitting dyes is given in figure 107 and the synthesis has been achieved by three different groups<sup>11-13</sup>. These molecules have the advantage that the emission is concentration independent. The white light-emitting dyad (**145**) creates the white light spectrum by frustrated energy transfer due to excited state intramolecular proton transfer from one hydroxytetraphenyl imidazole unit to the other. The second molecule (**146**) introduced by Yang *et.al.* emits white light only under very specific conditions like certain pH, solvent and irradiation wavelength. On the other hand with this fluorophore the emitted spectra can be tuned changing the named parameters. In the group of de Cola a white light emitting europium/indium complex (**147**) has been synthesized. Due to energy transfer with an efficiency of 38 % from the indium complex to the europium, center white light emission has been created.

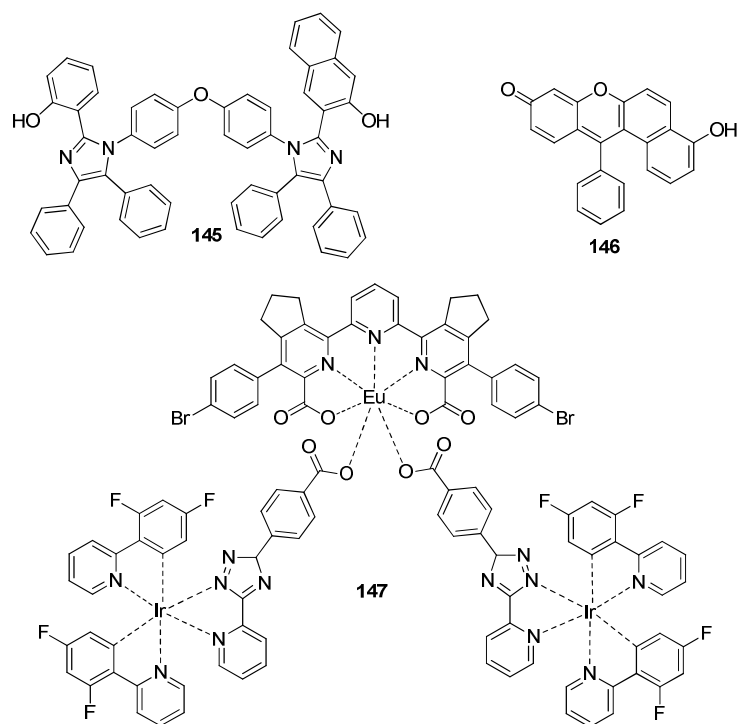


**Figure 107:** White light emitting dyad by Park, S. *et. al.* (**145**) and white light emitting benzo[a]xanthene by Yang, Y. *et. al.* (**146**) and white light emitting europium / iridium complex (**147**) by Coppo *et. al.*

Very few examples are known where energy transfer between the fluorophores is suppressed. The approach of white light emitting dyes using frustrated energy transfer had been shown and another approach is the physical separation of red green and blue emitting fluorophores with the help of surfactants for example. One such system has been presented by Wang *et.al.*<sup>14</sup> and was used to produce white light emitting surface coatings. Rhodamine 110 and sulforhodamine 101 have been encapsulated in the core of poly(styrene-block-4-vinylpyridine) micelles in toluene. Polyfluorene (PF) as a blue light emitting polymer has been added to that solution The mixed micelle solutions in presence of PF were then spin-coated onto a substrate to cover the surface with red and green emitting micelles in a matrix of PF to form a white light emitting monolayer. A schematic representation of the system is shown in figure 108.

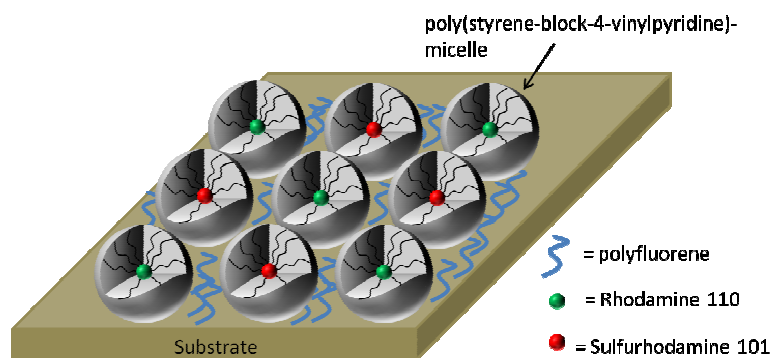


**Figure 108:** White light emitting spin coated film of red and green emitting polymer micelles and blue emitting polyfluorene in the periphery.

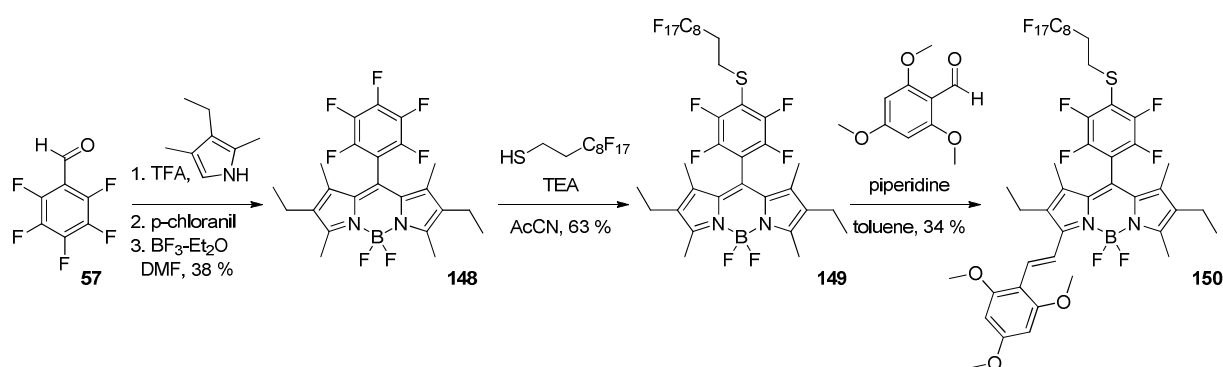
In the current work, a new approach towards white light emitting supramolecular assemblies is shown based on nanoconfinement. So far, white light emitting vesicles in aqueous solution or under pseudo-physiological conditions been described only once<sup>15</sup>. Therein the authors present white light emitting perylene bisimide vesicles at pH 9. Again, this white light emission occurs due to energy transfer from a donor molecule in the aqueous interior of the perylene vesicles and therefore molecular building blocks could not be distinguished.

In the following pages the idea of physical separation of fluorophores by encapsulating those in the membrane domain of orthogonal fluorinated vesicles is exploited, to use them as building blocks, which are subsequently sequestered in giant polymer vesicles. In doing so, white light emitting structures on the size of several  $\mu\text{m}$  are created, while retaining the ability to distinguish between the R G B building blocks. The only system known to us which possesses these qualities are the white light emitting micro-rods published by Lei *et.al.*<sup>16</sup>. The main difference however is the use of only two colours to prepare those white light emitting rods and the presence of these rods in non-aqueous media.

## 5.2 Synthesis of RGB fluorophores based on coumarin, fluorescein and BODIPY

The red light emitting fluorophore was based on the design of the perfluorinated BODIPY synthon which features a perfluorinated phenyl ring described in chapter 2 of this thesis<sup>17</sup>. A similar fluorophore has been published by Galangau *et al.*<sup>18</sup> The main difference in that

BODIPY is the presence of of ethyl groups in the  $\beta$ -position of the core, which leads to a bathochromic shift of 28 nm (516 nm  $\rightarrow$  544 nm) in the absorption and 31 nm (527 nm  $\rightarrow$  554 nm) in the emission spectra due to the more electron rich nature of the compound. An advantage of the compound is the enhanced chemical stability towards chromatography which leads to improved isolated yields (33 %  $\rightarrow$  38 %) and less loss of compound during purification since one purification step is sufficient to obtain the pure product. The synthesis of the red light emitting BODIPY is depicted in scheme 21.

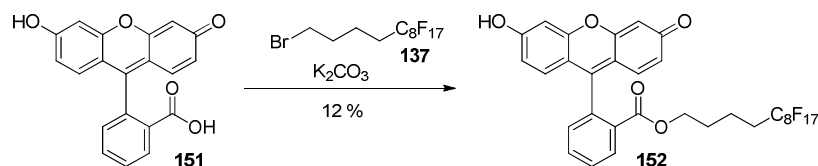


**Scheme 21:** Synthesis pathway of red light emitting BODIPY (**150**).

After the formation of the  $F_5$ -ethyl-BODIPY (**148**) a fluorinated chain bearing an heptafluorodecane thiol linker was introduced via  $S_NAr$  on the para position of the pentafluorophenyl ring using TEA as a base and acetonitrile as solvent. The substitution product (**149**) was obtained in 63 % yield after purification. The first tests on the incorporation of the fluorophore into the membrane of semi-fluorinated gemini amphiphile-based assembly were performed with this intermediate. In order to obtain a red light-emitting fluorophore, a Knoevenagel-type reaction has been performed to obtain an elongated aromatic structure in order to shift the emission wavelength towards longer wavelength. To that end, 2,4,6-trimethoxy benzaldehyde was boiled in dry toluene in presence of piperidine as a sterically hindered base. Mono and di-addition products were obtained during the reaction. By using 1.5 eq of the aldehyde and 2 eq of piperidine, monoaddition could be favoured and the final product BODred (**150**) was obtained in 34 % yield, which is in the range of published results on the monoaddition for Knoevenagel-type reactions on BODIPY<sup>18,19</sup>.

The synthesis of the green light emitting fluorophore started from commercially available fluorescein. A semi-fluorinated chain was introduced using a known procedure to form fluorescein esters<sup>20</sup>.  $C_8F_{17}$ -butyl bromide was reacted with fluorescein under basic conditions

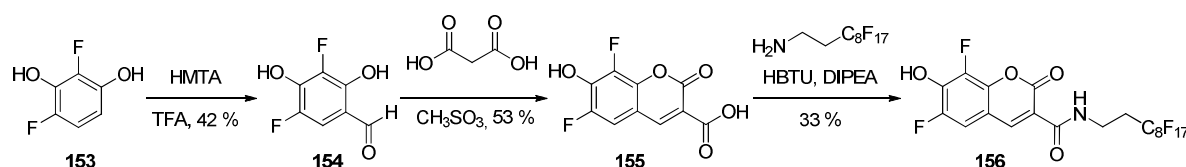
using  $K_2CO_3$  in DMF. The nucleophilic substitution occurs on the acid functionality of the molecule since the phenol is poorly reactive due to the mesomeric structure of the molecule.<sup>21</sup> The synthesis of the  $C_8F_{17}$ -fluorescein (**152**) is shown in scheme 22.



**Scheme 22:** Synthesis pathway of green light emitting  $C_8F_{17}$ -fluorescein (**152**).

The yield of the reaction was 12 % which is rather low and could be explained by the lower reactivity of long chained aliphatic compounds in polar solvents due to a coiling up of the molecule. Side products like partial alkylation of the phenols at  $60^\circ C$  could also participate to the lower reaction yield.

As blue light emitting fluorophore, a derivative of the commercially available pacific blue was envisaged. Due to the exorbitant price and the quantity of compound needed for functionalization it was decided to start the synthesis from commercially available difluoresorcinol (**153**). Following a procedure published by Weidner-Wells *et al.*<sup>22</sup>, the starting material was formylated with hexamethylenetetramine (HMTA) in strongly acid media giving 42 % of the aldehyde intermediate. The 3-carboxy-6,8-difluoro-7-hydroxycoumarin (**154**) was formed by the condensation of the aldehyde with malonic acid in methanesulfonic acid as shown by Sun *et.al.* yielding 53 % of the pacific blue fluorophore (**155**).<sup>23</sup>



**Scheme 23:** Synthesis pathway of blue light emitting  $C_8F_{17}$ -pacific (**156**).

In a last step a heptadecafluorodecane amine was introduced using a peptide coupling procedure with *N,N,N',N'*-Tetramethyl-*O*-(1*H*-benzotriazol-1-yl)uronium hexafluorophosphate HBTU and Diisopropylethylamin (DIPEA) in THF yielding the final product pacific- $C_8F_{17}$  (**156**) in 33 %.

---

### 5.3 Formation of fluorinated R G B vesicles via thinfilm hydration

Semi-fluorinated cationic vesicles loaded with red green and blue emitting dyes had been prepared using the thin film hydration procedure which is described in detail in the experimental section. The thin film was hydrated with a buffer containing 130 mg/ml sucrose, 100 mM KCl, 30 mM MOPS at pH 7.2 to obtain pseudo-intracellular conditions. The vesicle formulations had been extruded once through a 800 nm membrane in order to break large multilamellar structures. The size distribution was however rather large and vesicles of sizes ranging from 100 – 2400 nm were present as shown in figure 109

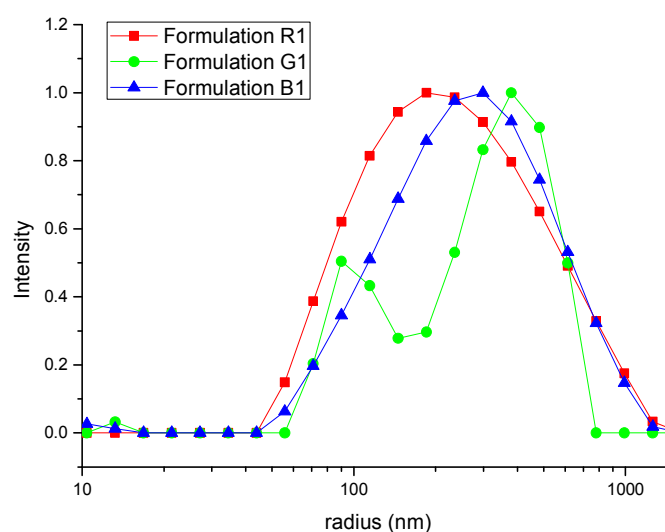


**Figure 109:** Graphical representation of the particle size measured by DLS for Formulation R1 (red), G1 (green) and B1 (blue).

While formulation R1 and B1 show a homogeneous distribution of particles, formulation G1 however shows two populations of vesicle sizes. These two populations have a maximum intensity at 180 nm and at 760 nm. Two explanations for this behaviour could be possible. A membrane during the extrusion process which was not well in place could lead to such an observation or the fluorophores themselves have an influence on the size distribution of the vesicles. For the preparation of multicompartimentalized, white light emitting supramolecular assemblies this behaviour was considered irrelevant and was not further pursued.

A summary of the fluorophore concentration in the vesicle membranes for formulation R1, G1 and B1 is given in table 13.

---

**Table 13:** Concentration and size of fluorinated R G B vesicles

Sample	Concentration of fluorophore	Concentration of amphiphile	Mean diameter
Formulation R1	3.2 $\mu\text{M}$	1.5 mM	452 nm
Formulation G1	20.3 $\mu\text{M}$	1.5 mM	520 nm
Formulation B1	4.2 $\mu\text{M}$	1.5 mM	524 nm

The loading efficiency of BODIPY-red was rather low. Samples were prepared to load a total of 10  $\mu\text{M}$  of fluorophore in the membrane of the vesicles. However, due to the large aromatic nature of the molecular structure the incorporation into membrane seemed unefficient and only 3.2  $\mu\text{M}$  of fluorophore were loaded. During the extrusion of the vesicles formulation a big part of the compound was precipitated on the extrusion membrane. Incorporation of Pacific- $\text{C}_8\text{F}_{17}$  and Fluorescein- $\text{C}_8\text{F}_{17}$  proceeded more smoothly aiming for a concentration of fluorophore in the membrane of 5  $\mu\text{M}$  (4.2  $\mu\text{M}$  incorporated) and 20  $\mu\text{M}$  (20.3  $\mu\text{M}$  incorporated), respectively.

#### 5.4 Spectral characterisation of fluorophores BODred (**150**), $\text{C}_8\text{F}_{17}$ -fluorescein (**152**), Pacific- $\text{C}_8\text{F}_{17}$ (**156**) and vesicle formulation B1, G1 and R1

Electronic absorption and emission spectra of the fluorophores were recorded in solution and incorporated in the vesicle membrane. The spectra are depicted in figure 110. The absorption spectrum of the pacific- $\text{C}_8\text{F}_{17}$  (**156**) shows a small hypsochromic shift of 3 nm upon incorporation into the membrane which can be attributed to the more apolar environment in the vesicle membrane. However, fluorescein- $\text{C}_8\text{F}_{17}$  (**152**) shows a small bathochromic shift of 5 nm in the vesicle membrane. To explain this behaviour two effects need to be considered. First, the effect of a more hydrophobic environment in the membrane leading to a blue-shift and second the physical separation of the fluorophores from each other. Molecules carrying a fluorinated chain tend to aggregate much easier due to their increased lipophilicity compared to their hydrocarbon analogs. The observed change in the absorption spectra is therefore a combination of the two effects. BODred (**150**) shows a small hypsochromic shift of 6 nm and behaves therefore more like the parent pacific blue derivative. For all three fluorophores a broadening of the absorption band has been observed due to the change in rotational and vibrational states in the amphiphile membrane.

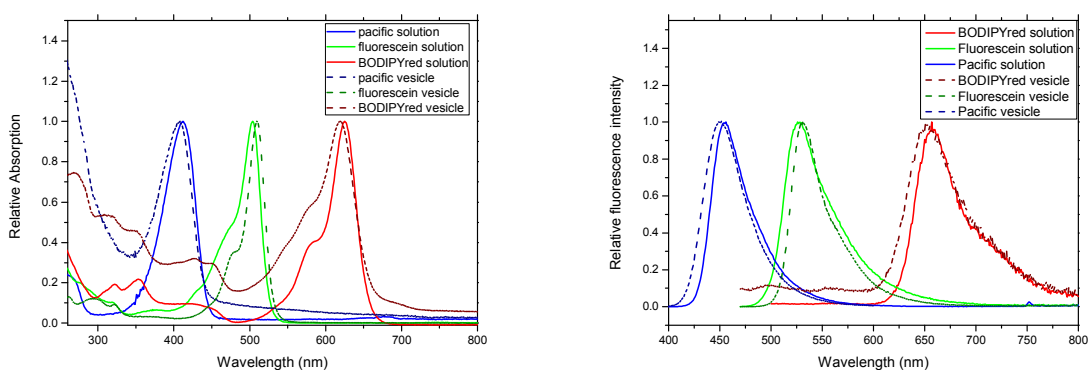


**Figure 110:** Absorption (left) and emission spectra (right) of pacific- $C_8F_{17}$  (**156**) (MeOH,  $\lambda_{exc} = 405$  nm), fluorescein- $C_8F_{17}$  (**152**) (MeOH,  $\lambda_{exc} = 458$  nm), BODred (**150**) (THF,  $\lambda_{exc} = 458$  nm) and Formulation R1, G1 and B1 in pseudo intracellular sucrose buffer ( $\lambda_{exc} =$  as corresponding fluorophore).

Quantum yields ( $\Phi_{em}$ ) in solution and in vesicles were established on comparing with a fluorescence standard, operating under dilute conditions and calculating the quantum yield of the desired compound by using equation 27. Where  $\Phi_r$  is the quantum yield of the reference  $A_r$  the absorption of the reference at the excitation wavelength,  $A$  the absorption of the fluorophore at the excitation wavelength,  $I$  is the integrated emission intensity,  $I_r$  the integrated emission intensity of the reference and  $\eta$  is the refractive index of the solvent used.

$$\Phi_F = \frac{\phi_r \times A_r \times I \times \eta^2}{A \times I_r \times \eta_r^2} \quad \text{equation 27}$$

For pacific- $C_8F_{17}$  (**156**) the blue emitting fluorescence standard 9,10-diphenylanthracene has been used in order to work at the same detector sensitivity.  $C_8F_{17}$ -fluorescein (**152**) was compared to fluorescein as a reference since the molecule shares the same core structure and similar absorption and emission characteristics. BODred (**150**) was measured against fluorescein and Rhodamine 101 to compare the results. In general it could be observed that quantum yields measured with the appropriate standard, meaning a standard which emits in the same spectral range results in a slightly higher quantum yield value for the measured chromophore. This is due to the decreased sensitivity of for higher wavelength and the overcorrection of the detector used in the experiment.

**Table 14:** Spectral characterization of fluorophores in solution and in vesicle membranes.

Sample	$\epsilon$ (l mol <sup>-1</sup> )	Abs. max.	Em. max.	$\Phi$ 375 nm	$\Phi$ 458 nm	$\Phi$ 561 nm
(1)	27940	412	455	0.97	-	
Form B		408	449	0.96		
(2)	51507	504	526	0.68	0.61	
Form G		509	531	0.52	0.69	
(3)	91228	625	657	0.63	0.54	0.68
Form R		619	651	0.26	0.22	0.32

While the fluorescence quantum yield of pacific-C<sub>8</sub>F<sub>17</sub> (**156**) seems to be unaffected by the incorporation into the vesicle membrane, C<sub>8</sub>F<sub>17</sub>-fluorescein (**152**) and BODred (**150**) show a difference. Upon excitation at 375 nm the quantum yield decreases 16 %. Considering that the vesicles themselves absorb a part of the light at 375 nm, that can explain the lower quantum yield. Upon excitation at 458 nm this effect should be negligible and in fact the quantum yield is increased by 8% compared to the molecule in solution. Taking the error of the measurement into account the values measured are comparable. The BODIPY derivative (**150**) however shows a decrease of 35 % on average when incorporated in the membrane of the vesicles. Since the emission of BODIPY meso-substituted with phenyl groups depend on the planarity of the structure and considering the size of the red light emitting elongated BODIPY, one can reason that there might a certain steric effect in the vesicle membrane and therefore a deformation of the BODIPY core and a loss of fluorescence emission. The influence of the orientation of BODIPY in a polymer film on the fluorescence quantum yield has been studied<sup>24</sup>. It was shown that depending on the polymer used (examples are given for different methacrylates like PMMA or fluorinated polymethacrylates like PFMA) and the orientation of BODIPY in the polymer film can lead to a 20 % lower quantum yield.

## 5.5 White light emission of mixed fluorocarbon vesicles bearing red, green and blue fluorophores

In order to obtain a white light emitting solution of vesicles one needs to determine the ideal ratio between red, green and blue light emitting formulations. To obtain the approximate ratio, titrations between blue and green blue and red emitting vesicle formulations had been conducted. Formulation B1 which has the coordinates (x = 0.1514 / y = 0.0880) is the most

outer point in the blue part of the CIE1931 graph represented in figure 11. Formulation G1 with the coordinates ( $x = 0.3271 / y = 0.6322$ ) is the most outer point in the green region of the graph and Formulation R ( $x = 0.6719 / y = 0.3012$ ) is the outer point in the red region. Mixtures of two formulations had been prepared in the ratio 1/4, 2/3, 1/1, 3/2 and 4/1 (v/v). The coordinates of the mixed solutions are located on a straight line between the coordinates of the pure formulations.

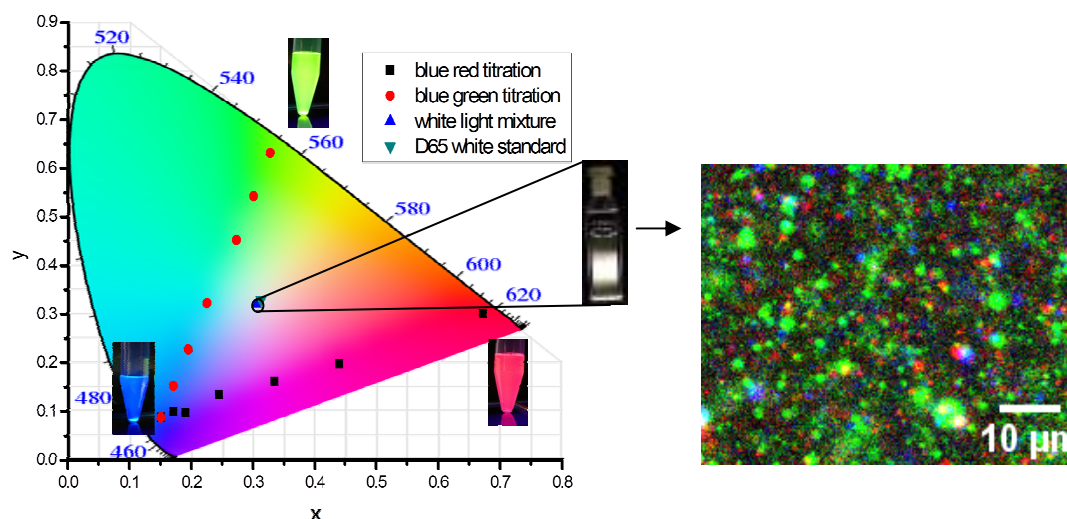


**Figure 111:** left: CIE1931 colour space of formulation R1 G1 B1. D65 white standard and coordinates for formulation W are highlighted ( $\lambda_{exc} = 375 \text{ nm}$ ,  $\text{H}_2\text{O}$ ). Images of the different formulations are placed beside their corresponding locations in the colour space. Right: confocal microscope image ( $\lambda_{exc} = 405 \text{ nm}$ ) of formulation W.

This is a general behaviour of mixed chromophores since the resulting colours of the mixed system are always a combination of the two emission spectra. The coordinates for the D65 daylight standard were envisaged for the white light emitting vesicle formulation. An appropriate mixture of formulation B and G was taken (1 eq. form. B1 / 2 eq. form. G1) and doped with formulation R to obtain a white light emitting mixture which will be called formulation W. The final ratio for formulation W was 1 eq form. B1/ 2 eq form. G1/ 2.5 eq form. R1, corresponding to a fluorophore concentration of  $0.76 \mu\text{M}$  (**156**),  $7.38 \mu\text{M}$  (**152**) and  $1.45 \mu\text{M}$  (**150**). The coordinates for the white light standard ( $x = 0.31271 / y = 0.32902$ ) and formulation W ( $x = 0.30639 / y = 0.32164$ ) are depicted in figure 111 and are in close proximity. On the right side of the same figure the confocal microscope image is shown. Using a confocal microscope, the macroscopically observed white light emission is broken down to its blue green and red parts and single separate vesicles can be observed, where each

colour corresponds to one of the formulations R1, G1 and B1. The fluorophores are well located in the vesicle membrane and no mixtures of two colours could be observed proving the rigidity and increased stability of the membrane<sup>25</sup> with slow amphiphile exchange rates. The image also reveals the polydisperse nature of the formulation which is in accordance with the DLS measurements depicted in table 14. The ratio of between blue green and red vesicles corresponds well to the experimental value of 1/2/2.5. Blue vesicles can be found as the minority whereas green and red vesicles are the majority in almost equal number. In this particular picture the size of formulation G1 seems to be superior to the other two formulations.

Another mean to prove the coexistence of R1, G1 and B1 vesicles is the recording of the fluorescence timetrace using a confocal fluorescence microscope. The observed volume was adjusted to 1 femtolitre and emissions of two colours inside the confocal volume were recorded simultaneously as a function of time. When the emitting individual micro-objects diffuse in the confocal volume fluorescence bursts were registered, see figure 112.

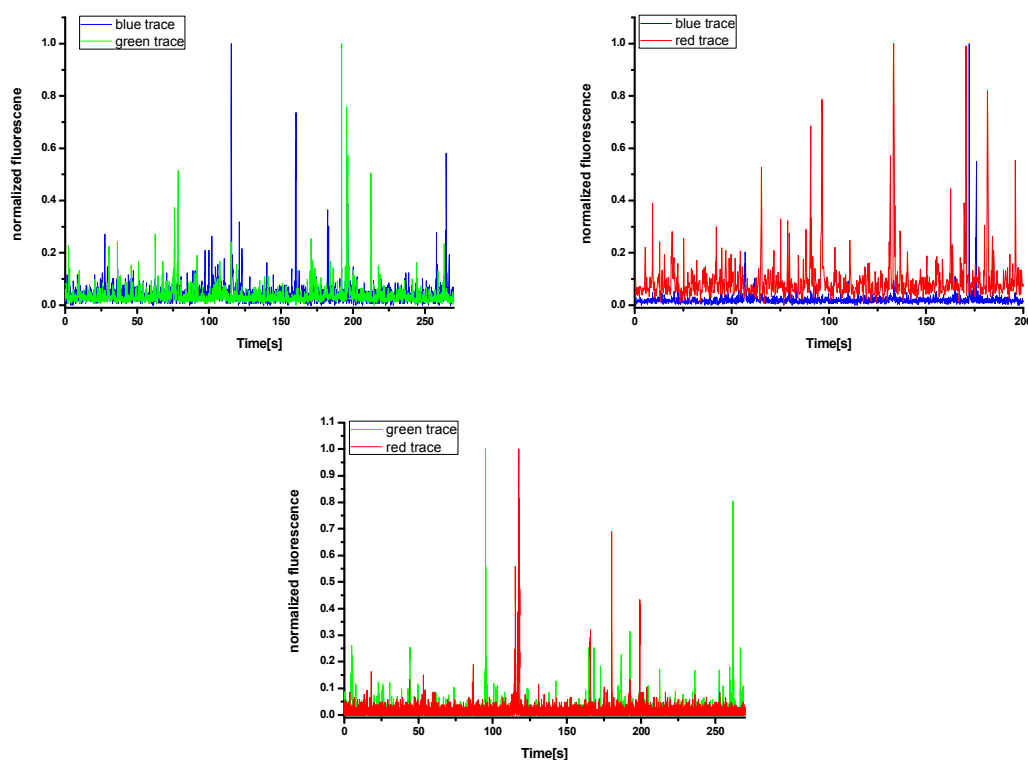


**Figure 112:** Fluorescence timetraces observed in a 1 femtoliter volume of formulation W ( $\lambda_{exc} = 375$  nm). Left: blue emission (375 – 475 nm) and green emission (500 – 580 nm), middle: blue emission (375 – 475 nm) and red emission (570 – 720 nm), right: green emission (500 – 580 nm) and red emission (570 – 720 nm).

The time traces confirm the observation of fluorophores separated in different vesicles, made in confocal fluorescence image. Bursts in the fluorescence intensity will occur every time a vesicle passes through the observed volume. In all three time traces it is shown that burst in the fluorescence intensity never occur at same time, indicating the absence of any other fluorophore in the vesicle membrane than the one prepared. It is important to mention, that only larger vesicles are recorded in this measurement due to sensitivity of the fluorescence detector. Smaller vesicles contain less amount of fluorophore and will be lost to, and aligned, the background of the measurement.

Fluorescence lifetimes of the fluorophores (**150**, **152** and **156**) in organic solvents and the liposome formulations (R1, G1, B1 and W) had been recorded via time correlated single photon counting spectrometry and compared in order to determine whether energy transfer occurs between the vesicles. The values obtained from time resolved fluorescence spectroscopy are highlighted in table 15. While the fluorophores in organic solvent display a monoexponential decay, which is an indication for the purity of the compound, vesicle formulations show multi-exponential decay. This behaviour previously studied by Krishna *et.al.*<sup>26</sup> and is related to the location of the fluorophore in the vesicle membrane. Essentially, there are three different locations possible, surface, interface and inner core. Fluorophores located close to the polar headgroups of the amphiphiles display a decreased lifetime due to solvent molecules, which can interact and contribute to vibrational loss pathways. Fluorophores located in the inner core are well protected from solvent interactions and show therefore no decrease in their fluorescence lifetime.

**Table 15:** Fluorescence lifetimes ( $\lambda_{exc} = 371$  nm) of fluorophores **150**, **152** and **156** in MeOH (**150** in THF) and form. R1, G1, B1 and W in Buffer (30 mM MOPS, 100 mM KCl, pH 7.2, 130 mg/ml sucrose)

	( <b>156</b> ) (ns)	Form. B (ns)	( <b>152</b> ) (ns)	Form. G (ns)	( <b>150</b> ) (ns)	Form. R (ns)	Form. W (450 nm) (ns)	Form. W (540 nm) (ns)	Form. W (651 nm) (ns)
$\tau_1$	3.54	3.81 (86%)	4.88	4.12 (80%)	5.28	4.38 (63%)	3.80 (85%)	4.13 (67%)	4.34 (58%)
$\tau_2$	-	2.23 (14%)	-	2.25 (20%)	-	2.43 (36%)	2.13 (15%)	2.53 (33%)	2.55 (42%)

The longer lifetime component in the membrane of the vesicles displays only little change. The fluorescence lifetime of pacific-C<sub>8</sub>F<sub>17</sub> (**156**) increases from 3.54 ns to 3.81 ns once

incorporated in the membrane with a shorter lifetime component of 2.23 ns with 14 % participation indicating that most of the fluorophore is located in the core region. C<sub>8</sub>F<sub>17</sub>-fluorescein (**152**) has a lifetime which is shortened (from 4.88 ns to 4.12 ns) in membrane indicating a closer proximity to the polar head groups with a shorter lifetime component (2.25 ns) corresponding to 20 % of the total lifetime. This behaviour can be explained by the increased size of the molecule, compared to fluorophore **152**. Molecule BODred (**150**) behaves similarly to molecule **152** showing a shorter lifetime in the membrane (from 5.28 ns in THF to 4.38 ns in vesicles) but with a higher percentage of the shorter lifetime component (2.43 ns, 36 %). Again the elongated BODIPY structure is larger than the fluorescein core and therefore penetrates deeper into the hydrophilic part of the membrane. The longer lifetime components in formulation W have approximately the same values as in formulation R1, G1 and B1, which implies that no energy transfer between the vesicles occurs and the fluorophores do not exchange between vesicles. Otherwise, Förster energy transfer would be anticipated due to spectral overlap and the fluorescence lifetime of the blue and green emission would be shortened. Figure 113 shows the spectral overlap of the absorption and emission for formulation R1, G1 and B1.

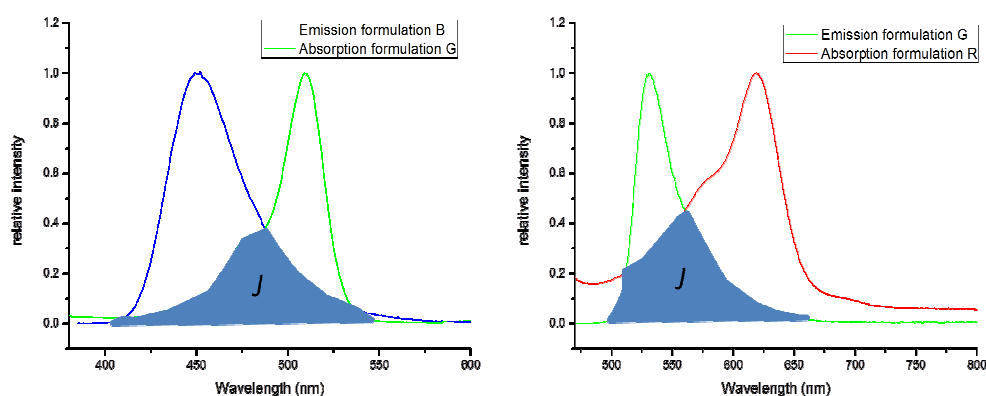


**Figure 113:** Spectral overlap for the emission of formulation B1 and the absorption of formulation G1 (left). Spectral overlap for the emission of formulation G1 and the absorption of formulation R1 (right).

It can be deduced that the parameters for energy transfer are given. The spectral overlap value  $J$  has been calculated using equation 26. The value for the blue green overlap is  $3.43 \cdot 10^{16} \text{ M}^{-1} \text{ cm}^{-1} \text{ nm}^4$  which results in an estimated Förster radius ( $R_0$ ) of 8.4 nm calculated by equation 25. In the same fashion, the  $J$  value for the green-red overlap has been calculated to be  $18.1 \cdot 10^{16} \text{ M}^{-1} \text{ cm}^{-1} \text{ nm}^4$  which yields a Förster radius ( $R_0$ ) of 9.8 nm. One can reason that

---

fluorophores incorporated in the vesicle membrane never come close enough to each other to undergo energy transfer. In addition being incorporated in the membrane the rotational freedom is reduced which results in an increased difficulty to align the dipoles and therefore  $K$  will be reduced.

## 5.6 White light emission in multicompartmentalized polymersomes

Giant white light emitting polymersomes had been prepared by emulsion centrifugation using formulation W as described in the experimental section and in chapter 4. A sample of formulation W containing 380 mOsm of sucrose was emulsified with the help of polybutadien-polyethylenoxide block copolymer in a solution of toluene. This emulsified solution was placed on top of an aqueous solution containing 380 mOsm glucose and the same ionic strength as formulation W. The remaining block copolymer forms a monolayer at the interface and after centrifugation, emulsified vesicle containing droplets will pass through the monolayer into the aqueous layer to form multicompartmentalized polymersomes according to the procedure published by Marguet *et. al.*<sup>27</sup> The sample was left at room temperature for at least one hour to obtain giant polymersomes in solution. A schematic representation of the preparation process is shown in figure 114.

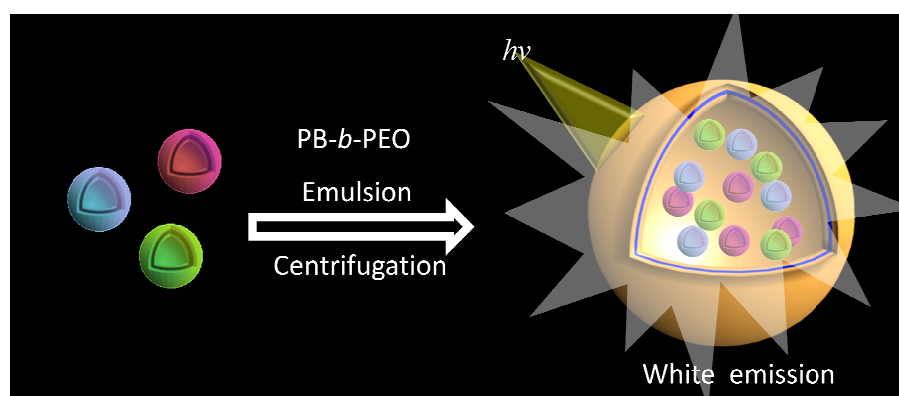


**Figure 114:** Schematic representation for the encapsulation process of formulation W and the preparation of white light emitting polymersomes.

The polymersome formulation was studied by confocal fluorescence microscopy and the observed results are highlighted in Figure 115. Using a pinhole value of 100 nm a slice of the polymersome is observed and the interior of the giant particles is revealed. By using blue, green and red detector channels separately only the corresponding vesicles are visible. Big

---

semi-fluorinated vesicles (circa 400 – 800 nm) in the interior of the polymersome appear as spherical objects, while smaller particles are visible as dots. The polydisperse nature of the sample can be seen in these images as the size distribution for the fluorinated vesicles is rather large. An overlay of the three detector channels is shown on the right side, which proves the presence of all three vesicles types at the same time. The giant polymersomes itself are polydisperse as well and range in diameter from 10  $\mu\text{m}$  to 80  $\mu\text{m}$ . Increasing the pinhole value to 300 nm and tuning the detector sensitivity of the blue, green and red channel to equal values one can create pseudo-epifluorescence image. A bigger slice of the polymersome is observed and therefore blue, green and red vesicles in the interior of the giant polymersomes are overlapping.

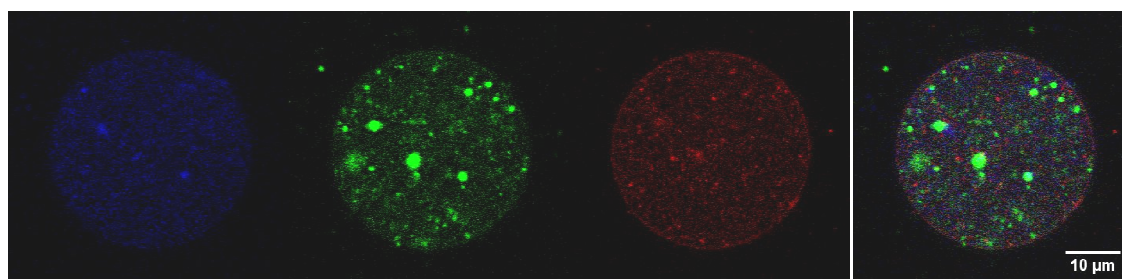
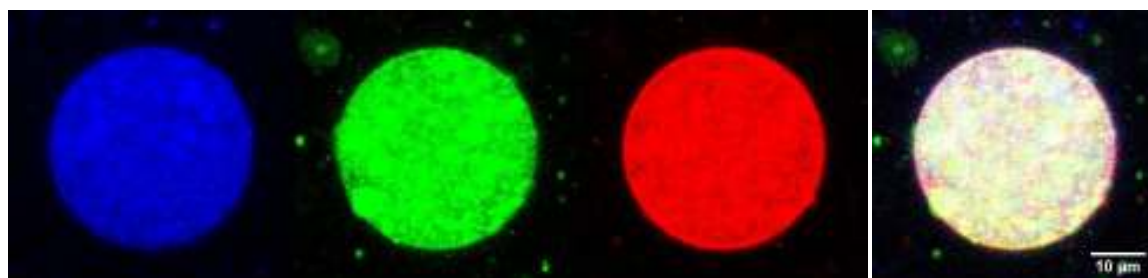


**Figure 115:** Confocal microscope image of a giant polymersomes. Red (600 – 750 nm), green (490- 600 nm) and blue (410 – 490 nm) detector channels are shown separately and the overlay shows the three detectors at the same time ( $\lambda_{\text{exc}} = 405 \text{ nm}$ ; pinhole = 100 nm).

The microscopy images for the pseudo-epifluorescence experiment are shown in figure 116. This creates a macroscopic effect in a micro-environment and white light emission can be observed. The three confocal microscope images on the left side show the three separate channels and vesicles in the interior appear diffuse and no longer well-defined. The image on the right side shows the channel overlay with equal detector intensities. The hole interior of the giant polymersome become a white smear, where vesicles shapes are insinuated.



---

**Figure 116:** Confocal microscope image of a giant polymersome using an increased pinhole value (300 nm). Blue, green and red detector channels on left and the overlay of the three detectors, tuned to the same equal sensitivity, on the right ( $\lambda_{\text{exc}} = 405 \text{ nm}$ ).

In order to prove that the white light emission observed in the giant polymersome is the same as that which was observed via a steady state spectra of the formulation W, the emission spectra was measured by a fluorescence spectrometer coupled to the confocal microscope. An overlay of the emission spectra of formulation W and the spectra measured inside the polymersome is depicted in figure 117. In the fluorescence spectrum of formulation W (red line) all three emissions corresponding to formulation R, G and B can be attributed without any deformation of the emission maxima. This is another indication for an absence of energy transfer between the fluorophores. The emission spectrum of the giant polymersome (black line) matches the emission spectrum of formulation W, with only minor intensity differences. These differences are related to the different set up and excitation power used for the measurement. In order to measure a fluorescence spectrum with a confocal microscope the sample needs to be irradiated more strongly since a much smaller volume is observed and therefore much less light is emitted.

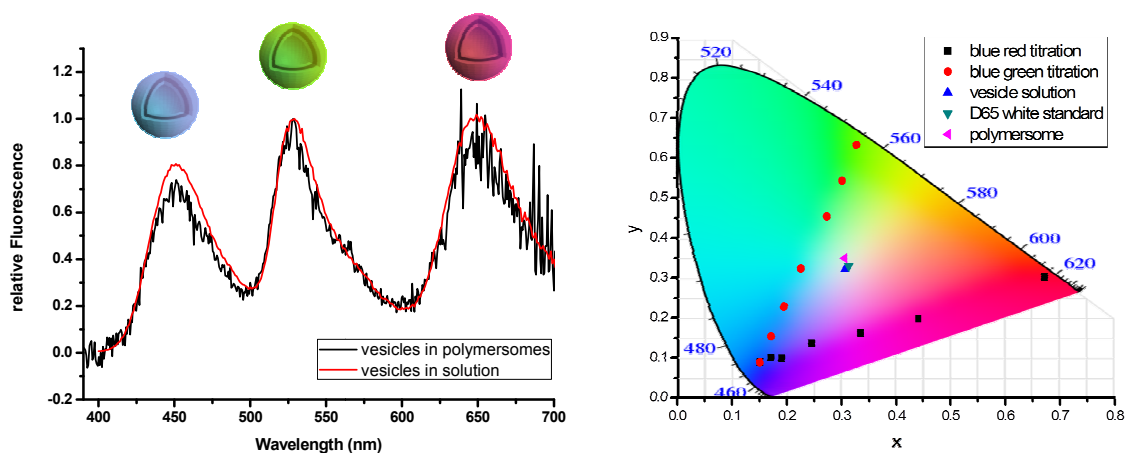


**Figure 117:** Fluorescence emission spectra of formulation W (red) recorded on a steady-state spectrofluorometer and fluorescence emission spectra of white light emitting polymersomes recorded with a confocal microscope coupled to a spectrometer.

Using a high laser intensity bleaches the fluorophores faster and during the accumulation of measured spectra the participation of the least stable fluorophore decreases, which is in the current experiment is the pacific blue derivative **156**. The green (**152**) and red (**150**)

---

fluorophores appears to resist the harsh irradiation conditions. Decreasing the blue intensity, the coordinates of the white light emission are green and red-shifted. The new coordinates determined by confocal microscopy are  $x = 0.3057$  /  $y = 0.3483$  (form. W  $x = 0.30639$  /  $y = 0.32164$ ) which is still in close proximity to the D65 white light standard and corresponds well to a white light emission. The CIE1931 colour space with all measured colours is shown in figure 117 on the right side. In figure 118 giant white light emitting polymersomes are shown in the presence of formulation W. The image has been recorded with increased pinhole value (300 nm) to obtain pseudo-epifluorescence. White light emitting polymersomes can be identified in the presence of red, green and blue vesicles. This image shows that the white light emission occurs due to confinement in the giant polymersome. Vesicles which are not confined can freely move on the cover slide and spread out over the surface, which decreases the local concentration of vesicles in the observed volume. In the interior of the polymersomes the local concentration is preserved and white light emission can occur.

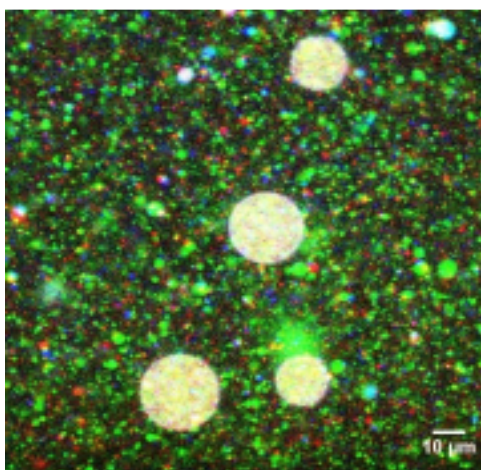


**Figure 118:** Confocal microscope image of a sample of white light emitting polymersomes in the presence of form. W. Observation with increased pinhole value (300 nm).

## 5.7 Conclusion

A new type of supramolecular white light emitting assembly has been prepared and characterized by confinement of red, green and blue emitting fluorinated vesicles in giant polymersomes. The absence of energy transfer between encapsulated vesicles has been proven and therefore the orthogonal coexistence of different fluorinated vesicles in the same compartment. Macroscopic white light emission of a formulation containing red, green and

---

blue emitting vesicles could be transferred into a micro-environment while the supramolecular building blocks can be identified via confocal microscopy.

This approach can be useful for future work regarding cascade reactions in confined compartment where isolated building blocks in the interior are needed. Moreover fluorinated amphiphiles have several advantages over polymer formulations like precise knowledge of the size and number of molecules per vesicle, while polymers mostly consist of a size distribution. The bilayer of these vesicles is much smaller than polymeric membranes providing easier access to membrane located molecules. The unique rigidity of fluorinated vesicles could be exploited under conditions where liposomes are not stable.

---

## References

- (1) Wright, W. *Transactions of the Optical Society* **1929**, 30.
- (2) Guild, J. *Philosophical Transactions of the Royal Society of London Series a-Containing Papers of a Mathematical or Physical Character* **1932**, 230, 149.
- (3) Ohta N.; Robertson, A. R. *Colorimetry (1. Edition)* **2006**.
- (4) Kido, J.; Kimura, M.; Nagai, K. *Science* **1995**, 267, 1332.
- (5) Forster, T. *Discuss. Faraday Soc.* **1959**, 7.
- (6) Corry, B.; Jayatilaka, D.; Rigby, P. *Biophys. J.* **2005**, 89, 3822.
- (7) Ego, C.; Marsitzky, D.; Becker, S.; Zhang, J. Y.; Grimsdale, A. C.; Mullen, K.; MacKenzie, J. D.; Silva, C.; Friend, R. H. *J. Am. Chem. Soc.* **2003**, 125, 437.
- (8) Vijayakumar, C.; Praveen, V. K.; Ajayaghosh, A. *Advanced Materials* **2009**, 21, 2059.
- (9) Giansante, C.; Raffy, G.; Schafer, C.; Rahma, H.; Kao, M. T.; Olive, A. G. L.; Del Guerzo, A. *J. Am. Chem. Soc.* **2011**, 133, 316.
- (10) Babu, S. S.; Aimi, J.; Ozawa, H.; Shirahata, N.; Saeki, A.; Seki, S.; Ajayaghosh, A.; Mohwald, H.; Nakanishi, T. *Angew. Chem. Int. Ed.* **2012**, 51, 3391.
- (11) Park, S.; Kwon, J. E.; Kim, S. H.; Seo, J.; Chung, K.; Park, S. Y.; Jang, D. J.; Medina, B. M.; Gierschner, J.; Park, S. Y. *J. Am. Chem. Soc.* **2009**, 131, 14043.
- (12) Yang, Y. J.; Lowry, M.; Schowalter, C. M.; Fakayode, S. O.; Escobedo, J. O.; Xu, X. Y.; Zhang, H. T.; Jensen, T. J.; Fronczek, F. R.; Warner, I. M.; Strongin, R. M. *J. Am. Chem. Soc.* **2007**, 129, 1008.
- (13) Coppo, P.; Duati, M.; Kozhevnikov, V. N.; Hofstraat, J. W.; De Cola, L. *Angew. Chem. Int. Ed.* **2005**, 44, 1806.
- (14) Wang, R. B.; Peng, J.; Qiu, F.; Yang, Y. L.; Xie, Z. Y. *Chem. Commun.* **2009**, 6723.
- (15) Zhang, X.; Rehm, S.; Safont-Sempere, M. M.; Wurthner, F. *Nature Chemistry* **2009**, 1, 623.
- (16) Lei, Y. L.; Liao, Q.; Fu, H. B.; Yao, J. N. *J. Am. Chem. Soc.* **2010**, 132, 1742.
- (17) Vives, G.; Giansante, C.; Bofinger, R.; Raffy, G.; Del Guerzo, A.; Kauffmann, B.; Batat, P.; Jonusauskas, G.; McClenaghan, N. D. *Chem. Commun.* **2011**, 47, 10425.
- (18) Galangau, O.; Dumas-Verdes, C.; Meallet-Renault, R.; Clavier, G. *Org. Biomol. Chem.* **2010**, 8, 4546.
- (19) Buyukcakir, O.; Bozdemir, O. A.; Kolemen, S.; Erbas, S.; Akkaya, E. U. *Org. Lett.* **2009**, 11, 4644.
- (20) Jiao, G. S.; Thoresen, L. H.; Kim, T. G.; Haaland, W. C.; Gao, F.; Topp, M. R.; Hochstrasser, R. M.; Metzker, M. L.; Burgess, K. *Chemistry-a European Journal* **2006**, 12, 7816.
- (21) Jing, B. W.; Zhang, D. Q.; Zhu, D. B. *Tetrahedron Lett.* **2000**, 41, 8559.
- (22) WeidnerWells, M. A.; FragaSpano, S. A. *Synth. Commun.* **1996**, 26, 2775.
- (23) Sun, W. C.; Gee, K. R.; Haugland, R. P. *Bioorg. Med. Chem. Lett.* **1998**, 8, 3107.
- (24) Jorge Bañuelos, F. L. A., Teresa Arbeloa, Virginia Martinez and Iñigo López Arbeloa *Applied Science Innovations Pvt. Ltd.* **2012**.
- (25) Riess, J. G. *J. Drug Targeting* **1994**, 2, 455.
- (26) Krishna, M. M. G.; Periasamy, N. *Journal of Fluorescence* **1998**, 8, 81.
- (27) Marguet, M.; Edembe, L.; Lecommandoux, S. *Angew. Chem. Int. Ed.* **2012**, 51, 1173.

---

---

---

## **6 General conclusion and perspectives**

---

---

The multidisciplinary approach of the thesis gave rise to a study using a wide range of techniques and comprising different disciplines of chemistry including supramolecular, photo- and materials chemistry. In chapter 2 a novel perfluorinated BODIPY fluorophore (**59**) had been synthesized which showed an approximately three times higher photostability than commercial fluorescein and a reactivity towards biologically interesting functional groups such as amines and thiols in organic solvent and aqueous DMF mixtures. The simultaneous reaction with thiols and amines present showed a 99 % selectivity for the thiol conjugate which gives rise to selective labeling applications of the amino acid cysteine in proteins. The 90-fold higher quantum yield for EtS-BODIPY (**60**) compared to BuNH-BODIPY (**61**) gives an approximate contrast of  $10^4$ . However, for future labeling applications the water solubility of the F<sub>5</sub>-BODIPY needs to be increased which can be achieved by incorporation of carboxylic or sulfonic acids on the BODIPY core in order to preserve the reactivity of the perfluorophenyl ring. Perfluorophenyl chemistry allowed the facile introduction of an azide functionality onto the aromatic ring. The azide-BODIPY (**63**) has been shown in some preliminary tests to be a reactive substrate for photoinduced surface patterning, on the micrometer scale, onto alkyne functionalized surfaces using a photoreducible click-catalyst (**64**). The quantity of azide-BODIPY (**63**) grafted onto the surface, was largely dependent on the irradiation power and the irradiation time, while the resolution was mostly dependent on the viscosity of the solvent. Confocal fluorescence microscopy images (FLIM) of the surface showed that in more viscous cyclohexanol a lower resolution was obtained than in toluene. For future studies on surface patterning several parameters of the system should be investigated like the solvent viscosity dependency. Control experiments with a non photoactive precatalyst analog of (**64**) need to be studied in order to attribute the reactivity to the employed photocatalyst (**64**) as well as the formation of an apparent side product resulting from irradiation with high laser intensities.

For the principle goal of the project, the essential Ca<sup>2+</sup>-sensors were successfully synthesized. Fluorescent water soluble BAPTA-BODIPYs (**72** and **76**) showed a fluorescence enhancement of 122 and 23 –fold respectively upon Ca<sup>2+</sup> complexation under pseudo-intracellular conditions. The rate of photoinduced electron transfer has been determined via transient absorption measurements to be  $3.3 \times 10^{12} \text{ s}^{-1}$  for BAPTA-BODIPY (**72**) and  $8.3 \times 10^{11} \text{ s}^{-1}$  for BAPTA-PH-BODIPY (**76**) with K<sub>d</sub> values of 0,53 and 0,16 μM respectively rendering these molecules interesting molecules for ion sensing in biological systems.

---

Amphiphilic  $\text{Ca}^{2+}$ -switches based on the BAPTA ionophore and BODIPY (**82**), naphthalimide (**79**) and furan (**97**) fluorophores have been designed.  $\text{Ca}^{2+}$  complexation studies yield binding affinities in the range of 0.076 – 0.724  $\mu\text{M}$  but with rather low fluorescence enhancement (4.3-fold max.) upon ion binding, which was attributed to aggregation in aqueous media. Water soluble DMNPE-4 (**99**) and amphiphilic (**122** and **124**)  $\text{Ca}^{2+}$ -decaging agents have been designed based and their decaging properties tested under pseudo-physiological conditions.  $K_d$  values and decaging efficiencies resemble those determined for DMNPE-4. The amphiphilic hydrocarbon analogue (**122**) is a promising candidate for applications in biological studies where  $\text{Ca}^{2+}$  from lipid membrane surfaces is desired. Equally, the amphiphilic decaging agents have been incorporated into the self-assembled membrane of synthetic amphiphiles and their decaging properties have been verified. The amphiphilic  $\text{Ca}^{2+}$ -sensors (**79**, **82** and **97**) showed increased fluorescence emission in vesicle membranes (one order of magnitude for **79** and **97** and two orders of magnitude for **82**). These amphiphilic fluorophores could be used for the sensing of  $\text{Ca}^{2+}$  close to biological membranes when equipped with hydrocarbon instead of fluorocarbon chains. Also the observed effect, namely the decrease in binding affinity towards  $\text{Ca}^{2+}$ , which was observed in cationic vesicles (circa 100-times lower for **82** and **97** and 10-times lower for **79**) would be probably present to a lesser extent in biological membranes since the charge on the surface is not exclusively positive.

Nevertheless, photoinduced  $\text{Ca}^{2+}$  transfer had been successfully shown between decaging vesicles and ion sensing vesicles under pseudo-intracellular conditions. Multicompartmentalized vesicle-in-polymerosome structures were achieved when using fluorocarbon vesicles, while hydrocarbon vesicles formed hybrid amphiphile polymer capsules which will be an interesting target for membrane permeability studies in the future, for example for oxygen transport etc. The ion transfer between fluorocarbon vesicles in the aqueous interior of polymerosomes had been achieved using UV-light as release trigger. The increase in fluorescence intensity of ion sensing vesicles gave direct proof of the occurrence of ion transfer. Fitting of the transfer kinetics revealed a slowed down decaging kinetic for DMNPE-4 based  $\text{Ca}^{2+}$ -decaging agents in aqueous polymer compartments. This multicompartmentalized system with  $\text{Ca}^{2+}$  ions bound to one internal vesicle could be exploited for more sophisticated architectures in the future. One could imagine internalization of biomolecules which are activated by  $\text{Ca}^{2+}$  incorporated in the membrane of one vesicle and

---

the  $\text{Ca}^{2+}$ -decaging agent to another. Upon photodecaging biochemical reactions in confined compartments could be photocontrolled biochemical microreactors. In the last part, the multicompartmentalization approach was extended to three different types of vesicles in the internal compartment of a giant polymersome. By incorporation of independent red (**150**), green (**152**) and blue (**156**) light-emitting dyes in the membrane of fluorinated vesicles, white light emission in the microcompartment of the polymersome could be achieved as a result of nanoconfinement. This system containing three types of 200 nanometer-sized vesicles in a micrometric polymersome could be exploited for cascade reactions in microenvironments.

In summary the goal of the project, namely the photoinduced ion transfer between synthetic vesicles in confined polymer compartments has been achieved and artificial mimicry for cellular communication has been shown. The most performant multicomponent system, namely fluorinated vesicles in polymersomes, opens the way towards some sophisticated future applications.

---

---

---

---

---

## **7 Experimental section**

---

---

## Solvents and chemical products

Commercially-available products were purchased from the Sigma Aldrich, Acros Chemicals, Lancaster and Fluka and were used as received. Solvents of technical grade were distilled and dried prior to utilization. Toluene was distilled over sodium, acetonitrile and dichloromethane were distilled over calcium hydride and dimethylformamide (DMF) was stored over molecular sieves. Deuterated solvents for NMR analysis were bought from Sigma-Aldrich and Euriso-top. Deionized water was obtained by purification over an ion exchange column and a membrane filter of 0.45  $\mu\text{m}$  (MSI, Micron separation, Inc.). Solvents for spectroscopy without the addition of stabilizing agents or other absorbing material were employed as bought.

## Thin layer chromatography and silica columns

Thin layer chromatography was performed on silica gel 60 F254 sheets on aluminium produced by Merck. Spots on the TLC plate were observed under UV light (254 nm / 365 nm) when appropriate for non-active compounds an appropriate staining agent were employed. Most frequently used staining agents comprised an ethanolic solution of fluorescein, dinitrophenylhydrazine staining agent for aldehydes, ninhydrin solution for amines, cerium molybdate staining agent for alcohols and as a general stain and phosphomolybdic acid stain as a general staining agent. Column chromatography for the separation of organic compounds was performed using silica gel from Merck with a particle size of 40 – 63  $\mu\text{m}$  (230 – 400 mesh). Organic compounds for separation were dissolved in a minimum amount of chromatography solvent and deposited on top of the column and subsequently eluted.

## Nuclear magnetic resonance spectroscopy (NMR)

$^1\text{H}$  and  $^{13}\text{C}$ -NMR experiments were performed at 295 K on a Bruker Avance 300 ( $^1\text{H}$ : 300 MHz,  $^{13}\text{C}$ : 75 MHz), Avance II 400 ( $^1\text{H}$ : 400 MHz,  $^{13}\text{C}$ : 100 MHz), and an Avance III 600 ( $^1\text{H}$ : 600 MHz,  $^{13}\text{C}$ : 150 MHz) spectrometer. Chemical shifts are reported in ppm ( $\delta$ ) and are referenced to the NMR solvent ( $\text{CDCl}_3$ ,  $\text{D}_2\text{O}$ , MeOD,  $\text{CD}_3\text{CN}$ , DMSO) residual peak. Abbreviations used are s = singlet, d = doublet, t = triplet, q = quartet, dd = doublet of doublets, dt = doublet of triplets and m = multiplet. The coupling constants ( $J$ ) are reported in Hertz (Hz).

---

### **Mass spectrometry**

Mass spectra are measured by the “Centre d’Etude Structurale et d’Analyse des Molecules Organique” (CESAMO) at the university of Bordeaux. The measurements were carried out on a QStar Elite mass spectrometer (Applied Biosystems). The instrument is equipped with an electrospray ionisation (ESI) source and the spectra were recorded in either positive or negative ionisation mode. The electrospray needle was maintained at 5000 V and operated at room temperature. Samples were introduced by injection through a 20  $\mu$ L sample lip into a 4500  $\mu$ L/min flow of methanol from the LC pump. Alternatively field desorption (FD) was used as ionization mode on a time of flight (TOF) mass spectrometer (Accu TOF GCv). The FD-emitter voltage was 10 kV and 1 – 2  $\mu$ L of sample solution was deposited on a 13  $\mu$ m emitter wire and inserted into the machine.

### **Electronic absorption (UV-Vis) and fluorescence spectroscopy**

Electronic absorption and emission spectra have been measured on a Varian UV-Vis-NIR spectrophotometer Cary 5000 or Cary 100. Heterogeneous samples were recorded on a Cary 100 equipped with an integrating sphere (labsphere DRA-CA-301). The wavelengths observed ranged from 200 – 800 nm. Sample solutions were measured in matched quartz cells with a pathlength of 10 mm. Before each measurement a baseline of pure solvent was been taken and was subtracted from the measured spectra. The fluorescence emission spectra were measured on a HORIBA Jobin-Yvon Fluorolog -3 equipped with a xenon lamp (450 W), with Hamamatsu R2658P and R928P photomultiplier (PMT) detection. Quartz cells of 10 mm length were employed for study of optically dilute samples with fluorescence emission being measured at a right angle with respect to the excitation beam. Time-correlated single photon counting was performed with a monochromatic pulsed light source (nanoLED 370 nm and 456 nm; 1.2 ns FWHM) on the Fluorolog-3.

---

### Fluorescence quantum yield calculation

The fluorescence quantum yield was determined by comparison to an optically dilute fluorescence standard with a known quantum yield according to the Parker method.<sup>1</sup> Mainly three different standards have been used namely fluorescein in 0.1 M NaOH ( $\phi = 0.95$ ) for green emitting dyes, 9,10-diphenylanthracene in cyclohexane ( $\phi = 0.90$ ) for blue emitting dyes and rhodamine 101 in ethanol containing 0.01 HCl ( $\phi = 1.00$ ) for red emitting dyes. The fluorescence quantum yield of the sample solution ( $\phi$ ) has then been calculated by equation xx1 where  $\phi_R$  is the fluorescence quantum yield of the reference,  $I$  is the integral of the fluorescence emission of the sample solution,  $I_R$  is the integral of the fluorescence emission of the reference,  $A$  is the absorption at the excitation wavelength and  $\eta$  is the refractive index of the solvent used.

$$\phi = \phi_R \times \frac{I}{I_R} \times \frac{A_R}{A} \times \frac{\eta^2}{\eta_R^2} \quad \text{equation 27}$$

### Transient absorption spectroscopy

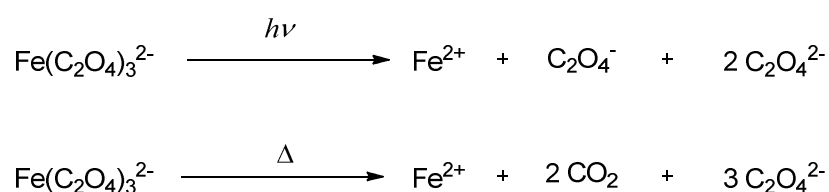
Transient absorption spectroscopy allows the observation and measurement of the evolution of the excited state of a molecule directly after its excitation and species with a very short time constant can be observed such as radicals or radical anions as well as dark non-radiative intersystem crossing processes giving triplet states. Two set-ups have been used to obtain transient absorption data, a femtosecond set up (1 ns – 200 fs) and a picosecond setup (1 ns – 1 ns). Transient absorption maps were constructed as follows: In order to generate the pump-probe pulses a tripled frequency Nd: YAG amplified laser (30 ps, 30 mJ, 1064 nm, 20 Hz, model Ekspla 401) was used to pump an optical parametric generator (PG model Ekspla 401) in order to produce the excitation pulse in the wavelength range between 410 – 2300 nm. The residual laser beam is focalised in a cell under high pressure of Xe, where a white light pulse is produced to measure the sample. All signals are analysed by a spectrograph (Princeton Instruments Acton model SP2300) coupled to a camera (Hamamatsu C7700). The accumulation of the pulses is stored and treated with the program HPDTA (Hamamatsu) in order to produce the transient absorption maps in two dimensions (wavelengths vs. time delay) of the absorption intensities between 300 and 800 nm.

---

### Photochemical quantum yield.

Montalti M., Credi A., Prodi L., Gandolfi M. T., *Handbook of photochemistry*, Taylor and Francis p601-604. ( $\phi_{\text{Fe}^{2+}} = 1.21$  at 365.6 nm)

Photochemical quantum yields have been determined according to a standard procedure using a ferrioxalate actinometer. A solution of potassium ferrioxalate (0.012 M) in  $\text{H}_2\text{SO}_4$  (0.05 M) and a solution of phenanthroline (0.1 %) in  $\text{H}_2\text{SO}_4$  (0.5 M) buffered with sodium acetate trihydrate (225 g/L) has been prepared. Ferrioxalate can be used as an actinometer up to 500 nm. The “micro-version” of the initial method by Hatchard and Parker and described by Fisher has been used. Under irradiation the ferrioxalate is decomposing according to the following equation.



After irradiating a solution of ferrioxalate (3 ml) for a certain time, the solution of phenanthroline (0.5 ml) is added, which forms a tris-phenanthroline complex only with the  $\text{Fe}^{2+}$  ions ( $\epsilon = 11100 \text{ cm}^{-1}\text{M}^{-1}$  at 510 nm) The absorption is compared to a non-irradiated reference solution which is kept in the dark and the difference between the two is noted and gives  $\Delta A$ . The molar amount of  $\text{Fe}^{2+}$  is given by equation 28.

$$\text{moles Fe}^{2+} = \frac{V \times \Delta A}{l \times \epsilon_{510}} \quad \text{equation 28}$$

Where  $V$  is the total volume (3.5 ml)  $l$  is the optical path of cell and  $\epsilon_{510}$  is the extinction coefficient of the  $\text{Fe}(\text{phen})^{2+}$  complex. Thus, the photons absorbed by the solution per time unit ( $Nh\nu/t$ ) is:

$$Nh\nu/t = \frac{V \times \Delta A}{l \times \epsilon_{510}} \quad \text{equation 29}$$

Where  $\phi_\lambda$  is the quantum yield for the formation of  $\text{Fe}^{2+}$ ,  $t$  is the irradiation time  $F$  is the fraction of photons absorbed by the ferrioxalate solution ( $F = 1 - 10^{-A}$ ). If the irradiated solution is sufficiently concentrated the  $F$  factor can be omitted. Upon irradiation of the sample solution it needs to be taken in account that the spectroscopical change should not surpass 10 % to obtain a reliable value for the photochemical quantum yield. The

---

concentration of the light induced change  $C_i$  (isomerisation or photocleavage) can be calculated as follows:

$$C_i = \frac{\Delta A}{\varepsilon - \varepsilon_{product}} \quad \text{equation 30}$$

$\varepsilon$  is the extinction coefficient of the starting material and  $\varepsilon_{product}$  is the extinction coefficient of the photoproduct. The photochemical quantum yield is then calculated as shown in equation xx6.

$$\phi_\lambda = \frac{C_i \times V_s}{\left(\frac{N h \nu}{t}\right) \times t} \quad \text{equation 31}$$

Here  $V_s$  is the irradiated volume of the sample and  $t$  stands for the irradiation time of the sample.

### Calcium titration

Two Calcium calibration stock solutions have been prepared, one containing 10 mM EGTA (0  $\mu\text{M}$   $\text{Ca}^{2+}$ -buffer) and another with 10 mM CaEGTA (39  $\mu\text{M}$   $\text{Ca}^{2+}$ -buffer). In addition both buffers were charged with 100 mM KCl and 30 mM 3-(N-Morpholino)-propanesulfonic acid (MOPS) adjusted at pH 7.2. In both buffers an equivalent amount of  $\text{Ca}^{2+}$ -binding probe was dissolved with a final concentration between 1-10  $\mu\text{M}$ . In order to determine the  $K_d$  both fluorescence and electronic absorption spectra have been taken after having adjusted the free  $\text{Ca}^{2+}$  concentration to 0.017  $\mu\text{M}$ , 0.038  $\mu\text{M}$ , 0.065  $\mu\text{M}$ , 0.100  $\mu\text{M}$ , 0.150  $\mu\text{M}$ , 0.225  $\mu\text{M}$ , 0.35  $\mu\text{M}$ , 1.35  $\mu\text{M}$  and 39  $\mu\text{M}$ . Therefore 2 mL of the 0  $\mu\text{M}$   $\text{Ca}^{2+}$ -sample was placed in a cuvette and the spectra were recorded. 200  $\mu\text{L}$  of the sample was discarded and replaced with 200  $\mu\text{L}$  of the 39  $\mu\text{M}$   $\text{Ca}^{2+}$ -sample. In that fashion a concentration of 0.017  $\mu\text{M}$   $\text{Ca}^{2+}$  can be obtained without changing the concentration of the analyte. The aforementioned  $\text{Ca}^{2+}$  concentrations were then adjusted by discarding 250, 222, 250, 286, 333, 400, 500, 667 and 1000  $\mu\text{L}$  and replacing the removed volume with an equivalent volume of the 39  $\mu\text{M}$   $\text{Ca}^{2+}$  sample. For the calculation of the free  $\text{Ca}^{2+}$ -concentration a constant room temperature of 21  $^\circ\text{C}$  was assumed.

The spectral change at a certain wavelength is then introduced into Hill plot which is the logarithm of  $(F - F_{\min}) / (F_{\max} - F)$  where  $F$  is the fluorescence emission or the absorption at a

---

certain wavelength plotted over the logarithm of the free  $\text{Ca}^{2+}$  concentration as obtained from the  $\text{Ca}^{2+}$ -buffers. A schematic representation of the obtained graph is shown in figure 119

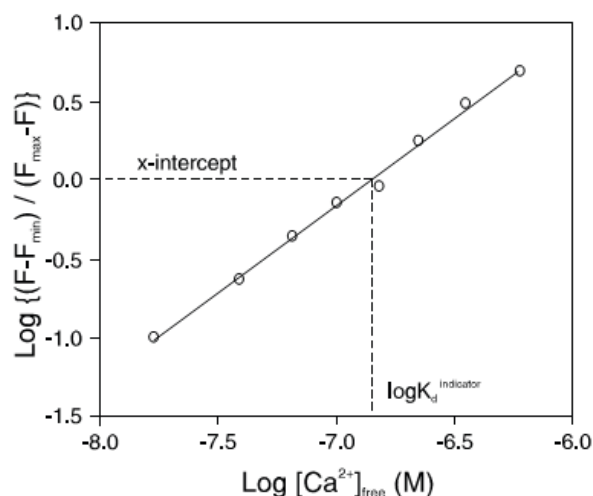


**Figure 119:** Schematic representation of the Hill plot obtained from a  $\text{Ca}^{2+}$  titration.

The x-intercept in this graph gives the logarithm of the  $K_d$  as shown in figure 119.

### Preparation of vesicles

Vesicles were prepared using a popular thin film hydration procedure. A solution of amphiphile and membrane fluorophores or  $\text{Ca}^{2+}$ -probes in a mixture of  $\text{CHCl}_3$  and MeOH (3:1, v/v) was prepared and the solvent was slowly evaporated on a rotary evaporator by increasing the vacuum stepwise until a thin film was obtained. After drying the thin film an additional 30 min, it was hydrated using an appropriate buffer (100 mM KCl, 30 mM MOPS, pH 7.2). The obtained polydisperse vesicle solution was passed through a membrane of 800 – 200  $\mu\text{m}$  pore size depending on the desired vesicle size.

### Preparation of multicompartmentalized polymersomes

A formulation of liposomes in pseudo-intracellular buffer loaded with 130 mg/ml sucrose which equals an osmotic pressure of 380 mOsm is emulsified in toluene using poly(butadiene)<sub>46</sub>-*b*-poly(ethylene oxide)<sub>30</sub> (PB-*b*-PEO) (3 mg/ml). The solution was gently shaken to produce droplets of a water-in-oil emulsion. The emulsion was then set on top of an aqueous pseudo intracellular buffer solution containing 380 mOsm of glucose. In a last step, the biphasic system is centrifuged, yielding giant polymersomes with the prepared vesicle solution in the aqueous interior.

## Optical and epifluorescence microscopy

Samples were sealed between a glass slide and cover glass and subsequently observed using a NIKON Eclipse Physio Station E600FN equipped with HAMAMATSU C4742-95 digital CCD Camera with either 10x/0.3, 20x/0.5 or 40x/0.75 Plan Fluor objectives with an adequate condenser and prism for DIC (differential interferential contrast) observation.

## Confocal fluorescence microscopy

A Picoquant Microtime 200 with two MPD SPADs and a Ti-Sa laser chain (Coherent) yielding 4–6 ps pulses at 4.75 MHz. An 80% T/20% and R spectrally flat beam splitter was used in combination with a microscope objective (100× UPLSAPO, NA 1.4), suitable interferential filters, a 50 μm pinhole and, when specified, a polarizing beam splitter and two Glan-Thompson polarizers. Laser powers were adjusted as described in the result section. Spectroscopy was performed with an Andor system, collecting after the pinhole. The spectra were intensity corrected for instrumental response, measuring suitable reference solutions that cover the whole spectral range. A schematic representation of the setup is given in figure 120.

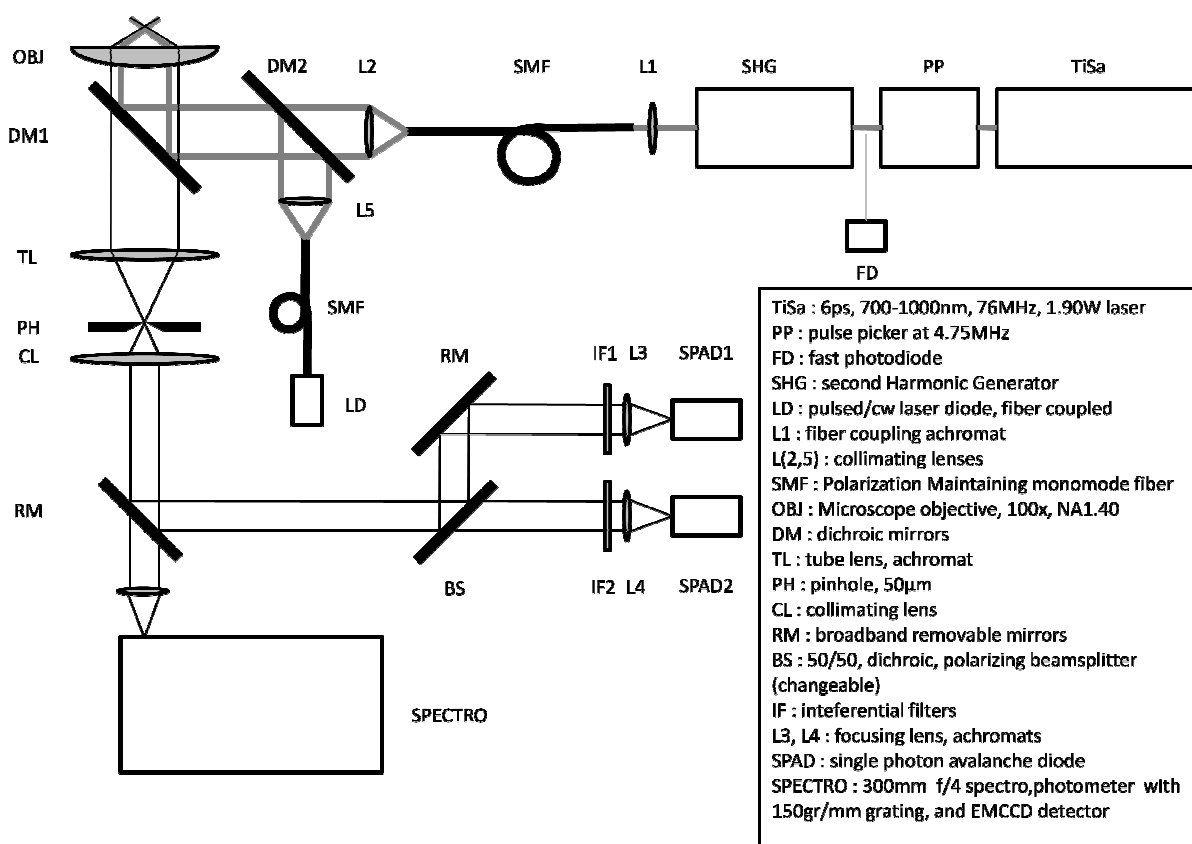


**Figure 120:** Scheme of the confocal fluorescence microscopy setup used in the surface patterning experiments.



---

followed by recrystallisation from chloroform, then toluene to give 347 mg (0.83 mmol, 33 % yield) of product as an orange crystalline solid.

$^1\text{H}$  NMR (300 MHz,  $\text{CDCl}_3$ ):  $\delta$  = 6.05 (s, 2H), 2.57 (s, 6H), 1.62 (s, 6H).

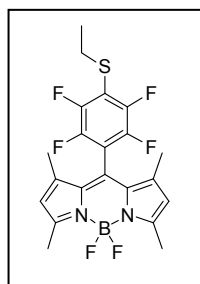
$^{13}\text{C}$  NMR (75 MHz,  $\text{CDCl}_3$ ):  $\delta$  = 157.81, 141.70, 141.53, 131.00, 122.77, 122.29, 14.78, 13.58.

$^{19}\text{F}$  NMR (400 MHz,  $\text{CDCl}_3$ ):  $\delta$  = -161.93 (m, 2F), -153.04 (t, 1F,  $J$  = 20.2 Hz), -146.69 (q, 2F,  $J$  = 32.1 Hz), -143.53 (dd, 2F,  $J$  = 22.0 Hz,  $J$  = 7.6 Hz).

HRMS (ESI): Calc.  $m/z$  = 437.1034 for  $\text{C}_{19}\text{H}_{14}\text{BF}_7\text{N}_2\text{Na}$

Found  $m/z$  = 437.1046  $[\text{M}+\text{Na}]^+$

### EtS-BODIPY (60)



$\text{F}_5$ -BODIPY (10 mg, 24  $\mu\text{mol}$ ) was dissolved in DMF (1 mL) and ethane thiol (10  $\mu\text{l}$ , 144  $\mu\text{mol}$ .) and  $\text{K}_2\text{CO}_3$  (2 mg, 15  $\mu\text{mol}$ ) were added. The reaction was followed by means of normal phase HPLC using a Kromasil SI-100 column (250 mm x 4.6 mm, 5  $\mu\text{m}$ ). Water was added and the aqueous phase was extracted with  $\text{Et}_2\text{O}$ . The organic phase was washed with water and dried over  $\text{Na}_2\text{SO}_4$ . The solvent was then removed under reduced pressure yielding the crude product (9 mg).  $^{19}\text{F}$ -NMR was recorded with the crude product. The rest of the sample was dissolved in a mixture of cyclohexane / EtAc (95/5, v/v) and passed through a short  $\text{SiO}_2$  plug to obtain the pure product as a red solid 7 mg (15  $\mu\text{mol}$ , 63 % yield).

$^1\text{H}$  NMR (300 MHz,  $\text{CDCl}_3$ ):  $\delta$  = 6.21 (s, 2H), 3.08 (q,  $J$  = 7.3 Hz, 2H), 2.54 (s, 6H), 1.68 (s, 6H), 1.26 (t,  $J$  = 7.3 Hz, 3H).

$^{13}\text{C}$  NMR (75 MHz,  $\text{CDCl}_3$ ):  $\delta$  = 206.73, 123.40, 122.61, 78.52, 78.19, 77.87, 30.13, 28.68, 14.57, 14.18, 13.04.

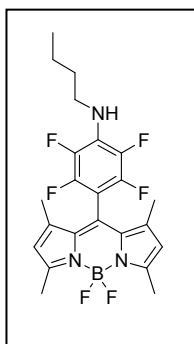
$^{19}\text{F}$  NMR (400 MHz,  $\text{CDCl}_3$ ):  $\delta$  = -134.13 (m, 2F), -143.65 (m, 2F), -147.69 (q, 2F,  $J$  = 32.0 Hz).

HRMS (ESI): Calc.  $m/z$  = 479.1158 for  $\text{C}_{21}\text{H}_{19}\text{B N}_2\text{F}_6\text{SNa}$

Found  $m/z$  = 479.1179  $[\text{M}+\text{Na}]^+$

---

### BuNH-BODIPY (61)



F5-BODIPY (10 mg, 24  $\mu\text{mol}$ ) was dissolved in DMF (1 mL) and *n*-butylamine (20  $\mu\text{l}$ , 192  $\mu\text{mol}$ ) was added. The reaction was followed by means of normal phase HPLC using a Kromasil SI-100 column (250 mm x 4.6 mm, 5  $\mu\text{m}$ ). Water was added and the aqueous phase was extracted with  $\text{Et}_2\text{O}$ . The organic phase was washed with water and dried over  $\text{Na}_2\text{SO}_4$ . The solvent was removed under reduced pressure yielding the crude product (10 mg).  $^{19}\text{F}$ -NMR was recorded using the crude product. The rest of the sample was dissolved in a mixture of cyclohexane / EtAc (95/5, v/v) and passed through a short  $\text{SiO}_2$  plug to obtain 8 mg (17  $\mu\text{mol}$ , 70 %) of pure product.

$^1\text{H}$  NMR (300 MHz,  $\text{CDCl}_3$ ):  $\delta$  = 6.20 (s, 2H), 4.95 (s, br, 1H), 3.43-3.51 (m, 2H), 2.53 (s, 6H), 1.73 (s, 6H), 1.58-1.68 (m, 2H), 1.36-1.49 (m, 2H), 0.97 (t,  $J$  = 7.3, 3H).

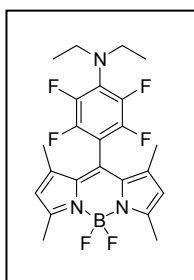
$^{13}\text{C}$  NMR (75 MHz,  $\text{CDCl}_3$ ):  $\delta$  = 193.54, 157.33, 143.12, 122.17, 78.49, 78.16, 77.83, 44.96, 32.54, 19.72, 14.11, 13.32, 13.03.

$^{19}\text{F}$  NMR (400 MHz,  $\text{CDCl}_3$ ):  $\delta$  = -146.74 (q, 2F,  $J$  = 32.3 Hz), -147.60 (m, 2F), -161.61 (m, 2F).

HRMS (ESI): Calc.  $m/z$  = 490.1859 for  $\text{C}_{23}\text{H}_{24}\text{B N}_3\text{F}_6\text{Na}$

Found  $m/z$  = 490.1860  $[\text{M}+\text{Na}]^+$

### $\text{Et}_2\text{N}$ -BODIPY (62)



$\text{F}_5$ -BODIPY (10 mg, 24  $\mu\text{mol}$ ) was dissolved in a Schlenk tube under nitrogen in DMF (1 mL) and diethylamine (0.1 mL, 957  $\mu\text{mol}$ ) was added. The mixture was heated at 120°C overnight. Water was added and the crude product was extracted with  $\text{Et}_2\text{O}$  and further washed with water. The organic phase was dried over  $\text{MgSO}_4$ , filtered and the solvent was evaporated under reduced pressure to yield the crude product (6 mg). The crude sample was dissolved in a mixture of cyclohexane / Ethylacetate (95/5, v/v) and passed through a short  $\text{SiO}_2$  plug to obtain the pure (4 mg, 8  $\mu\text{mol}$ , 36 %) product.

$^1\text{H}$  NMR (300 MHz,  $\text{CDCl}_3$ ):  $\delta$  = 6.04 (s, 2H), 4.33 (q,  $J$  = 7.1 Hz, 4H), 2.56 (s, 6H), 1.65 (s, 6H), 1.12 (t,  $J$  = 7.1 Hz, 6H).

---

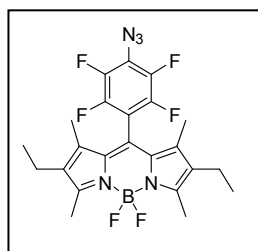
$^{13}\text{C}$  NMR (75 MHz,  $\text{CDCl}_3$ ):  $\delta = 206.12, 123.40, 194.08, 155.78, 30.13, 26.85, 12.92, 12.72.$

$^{19}\text{F}$  NMR (400 MHz,  $\text{CDCl}_3$ ):  $\delta = -143$  (m, 2F),  $-147$  (m, 2F),  $-153$  (m, 2F). ).

HRMS (ESI): Calc.  $m/z = 490.1859$  for  $\text{C}_{23}\text{H}_{24}\text{B N}_3\text{F}_6\text{Na}$

Found  $m/z = 490.1854$   $[\text{M}+\text{Na}]^+$

### azide-BODIPY (63)



$\text{F}_5$ -BODIPY (300 mg, 0.638 mmol) and sodium azide (124 mg, 1.913 mmol) were dissolved in DMF (1 mL). The reaction mixture was stirred for 1 h, then diluted with brine (20 mL) and the aqueous phase was extracted with  $\text{Et}_2\text{O}$  (3x). The organic phase was washed with brine and dried over  $\text{MgSO}_4$ . After filtration, the solvent was evaporated under reduced pressure and the crude product was purified by column chromatography using PTE/DCM (80/20, v/v) as eluent to obtain 69 mg (0.14 mmol, 22 %) of product as a red powder.

$^1\text{H}$  NMR (300 MHz,  $\text{CDCl}_3$ ):  $\delta = 3.48$  (q,  $J = 7.02$  Hz, 4H), 2.54 (s, 6H); 1.53 (s, 6H), 1.21 (t, 6H,  $J = 7.01$  Hz).

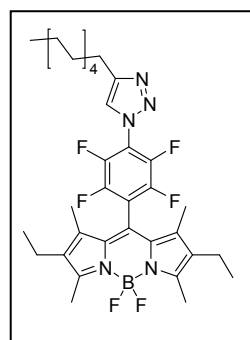
$^{13}\text{C}$  NMR (75 MHz,  $\text{CDCl}_3$ ):  $\delta = 156.14, 136.80, 133.97, 130.55, 17.24, 14.70, 12.88, 11.08.$

$^{19}\text{F}$  NMR (400 MHz,  $\text{CDCl}_3$ ):  $\delta = -140.78$  (dd,  $J = 10.09$  Hz,  $J = 21.81$  Hz, 2F),  $-146.73$  (dd,  $J = 32.46$  Hz,  $J = 65.26$  Hz, 2F),  $-151.33$  (dd,  $J = 10.22$  Hz,  $J = 21.81$  Hz, 2F),

HRMS (ESI): Calc.  $m/z = 516.1775$  for  $\text{C}_{23}\text{H}_{22}\text{BN}_5\text{F}_6\text{Na}$

Found  $m/z = 516.1764$   $[\text{M}+\text{Na}]^+$

### triazole-BODIPY (65)



azide-BODIPY (25 mg, 51.6  $\mu\text{mol}$ ) and  $[\text{Cutren}(\text{CH}_2\text{PhtBu})_3](\text{kt})_2$  (0.58 mg, 0.5  $\mu\text{mol}$ ) are dissolved in toluene (0.75 mL) and dodec-1-yne (12  $\mu\text{L}$ , 55.6  $\mu\text{mol}$ ) was added in a NMR tube. The solution was bubbled with argon during 20 min, sealed and irradiated at 365 nm with a TLC-lamp. After 28.5 h the reaction had reached 78 % completion. The volatiles were evaporated and crude product was purified by column chromatography using PTE/DCM (80/20, v/v). The 20 mg (31  $\mu\text{mol}$ ,

---

60 % yield) of product was obtained as a red crystalline solid.

$^1\text{H}$  NMR (400 MHz,  $\text{CDCl}_3$ ):  $\delta$  = 7.70 (s, 1H), 2.86 (t,  $J$  = 7.71 Hz, 2H), 2.56 (s, 6H), 2.35 (q,  $J$  = 7.56 Hz, 4H), 1.81 – 1.74 (m, 2H), 1.58 (s, 6H), 1.46 – 1.25 (m, 16H), 1.03 (t,  $J$  = 7.56 Hz, 6H), 0.88 (t,  $J$  = 6.81 Hz, 3H).

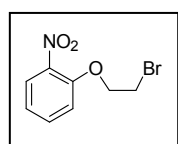
$^{19}\text{F}$  NMR (400 MHz,  $\text{CDCl}_3$ ):  $\delta$  = -183.52 – -183.62 (m, 2F), -145.90 – -145.98 (m, 2F), -146.56 – -146.82 (m, 2F).

$^{13}\text{C}$  NMR (150 MHz,  $\text{CDCl}_3$ ):  $\delta$  = 156.61, 149.20, 145.36 – 145.28 (m), 143.70 – 143.62 (m), 142.67 (d,  $J$  = 14.31 Hz), 140.94 (d,  $J$  = 12.76 Hz), 136.59, 134.26, 130.13, 123.02, 120.95, 118.37 – 118.20 (m), 116.46 (t,  $J$  = 19.29 Hz), 32.05, 29.72 (d,  $J$  = 7.59 Hz), 29.49 (d,  $J$  = 4.21 Hz), 29.35 (d,  $J$  = 8.73 Hz), 25.84, 22.84, 17.27, 14.70, 14.27, 12.95, 11.23.

HRMS (FD): Calc.  $m/z$  = 658.3602 for  $\text{C}_{35}\text{H}_{44}\text{BN}_5\text{F}_6$

Found  $m/z$  = 658.3630  $[\text{M}]^+$

#### 1-(2-Bromoethoxy)-2-nitrobenzene (**66**)<sup>5</sup>

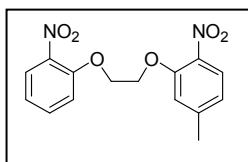


2-Nitrophenol (100 g, 719 mmol) was solubilized in hot MeOH and a mixture of KOH (40 g, 719 mmol) in MeOH was added and a red precipitate was formed. The solvent was evaporated and the solid was dissolved in a minimum amount of DMF (circa 200 mL). 1,2-dibromoethane (247 ml, 2.88 mol) is added and the reaction mixture heated to 120 °C for 4 h. After cooling, the reaction mixture was filtered and the filtrate washed with DCM and a small volume of water. The organic phase was washed with NaOH (10 %, 3x) and brine (3x). The organic phase was dried over  $\text{MgSO}_4$ , filtered and evaporated. The crude product was recrystallized from hot EtOH containing a few drops of water to obtain 64.5 g (263 mmol, 36.5 %) of the product as a beige solid.

$^1\text{H}$  NMR (300 MHz,  $\text{CDCl}_3$ ):  $\delta$  = 7.79 – 7.06 (m, 8H), 4.41 (t,  $J$  = 7.02 Hz, 4H), 3.67 (t,  $J$  = 7.04 Hz, 2H).

Spectra conform with literature

#### 4-methyl-1-nitro-2-(2-(2-nitrophenoxy)ethoxy)-benzene (**67**)<sup>5</sup>

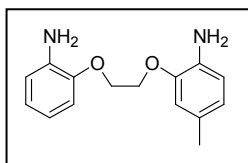


5-methyl-2-nitrophenol (30 g, 196 mmol) was solubilized in hot MeOH and a mixture of KOH (11 g, 196 mmol) in MeOH was added to form a red precipitate. The solvent was evaporated and the residue was dissolved in DMF (90 mL). 1-(2-Bromoethoxy)-2-nitrobenzene (45 g, 196 mmol) was added and the mixture was stirred at 120°C for 2 h. After cooling to room temperature, the reaction mixture was diluted with water (800 mL) and filtered. The precipitate was dried and recrystallized from hot EtOH containing 5 % water to yield 41.8 g (131.5 mmol, 67 %) of the product as a white powder.

$^1\text{H NMR}$  (300 MHz,  $\text{CDCl}_3$ ):  $\delta = 7.79 - 6.85$  (m, 7H), 4.53 (s, 4H), 2.44 (s, 3H)

Spectra conform with literature

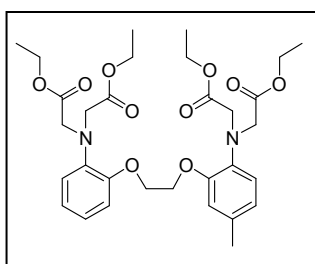
#### 2-(2-(2-aminophenoxy)ethoxy)-4-methylaniline (**68**)<sup>5</sup>



4-methyl-1-nitro-2-(2-(2-aminophenoxy)ethoxy)-benzene (20 g, 62.8 mmol) was dissolved in EtOH (200 mL). Pd/C (2 g) was added and the flask placed under hydrogen atmosphere and stirred for 24 h. The reaction mixture was filtered over celite, washed with hot EtOH and the solvent was evaporated. The crude product was taken up in  $\text{Et}_2\text{O}$ , sonicated and filtered. The precipitate was washed with cold  $\text{Et}_2\text{O}$  and dried under vacuum to yield 23.8 g (91.1 mmol, 71 %) of product.

$^1\text{H NMR}$  (300 MHz,  $\text{CDCl}_3$ ):  $\delta = 6.84 - 6.63$  (m, 7H), 4.35 (s, 4H), 3.73 (s, br, 4H), 2.26 (s, 3H). Spectra conform with literature

#### Methyl-BAPTA (**69**)<sup>5</sup>



2-(2-(2-aminophenoxy)ethoxy)-4-methylaniline (22 g, 85.2 mmol) was dissolved in dry AcCN (150 ml), NaI (5.02 g, 33.2 mmol),  $\text{Na}_2\text{HPO}_4$  (60.5 g, 425.9 mmol) and ethyl bromoacetate (52 ml, 468.6 mmol) were added and the reaction mixture was heated at reflux overnight. After cooling to room temperature the solution

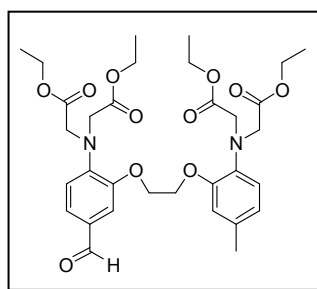
---

was diluted with toluene and washed with water. The organic phase was dried over  $\text{MgSO}_4$ , filtered and evaporated to dryness. The crude product was recrystallized from hot EtOH to yield 18.1 g (30.1 mmol, 35 %) of product.

$^1\text{H}$  NMR (300 MHz,  $\text{CDCl}_3$ ):  $\delta$  = 6.88 – 6.67 (m, 7H), 4.27 (s, 4H), 4.13 (m, 8H), 4.04 (m, 8H), 2.26 (s, 3H), 1.49 (m, 12H).

Spectra conform with literature

### BAPTA-aldehyde (**70**)<sup>5</sup>

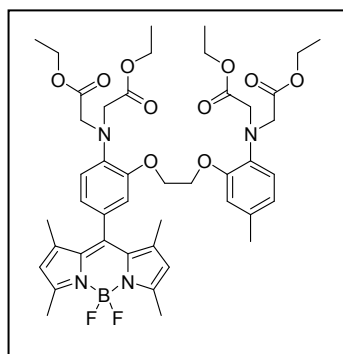


methyl-BAPTA (0.76 g, 1.26 mmol) was dissolved in a mixture of DMF (11 mL) and pyridine (0.14 mL).  $\text{POCl}_3$  (1.0 mL, 11.1 mmol) was added dropwise and the reaction mixture stirred at room temperature overnight. Then the reaction was heated to 60 °C for 1 h. The reaction was quenched with a solution of NaOH (1 M) and the aqueous phase was extracted with DCM (3x). After washing the organic phase with brine (2x), the organic phase was dried over  $\text{MgSO}_4$ , filtered and the solvent evaporated under reduced pressure. The crude product was triturated with isopropanol to yield 345 mg (0.55 mmol, 43 %) of pure product.

$^1\text{H}$  NMR (300 MHz,  $\text{CDCl}_3$ ):  $\delta$  = 9.78 (s, 1H), 7.38 (dd,  $J$  = 1.73 Hz,  $J$  = 5.88 Hz, 1H), 6.88 – 6.82 (m, 1H), 6.77 – 6.72 (m, 2H), 6.67 – 6.58 (m, 2H), 4.33 – 4.26 (m, 4H), 4.23 (s, 4H), 4.11 – 4.00 (m, 12H), 2.25 (s, 3H), 1.18 – 1.12 (m, 12H).

Spectra conform with literature

### BAPTA-BODIPY ester (**71**)



In a two neck round bottom flask under  $\text{N}_2$ , BAPTA carboxaldehyde (0.4 g, 0.63 mmol) was dissolved in freshly distilled dichloromethane (80 mL). 2,4-dimethylpyrrole (0.2 mL, 1.9 mmol) and a drop of TFA were added and the mixture was stirred at room temperature overnight. *p*-Chloranil (0.16 mg, 0.63 mmol) in DCM (20 mL) was added dropwise and the mixture was stirred for 30 min at room temperature. Then

---

triethylamine (4.0 mL) and borontrifluoride etherate (4.0 mL) were added and the mixture was stirred for two additional hours. Water was added and the product was extracted with DCM. The organic phase was dried over MgSO<sub>4</sub> and the solvent was evaporated. The crude product was purified by chromatography PTE/EtAc, 80:20, v/v) followed by a recrystallization in ethanol to give 0.14 g of product as an orange solid, (0.16 mmol, 26 % yield).

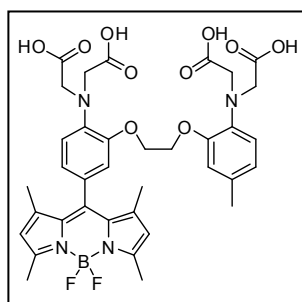
<sup>1</sup>H NMR (300 MHz, CDCl<sub>3</sub>): δ = 6.87 (d, *J* = 8.5 Hz, 1H), 7.79-7.74 (m, 3H), 6.67 (d, *J* = 7.2 Hz, 2H), 5.97 (s, 2H), 4.25 (m, 4H), 4.21 (s, 4H), 4.10 (q, *J* = 7.1 Hz, 4H), 4.09 (s, 4H), 4.07 (q, *J* = 7.1 Hz, 2H), 2.54 (s, 6H), 2.24 (s, 3H), 1.48 (s, 6H), 1.19 (t, *J* = 7.1 Hz, 6H), 1.16 (t, *J* = 7.1 Hz, 6H).

<sup>13</sup>C NMR (75 MHz, CDCl<sub>3</sub>): δ = 171.33, 171.23, 155.28, 150.79, 150.28, 143.10, 140.12, 137.10, 132.24, 128.04, 122.26, 121.13, 121.02, 119.76, 119.08, 115.40, 113.22, 67.55, 67.23, 60.84, 60.52, 53.67, 20.86, 14.53, 14.13, 14.09.

HRMS (ESI): Calc. *m/z* = 871.3871 for C<sub>44</sub>H<sub>55</sub>BF<sub>2</sub>N<sub>4</sub>O<sub>10</sub>Na

Found *m/z* = 871.3871 [M+Na]<sup>+</sup>

### BAPTA-BODIPY (72)



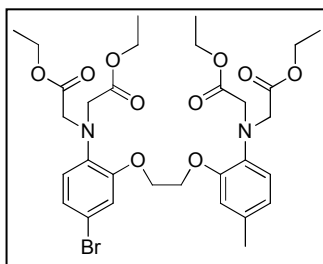
The BAPTA-BODIPY-ester (5 mg, 6 μmol) was dissolved in a mixture of THF (1 mL) and MeOH (1 mL), then LiOH.H<sub>2</sub>O (5 mg, 120 μmol) and a drop of water was added and the mixture was stirred at room temperature overnight. The solvent was evaporated under reduced pressure and the crude product was dispersed in ethyl acetate and centrifuged. The solvent was pipetted off, the solid dissolved in water and acidified with 1M HCl. The precipitate was dissolved in an appropriate amount of KOH solution to form the potassium salt and freeze dried to yield the title compound quasi-quantitatively.

HRMS (FD): Calc. *m/z* = 736.2727 for C<sub>36</sub>H<sub>39</sub>BF<sub>2</sub>N<sub>4</sub>O<sub>10</sub>

Found *m/z* = 736.2718 [M]<sup>+</sup>

---

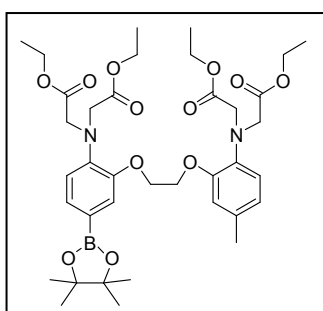
### Bromo BAPTA (73)<sup>6</sup>



BAPTA (1.5 g, 2.5 mmol), was dissolved in dry DCM (60 ml) under argon atmosphere and cooled to 0 °C. Br<sub>2</sub> (0.25 ml, 4.9 mmol) in dry DCM (10 ml) was added dropwise via a syringe and the resulting solution was stirred at room temperature overnight. The reaction was quenched with 10 % aqueous NaOH, extracted with DCM and washed with water and brine. The combined organic phase was dried over MgSO<sub>4</sub>, filtered and the solvent evaporated. The crude was purified by recrystallization from ethanol yielding 1.23 g (1.80 mmol, 72 %) title compound.

<sup>1</sup>H NMR (300 MHz, CDCl<sub>3</sub>): δ = 7.38 (dd, *J* = 1.7 Hz, *J* = 5.8 Hz, 1H), 6.88 – 6.82 (m, 1H), 6.77 – 6.72 (m, 2H), 6.67 – 6.58 (m, 2H), 4.33 – 4.26 (m, 4H), 4.23 (s, 4H), 4.11 – 4.00 (m, 12H), 2.25 (s, 3H), 1.18 – 1.12 (m, 12H). Spectra conform with literature

### BAPTA boronic ester (74)



In a sealed tube, bromo-BAPTA (100 mg, 0.15 mmol), bis(pinacolato) diboron (41 mg, 0.16 mmol), potassium acetate (43 mg, 0.44 mmol) and dry DMF (2 mL) were degassed under argon during 20 min. PdCl<sub>2</sub>(dppf) (5 mg, 7 μmol, 5%) was added and the mixture was heated under microwave irradiation at 120 °C for 15 min. The crude reaction mixture was passed through a silica plug eluting with Et<sub>2</sub>O and the solvent was removed under reduced pressure. The product was further purified by recrystallisation in ethanol to yield **6** as a white solid (70 mg, 65%).

<sup>1</sup>H NMR (300 MHz, CDCl<sub>3</sub>): δ = 7.32 (dd, *J* = 7.9 Hz, *J* = 1.2 Hz, 1H), 7.24 (d, *J* = 1.2 Hz, 1H), 6.77 - 6.64 (m, 4H), 4.29 - 4.27 (m, 4H), 4.17 (s, 4H), 4.15 (s, 4H), 4.05 (q, *J* = 7.1 Hz, 4H), 4.04 (q, *J* = 7.1 Hz, 2H), 2.25 (s, 3H), 1.31 (s, 12H), 1.13 (t, *J* = 7.1 Hz, 12H).

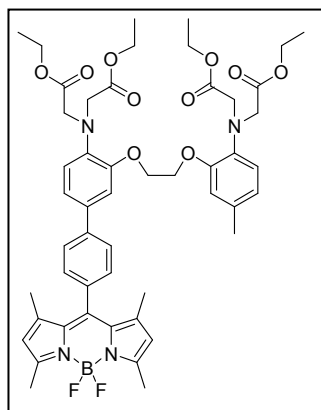
<sup>13</sup>C NMR (75 MHz, CDCl<sub>3</sub>): δ = 171.58, 171.36, 150.27, 149.24, 142.04, 136.87, 131.94, 128.71, 121.71, 119.26, 118.65, 117.54, 114.33, 83.50, 67.05, 66.97, 60.76, 60.60, 53.60, 53.53, 24.82, 20.90, 14.05, 14.02.

HRMS (ESI): Calc. *m/z* = 751.3583 for C<sub>37</sub>H<sub>53</sub>BN<sub>2</sub>O<sub>12</sub>Na

Found *m/z* = 751.3578 [M+Na]<sup>+</sup>

---

### BAPTA-PH-BODIPY ester (**75**)



In a Schlenk tube, BAPTA boronic ester (50 mg, 0.07 mmol), iodoBODIPY (28 mg, 0.06 mmol) and Pd(PPh<sub>3</sub>)<sub>4</sub> (7 mg, 6 μmol, 10 mol%), were dissolved in freshly distilled THF (5 mL). An aqueous solution of Na<sub>2</sub>CO<sub>3</sub> (0.1 mL, 2 M), previously degassed by 20 min argon bubbling, was added and the mixture was heated at 65 °C overnight. The crude reaction mixture was evaporated under reduced pressure and the product was purified by column chromatography PTE/EtAc (70/30, v/v) followed by recrystallisation in EtOH to yield 38 mg (0.041 mmol, 45 %) as an orange-red crystalline powder.

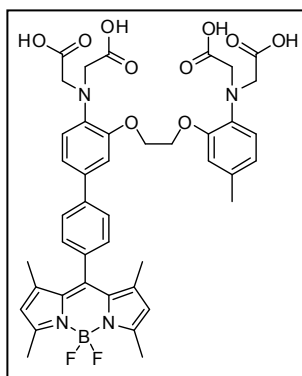
<sup>1</sup>H NMR (300 MHz, CDCl<sub>3</sub>): δ = 7.67 (d, *J* = 8.2 Hz, 2H), 7.30 (d, *J* = 7.9 Hz, 2H), 7.23 – 7.19 (m, 2H), 6.90 (d, *J* = 8.2 Hz, 1H), 6.77 (d, *J* = 7.8 Hz, 1H), 6.70 - 6.67 (m, 2H), 5.99 (s, 2H), 4.40 (m, 2H), 4.32 (m, 2H), 4.21 (s, 4H), 4.13 (s, 4H), 4.10 (q, *J* = 7.1 Hz, 4H), 4.06 (q, *J* = 7.1 Hz, 2H), 2.56 (s, 6H), 2.26 (s, 3H), 1.45 (s, 6H), 1.19 (t, *J* = 7.1 Hz, 6H), 1.16 (t, *J* = 7.1 Hz, 6H);

<sup>13</sup>C NMR (75 MHz, CDCl<sub>3</sub>): δ = 171.59, 171.50, 171.37, 171.33, 155.41, 150.53, 150.28, 149.25, 143.13, 142.05, 141.65, 141.19, 139.39, 136.95, 136.88, 133.74, 133.34, 132.13, 131.96, 131.48, 128.72, 128.68, 128.41, 127.01, 126.67, 121.95, 121.72, 121.17, 121.13, 120.15, 119.46, 119.27, 119.18, 118.66, 117.55, 114.72, 114.35, 112.42, 83.51, 67.53, 67.08, 66.98, 60.80, 60.60, 53.62, 24.83, 20.92, 14.60, 14.09.

HRMS (ESI): Calc. *m/z* = 947.4184 for C<sub>50</sub>H<sub>59</sub>BF<sub>2</sub>N<sub>4</sub>O<sub>10</sub>Na

Found *m/z* = 947.4183 [M+Na]<sup>+</sup>

### BAPTA-PH-BODIPY (76)

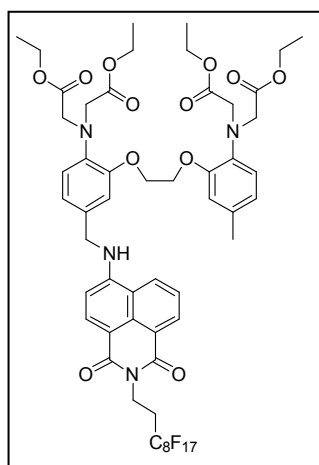


The BAPTA-PH-BODIPY-ester (8 mg, 9  $\mu\text{mol}$ ) was dissolved in a mixture of THF (1 mL) and MeOH (1 mL), then LiOH.H<sub>2</sub>O (5 mg, 120  $\mu\text{mol}$ ) and a drop of water was added and the mixture was stirred at room temperature overnight. The solvent was evaporated under reduced pressure and the crude product was dispersed in ethyl acetate and centrifuged. The solvent was pipetted off, the solid was dissolved in water and acidified with 1M HCl. The precipitate was dissolved in an appropriate amount of KOH solution to form the potassium salt and freeze dried to yield the title compound quasi quantitatively.

HRMS (FD): Calc.  $m/z = 812.3040$  for C<sub>42</sub>H<sub>43</sub>BF<sub>2</sub>N<sub>4</sub>O<sub>10</sub>

Found  $m/z = 812.3041$  [M]<sup>+</sup>

### BANIF ester (78)



BAPTA-aldehyde (55 mg, 0.087 mmol) and C<sub>8</sub>F<sub>17</sub>-aminonaphthalimide (52 mg, 0.079 mmol) were dissolved in hexafluoroisopropanol (1 mL) and 5 drops of TFA were added. The reaction mixture was stirred at 80 °C for 2 h. The reaction was followed by TLC using PTE/EtAc (60/40, v/v). After cooling to room temperature (9 mg, 0.237 mmol) NaBH<sub>4</sub> was added and the reaction was followed by TLC using DCM/EtAc (90/10, v/v). Since the reaction did not proceed to completion, the reaction media was acidified with TFA and another equivalent of aldehyde was added.

After repeating the reduction with NaBH<sub>4</sub>, the mixture was filtered, evaporated and the crude product was purified by column chromatography using DCM/EtAc (90/10, v/v). 50 mg (0.039 mmol, 47 % yield) of the product was obtained as a yellow solid.

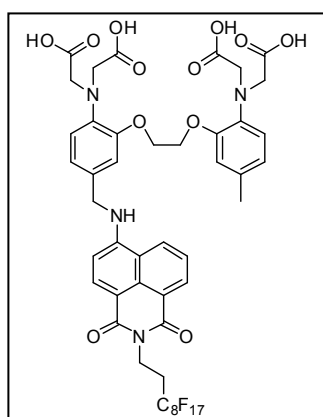
<sup>1</sup>H NMR (300 MHz, CDCl<sub>3</sub>):  $\delta = 8.59$  (d,  $J = 8.5$  Hz, 1H), 8.45 (d,  $J = 8.3$  Hz, 1H), 8.14 (d,  $J = 8.3$  Hz, 1H), 7.61 (t,  $J = 7.3$  Hz, 1H), 6.97 – 6.92 (m, 2H), 6.83 (d,  $J = 7.2$  Hz, 1H), 6.78 – 6.75 (m, 2H), 6.68 – 6.65 (m, 2H), 5.70 (m, 1H), 4.54 – 4.59 (m, 4H), 4.30 – 4.26 (m, 4H), 4.16 – 3.99 (m, 16H), 2.66 – 2.49 (m, 2H), 2.24 (s, 3H), 1.20 – 1.12 (m, 12H).

---

$^{13}\text{C}$  NMR (75 MHz,  $\text{CDCl}_3$ ):  $\delta = 171.66, 171.48, 164.56, 163.81, 150.88, 150.47, 139.63, 137.01, 125.06, 122.88, 120.50, 119.36, 114.92, 60.97, 60.74, 53.78, 21.05, 14.25$ .

$^{19}\text{F}$  NMR (400 MHz,  $\text{CDCl}_3$ ):  $\delta = -81.71$  (t,  $J = 10.2$  Hz, 3F),  $-115.26 - -115.42$  (m, 2F),  $-122.59$  (s, br, 2F),  $-122.83$  (s, br, 4F),  $-123.64$  (s, br, 2F),  $-124.37$  (s, br, 2F),  $-127.03$  (s, br, 2F).

### BANIF (79)

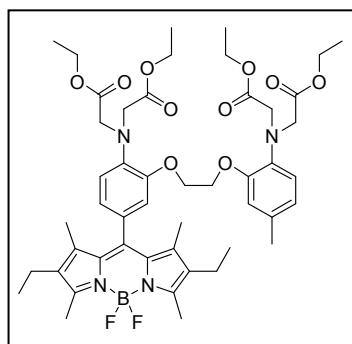


The BANIF-ester (15 mg, 12  $\mu\text{mol}$ ) was dissolved in a mixture of THF (1 mL) and MeOH (1 mL), then LiOH.H<sub>2</sub>O (10 mg, 250  $\mu\text{mol}$ ) and a drop of water was added and the mixture was stirred at room temperature overnight. The solvent was evaporated under reduced pressure and the crude product was dispersed in ethyl acetate and centrifuged. The solvent was pipetted off, the solid was dissolved in water and acidified with 1M HCl. The precipitate was dissolved in an appropriate amount of KOH solution to form the potassium salt and freeze dried to yield the title compound quasi-quantitatively.

MS (MALDI): Calc.  $m/z = 1312.0$  for  $\text{C}_{46}\text{H}_{34}\text{F}_{17}\text{N}_4\text{O}_{12}\text{K}_4$

Found  $m/z = 1312.5$  [ $\text{M}$ ]<sup>+</sup> (Potassium salt)

### BAPTA-BODIPY2 ester (80)



In a round bottom flask, BAPTA-aldehyde (345 mg, 0.55 mmol) and kryptopyrrole (0.22 mL, 1.64 mmol) were dissolved in freshly-distilled DCM (80 mL) and a drop of TFA was added. The reaction mixture was stirred at room temperature until the aldehyde was consumed. The p-chloranil (135 mg, 0.55 mmol) in DCM (20 mL) was added and stirring was continued for 30 min. Borontrifluoride diethyl etherate (3.45 mL) and TEA (3.45 mL) were added and stirring was continued for 2 h. H<sub>2</sub>O was added and the aqueous phase was extracted with DCM (3x) and dried over MgSO<sub>4</sub>. After filtration, the solvent was evaporated and the crude product was purified by column chromatography using

cyclohexane/EtAc (80/20, v/v). The product was further purified by recrystallisation from hot EtOH, yielding 232 mg (0.26 mmol, 47 % yield).

$^1\text{H}$  NMR (400 MHz,  $\text{CDCl}_3$ ):  $\delta$  = 6.88 (d,  $J$  = 8.57 Hz, 1H), 6.78 – 6.76 (m, 3H), 6.69 – 6.67 (m, 2H), 4.28 – 4.23 (m, 4H), 4.22 (s, 4H), 4.15 – 4.03 (m, 12H), 2.52 (s, 6H), 2.30 (q,  $J$  = 7.48 Hz, 4H), 2.24 (s, 3H), 1.39 (s, 6H), 1.22 – 1.16 (m, 12H), 0.98 (t,  $J$  = 7.50 Hz, 6H).

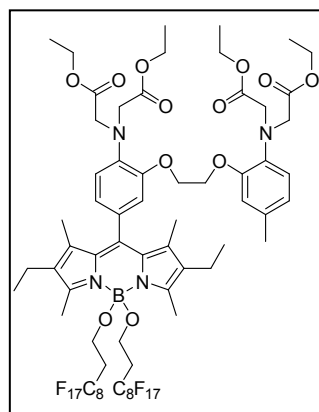
$^{13}\text{C}$  NMR (75 MHz,  $\text{CDCl}_3$ ):  $\delta$  = 171.54, 171.46, 153.72, 150.90, 150.45, 140.13, 138.55, 137.25, 132.77, 132.39, 131.13, 129.10, 122.37, 121.57, 119.89, 77.37, 61.01, 60.70, 53.83, 21.05, 17.22, 14.76, 14.28, 12.01.

$^{19}\text{F}$  NMR (400 MHz,  $\text{CDCl}_3$ ):  $\delta$  = -146.82 (dd,  $J$  = 30.59 Hz,  $J$  = 65.61 Hz, 2F).

HRMS (FD): Calc.  $m/z$  = 927.4498 for  $\text{C}_{48}\text{H}_{63}\text{BN}_4\text{O}_{10}\text{F}_2\text{Na}$

Found  $m/z$  = 927.4497  $[\text{M}+\text{Na}]^+$

#### $\text{C}_8\text{F}_{17}$ -BAPTA-BODIPY ester (**81**)



BAPTA-BODIPY2 (50 mg, 0.055 mmol) was dissolved in DCM (5 ml) and  $\text{AlCl}_3$  (11 mg, 0.082 mmol) was added portion wise. The reaction was stirred for 20 min at room temperature, then  $\text{C}_8\text{F}_{17}$ -ethanol (56 mg, 0.121 mmol) was added in one portion and stirring was continued for 1 h. The reaction was cooled in an ice bath and sat. Sodium bicarbonate solution was added until  $\text{CO}_2$  development stopped. The aqueous phase was extracted with DCM (3x) and the organic phase was washed with brine (2x). The aqueous phase was

dried over  $\text{MgSO}_4$ , filtered and evaporated to dryness. The crude product was purified by column chromatography using PTE/EtAc (90/10, v/v) to obtain 25 mg (0.014 mmol, 26 % yield) of the product as an amorphous orange solid.

$^1\text{H}$  NMR (400 MHz,  $\text{DMSO-d}_6$ ):  $\delta$  = 6.89 (d,  $J$  = 7.90 Hz, 1H), 6.79 – 6.74 (m, 3H), 6.69 – 6.68 (m, 2H), 4.27 (s, br, 4H), 4.23 (s, 4H), 4.13 – 4.05 (m, 12H), 4.00 (dd,  $J$  = 6.02 Hz,  $J$  = 11.95 Hz, 4H), 3.35 – 3.26 (m, 4H), 2.51 (s, 6H), 2.31 (q,  $J$  = 6.87 Hz, 4H), 2.25 (s, 3H), 1.40 (s, 6H), 1.21 – 1.16 (m, 12H), 0.98 (t,  $J$  = 7.44 Hz, 6H).

$^{13}\text{C}$  NMR (75 MHz,  $\text{CDCl}_3$ ):  $\delta$  = 171.54, 153.98, 150.93, 150.45, 140.38, 140.08, 137.60, 137.26, 133.01, 132.41, 132.35, 129.34, 122.37, 121.72, 119.91, 119.28, 115.48, 113.49,

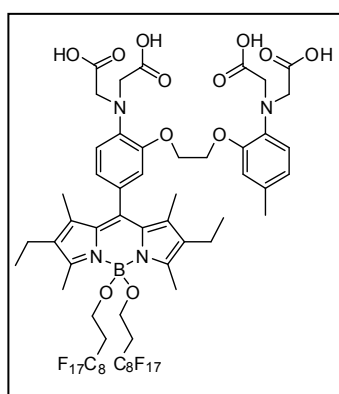
---

110.92, 108.47, 67.61, 67.32, 61.01, 60.66, 55.43, 53.82, 34.07, 33.28, 29.85, 21.01, 17.24, 14.63, 14.25, 12.56, 12.09.

$^{19}\text{F}$  NMR (400 MHz,  $\text{CDCl}_3$ ):  $\delta = -81.73$  (t,  $J = 9.71$  Hz, 6F),  $-114.30 - -114.77$  (m, 4F),  $-122.68$  (s, 4F),  $-122.89$  (s, 8F),  $-123.68$  (s, 4F),  $-124.65$  (s, 2F),  $-124.87$  (s, 2F),  $-127.07$  (s, 4F).

HRMS (FD):            Calc.  $m/z = 1815.4628$  for  $\text{C}_{68}\text{H}_{71}\text{BN}_4\text{O}_{12}\text{F}_{34}\text{Na}$   
                             Found  $m/z = 1815.4510$   $[\text{M}+\text{Na}]^+$

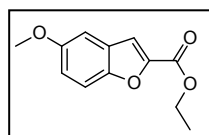
### $\text{C}_8\text{F}_{17}$ -BAPTA-BODIPY (**82**)



The  $\text{C}_8\text{F}_{17}$ -BAPTA-BODIPY-ester (20 mg, 11  $\mu\text{mol}$ ) was dissolved in a mixture of THF (1 mL) and MeOH (1 mL), then LiOH.H<sub>2</sub>O (10 mg, 250  $\mu\text{mol}$ ) and a drop of water was added and the mixture was stirred at room temperature overnight. The solvent was evaporated under reduced pressure and the crude product was dispersed in ethyl acetate and centrifuged. The solvent was pipetted off, the solid was dissolved in water and acidified with 1M HCl. The precipitate was dissolved in an appropriate amount of KOH solution to form the potassium salt and freeze dried to yield the title compound quasi-quantitatively.

MS (MALDI)            Calc.  $m/z = 1704.4$  for  $\text{C}_{60}\text{H}_{51}\text{BF}_{34}\text{N}_4\text{O}_{12}\text{Li}_4$   
                             Found  $m/z = 1704.9$   $[\text{M}]^+$  (Lithium salt)

### Ethyl 5-methoxybenzofuran-2-carboxylate (**84**)



5-Methoxysalicylaldehyde (5.5 g, 36.2 mmol) and ethyl bromo-acetate (4.7 ml, 43.1 mmol) were dissolved in AcCN (200 mL) and  $\text{K}_2\text{CO}_3$  (14.9 g, 108 mmol) was added. The reaction mixture was stirred under reflux overnight, then cooled to room temperature and filtered. The solvent was evaporated and the crude product was purified by column chromatography using PTE/EtAc (90/10, v/v) to yield 3.5 g (15.9 mmol, 44 %) of the product as a white solid.

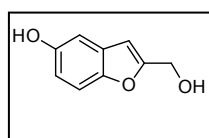
---

$^1\text{H}$  NMR (300 MHz, DMSO):  $\delta$  = 7.63 (d,  $J$  = 9.0 Hz, 1H), 7.27 (d,  $J$  = 2.6 Hz, 1H), 7.12 (dd,  $J$  = 9.0 Hz,  $J$  = 2.6 Hz, 1H), 6.85 (s, 1H), 4.35 (q,  $J$  = 7.2 Hz, 2H), 3.80 (s, 3H), 1.33 (t,  $J$  = 7.2 Hz, 3H).

$^{13}\text{C}$  NMR (75 MHz,  $\text{CDCl}_3$ ):  $\delta$  = 159.65, 156.64, 150.95, 146.44, 127.58, 117.59, 113.91, 113.08, 103.87, 61.58, 55.95, 14.46

HRMS (EI):                Calc.  $m/z$  = 220.0713 for  $\text{C}_{12}\text{H}_{12}\text{O}_4$   
                                 Found  $m/z$  = 220.7356  $[\text{M}]^+$

### 2-(Hydroxymethyl)benzofuran-5-ol (**85**)



Ethyl 5-methoxybenzofuran-2-carboxylate (5.7 g, 25.9 mmol) was dissolved in DCM (70 mL) and cooled to  $-60\text{ }^\circ\text{C}$ . A 1 M solution of  $\text{BBr}_3$  in DCM (53 mL) was added dropwise via a syringe pump. The reaction was stirred for 2 h and subsequently a saturated solution of  $\text{NaHCO}_3$  was added, the phases were separated and the aqueous phases were extracted with EtAc. The combined organic phases were dried over  $\text{MgSO}_4$ , filtered and evaporated. The crude product was dissolved in THF (10 mL) and added dropwise to a solution of  $\text{LiAlH}_4$  (994 mg, 26.8 mmol) in THF (130 mL) and stirred for 30 min. A saturated  $\text{NH}_4\text{Cl}$  solution was added and extracted with EtAc, dried over  $\text{MgSO}_4$  and evaporated after filtration. The crude product was purified by column chromatography using PTE/EtAc (50/50, v/v) to yield 2.0 g (12.1 mmol, 48 %) of product.

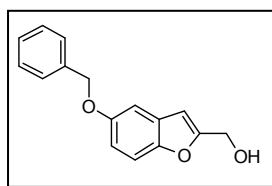
$^1\text{H}$  NMR (300 MHz, MeOD):  $\delta$  = 7.18 (d,  $J$  = 8.5 Hz, 1H), 6.70 (dd,  $J$  = 9.8 Hz,  $J$  = 2.4 Hz, 1H), 6.45 (s, 1H), 4.59 (s, 2H), 3.46 (s, 3H).

$^{13}\text{C}$  NMR (75 MHz, MeOD):  $\delta$  = 159.80, 154.60, 130.93, 114.23, 112.47, 107.08, 105.01, 58.48.

HRMS (ESI): Calc.  $m/z$  = 163.0399 for  $\text{C}_9\text{H}_7\text{O}_3$   
                                 Found  $m/z$  = 163.0400  $[\text{M}-\text{H}]^-$

---

(5-(Benzyloxy)benzofuran-2-yl)methanol (**86**)



2-(Hydroxymethyl)benzofuran-5-ol (1.9 g, 11.6 mmol) and benzyl bromide (1.5 ml, 12.7 mmol) were dissolved in AcCN (70 mL) and  $K_2CO_3$  (3.0 g, 21.7 mmol) was added. The reaction mixture was heated to reflux for 5 h, then subsequently cooled to room temperature and filtered. The crude product was purified by column chromatography using PTE/EtAc (60/40, v/v) to yield 2.67 g (10.5 mmol, 95 %) of product.

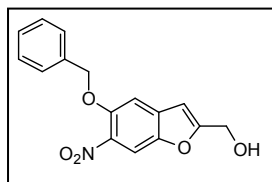
$^1H$  NMR (300 MHz,  $CDCl_3$ ):  $\delta$  = 7.47 – 7.33 (m, 6H), 7.09 (d,  $J$  = 2.6 Hz, 1H), 6.97 (dd,  $J$  = 8.9 Hz,  $J$  = 2.4 Hz, 1H), 6.59 (s, 1H), 5.09 (s, 1H), 4.75 (s, 1H), 1.31 (s, br, 1H).

$^{13}C$  NMR (75 MHz,  $CDCl_3$ ):  $\delta$  = 157.41, 155.20, 137.3, 128.66, 127.59, 114.02, 111.80, 105.26, 104.42, 71.00, 58.27.

HRMS (ESI): Calc.  $m/z$  = 255.0943 for  $C_{16}H_{15}O_3$

Found  $m/z$  = 255.0948  $[M+H]^+$

(5-(benzyloxy)-6-nitrobenzofuran-2-yl)methanol (**87**)



(5-(Benzyloxy)benzofuran-2-yl)methanol (2.7g, 10.5 mmol) were dissolved in DCM (60 mL) and cooled to  $-20$  °C. Fuming  $HNO_3$  (1.06 mL, 25.2 mmol) in DCM (30 mL) was added dropwise via a syringe pump. After the completion of the reaction, water was added and the aqueous phase was extracted with DCM (3x) The organic phase was washed with saturated NaCl solution and then dried over  $MgSO_4$ . The solvent was evaporated after filtration and the crude product was purified by column chromatography using PTE/EtAc (50/50, v/v) to yield 2.0 g (6.69 mmol, 63 %) of product.

$^1H$  NMR (300 MHz,  $CDCl_3$ ):  $\delta$  = 8.02 (s, 1H), 7.51 – 7.50 (m, 2H), 7.43 – 7.33 (m, 3H), 7.20 (s, 1H), 6.67 (s, 1H), 5.25 (s, 2H), 4.79 (s, 2H), 1.99 (s, br, 1H).

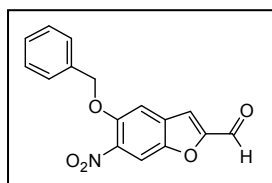
$^{13}C$  NMR (75 MHz,  $CDCl_3$ ):  $\delta$  = 162.49, 149.09, 147.78, 135.97, 133.40, 128.81, 128.31, 127.22, 109.15, 106.73, 104.11, 72.29, 58.19.

HRMS (ESI): Calc.  $m/z$  = 322.0690 for  $C_{16}H_{13}NO_5Na$

Found  $m/z$  = 322.0685  $[M+Na]^+$

---

5-(benzyloxy)-6-nitrobenzofuran-2-carbaldehyde (**88**)



PCC (2.9 g, 13.4 mmol) was dissolved in DCM (20 mL) and a solution of (5-(benzyloxy)-6-nitrobenzofuran-2-yl)methanol (2.0 g, 6.6 mmol) in DCM (60 mL) was added in one shot. The reaction mixture was stirred at room temperature for 4 h and subsequently washed with a saturated solution of NaCl (2x) NaHCO<sub>3</sub> (2x) and water. The organic phase was dried over MgSO<sub>4</sub>, filtered and evaporated. The crude product was purified by column chromatography using PTE/EtAc (60/40, v/v) to yield 1.3 g (4.37 mmol, 66 %) of the aldehyde.

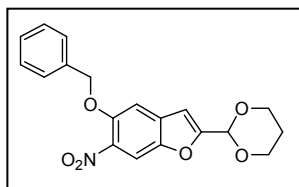
<sup>1</sup>H NMR (300 MHz, CDCl<sub>3</sub>): δ = 9.91 (s, 1H), 8.07 (s, 1H), 7.50 – 7.36 (m, 6H), 5.27 (s, 1H).

<sup>13</sup>C NMR (75 MHz, CDCl<sub>3</sub>): δ = 179.70, 156.04, 148.96, 141.62, 135.39, 130.65, 128.93, 128.51, 127.17, 115.47, 110.23, 108.21, 72.15.

HRMS (ESI): Calc. m/z = 296.0570 for C<sub>16</sub>H<sub>10</sub>NO<sub>5</sub>

Found m/z = 296.0564 [M-H]<sup>-</sup>

5-(Benzyloxy)-2-(1,3-dioxan-2-yl)-6-nitrobenzofuran (**89**)



5-(benzyloxy)-6-nitrobenzofuran-2-carbaldehyde (1.4 g, 4.7 mmol), propane diol (5 mL) and p-TsOH monohydrate (0.2 g, 1.05 mmol) were dissolved in DCM (30 mL) and heated to reflux for 1 h. After 30 min, some molecular sieves were added. The reaction was stopped by the addition of a saturated solution of NaHCO<sub>3</sub> and the aqueous phase was extracted (3x) with DCM. The combined organic phases were washed with brine (2x) and water and subsequently dried over MgSO<sub>4</sub>. After filtration, the solvent was evaporated to yield 1.6 g (4.5 mmol, 95 %) of product.

<sup>1</sup>H NMR (300 MHz, CDCl<sub>3</sub>): δ = 8.03 (s, 1H), 7.49 – 7.46 (m, 2H), 7.42 – 7.32 (m, 3H), 7.23 (s, 1H), 6.80 (s, 1H), 5.70 (s, 1H), 5.24 (s, 2H), 4.30 (dd, *J* = 10.8 Hz, *J* = 5.2 Hz, 2H), 4.02 (dt, *J* = 12.1 Hz, *J* = 2.6 Hz, 2H), 2.36 – 2.202 (m, 1H), 1.55 – 1.47 (m, 1H).

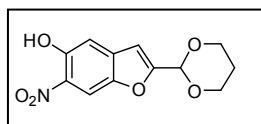
<sup>13</sup>C NMR (75 MHz, CDCl<sub>3</sub>): δ = 158.72, 149.01, 138.30, 135.94, 132.58, 128.78, 127.22, 109.49, 107.12, 104.42, 95.78, 72.25, 7.48, 25.69.

---

HRMS (FD): Calc.  $m/z = 355.1062$  for  $C_{19}H_{17}NO_6$

Found  $m/z = 355.1056$   $[M]^+$

2-(1,3-Dioxan-2-yl)-6-nitrobenzofuran-5-ol (**90**)



5-(Benzyloxy)-2-(1,3-dioxan-2-yl)-6-nitrobenzofuran (1.1 g, 3.1 mmol) was dissolved in  $CHCl_3$  (85 mL) and cooled to  $0\text{ }^\circ\text{C}$ .  $AlCl_3$  (0.8 g, 6.1 mmol) was added in small portions and the reaction mixture was

heated to  $60\text{ }^\circ\text{C}$  for 1 h. The reaction was cooled, a saturated solution of  $NaHCO_3$  was added and the aqueous phase was extracted with DCM. The combined organic phases were dried over  $MgSO_4$ , filtered and evaporated and the crude product was purified by column chromatography using PTE/DCM (50/50, v/v) to yield 570 mg (2.15 mmol, 69 %) of product.

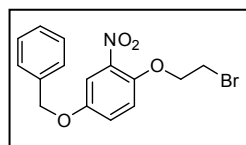
$^1H$  NMR (300 MHz,  $CDCl_3$ ):  $\delta = 10.48$  (s, 1H), 8.23 (s, 1H), 7.23 (s, 1H), 6.78 (s, 1H), 5.69 (s, 1H), 4.35 – 4.26 (m, 2H), 4.08 – 3.95 (m, 2H), 2.40 – 2.16 (s, 1H), 1.55 – 1.48 (s, 1H).

$^{13}C$  NMR (75 MHz,  $CDCl_3$ ):  $\delta = 160.80$ , 151.54, 147.75, 137.05, 131.44, 109.79, 17.81, 104.25, 95.66, 67.50, 25.68.

HRMS (ESI): Calc.  $m/z = 264.0517$  for  $C_{12}H_{10}NO_6$

Found  $m/z = 264.0513$   $[M-H]^-$

4-(benzyloxy)-1-(2-bromoethoxy)-2-nitrobenzene (**90-1**)



4-(Benzyloxy)-2-nitrophenol (1.0 g, 3.5 mmol) was dissolved in AcCN (40 mL) and  $K_2CO_3$  (1.4 g, 10.6 mmol) was added. The mixture was heated to  $60\text{ }^\circ\text{C}$  and a solution of 1,2-dibromoethane (3.0 mL, 35 mmol) in

AcCN (50 mL) was added dropwise. The reaction mixture was refluxed for 3 h, then cooled and filtered. The solid was washed with DCM and the combined filtrates were evaporated. The crude product was purified by column chromatography using PTE/DCM (60/40, v/v) to yield 0.78 g (2.22 mmol, 64 %) of product.

$^1H$  NMR (300 MHz,  $CDCl_3$ ):  $\delta = 7.46$  (d,  $J = 3.0$  Hz, 1H), 7.42 – 7.32 (m, 5H), 7.16 (dd,  $J = 9.0$  Hz,  $J = 3.0$  Hz, 1H), 7.06 (d,  $J = 9.4$  Hz, 1H), 5.07 (s, 2H), 4.36 (t,  $J = 6.6$  Hz, 2H), 3.65 (t,  $J = 6.6$  Hz, 2H).

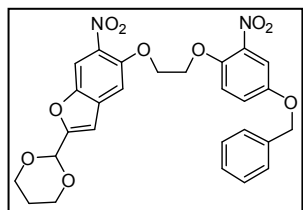
---

$^{13}\text{C}$  NMR (75 MHz,  $\text{CDCl}_3$ ):  $\delta = 153.14, 145.91, 136.00, 128.87, 128.50, 127.66, 121.62, 118.36, 111.28, 71.12, 28.56$ .

HRMS (FD): Calc.  $m/z = 351.0095$  for  $\text{C}_{15}\text{H}_{14}\text{NO}_4\text{Br}$

Found  $m/z = 351.01062$   $[\text{M}]^+$

#### 5-(2-(4-(benzyloxy)-2-nitrophenoxy)ethoxy)-2-(1,3-dioxan-2-yl)-6-nitrobenzofuran (**91**)



2-(1,3-Dioxan-2-yl)-6-nitrobenzofuran-5-ol (0.50 g, 1.88 mmol) and 4-(benzyloxy)-1-(2-bromoethoxy)-2-nitrobenzene (0.64 g, 1.82 mmol) were dissolved in DMF and  $\text{K}_2\text{CO}_3$  (0.13 g, 0.94 mmol) was added. The reaction mixture was heated to  $120\text{ }^\circ\text{C}$  for 1 h, then cooled to room temperature and brine was added. The aqueous phase was extracted with EtAc (3x) and the combined organic phases were washed with brine (2x) and water. The organic phase was dried over  $\text{MgSO}_4$ , filtered and evaporated. The crude was dissolved in a minimum amount of acetone and under stirring PTE was added. The product precipitated from the solution to yield 0.74 g (1.37 mmol, 75 %) of pure product.

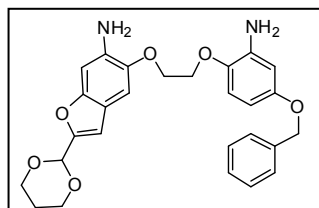
$^1\text{H}$  NMR (300 MHz,  $\text{CDCl}_3$ ):  $\delta = 8.00$  (s, 1H), 7.45 – 7.44 (m, 1H), 7.41 – 7.34 (m, 6H), 7.19 (d,  $J = 1.6$  Hz, 2H), 6.87 (s, 1H), 5.71 (s, 1H), 5.06 (s, 2H), 4.52 – 4.46 (m, 4H), 4.30 (dd,  $J = 10.8$  Hz,  $J = 4.7$  Hz, 2H), 4.02 (dt,  $J = 12.4$  Hz,  $J = 2.6$  Hz, 2H), 2.36 – 2.20 (m, 1H), 1.54 – 1.48 (m, 1H).

$^{13}\text{C}$  NMR (75 MHz,  $\text{CDCl}_3$ ):  $\delta = 158.81, 153.00, 149.15, 147.89, 146.56, 140.73, 138.35, 136.10, 132.85, 128.84, 128.45, 127.68, 121.79, 118.53, 111.27, 109.35, 108.31, 104.64, 95.80, 71.11, 70.15, 67.49, 25.70$ .

HRMS (FD): Calc.  $m/z = 559.1344$  for  $\text{C}_{27}\text{H}_{24}\text{N}_2\text{O}_{10}\text{Na}$

Found  $m/z = 559.1323$   $[\text{M}+\text{Na}]^+$

#### 5-(2-(2-amino-4-(benzyloxy)phenoxy)ethoxy)-2-(1,3-dioxan-2-yl)benzofuran-6-amine (**92**)



5-(2-(4-(benzyloxy)-2-nitrophenoxy)ethoxy)-2-(1,3-dioxan-2-yl)-6-nitrobenzofuran (200 mg, 0.37 mmol) was dissolved in a mixture of EtOH and EtAc (1:1, v/v) and Pt/C (20 mg) was added. The reaction mixture was placed under a hydrogen atmosphere and

---

stirred overnight. The reaction was filtered over celite and washed with EtOH. The solvent was evaporated and the crude was purified by column chromatography using DCM/EtAc (90/10, v/v) to yield 130 mg (0.27 mmol, 73 %) of the diamine.

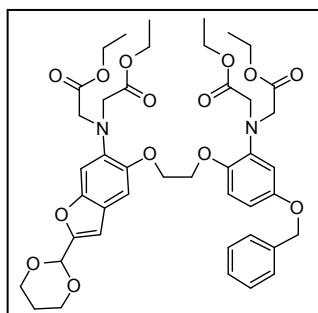
$^1\text{H}$  NMR (300 MHz,  $\text{CDCl}_3$ ):  $\delta$  = 7.43 – 7.31 (m, 5H), 6.96 (s, 1H), 6.85 (s, 1H), 6.77 (d,  $J$  = 8.7 Hz, 1H), 6.65 (s, 1H), 6.40 (d,  $J$  = 3.0 Hz, 1H), 6.31 (dd,  $J$  = 8.9 Hz,  $J$  = 2.8 Hz, 1H), 5.65 (s, 1H), 4.98 (s, 2H), 4.34 – 4.27 (m, 6H), 4.03 – 3.95 (m, 2H), 2.34 – 2.22 (m, 1H), 1.50 – 1.45 (m, 1H).

$^{13}\text{C}$  NMR (75 MHz,  $\text{CDCl}_3$ ):  $\delta$  = 154.44, 151.13, 150.95, 144.19, 140.90, 138.33, 137.55, 136.04, 128.63, 127.91, 127.54, 118.19, 114.39, 104.54, 104.39, 103.52, 103.17, 97.77, 96.52, 70.49, 68.69, 68.45, 67.44, 25.79.

HRMS (FD): Calc.  $m/z$  = 477.1981 for  $\text{C}_{25}\text{H}_{30}\text{N}_2\text{O}_6\text{Na}$

Found  $m/z$  = 477.1996  $[\text{M}+\text{Na}]^+$

### Bz-BAPTA-acetal (**93**)



5-(2-(2-amino-4-(benzyloxy)phenoxy)ethoxy)-2-(1,3-dioxan-2-yl)benzofuran-6-amine (150 mg, 0.31 mmol), ethyl bromoacetate (348  $\mu\text{L}$ , 3.1 mmol) and diisopropylethylamine (DIPEA) (263  $\mu\text{L}$ , 1.55 mmol) were dissolved in NMP (6 mL) and heated to 120°C for 3 h. The reaction mixture was cooled to room temperature and diluted with EtAc. The organic phase was washed with brine (3x)

and water (3x) and dried over  $\text{MgSO}_4$ . After filtration and evaporation of all volatiles, the crude was purified by column chromatography using PTE/EtAc (60/40, v/v) to yield 130 mg (0.16 mmol, 51 %) of product.

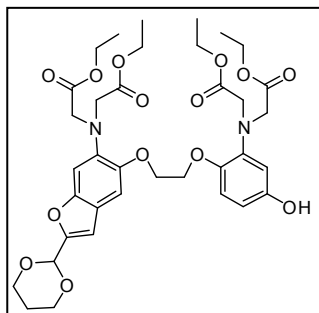
$^1\text{H}$  NMR (300 MHz,  $\text{CDCl}_3$ ):  $\delta$  = 7.42 – 7.30 (m, 5H), 6.99 (d,  $J$  = 8.7 Hz, 2H), 6.77 (d,  $J$  = 9.0 Hz, 1H), 6.66 (s, 1H), 6.48 – 6.45 (m, 2H), 5.66 (s, 1H), 4.97 (s, 2H), 4.32 – 4.24 (m, 6H), 4.17 (s, 4H), 4.14 (s, 4H), 4.10 – 3.96 (m, 10H), 2.36 – 2.20 (m, 1H), 1.50 – 1.45 (m, 1H), 1.18 – 1.10 (m, 12H).

$^{13}\text{C}$  NMR (75 MHz,  $\text{CDCl}_3$ ):  $\delta$  = 171.50, 171.46, 153.78, 152.51, 150.31, 148.34, 144.91, 140.75, 138.53, 137.39, 128.64, 127.99, 127.63, 121.35, 107.40, 106.61, 104.94, 104.36, 102.61, 96.40, 70.60, 68.03, 67.45, 60.91, 53.93, 53.62, 25.78, 14.20, 14.17.

---

HRMS (FD):            Calc.  $m/z = 820.3456$  for  $C_{43}H_{52}N_2O_{14}$   
                             Found  $m/z = 820.3419$   $[M]^+$

HO-BAPTA-acetal (**94**)



Bz-BAPTA-acetal (40 mg, 0.05 mmol) was dissolved in EtAc (2 mL) and Pd/C (10 mg) was added. The reaction mixture was placed under a hydrogen atmosphere, stirred overnight and subsequently filtered over celite and washed with EtAc. The solvent was evaporated and the crude product was purified by column chromatography using PTE/EtAc (50/50, v/v) to yield

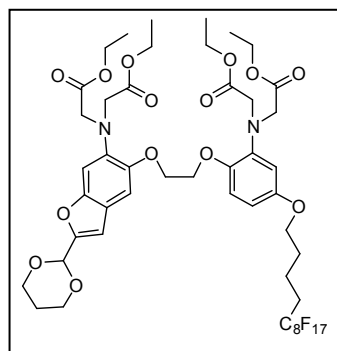
31 mg (0.04 mmol, 88 %) of product.

$^1H$  NMR (300 MHz,  $CDCl_3$ ):  $\delta = 6.99$  (d,  $J = 18.0$  Hz, 2H), 6.71 (d,  $J = 6.3$  Hz, 1H), 6.66 (s, 1H), 6.38 – 6.32 (m, 2H), 5.66 (s, 1H), 4.30 – 4.21 (m, 6H), 4.17 (s, 4H), 4.14 (s, 4H), 4.11 – 3.98 (m, 10H), 2.32 – 2.24 (m, 1H), 1.49 – 1.46 (m, 1H), 1.21 – 1.16 (m, 12H).

$^{13}C$  NMR (75 MHz,  $CDCl_3$ ):  $\delta = 171.61, 171.56, 152.48, 150.49, 150.29, 148.32, 144.51, 140.77, 138.49, 121.33, 115.15, 107.81, 106.79, 104.80, 104.39, 102.57, 96.41, 68.08, 67.48, 60.98, 53.92, 25.77, 14.24, 14.20$ .

HRMS (FD):            Calc.  $m/z = 730.2924$  for  $C_{36}H_{46}N_2O_{14}$   
                             Found  $m/z = 730.2949$   $[M]^+$

$C_8F_{17}$ -BAPTA-acetal (**95**)



HO-BAPTA acetal (110 mg, 0.15 mmol) and  $C_8F_{17}$ -butyl bromide (91 mg, 0.16 mmol) were dissolved in AcCN (5 mL).  $K_2CO_3$  (41 mg, 0.29 mmol) was added and the reaction was refluxed for 6 h. After cooling, the reaction was filtered and the filtered product was washed with DCM. The combined organic phases were dried over  $MgSO_4$ , filtered and evaporated. The crude product was purified using PTE/EtAc (70/30, v/v) to yield

120 mg (0.1 mmol, 66 %) of product.

---

$^1\text{H}$  NMR (400 MHz,  $\text{CDCl}_3$ ):  $\delta$  = 6.99 (d,  $J$  = 10.7 Hz, 2H), 6.77 (d,  $J$  = 8.5 Hz, 1H), 6.66 (s, 1H), 6.41 – 6.38 (m, 2H), 5.65 (s, 1H), 4.30 – 4.23 (m, 6H), 4.17 (s, 4H), 4.14 (s, 4H), 4.09 – 4.00 (m, 10H), 3.90 (t,  $J$  = 5.4 Hz, 2H), 2.34 – 2.23 (m, 1H), 2.21 – 2.08 (m, 2H), 1.81 – 1.76 (m, 4H), 1.49 – 1.46 (m, 1H), 1.20 – 1.11 (m, 12H).

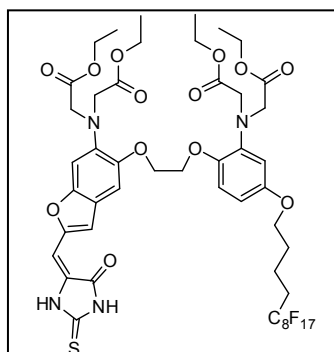
$^{13}\text{C}$  NMR (75 MHz,  $\text{CDCl}_3$ ):  $\delta$  = 171.63, 171.59, 153.92, 152.59, 150.40, 148.41, 144.95, 140.87, 138.59, 121.45, 114.97, 107.17, 106.30, 105.04, 104.45, 102.70, 96.48, 68.09, 67.80, 67.55, 61.00, 54.02, 53.72, 30.92, 28.99, 25.84, 17.48, 14.27, 14.23.

$^{19}\text{F}$  NMR (400 MHz,  $\text{CDCl}_3$ ):  $\delta$  = -81.74 (t,  $J$  = 10.2 Hz, 3F), -115.50 – -115.67 (m, 2F), -122.90 (s, br, 2F), -123.09 (s, br, 4F), -123.88 (s, br, 2F), -124.65 (s, br, 2F), -127.27 (s, br, 2F).

HRMS (FD): Calc.  $m/z$  = 1204.3196 for  $\text{C}_{48}\text{H}_{53}\text{F}_{17}\text{N}_2\text{O}_{14}$

Found  $m/z$  = 1204.3225  $[\text{M}]^+$

#### $\text{C}_8\text{F}_{17}$ -fura red ester (**96**)



$\text{C}_8\text{F}_{17}$ -BAPTA-acetal (50 mg, 0.04 mmol) and 2-thiohydantoin (5.3 mg, 0.05 mmol) were dissolved in AcOH (2.5 mL) along with  $\text{NH}_4\text{OAc}$  (11 mg, 0.14 mmol). The reaction mixture was stirred at 60 °C for 2 h, cooled and water was added. The aqueous phase was extracted with EtAc (3x) and the combined organic phases washed with a saturated solution of  $\text{NaHCO}_3$ . The organic phase was dried over  $\text{Na}_2\text{SO}_4$ , filtered and evaporated. The crude

product was purified by column chromatography using DCM/EtAc (90/10, v/v) to yield 40 mg (0.03 mmol, 80 %) of product.

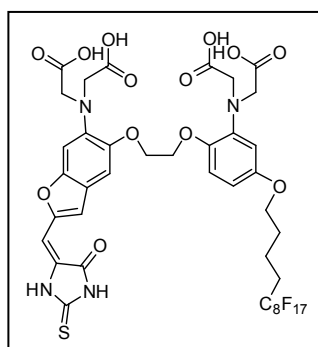
$^1\text{H}$  NMR (400 MHz,  $\text{CDCl}_3$ ):  $\delta$  = 9.61 (s, 1H), 9.96 (s, 1H), 7.12 (s, 1H), 6.99 (s, 1H), 6.91 (s, 1H), 6.78 (d,  $J$  = 8.6 Hz, 1H), 6.50 (s, 1H), 6.42 (d,  $J$  = 9.3 Hz, 2H), 4.27 – 4.23 (m, 8H), 4.17 (s, 4H), 4.13 – 4.03 (m, 8H), 3.90 (t,  $J$  = 5.7 Hz, 2H), 2.19 – 2.09 (m, 2H), 1.85 – 1.78 (m, 4H), 1.21 – 1.14 (m, 12H).

---

$^{13}\text{C}$  NMR (75 MHz,  $\text{CDCl}_3$ ):  $\delta = 175.08, 171.52, 171.32, 163.60, 154.00, 152.29, 150.65, 148.97, 144.77, 141.13, 140.84, 125.73, 121.80, 115.15, 113.51, 107.24, 106.32, 104.43, 101.60, 100.72, 67.99, 67.73, 61.37, 60.94, 54.07, 53.64, 30.84, 28.92, 17.42, 14.24, 14.19,$   
 $^{19}\text{F}$  NMR (400 MHz,  $\text{CDCl}_3$ ):  $\delta = -81.94$  (t,  $J = 9.5$  Hz, 3F),  $-115.55 - -115.62$  (m, 2F),  $-122.90$  (s, br, 2F),  $-123.09$  (s, br, 4F),  $-123.88$  (s, br, 2F),  $-124.65$  (s, br, 2F),  $-127.27$  (s, br, 2F).

HRMS (FD):            Calc.  $m/z = 1244.2774$  for  $\text{C}_{48}\text{H}_{49}\text{F}_{17}\text{N}_4\text{O}_{13}\text{S}$   
                             Found  $m/z = 1244.2745$   $[\text{M}]^+$

**$\text{C}_8\text{F}_{17}$ -fura red ester (**97**)**

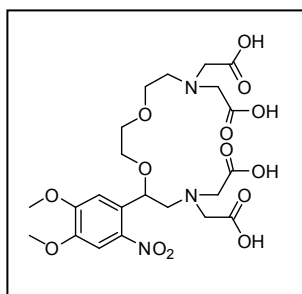


$\text{C}_8\text{F}_{17}$ -fura red-ester (15 mg, 12  $\mu\text{mol}$ ) was dissolved in a mixture of THF (1 mL) and MeOH (1 mL), then  $\text{LiOH}\cdot\text{H}_2\text{O}$  (10 mg, 250  $\mu\text{mol}$ ) and a drop of water was added and the mixture was stirred at room temperature overnight. The solvent was evaporated under reduced pressure and the crude product was dispersed in ethyl acetate and centrifuged. The solvent was pipetted off, the solid was dissolved in water and acidified with 1M HCl. The precipitate was dissolved in an appropriate amount of KOH solution to form the potassium salt and freeze dried to yield the title compound quasi-quantitatively.

HRMS (FD):            Calc.  $m/z = 1133.1566$  for  $\text{C}_{40}\text{H}_{34}\text{F}_{17}\text{N}_4\text{O}_{13}\text{S}$   
                             Found  $m/z = 1133.1571$   $[\text{M}]^+$

---

### DMNPE-4 (99)

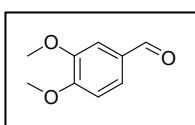


DMNPE-4-ester (20 mg, 35  $\mu\text{mol}$ ) was dissolved in a mixture of THF (1 ml) and MeOH (1 ml), then LiOH.H<sub>2</sub>O (10 mg, 250  $\mu\text{mol}$ ) and a drop of water was added and the mixture was stirred at room temperature overnight. The solvent was evaporated under reduced pressure and the crude product was dispersed in ethyl acetate and centrifuged. The solvent was pipetted off and the solid was dissolved in water and acidified with 1M HCl. The precipitate was dissolved in an appropriate amount of KOH-solution to form the potassium salt and freeze dried to yield the title compound quasi-quantitatively.

HRMS (FD): Calc.  $m/z$  = 583.1631 for C<sub>22</sub>H<sub>30</sub>N<sub>3</sub>O<sub>14</sub>Na

Found  $m/z$  = 583.1625 [M-H+Na]<sup>+</sup>

### 3,4-dimethoxybenzaldehyde (105)<sup>3</sup>



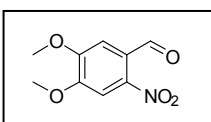
(3,4-Dimethoxyphenyl)methanol (1 g, 5.95 mmol), potassium iodide (0.25 g, 1.50 mmol), iodine (1.52 g, 5.99 mmol) and K<sub>2</sub>CO<sub>3</sub> (1.24 g, 8.97 mmol) were and heated at 90 °C in H<sub>2</sub>O (24 mL) for 1 h. The reaction mixture was cooled to room temperature and extracted with diethyl ether (3x) and washed with saturated Na<sub>2</sub>SO<sub>3</sub>-solution (3x). The organic phase was dried over MgSO<sub>4</sub>, filtered and evaporated to dryness. The crude product was purified by column chromatography using petroleum ether / ethyl acetate (80 / 20, v/v) to obtain 0.515 g of product (52 % yield).

<sup>1</sup>H NMR (300 MHz, CD<sub>3</sub>Cl):  $\delta$  = 9.85 (s, 1H), 7.46 (dd,  $J$  = 1.87 Hz,  $J$  = 8.16 Hz, 1H), 7.42 (d,  $J$  = 1.87 Hz, 1H), 6.98 (d,  $J$  = 8.16 Hz, 1H), 3.97 (s, 3H), 3.97 (s, 3H).

Spectra conform with literature

Kamimura, A.; Komatsu, H.; Moriyama, T.; Nozaki, Y. *Tetrahedron* **2013**, *69*, 5968.

### 4,5-dimethoxy-2-nitrobenzaldehyde (106)<sup>3</sup>



3,4-dimethoxybenzaldehyde (2 g, 12 mmol) was added at 0 °C, over a period of 5 min to a cooled solution of HNO<sub>3</sub> (65 % in water). The reaction

---

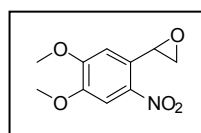
mixture was stirred for 10 min at 0 °C followed by 60 min at room temperature. The reaction mixture was poured into an ice-cooled aqueous solution and filtered. The yellow solid was recrystallised from ethanol to give 2.3 g (90 % yield) of product as a yellow powder.

<sup>1</sup>H NMR (200 MHz, CD<sub>3</sub>Cl): δ = 10.45 (s, 1H), 7.61 (d, *J* = 3.90 Hz, 1H), 7.42 (d, *J* = 3.93 Hz, 1H), 4.03 (s, 3H), 4.01 (s, 3H).

Spectra conform with literature

Gavara, L.; Boisse, T.; Henichart, J. P.; Daich, A.; Rigo, B.; Gautret, P. *Tetrahedron* **2010**, *66*, 7544.

### 2-(4,5-dimethoxy-2-nitrophenyl)oxirane (**107**)<sup>3</sup>



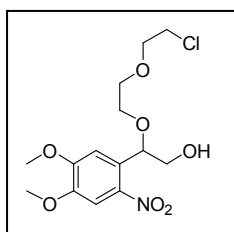
NaH (0.25 g, 10.42 mmol) was set in a round bottom flask and 20 mL THF was added at 0 °C. Trimethylsulfonium iodide (2.08 g 10 mmol) in dry DMSO (20 mL) was added dropwise at 0 °C. After a few minutes of stirring a solution of 2,4-dimethoxy-2-nitrobenzaldehyde (2.13 g, 10 mmol) in THF (5 mL) was rapidly added. The reaction was stirred at 0 °C until completed (circa 20 min) then water was added. The mixture was extracted with diethyl ether (3x) and the organic phase was washed with water and brine (5x). The organic phase was dried over MgSO<sub>4</sub>, filtered and evaporated. The crude product was purified by column chromatography PTE/EtAc (70/30, v/v) to yield 1.13 g (50 %) of the epoxide.

<sup>1</sup>H NMR (300 MHz, CD<sub>3</sub>Cl): δ = 7.73 (s, 1H), 7.04 (s, 1H), 4.53 (dd, *J* = 2.65 Hz, *J* = 4.32 Hz, 1H), 3.97 (s, 3H), 3.95 (s, 3H), 3.29 (dd, *J* = 4.48 Hz, *J* = 5.49 Hz, 1H), 2.64 (dd, *J* = 2.63 Hz, *J* = 5.53 Hz, 1H).

<sup>13</sup>C NMR (75 MHz, CDCl<sub>3</sub>): δ = 154.36, 148.32, 140.25, 129.91, 108.11, 107.91, 56.65, 56.55, 51.32, 50.68.

---

2-(2-(2-chloroethoxy)ethoxy)-2-(4,5-dimethoxy-2-nitrophenyl)ethanol (**108**)



2-(4,5-dimethoxy-2-nitrophenyl)oxirane (1.50 g, 6.66 mmol)  $\text{Eu}(\text{CF}_3\text{SO}_3)_3$  (39.5 mg, 0.066 mmol) and 2-(2-Chloro-ethoxy)ethanol (7.0 ml, 66.6 mmol) were mixed in a round bottom flask and a minimum amount of THF was added to solubilise all solids. The reaction mixture was stirred for 1 h at room temperature then separated between  $\text{H}_2\text{O}$  and DCM. The aqueous phase was extracted with DCM (3x) and the organic phase dried over  $\text{MgSO}_4$ . After filtration and evaporation of the volatiles, the crude product was purified by column chromatography. First two column volumes of a mixture PTE/EtAc (85/15, v/v) was used to wash of the excess alcohol then PET/EtAc was used to eluted 1.8 g (77 %) of the product, which was a light yellowish oil.

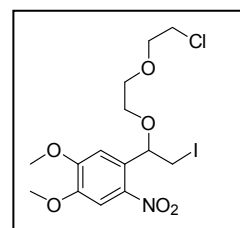
$^1\text{H}$  NMR (200 MHz,  $\text{CD}_3\text{Cl}$ ):  $\delta$  = 7.64 (s, 1H), 7.27 (s, 1H), 5.25 (dd,  $J$  = 3.18 Hz,  $J$  = 7.31 Hz, 1H), 3.99 (s, 3H), 3.95 (s, 3H), 3.57-3.79 (m, 11H).

$^{13}\text{C}$  NMR (75 MHz, DMSO):  $\delta$  = 109.92, 108.11, 79.12, 72.43, 71.46, 71.28, 70.58, 69.15, 66.55, 61.89, 56.68, 56.53, 56.50, 42.86.

HRMS (ESI): Calc.  $m/z$  = 372.0805 for  $\text{C}_{14}\text{H}_{20}\text{NO}_7\text{ClNa}$

Found  $m/z$  = 372.0820  $[\text{M}+\text{Na}]^+$

1-(1-(2-(2-chloroethoxy)ethoxy)-2-iodoethyl)-4,5-dimethoxy-2-nitrobenzene (**109**)



$\text{PPh}_3$  (2.00 g, 7.62 mmol) was added in one portion to a stirred solution of 1-(1-(2-(2-chloroethoxy)ethoxy)-2-iodoethyl)-4,5-dimethoxy-2-nitrobenzene (1.80 g, 5.15 mmol) and imidazole (880 mg, 12.93 mmol) in toluene.  $\text{I}_2$  (1.95 g, 7.68 mmol) was added and the reaction mixture was refluxed for 2 h, then the reaction was cooled and diluted with EtAc. The organic phase was washed with saturated  $\text{Na}_2\text{S}_2\text{O}_3$ -solution until the iodine color disappeared, followed by 2 washings with brine and water. The organic phase was dried over  $\text{MgSO}_4$ , filtered and the solvent evaporated. The crude product was purified by column chromatography PTE/EtAc (60/40, v/v) to obtain 1.1 g (48 % yield) of the product as a yellow oil.

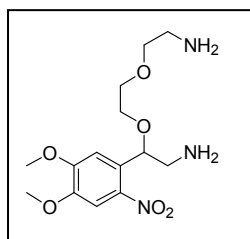
$^1\text{H}$  NMR (300 MHz,  $\text{CD}_3\text{Cl}$ ):  $\delta$  = 7.64 (s, 1H), 7.30 (s, 1H), 5.19 (dd,  $J$  = 2.79 Hz,  $J$  = 8.07 Hz, 1H), 4.01 (s, 3H), 3.96 (s, 3H), 3.81-3.74 (m, 3H), 3.70-3.56 (m, 6H) 3.33-3.28 (m, 1H).

---

HRMS (ESI): Calc.  $m/z = 481.9849$  for  $C_{14}H_{19}NO_6ClNa$

Found  $m/z = 481.9837 [M+Na]^+$

2-(2-(2-aminoethoxy)ethoxy)-2-(4,5-dimethoxy-2-nitrophenyl)ethanamine (**110**)



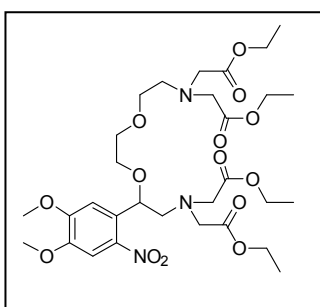
1-(1-(2-(2-chloroethoxy)ethoxy)-2-iodoethyl)-4,5-dimethoxy-2-nitrobenzene (0.85 g, 1.92 mmol) was dissolved in DMF (4 mL) and sodium azide (0.28 g, 4.3 mmol) was added. The reaction mixture was heated to 90 °C and stirred for 5 h. The solvent was evaporated under reduced pressure, the residue dissolved in EtAc and washed with water and brine. The organic phase was dried over  $MgSO_4$ , filtered and the solvent evaporated. To the crude product was added THF (8 ml)  $PPh_3$  (1.05 g, 4.00 mmol) and  $H_2O$  (200  $\mu$ l). The reaction mixture was stirred at 40 °C over night. The solvent was evaporated and the crude mixture purified by column chromatography using DCM/MeOH/TEA (80/20/1, v/v/v) to yield 0.50 mg (1.52 mmol, 79 %) product as a light yellow liquid.

$^1H$  NMR (300 MHz,  $CD_3Cl$ ):  $\delta = 7.63$  (s, 1H), 7.24 (s, 1H), 5.08 (dd,  $J = 2.91$  Hz,  $J = 7.85$  Hz, 1H), 3.98 (s, 3H), 3.95 (s, 3H), 3.72-3.51 (m, 4H), 3.49 (t,  $J = 5.16$ , 2H), 3.06 (dd,  $J = 2.93$ ,  $J = 13.59$ , 1H), 2.87 (t,  $J = 5.30$ , 2H), 2.80 (dd,  $J = 7.87$ ,  $J = 13.59$ , 1H).  $^{13}C$  NMR (75 MHz,  $CD_3Cl$ ):  $\delta = 153.94$ , 148.10, 140.84, 132.13, 109.39, 108.06, 80.61, 73.47, 70.46, 69.18, 56.59, 56.48, 48.72, 41.81.

HRMS (ESI): Calc.  $m/z = 352.1493$  for  $C_{14}H_{23}N_3O_6Na$

Found  $m/z = 352.1479 [M+Na]^+$

DMNPE-4 ester (**111**)



In a round bottom flask, 2-(2-(2-aminoethoxy)ethoxy)-2-(4,5-dimethoxy-2-nitrophenyl)ethanamine (0.50 g, 1.52 mmol) and ethyl bromoacetate (1.68 mL, 15.2 mmol) were dissolved in AcCN (15 mL), then  $Na_2HPO_4$  (0.87 g, 6.12 mmol) and NaI (0.11 g, 0.74 mmol) were added. The reaction mixture was heated to reflux over night. The reaction was cooled to room temperature and the solids filtered off. The solvent was removed under reduced pressure and the crude product

---

purified by column chromatography using PET/EtAc (30/70, v/v) to obtain 0.76 g (1.12 mmol, 74 % yield) of the shown compound as a light yellow oil.

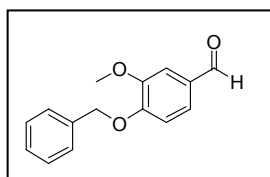
$^1\text{H}$  NMR (300 MHz,  $\text{CD}_3\text{Cl}$ ):  $\delta$  = 7.61 (s, 1H), 7.28 (s, 1H), 5.29 (dd,  $J$  = 2.67 Hz,  $J$  = 7.20 Hz, 1H), 4.22-4.07 (m, 8H), 3.99 (s, 3H), 3.93 (s, 3H), 3.75 (s, 4H), 3.58 (s, 4H) 3.56-3.41 (m, 6H), 3.11 (dd,  $J$  = 2.68,  $J$  = 14.72, 1H), 3.03 (dd,  $J$  = 6.93,  $J$  = 14.14, 1H), 2.92 (t,  $J$  = 5.77, 2H), 1.30-1.20 (m, 12H)

$^{13}\text{C}$  NMR (75 MHz,  $\text{CD}_3\text{Cl}$ ):  $\delta$  = 171.96, 171.41, 153.97, 147.99, 140.50, 132.44, 109.87, 107.93, 78.35, 70.52, 70.46, 68.97, 61.34, 60.53, 60.45, 56.72, 56.46, 55.98, 55.82, 53.74, 14.39, 14.35.

HRMS (ESI): Calc.  $m/z$  = 696.2952 for  $\text{C}_{30}\text{H}_{47}\text{N}_3\text{O}_{14}\text{Na}$

Found  $m/z$  = 696.2950  $[\text{M}+\text{Na}]^+$

#### 4-(benzyloxy)-3-methoxybenzaldehyde (**113**)



Vanilin (3.00 g, 19.72 mmol) and benzyl bromide (3.51 ml, 29.55 mmol) were dissolved in acetone (20 mL).  $\text{K}_2\text{CO}_3$  (4.08 g, 29.55 mmol) was added and the reaction mixture heated at reflux for 5 h. The solution was cooled to room temperature and filtered. The

solid was washed with acetone several times and the combined organic phases were evaporated. The crude product was purified by column chromatography using PTE/DCM (40/60, v/v) to yield 3.8 g (15.7 mmol, 80 % yield).

$^1\text{H}$  NMR (300 MHz,  $\text{CD}_3\text{Cl}$ ):  $\delta$  = 9.83 (s, 1H), 7.46-7.32 (m, 7H), 6.99 (d,  $J$  = 8.17, 1H), 5.25 (s, 2H), 3.95 (s, 3H).

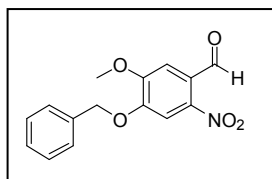
$^{13}\text{C}$  NMR (75 MHz,  $\text{CD}_3\text{Cl}$ ):  $\delta$  = 190.95, 153.70, 150.19, 136.13, 130.42, 128.81, 128.29, 127.30, 126.63, 112.53, 109.52, 70.97.56.15

HRMS (ESI): Calc.  $m/z$  = 243.1019 for  $\text{C}_{15}\text{H}_{15}\text{O}_3$

Found  $m/z$  = 243.1015  $[\text{M}+\text{H}]^+$

#### 4-(benzyloxy)-5-methoxy-2-nitrobenzaldehyde (**114**)

---



4-Benzyloxy-3-methoxybenzaldehyde (3.7 g, 15.3 mmol) was solubilized in acetic acid (6 mL) and cooled in an ice bath. HNO<sub>3</sub> 65 % in water (20 mL) was added dropwise over 10 min. After the addition the mixture was stirred at room temperature for 1 h until all starting material was consumed. The reaction mixture was poured into an ice water mixture and the precipitated solid was filtered off and washed with H<sub>2</sub>O. The crude product was purified by column chromatography using gradient elution starting from PTE/DCM (40/60, v/v) to pure DCM yielding 3 g (10.4 mmol, 68% yield) of a yellowish solid.

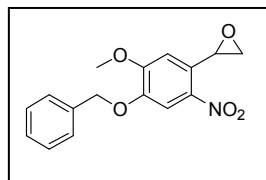
<sup>1</sup>H NMR (300 MHz, CD<sub>3</sub>Cl): δ = 10.43 (s, 1H), 7.66 (s, 1H), 7.49-7.35 (m, 6H), 5.27 (s, 2H), 4.01 (s, 3H).

<sup>13</sup>C NMR (75 MHz, CD<sub>3</sub>Cl): δ = 187.84, 153.86, 151.54, 143.74, 134.99, 129.02, 128.82, 127.70, 125.85, 110.16, 109.04, 71.69, 56.84.

HRMS (ESI): Calc. m/z = 288.0866 for C<sub>15</sub>H<sub>14</sub>NO<sub>5</sub>

Found m/z = 288.0866 [M+H]<sup>+</sup>

#### 2-(4-(benzyloxy)-5-methoxy-2-nitrophenyl)oxirane (**115**)



A suspension of NaH (275 mg, 11.47 mmol) in DMSO (20 ml) was prepared and stirred under an argon atmosphere for 30 min at 60 °C. The mixture was diluted with THF (20 mL) and cooled to 0 °C. Trimethylsulfonium iodide (1.72 g, 8.43 mmol) in DMSO (5 mL) was added dropwise and subsequently 4-(benzyloxy)-5-methoxy-2-nitrobenzaldehyde (2.20 g, 7.66 mmol) dissolved in THF (5 mL) was added dropwise. After 15 min, another portion of NaH (275 mg, 11.47 mmol) was added. The reaction progression was monitored by TLC PET/EtAc (70/30, v/v). Once the reaction was complete water was added (150 mL) and the mixture was extracted with Et<sub>2</sub>O (3x). The ether phase was washed with brine (2x) and water (2x). The organic phase was dried over MgSO<sub>4</sub> and after filtration, the solution was concentrated to approximately 10 mL and passed through a silica plug eluting with Et<sub>2</sub>O. After evaporation of the solvent in vacuo 1.82 g (6.04 mmol, 79 % yield) of product was obtained.

---

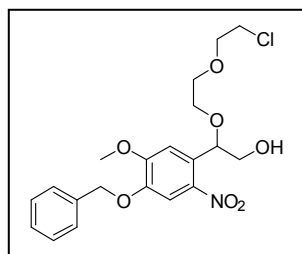
$^1\text{H}$  NMR (300 MHz,  $\text{CDCl}_3$ ):  $\delta$  = 7.79 (s, 1H), 7.49-7.33 (m, 5H), 7.05 (s, 1H), 5.20 (s, 2H), 4.52 (dd,  $J$  = 2.63,  $J$  = 4.40, 1H), 3.97 (s, 3H) 4.29 (dd,  $J$  = 4.46,  $J$  = 5.53, 1H), 2.64 (dd,  $J$  = 2.59,  $J$  = 5.55, 1H).

$^{13}\text{C}$  NMR (75 MHz,  $\text{CDCl}_3$ ):  $\delta$  = 154.96, 147.27, 140.05, 135.76, 130.18, 128.86, 128.50, 127.68, 110.05, 108.36, 71.44, 56.63, 51.35, 50.68.

HRMS (ESI): Calc.  $m/z$  = 302.1029 for  $\text{C}_{16}\text{H}_{16}\text{NO}_5$

Found  $m/z$  = 302.1022  $[\text{M}+\text{H}]^+$

### 2-(4-(benzyloxy)-5-methoxy-2-nitrophenyl)-2-(2-(2-chloroethoxy)ethoxy)ethanol (**116**)



In a round bottom flask, 2-(4-(benzyloxy)-5-methoxy-2-nitrophenyl)oxirane (1.80 g, 5.97 mmol) was dispersed in 2-(2-chloroethoxy)ethanol (6.9 ml, 66.0 mmol) and a minimum amount of THF was added to solubilise all solids.  $\text{Eu}(\text{CF}_3\text{SO}_3)_3$  (50.0 mg, 0.083 mmol) was added and the reaction mixture stirred at 50 °C for

2 h. Water was added and the aqueous phase extracted with DCM (3x) The organic phase was dried over  $\text{MgSO}_4$ , filtered and evaporated to dryness. The crude product was purified by column chromatography starting with two column volumes PTE/EtAc (80/20, v/v) to wash of the excess of 2-(2-chloroethoxy)ethanol then eluting the rest with PTE/EtAc (50/50, v/v). 1.81 g (4.26 mmol, 71 % yield) of the product was obtained.

$^1\text{H}$  NMR (300 MHz,  $\text{DMSO}-d_6$ ):  $\delta$  = 7.71 (s, 1H), 7.50-7.31 (m, 5H), 7.24 (s, 1H), 5.19 (s, 2H), 5.03 (dd,  $J$  = 4.25,  $J$  = 6.01, 1H), 3.90 (s, 3H) 3.73-3.43 (m, 11H).

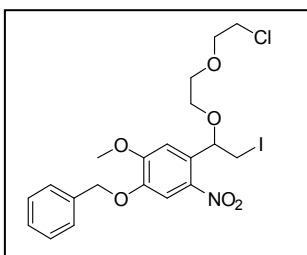
$^{13}\text{C}$  NMR (75 MHz, DMSO):  $\delta$  = 153.37, 146.53, 140.63, 136.25, 130.43, 128.49, 128.11, 127.94, 110.19, 109.24, 78.66, 70.58, 70.33, 69.75, 68.61, 56.10, 43.49.

HRMS (ESI): Calc.  $m/z$  = 448.1114 for  $\text{C}_{20}\text{H}_{24}\text{NO}_7\text{ClNa}$

Found  $m/z$  = 448.1133  $[\text{M}+\text{Na}]^+$

---

1-(benzyloxy)-4-(1-(2-(2-chloroethoxy)ethoxy)-2-iodoethyl)-2-methoxy-5-nitrobenzene (**117**)



In a round bottom flask, imidazole (0.74 g, 10.80 mmol) and 2-(4-(benzyloxy)-5-methoxy-2-nitrophenyl)-2-(2-(2-chloro-ethoxy)ethoxy)ethanol (1.60 g, 3.76 mmol) were dissolved in toluene (40 mL), then PPh<sub>3</sub> (2.10 g, 8.01 mmol) and I<sub>2</sub> (1.46 g, 5.76 mmol) were added. The reaction mixture was heated to 80 °C for 1.5 h.

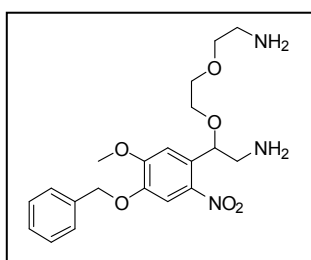
After cooling to room temperature, the solution was diluted with EtAc and washed with a saturated aqueous Na<sub>2</sub>SO<sub>4</sub> solution and then a saturated aqueous NaHCO<sub>3</sub> solution. The organic phase was dried over MgSO<sub>4</sub>, filtered and the solvent was evaporated. The crude product was then purified by column chromatography using first PTE/EtAc (90/10, v/v) then PTE/EtAc (70/30, v/v) to yield 1.40 g (2.62 mmol, 70 % yield) of pure product.

<sup>1</sup>H NMR (300 MHz, DMSO-*d*<sub>6</sub>): δ = 7.76 (s, 1H), 7.49-7.35 (m, 5H), 7.29 (s, 1H), 5.21 (s, 2H), 5.09 (dd, *J* = 2.78, *J* = 8.43, 1H), 3.93 (s, 3H) 3.71-3.36 (m, 10H). <sup>13</sup>C NMR (75 MHz, DMSO): δ = 153.69, 146.94, 140.07, 136.13, 130.89, 128.50, 128.14, 127.95, 109.64, 109.38, 77.02, 70.56, 70.37, 69.64, 68.82, 56.23, 43.45.

HRMS (ESI): Calc. *m/z* = 558.0162 for C<sub>20</sub>H<sub>23</sub>NO<sub>6</sub>IClNa

Found *m/z* = 558.0150 [M+Na]<sup>+</sup>

2-(2-(2-aminoethoxy)ethoxy)-2-(4-(benzyloxy)-5-methoxy-2-nitrophenyl)ethanamine (**118**)



Sodium azide (0.60 g, 9.23 mmol) and 1-(benzyloxy)-4-(1-(2-(2-chloroethoxy)ethoxy)-2-iodoethyl)-2-methoxy-5-nitrobenzene

(1.30 g, 2.43 mmol) were dissolved in DMF (6 mL) and stirred for 6 h at room temperature so that double substitution could be observed on the TLC PTE/EtAc (80/20, v/v). The solution was

cooled, diluted with EtAc and washed with brine (2x) and water (1x). The organic phase was dried over MgSO<sub>4</sub>, filtered and the volatiles were evaporated. To the crude product was solubilized in THF (10 ml) and H<sub>2</sub>O (200 μL), subsequently PPh<sub>3</sub> (1.32 g, 5.03 mmol) was added and the reaction mixture was stirred at room temperature overnight. The solvent was evaporated and the product was purified by column chromatography using DCM/MeOH/TEA (90/10/1, v/v/v) to yield 0.82 g (2.02 mmol, 83 % yield) of product as a yellowish oil.

---

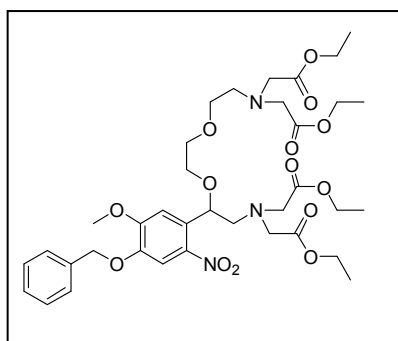
---

$^1\text{H}$  NMR (300 MHz,  $\text{CDCl}_3$ ):  $\delta$  = 7.70 (s, 1H), 7.48-7.34 (m, 5H), 7.28 (s, 1H), 5.19 (s, 2H), 5.07 (dd,  $J$  = 2.84,  $J$  = 7.77, 1H), 3.99 (s, 3H) 3.75-3.56 (m, 6H) 3.06 (dd,  $J$  = 2.86,  $J$  = 13.6, 1H) 2.88-2.76 (m, 3H).

$^{13}\text{C}$  NMR (75 MHz,  $\text{CDCl}_3$ ):  $\delta$  = 154.51, 147.09, 140.62, 135.83, 132.43, 128.85, 128.47, 127.66, 110.13, 109.65, 80.73, 73.59, 71.37, 70.46, 69.20, 56.56, 48.76, 41.85.

MS (ESI): Calc.  $m/z$  = 405.190 for  $\text{C}_{20}\text{H}_{27}\text{N}_3\text{O}_6$   
Found  $m/z$  = 406.2  $[\text{M}+\text{H}]^+$

### Bz-DMNPE-4 ester (**119**)



In a round bottom flask equipped with a reflux condenser,  $\text{Na}_2\text{HPO}_4$  (1.40 g, 9.86 mmol), NaI (0.15 g, 1.00 mmol), ethyl bromoacetate (2.2 mL, 19.7 mmol) and 2-(2-(2-aminoethoxy)ethoxy)-2-(4-(benzyloxy)-5-methoxy-2-nitrophenyl)ethanamine (0.80 g, 1.97 mmol) were dispersed in acetonitrile (25 mL). The reaction mixture was heated under reflux overnight. The solution was cooled

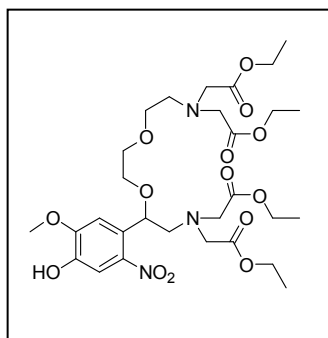
to room temperature and filtered. The solid was filtered off and washed with acetonitril. The filtrate was evaporated to dryness and the crude product was purified by column chromatography using PTE/EtAc (30/70, v/v) to yield 1.13 g (1.51 mmol, 76 %) product as a light yellow oil.

$^1\text{H}$  NMR (300 MHz,  $\text{CDCl}_3$ ):  $\delta$  = 7.66 (s, 1H), 7.46-7.32 (m, 5H), 7.28 (s, 1H), 5.27 (dd,  $J$  = 2.29,  $J$  = 7.59, 1H), 5.17 (s, 2H), 4.18-4.09 (m, 8H), 3.98 (s, 3H), 3.75 (s, 4H), 3.57 (s, 4H), 3.57-3.37 (m, 6H), 3.08 (dd,  $J$  = 2.37,  $J$  = 14.70, 1H), 2.98 (dd,  $J$  = 8.28,  $J$  = 15.39, 1H), 2.92 (t,  $J$  = 5.79, 2H), 1.28-1.21 (m, 12H).

$^{13}\text{C}$  NMR (75 MHz,  $\text{CDCl}_3$ ):  $\delta$  = 171.98, 171.43, 154.57, 146.98, 140.28, 135.94, 132.72, 128.86, 128.46, 127.67, 120.00, 110.08, 78.38, 71.39, 70.51, 70.47, 68.97, 61.35, 60.56, 60.47, 56.71, 55.99, 55.81, 53.74, 14.40, 14.36.

HRMS (ESI): Calc.  $m/z$  = 772.3259 for  $\text{C}_{36}\text{H}_{51}\text{N}_3\text{O}_{14}\text{Na}$   
Found  $m/z$  = 772.3263  $[\text{M}+\text{Na}]^+$

### HO-DMNPE-4 ester (**120**)



To a solution of benzyl-protected DMNPE-4-ester (1.10 g, 1.46 mmol) in DCM (10 mL) was added dropwise at room temperature to a mixture of  $\text{Et}_2\text{O}\cdot\text{BF}_3$  (1.86 ml, 15.9 mmol) and ethane thiol (2.22 ml, 30.8 mmol). After addition, the reaction mixture was heated at 38 °C overnight. The progression of the reaction was monitored by TLC using DCM/MeOH (95/5, v/v). Then, saturated  $\text{NaHCO}_3$ -solution was added to stop the reaction.

The aqueous phase was extracted with DCM (3x) and the combined organic phases were washed with  $\text{H}_2\text{O}$  (2x) and dried over  $\text{MgSO}_4$ . After filtration, the solvent was evaporated under reduced pressure and the crude product was purified by column chromatography using PTE/EtAc (30/70, v/v) yielding 0.69 g (1.05 mmol, 71 %) of product as a light yellow oil.

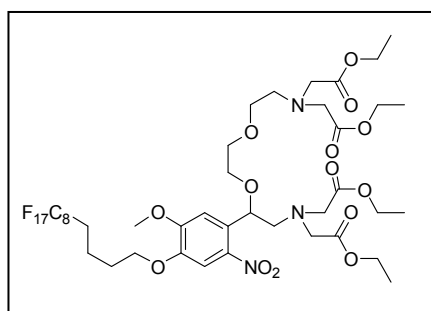
$^1\text{H}$  NMR (300 MHz,  $\text{CDCl}_3$ ):  $\delta$  = 7.64 (s, 1H), 7.29 (s, 1H), 5.22 (dd,  $J$  = 2.28,  $J$  = 7.48, 1H), 4.21-4.08 (m, 8H), 4.02 (s, 3H), 3.74 (s, 4H), 3.58 (s, 4H), 3.57-3.39 (m, 6H), 3.11 (dd,  $J$  = 2.27,  $J$  = 14.61, 1H), 3.04-2.90 (m, 3H), 1.30-1.21 (m, 12H).

$^{13}\text{C}$  NMR (75 MHz,  $\text{CDCl}_3$ ):  $\delta$  = 172.04, 171.47, 144.83, 141.20, 111.37, 109.59, 70.41, 68.87, 61.40, 60.59, 60.51, 56.78, 55.88, 53.72, 21.14, 14.36, 14.32.

HRMS (ESI): Calc.  $m/z$  = 682.2786 for  $\text{C}_{36}\text{H}_{51}\text{N}_3\text{O}_{14}\text{Na}$

Found  $m/z$  = 682.2793  $[\text{M}+\text{Na}]^+$

### $\text{C}_8\text{F}_{17}$ -DMNPE-4 ester (**121**)



In a round bottom flask HO-DMNPE-4-ester (100 mg, 0.15 mmol) and heptafluoro-1-dodecanol (100 mg, 0.18 mmol) were dissolved in AcCN (3 mL).  $\text{Cs}_2\text{CO}_3$  (98 mg, 0.30 mmol) was added and the reaction mixture was stirred at room temperature overnight. The solution was filtered and the solvent was evaporated under reduced

pressure. The crude product was purified by column chromatography using PTE/EtAc (70/30, v/v) which yielded 100 mg (0.09 mmol, 58 %) of product as a yellow oil.

---

$^1\text{H}$  NMR (300 MHz,  $\text{CDCl}_3$ ):  $\delta$  = 7.59 (s, 1H), 7.27 (s, 1H), 5.29 (dd,  $J$  = 2.73,  $J$  = 7.08, 1H), 4.20-4.06 (m, 10H), 3.96 (s, 3H), 3.75 (s, 3H), 3.58 (s, 4H), 3.56-3.38 (m, 6H), 3.10 (dd,  $J$  = 2.60,  $J$  = 14.69, 1H), 3.04-2.89 (m, 3H), 2.35-2.08 (m, 2H), 2.04-1.75 (m, 4H), 1.30-1.20 (m, 12H).

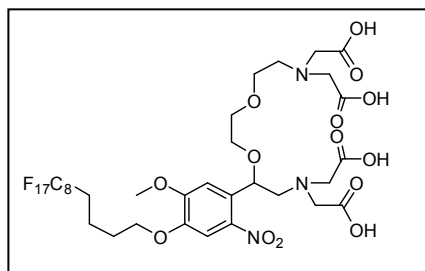
$^{13}\text{C}$  NMR (75 MHz,  $\text{CDCl}_3$ ):  $\delta$  = 172.00, 171.45, 154.41, 147.19, 140.35, 132.65, 110.02, 109.26, 78.36, 70.52, 70.48, 69.00, 61.35, 60.58, 60.50, 56.62, 55.99, 55.82, 53.74, 30.82, 28.50, 17.53, 14.41, 14.36.

$^{19}\text{F}$  NMR (400 MHz,  $\text{CDCl}_3$ ):  $\delta$  = -81.72 (t,  $J$  = 9.98 Hz, 3F), -115.35—115.52 (m, 2F), -122.65 (s, br, 2F), -122.87 (s, br, 4F), -123.68 (s, br, 2F), 124.46 (s, br, 2F), 127.04 (s, br, 2F).

HRMS (ESI): Calc.  $m/z$  = 1133.3136 for  $\text{C}_{41}\text{H}_{52}\text{F}_{17}\text{N}_3\text{O}_{14}$

Found  $m/z$  = 1133.3178  $[\text{M}+\text{H}]^+$

#### $\text{C}_8\text{F}_{17}$ -DMNPE-4 (**122**)



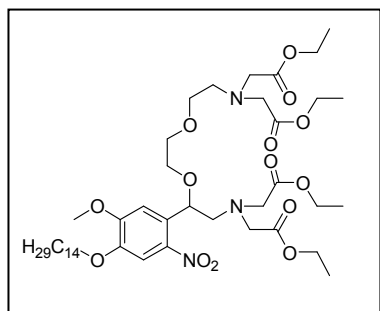
$\text{C}_8\text{F}_{17}$ -DMNPE-4 ester (20 mg, 18  $\mu\text{mol}$ ) was dissolved in a mixture of THF (1 mL) and MeOH (1 mL), then  $\text{LiOH}\cdot\text{H}_2\text{O}$  (10 mg, 250  $\mu\text{mol}$ ) and a drop of water was added and the mixture was stirred at room temperature overnight. The solvent was evaporated under reduced pressure and the crude product was dispersed in ethyl acetate and centrifuged. The solvent was pipetted off, the solid dissolved in water and acidified with 1M HCl. The precipitate was dissolved in an appropriate amount of KOH solution to form the potassium salt and freeze-dried to yield the title compound quasi-quantitatively.

MS (MALDI): Calc.  $m/z$  = 1173.0 for  $\text{C}_{31}\text{H}_{32}\text{F}_{17}\text{N}_3\text{O}_{14}\text{K}$

Found  $m/z$  = 1173.6  $[\text{M}]^+$  (Potassium salt)

---

**C<sub>14</sub>H<sub>29</sub>-DMNPE-4 ester (123)**



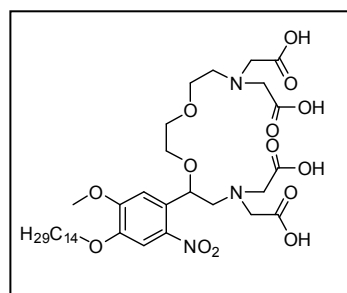
HO-DMNPE-4-ester (200 mg, 0.30 mmol), 1-bromotetradecane (107  $\mu$ L, 0.36 mmol) were dissolved in AcCN (5 ml) and Cs<sub>2</sub>CO<sub>3</sub> (195 mg, 0.6 mmol) was added. The reaction mixture was refluxed for 1 h, cooled to room temperature and filtered. The solvent was evaporated under reduced pressure and the crude product was purified by column chromatography using PTE/EtAc (80/20, v/v) to yield 180 mg (0.21 mmol, 70 %) of product as a light yellow oil.

<sup>1</sup>H NMR (400 MHz, CDCl<sub>3</sub>):  $\delta$  = 7.58 (s, 1H), 7.24 (s, 1H), 5.27 (dd,  $J$  = 2.12,  $J$  = 7.76, 1H), 4.17-4.10 (m, 8H), 4.03 (t,  $J$  = 6.81, 2H), 3.96 (s, 3H), 3.75 (s, 4H), 3.57 (s, 4H), 3.56-3.38 (m, 6H), 3.08 (dd,  $J$  = 2.18,  $J$  = 14.69, 1H), 2.98 (dd,  $J$  = 7.80,  $J$  = 14.75, 1H), 2.92 (t,  $J$  = 5.77, 2H), 1.88-1.75 (m, 3H), 1.48-1.41 (m, 2H), 1.36-1.21 (m, 31H) 0.87 (t,  $J$  = 6.84, 3H). <sup>13</sup>C NMR (75 MHz, CDCl<sub>3</sub>):  $\delta$  = 172.00, 171.43, 154.31, 147.51, 140.40, 132.06, 109.84, 108.97, 78.31, 70.46, 69.58, 68.89, 61.32, 60.55, 60.48, 56.67, 55.96, 55.78, 53.72, 32.04, 29.78, 29.48, 29.02, 26.02, 22.81, 14.37.

HRMS (ESI): Calc.  $m/z$  = 878.4994 for C<sub>43</sub>H<sub>73</sub>N<sub>3</sub>O<sub>14</sub>Na

Found  $m/z$  = 878.4984 [M+Na]<sup>+</sup>

**C<sub>14</sub>H<sub>29</sub>-DMNPE-4 (124)**



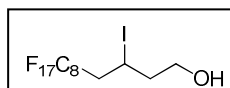
C<sub>14</sub>H<sub>29</sub>-DMNPE-4-ester (15 mg, 18  $\mu$ mol) was dissolved in a mixture of THF (1 mL) and MeOH (1 mL), then LiOH.H<sub>2</sub>O (10 mg, 250  $\mu$ mol) and a drop of water was added and the mixture was stirred at room temperature overnight. The solvent was evaporated under reduced pressure and the crude product was dispersed in ethyl acetate and centrifuged. The solvent was pipetted off, the solid was dissolved in water and acidified with 1M HCl. The precipitate was dissolved in an appropriate amount of KOH solution to form the potassium salt and freeze-dried to yield the title compound quasi-quantitatively.

---

HRMS (FD): Calc.  $m/z = 782.3478$  for  $C_{35}H_{57}N_3O_{14}K$

Found  $m/z = 782.34832$   $[M+K]^+$

### Heptadecafluoro-3-iodododecan-1-ol (**135**)<sup>2</sup>



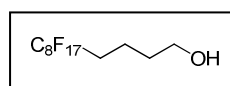
Fine copper powder (283 mg), 1-iodoperfluorooctane (11.88 ml, 45 mmol) and 3-butan-1-ol (4.5 ml, 54 mmol) were mixed in a pressure tube and heated to 120 °C overnight. The reaction mixture was cooled to room temperature and the obtained solid was dissolved in warm chloroform and filtered hot. The solvent of the filtrate was evaporated and the crude product was recrystallized from hot hexane upon standing in the fridge. The product was obtained in 87 % (24.3 g, 39 mmol) yield.

<sup>1</sup>H NMR (300 MHz, CDCl<sub>3</sub>):  $\delta = 4.53$ -4.62 (m, 1H), 3.90-3.97 (m, 1H), 3.80-3.87 (m, 1H), 2.81-3.13 (m, 2H) 1.99-2.17 (m, 2H), 1.53 (s, br, 1H).

<sup>13</sup>C NMR (75 MHz, CDCl<sub>3</sub>):  $\delta = 62.55$ , 42.37, 42.34, 41.99, 16.64.

<sup>19</sup>F NMR (400 MHz, CDCl<sub>3</sub>):  $\delta = -80.74$  (s, br., 3F), -110.52-114.97 (m, 2F), -121.55 (s, br, 2F), -121.85 (s, br, 4F), 122.68 (s, br, 2F), 123.56 (s, br, 2F), 126.06 (s, br, 2F).

### Heptadecafluorododecan-1-ol (**136**)<sup>2</sup>



Heptadecafluoro-3-iodododecan-1-ol (12 g, 19.4 mmol) and tributyltin hydride (6.25 ml, 23.3 mmol) were mixed in a pressure tube, sealed and heated to 80 °C for 2 h with vigorous stirring. The reaction mix was cooled to room temperature and dissolved in hot hexane then filtered hot. The product crystallized upon standing in the fridge and was recrystallized from hot hexane to yield (8.4 g, 17.1 mmol) 88 % pure product as a white powder.

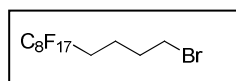
<sup>1</sup>H NMR (300 MHz, CDCl<sub>3</sub>):  $\delta = 3.73$ -3.76 (m, 2H), 2.06-2.21 (m, 2H), 1.67-1.81 (m, 4H) 1.54 (s, br, 1H).

<sup>13</sup>C NMR (75 MHz, CDCl<sub>3</sub>):  $\delta = 62.23$ , 31.92, 30.74, 16.86

<sup>19</sup>F NMR (400 MHz, CDCl<sub>3</sub>):  $\delta = -83.34$  (t,  $J = 10.16$  Hz, 3F), -116.35 (s, br, 2F), -123.70 (s, br, 2F), -123.34 (s, br, 4F), -124.71 (s, br, 2F), 125.47 (s, br, 2F), 128.25 (s, br, 2F).

---

### Heptadecafluorododecyl bromide (**137**)<sup>2</sup>



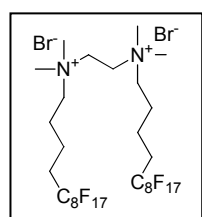
Heptadecafluorododecan-1-ol (7.8 g, 15.8 mmol) was dissolved in anhydrous THF (150 mL) and the solution was cooled in an ice bath. Methanesulfonic anhydride (4.1 g, 23.7 mmol) and ethyldiisopropylamine (5.4 mL, 31.6 mmol) were added and the reaction mixture was stirred at 0 °C for 1 h, followed by 2 h at room temperature. The mixture was filtered and the solvent evaporated. The crude product was dissolved in acetone (60 mL) and LiBr (10 g, 115 mmol) was added and the suspension heated under reflux overnight. The acetone was evaporated and the crude product was passed through a short silica pad eluting with hexane. The organic phase was concentrated to 100 mL and the product crystallized upon standing in the freezer overnight to yield the product (86 %, 7.5 g, 13.6 mmol) as a white solid.

<sup>1</sup>H NMR (300 MHz, CDCl<sub>3</sub>): δ = 3.47 (t, *J* = 6.45 Hz, 2H), 2.07-2.19 (m, 2H), 1.95-2.04 (m, 2H), 1.78-1.87 (m, 2H).

<sup>13</sup>C NMR (75 MHz, CDCl<sub>3</sub>): δ = 32.40, 31.91, 30.12, 19.12.

<sup>19</sup>F NMR (400 MHz, CDCl<sub>3</sub>): δ = -81.74 (t, *J* = 8.96, 3F), -115.16-115.38 (m, 2F), 122.67 (s, br, 2F), 122.88 (s, br, 4F), 123.67 (s, br, 2F), 124.44 (s, br, 2F), 127.07 (s, br, 2F).

### Fluorinated gemini (**138**)<sup>2</sup>



Heptadecafluoro-1-bromo dodecane (1 g, 1.8 mmol) and tetramethylethylenediamine (127 μL, 0.85 mmol) were added to a pressure tube and the dissolved in AcCN (5 mL). The sealed pressure tube was heated at 80 °C for 3 days. The solvent was evaporated and the crude product was recrystallized two times from a 1:1 mixture of chloroform and acetone to give the product as a white solid in 58 % yield (620 mg, 0.59 mmol).

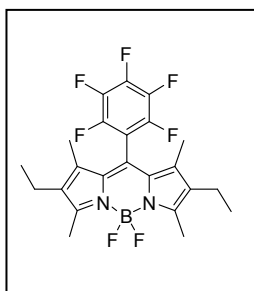
<sup>1</sup>H NMR (300 MHz, CD<sub>3</sub>OD): δ = 4.10 (s, 4H), 3.56-3.62 (m, 4H), 3.32-3.34 (m, 12H), 2.29-2.47 (m, 4H), 1.96-2.07 (m, 4H), 1.71-1.82 (m, 4H).

<sup>1</sup>H NMR (300 MHz, CD<sub>3</sub>Cl / CD<sub>3</sub>OD): δ = 4.30 (s, 4H), 3.75 (s, 12H), 3.56-3.64 (m, 4H), 3.21-3.38 (m, 4H), 1.87-1.97 (m, 4H), 1.69-1.89 (m, 4H).

Spectra conform with literature

---

### F<sub>5</sub>-ethyl-BODIPY (**148**)<sup>4</sup>



Kryptopyrrole (1.00 g, 8.12 mmol), perfluorobenzaldehyde (0.80 g, 4.06 mmol) and few drops of TFA were dissolved in DCM (100 mL). The reaction was monitored by TLC and after consumption of the aldehyde, chloranil (1 g, 4.06 mmol) was added. The reaction mixture was stirred for 15 min. Diisopropylethylamine (4.83 mL, 28.4 mmol) was added and the reaction was further stirred for a further 5 min. Boron trifluoride etherate (6.34 g, 44.6 mmol) was added and the reaction mixture was stirred for 1 h. Water was added and the phases were separated. The organic phase was washed with water (3x) and reextracted (1x). The organic phase was dried over MgSO<sub>4</sub>, filtered and evaporated. The crude product was purified by column chromatography using PTE/DCM (70/30, v/v) to yield 0.73 g (1.6 mmol, 38 %) of the product as a golden brown powder.

<sup>1</sup>H NMR (300 MHz, CDCl<sub>3</sub>): δ = 2.54 (s, 6H); 2.33 (q, 4H, *J* = 7.58 Hz), 1.51 (s, 6H), 1.02 (t, 6H, *J* = 7.58 Hz).

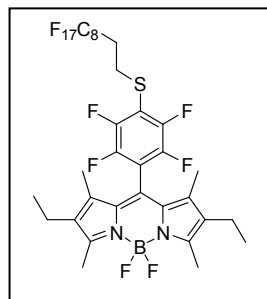
<sup>13</sup>C NMR (75 MHz, CDCl<sub>3</sub>): δ = 156.27, 136.70, 134.07, 130.48, 17.24, 14.70, 12.89, 11.01.

<sup>19</sup>F NMR (400 MHz, CDCl<sub>3</sub>): δ = -159.04 – -159.12 (m, 2F), -152.40 (t, *J* = 21.73 Hz, 1F), -146.61 (q, *J* = 30.72 Hz, 2F), -138.40 – -138.69 (m, 2F).

HRMS (ESI): Calc. *m/z* = 493.1667 for C<sub>23</sub>H<sub>22</sub>BN<sub>2</sub>F<sub>7</sub>Na

Found *m/z* = 493.1656 [M+Na]<sup>+</sup>

### C<sub>8</sub>F<sub>17</sub>-BODIPY (**149**)



F<sub>5</sub>-BODIPY (80 mg, 0.17 mmol) and heptadecafluorodecane-1-thiol (97 mg, 0.20 mmol) were dissolved in AcCN (5 mL) and TEA (86 μL, 0.6 mmol) was added. The reaction mixture was stirred at room temperature for 2 h. The volatiles were evaporated under reduced pressure and the crude product was purified by column chromatography using PTE/DCM (80/20, v/v) to yield 100 mg (0.11 mmol, 63 %) of product as a red powder.

$^1\text{H}$  NMR (300 MHz,  $\text{CDCl}_3$ ):  $\delta$  = 3.22-3.14 (m, 2H), 2.50 (s, 6H), 2.40-2.23 (m, 6H), 1.45 (s, 6H), 0.97 (t,  $J$  = 7.58 Hz, 6H).

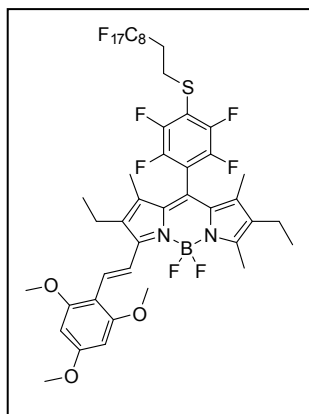
$^{13}\text{C}$  NMR (75 MHz,  $\text{CDCl}_3$ ):  $\delta$  = 156.24, 136.60, 134.05, 130.19, 17.23, 14.63, 12.91, 10.78.

$^{19}\text{F}$  NMR (400 MHz,  $\text{CDCl}_3$ ):  $\delta$  = -81.68 (t,  $J$  = 9.91 Hz, 3F), -114.88 – -115.04 (m, 2F), -122.60 (s, 2F), -122.83 (s, 4F), -123.64 (s, 2F), -124.37 (s, 2F), -127.04 (2F), -132.07 (dd,  $J$  = 12.44 Hz,  $J$  = 24.40 Hz, 2F), -139.57 (dd,  $J$  = 12.47 Hz,  $J$  = 24.35 Hz, 2F), -146.73 (q,  $J$  = 32.47 Hz, 2F).

HRMS (ESI): Calc.  $m/z$  = 929.1623 for  $\text{C}_{33}\text{H}_{26}\text{B N}_2\text{F}_{23}\text{S}$

Found  $m/z$  = 929.1579  $[\text{M}+\text{H}]^+$

### BODred (150)



$\text{C}_8\text{F}_{17}$ -BODIPY (30 mg, 0.032 mmol) and 2,4,6-trimethoxybenzaldehyde (9.4 mg, 0.048 mmol) were dissolved in toluene (2 mL) and piperidine (6.3  $\mu\text{L}$ , 0.064 mmol) was added. The reaction mixture was heated at reflux for 6 h, cooled to room temperature and diluted with DCM. The organic phase was washed with brine (2x) and water (2x). After drying over  $\text{MgSO}_4$ , the solution was filtered and evaporated to dryness. The crude product was purified by column chromatography using PTE/DCM (30/70,

v/v) as eluent to obtain a blue solid 12 mg (0.011 mmol, 34 %).

$^1\text{H}$  NMR (300 MHz,  $\text{CDCl}_3$ ):  $\delta$  = 8.23 (d,  $J$  = 17.04 Hz, 1H), 7.72 (d,  $J$  = 17.02 Hz, 1H), 6.17 (s, 2H), 3.94 (s, 6H), 3.88 (s, 3H), 3.27 – 3.23 (m, 2H), 2.66 (q,  $J$  = 7.45 Hz, 2H), 2.49 – 2.39 (m, 2H), 2.35 (q,  $J$  = 7.51 Hz, 2H), 1.58 (s, 3H), 1.55 (s, 3H), 1.51 (s, 3H), 1.22 (t,  $J$  = 7.61 Hz, 3H), 1.02 (t,  $J$  = 7.53 Hz, 3H).

$^{13}\text{C}$  NMR (75 MHz,  $\text{CDCl}_3$ ):  $\delta$  = 162.01, 160.75, 155.50, 154.24, 148.84, 148.72, 146.38, 146.23, 145.68, 143.18, 143.03, 137.20, 134.75, 134.47, 133.44, 131.78, 130.30, 130.08, 120.58, 119.32, 117.00, 108.83, 90.94, 56.08, 55.54, 32.28, 32.07, 29.86, 25.60, 18.79, 17.29, 14.73, 12.90, 10.70, 10.55.

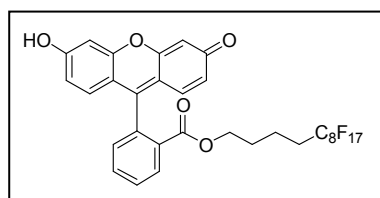
$^{19}\text{F}$  NMR (400 MHz,  $\text{CDCl}_3$ ):  $\delta$  = -81.69 (t,  $J$  = 9.92 Hz, 3F), -114.87 – -115.04 (m, 2F), -122.59 (s, 2F), -122.83 (s, 4F), -123.63 (s, 2F), -124.36 (s, 2F), -127.03 (s, 2F), -133.26 – -133.35 (m, 2F), -139.24 – -139.34 (m, 2F), -144.25 – -144.51 (m, 2F).

---

HRMS (FD): Calc.  $m/z = 1108.2282$  for  $C_{43}H_{36}B F_{23}N_2O_3S$

Found  $m/z = 1107.22087$   $[M-H]^+$

### $C_8F_{17}$ -fluorescein (**152**)



Fluorescein (130 mg, 0.39 mmol) and  $C_8F_{17}$ -butyl bromide (242 mg, 0.45 mmol) were dissolved in DMF (2 mL). The reaction mixture was stirred overnight at 60 °C. The solvent was evaporated and the crude product was purified by column

chromatography starting with pure DCM to DCM/MeOH (90/10, v/v) to yield 40 mg (0.05 mmol, 12 %) of product.

$^1H$  NMR (400 MHz,  $CD_3OD$ ):  $\delta = 8.29$  (dd,  $J = 1.41$  Hz,  $J = 7.78$  Hz, 1H), 7.86 – 7.76 (m, 2H), 7.43 (dd,  $J = 1.31$  Hz,  $J = 7.53$  Hz, 1H), 7.01 (d,  $J = 9.20$  Hz, 2H), 6.74 (d,  $J = 2.06$  Hz, 2H), 6.69 (dd,  $J = 2.16$  Hz,  $J = 9.22$  Hz, 2H), 4.01, (t,  $J = 5.84$  Hz, 2H), 2.09 – 1.96 (m, 2H), 1.47 – 1.29 (m, 5H).

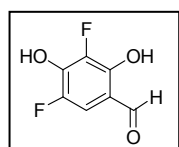
$^{13}C$  NMR (75 MHz,  $CD_3OD$ ):  $\delta = 166.86, 159.03, 156.57, 135.19, 134.02, 132.23, 131.94, 131.74, 131.24, 116.38, 104.33, 65.92, 31.12, 30.90, 28.80, 18.00$ .

$^{19}F$  NMR (400 MHz,  $CD_3OD$ ):  $\delta = -83.32$  (t,  $J = 10.15$  Hz, 3F), -116.27 – -116.44 (m, 2F), .123.61 (s, 2F), -123.84 (s, 4F), -124.68 (s, 2F), -125.46 (s, 2F), -128.22 (s, 2F).

HRMS (FD): Calc.  $m/z = 806.0992$  for  $C_{32}H_{19}F_{17}O_5$

Found  $m/z = 806.0961$   $[M]^+$

### 2,4-Dihydroxy-3,5-difluoro benzaldehyde (**154**)<sup>7</sup>



In a Schlenk tube, 2,4-difluororesorcinol (100 mg, 0.68 mmol) was dissolved in TFA (1 mL) and hexamethylenetetramine (190 mg, 1.36 mmol) was slowly added under stirring. The tube was placed under a  $N_2$ -atmosphere and heated to reflux overnight. The reaction mixture was cooled and  $H_2SO_4$  (50 %, 2 mL) was added and stirred for 2 h. The acidic aqueous phase was extracted EtAc (3x) and the combined organic phases were washed with HCl (1 N, 3x) and water (1x). The organic solution was dried over  $MgSO_4$ , filtered and the solvent was evaporated under reduced pressure to yield 50 mg (0.287 mmol, 42 %) product as a white solid.

---

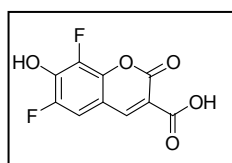
---

$^1\text{H}$  NMR (300 MHz,  $\text{CDCl}_3$ ):  $\delta = 9.63$  (d,  $J = 1.93$  Hz, 1H),  $7.03$  (dd,  $J = 2.06$  Hz,  $J = 9.76$  Hz, 1H).

Spectra conform with literature

Gee, Kyle R.; Haugland, Richard P.; Sun, Wei Chuan. UK Pat. Appl. (1998), GB 2319250 A 19980520

### Pacific blue (155)<sup>8</sup>



2,4-Dihydroxy-3,5-difluoro benzaldehyde (50 mg, 0.287 mmol) and malonic acid (32 mg, 0.316 mmol) were dissolved in methanesulfonic acid (2 mL) and the reaction mixture was stirred at room temperature overnight. The solution was diluted with brine and extracted with a THF/EtAc mixture (3x). The organic phase was dried over  $\text{MgSO}_4$ , filtered and evaporated. The crude product was purified by column chromatography using DCM/MeOH/Formic acid (80/20/1, v/v/v) as eluent to obtain 40 mg (0.165 mmol, 53 %) of pure product.

$^1\text{H}$  NMR (400 MHz,  $\text{DMSO-d}_6$ ):  $\delta = 8.50$  (s, br, 1H),  $8.20$  (s, 1H),  $7.18$  (d,  $J = 11.49$  Hz, 1H).

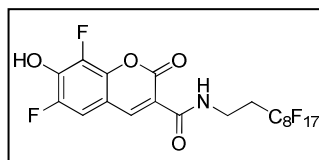
$^{13}\text{C}$  NMR (75 MHz,  $\text{CDCl}_3$ ):  $\delta = 171.76$ ,  $164.13$ ,  $149.25$ ,  $142.70$ ,  $142.59$ ,  $108.79$ ,  $108.62$ ,  $99.81$ ,  $99.73$ ,  $28.73$ .

$^{19}\text{F}$  NMR (400 MHz,  $\text{CDCl}_3$ ):  $\delta = -74.51$  (s, br, 1F),  $-136.73$  (s, br, 1F)

HRMS (FD): Calc.  $m/z = 242.0020$  for  $\text{C}_{10}\text{H}_4\text{F}_2\text{O}_5$

Found  $m/z = 242.0027$   $[\text{M}]^+$

### Pacific- $\text{C}_8\text{F}_{17}$ (156)



Pacific blue (20 mg, 0.076 mmol) and HBTU (86 mg, 0.228 mmol) were dissolved in THF (2 mL) and diisopropylethylamine (100  $\mu\text{L}$ ) was added. The reaction was stirred for 5 h at room temperature and subsequently water and DCM were added. The aqueous phase was extracted with DCM (3x) and the organic phase washed with brine (2x), HCl (1 N, 2x) and water (2x). The organic phase was dried over  $\text{MgSO}_4$ , filtered and evaporated. The crude product was purified by column chromatography using DCM/MeOH (90/10, v/v) to yield 17 mg (0.025 mmol, 33 %) of the product as a yellowish powder.

---

$^1\text{H}$  NMR (400 MHz, MeOD):  $\delta$  = 8.70 (s, 1H), 7.31 (d,  $J$  = 10.35 Hz, 1H), 3.75 (t,  $J$  = 7.04 Hz, 2H), 2.62 – 2.49 (m, 2H).

$^{13}\text{C}$  NMR (75 MHz, MeOD):  $\delta$  = 164.82, 162.37, 151.62, 149.49, 110.85, 110.65, 107.95, 33.03, 31.50.

$^{19}\text{F}$  NMR (400 MHz, MeOD):  $\delta$  = -83.31 (t,  $J$  = 9.97 Hz, 3F), -116.07 – -116.24 (m, 2F), -123.60 (s, 2F), -123.84 (s, 4F), -124.68 (s, 2F), -125.56 (s, 2F), -128.22 (s, 2F), -138.51 – -138.57 (m, 1F), -160.05 (d,  $J$  = 13.74 Hz, 1F).

HRMS (FD):            Calc.  $m/z$  = 687.0150 for  $\text{C}_{20}\text{H}_8\text{F}_{19}\text{O}_4$

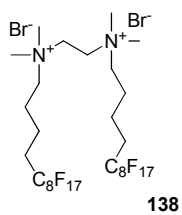
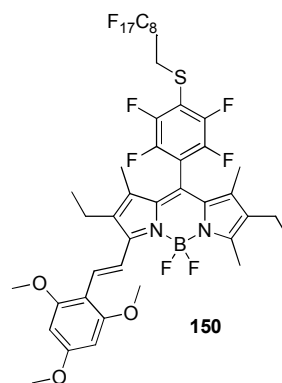
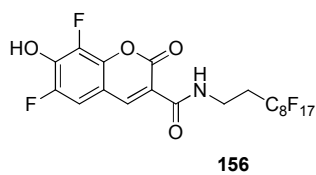
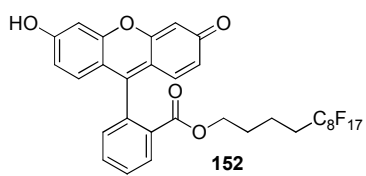
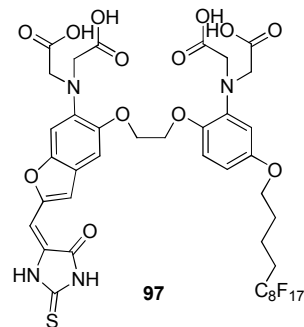
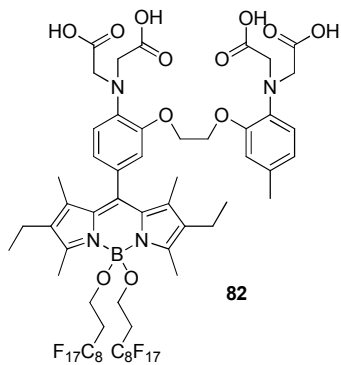
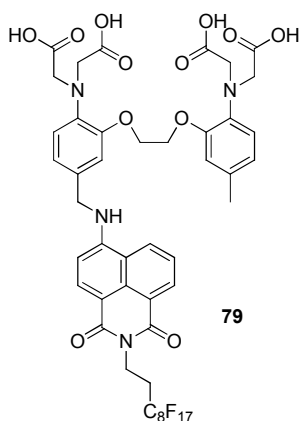
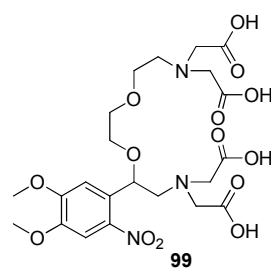
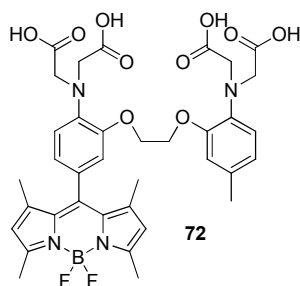
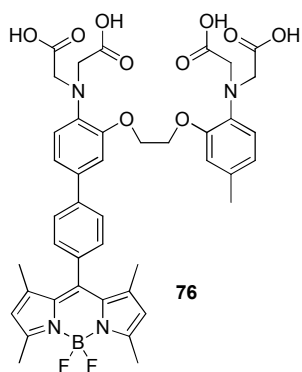
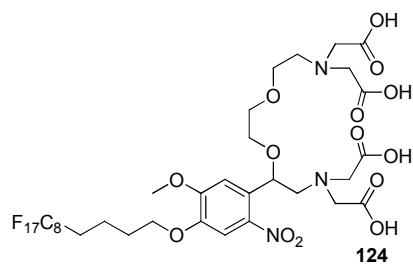
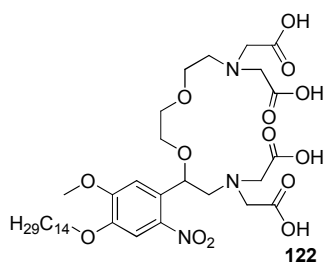
                         Found  $m/z$  = 687.01499  $[\text{M}]^+$

---

## References:

- (1) Parker, C. A.; Rees, W. T. *Analyst* **1960**, *85*, 587.
- (2) Oda, R.; Huc, I.; Danino, D.; Talmon, Y. *Langmuir* **2000**, *16*, 9759.
- (3) Ellis-Davies, G. C. R. *Tetrahedron Lett.* **1998**, *39*, 953.
- (4) Galangau, O.; Dumas-Verdes, C.; Meallet-Renault, R.; Clavier, G. *Org. Biomol. Chem.* **2010**, *8*, 4546.
- (5) Gryniewicz, G.; Poenie, M.; Tsien, R. Y. *J. Biol. Chem.* **1985**, *260*, 3440.
- (6) Tsien, R. Y. *Biochemistry* **1980**, *19*, 2396.
- (7) WeidnerWells, M. A.; FragaSpano, S. A. *Synth. Commun.* **1996**, *26*, 2775.
- (8) Sun, W. C.; Gee, K. R.; Haugland, R. P. *Bioorg. Med. Chem. Lett.* **1998**, *8*, 3107.

## Formulae of key molecules



---

## **Communication moléculaire biomimétique entre molécules et nanosystèmes photocontrôlés dans compartiments confiné**

Cette thèse se focalise sur la synthèse et l'étude de nouvelles molécules photoactives et leurs applications en tant que marqueurs, senseurs moléculaires et récepteurs d'ions photomodulables en milieux aqueux et organisés. Les fluorophores développés sont principalement des dérivés du bore-dipyrométhène (BODIPY), comportant des groupements réactifs (azoture, perfluorophényle), des chaînes hydrophobes, ou sont intégrés à un récepteur de calcium biocompatible. Le développement d'architectures auto-assemblées multicompartimentées de type vésicules dans des polymersomes géant y est décrit. Ces architectures ont été utilisées pour la génération de lumière blanche dans un micro-domaine, et constitue un modèle pour l'étude de transfert d'ions calcium entre vésicules localisées dans des polymersomes individuels. Ce transfert entre nano-objets confinés à l'intérieur d'un polymersome géant représente un système prototype de communication cellulaire artificiel rudimentaire.

Mots clefs: Chimie supramoléculaire, auto-assemblage, photochimie, multicompartimentation, liposome, polymersome, récepteur d'ion, fluorescence, libération d'ion.

## **Photocontrolled biomimetic communication between molecules and nanosystems in confined compartments**

The thesis focuses on the study and design of novel photoactive molecules and their application as labeling agents, fluorescent molecular  $\text{Ca}^{2+}$ -sensors and photolabile  $\text{Ca}^{2+}$ -decaging agents in aqueous media and organized supramolecular assemblies. The designed fluorophores are based on boron-dipyromethene (BODIPY) bearing hydrophobic chains or a reactive group like an azide or a perfluorophenyl moiety. Biocompatible calcium receptors have been prepared harnessing the fluorescence properties of BODIPY, naphthalimide and furan fluorophores. The development of self-assembled multicompartmentalized architectures, namely fluorocarbon vesicles in giant polymersomes is reported and the system has been used to create white light emission in confined microdomains. The  $\text{Ca}^{2+}$ -based ion transfer ion the confined polymer compartments between individual fluorinated vesicles has been studied. The ion transfer in between vesicles in polymer microcompartments has been established as an artificial prototype system for cellular communication.

Keywords: Supramolecular chemistry, self-assembly, photochemistry, multicompartmentalization, liposome, polymersome, ion receptor, fluorescence, ion decaging.